Large Engine Technology (LET) Task XXXVII Low-Bypass Ratio Mixed Turbofan Engine Subsonic Jet Noise Reduction Program Test Report

Joseph R. Hauser, Steven H. Zysman, and Thomas J. Barber
United Technologies Corporation, East Hartford, Connecticut

Since its founding, NASA has been dedicated to the advancement of aeronautics and space science. The NASA Scientific and Technical Information (STI) Program Office plays a key part in helping NASA maintain this important role.

The NASA STI Program Office is operated by Langley Research Center, the Lead Center for NASA's scientific and technical information. The NASA STI Program Office provides access to the NASA STI Database, the largest collection of aeronautical and space science STI in the world. The Program Office is also NASA's institutional mechanism for disseminating the results of its research and development activities. These results are published by NASA in the NASA STI Report Series, which includes the following report types:

- TECHNICAL PUBLICATION. Reports of completed research or a major significant phase of research that present the results of NASA programs and include extensive data or theoretical analysis. Includes compilations of significant scientific and technical data and information deemed to be of continuing reference value. NASA's counterpart of peer-reviewed formal professional papers but has less stringent limitations on manuscript length and extent of graphic presentations.

- TECHNICAL MEMORANDUM. Scientific and technical findings that are preliminary or of specialized interest, e.g., quick release reports, working papers, and bibliographies that contain minimal annotation. Does not contain extensive analysis.

- CONTRACTOR REPORT. Scientific and technical findings by NASA-sponsored contractors and grantees.

- CONFERENCE PUBLICATION. Collected papers from scientific and technical conferences, symposia, seminars, or other meetings sponsored or cosponsored by NASA.

- SPECIAL PUBLICATION. Scientific, technical, or historical information from NASA programs, projects, and missions, often concerned with subjects having substantial public interest.

- TECHNICAL TRANSLATION. English-language translations of foreign scientific and technical material pertinent to NASA's mission.

Specialized services that complement the STI Program Office's diverse offerings include creating custom thesauri, building customized data bases, organizing and publishing research results . . . even providing videos.

For more information about the NASA STI Program Office, see the following:

- Access the NASA STI Program Home Page at *http://www.sti.nasa.gov*

- E-mail your question via the Internet to help@sti.nasa.gov

- Fax your question to the NASA Access Help Desk at 301–621–0134

- Telephone the NASA Access Help Desk at 301–621–0390

- Write to:
  NASA Access Help Desk
  NASA Center for AeroSpace Information
  7121 Standard Drive
  Hanover, MD 21076

NASA/CR—2001-210571

Large Engine Technology (LET) Task XXXVII Low-Bypass Ratio Mixed Turbofan Engine Subsonic Jet Noise Reduction Program Test Report

Joseph R. Hauser, Steven H. Zysman, and Thomas J. Barber
United Technologies Corporation, East Hartford, Connecticut

National Aeronautics and
Space Administration

Glenn Research Center

March 2001

Acknowledgments

The authors would like to thank Mr. Naseem Saiyed and Dr. James Bridges of NASA Glenn Research Center for their support of the entire model test program.

TABLE OF CONTENTS

LIST OF SYMBOLS / NOMENCLATURE

A   Area
a or C   Speed of sound
BPR   Bypass ratio, m_{Bypass}/m_{Core},
D   Nozzle diameter
f   Observed frequency
g   Shielding function
k   Turbulence kinetic energy
m   Mass flow
M   Mach Number
P   Pressure
r   Radial coordinate
R   Distance to observer
T   Temperature
U   Axial velocity component
V   Vertical velocity component
x   Axial coordinate

$\alpha, \alpha_T, \beta_c$ Empirical constants
ε Turbulent dissipation
η Temperature mixedness
ρ Density
τ Characteristic time delay
Ω Source frequency
θ Viewing angle referred to upstream

Subscripts
0   Stagnation condition
b   Bypass stream condition
c   Convective reference
cl   Centerline
fs   Full or engine scale
j   Jet exit plane condition
m   Fully mixed out plane
p   Primary stream condition
ss   Small or model scale
x   Axial location
∞ Freestream condition

Superscripts
$(\,)'$ Turbulent fluctuation

LIST OF FIGURES

LIST OF TABLES

1.0   SUMMARY

In 1993, NASA Lewis Research Center initiated a three year effort to research, design, and develop internal mixers for reducing subsonic jet noise of both low-bypass ratio (approximately 1.7) and high-bypass ratio (approximately 6.0) turbofan engines. The goal of the program was to reduce sideline during takeoff noise by 3 EPNdB (Effective Perceived Noise Level in deciBel) relative to noise levels consistent with 1992 mixer technology. This program was known as LET (Large Engine Technology) Task XXXVII, Subsonic Jet Noise Reduction NASA contract NAS3-26618. In 1994, Pratt & Whitney (P&W) was awarded this contract in order to pursue the mixer design for low-bypass ratio engines.

An objective under this NASA contract is to assess design methods based on computational fluid dynamics (CFD) and computational aeroacoustics (CAA) codes that are capable of predicting both the far-field jet noise and performance impact of mixed nozzle exhaust systems.   This capability will permit analytical evaluation of promising concepts and minimize reliance on costly and time consuming "cut and try" development methods.

In 1994, (under internal funding) Pratt & Whitney used CFD (i.e., NASTAR) to guide the design of a mixer that would achieve a noise reduction relative to an existing P&W 12-lobe mixer. Since lower jet noise corresponds to reduced peak velocity and temperature profile at the exit plane of the nozzle, the objective was to achieve the most uniform velocity profile possible. Analysis of CFD for the baseline 12-lobe mixer indicated that there were 12 "regions of high temperature" located at the exit plane of the exhaust nozzle, and each were aligned with a mixer lobe. The output of CFD for the 12-lobe mixer at 4 axial locations downstream of the nozzle exit plane are shown on Figures 7.3.5 and 7.3.6. Since the goal was to achieve a uniform velocity profile, elimination of the "regions of high temperature" were necessary. This was accomplished by introducing a mini-chute at each primary lobe of a 16-lobe mixer to provide additional cooler fan air at the location of the "region of high temperature". The incorporation of a mini-chute as can be seen from Figure 4.0.1 results in a mixer that appears to have a "double lobe" at each primary lobe location. This mixer was designated the Advanced Technology Mixer (ATM). A photo of the ATM can be found on Figure 4.2.6.1.   Pre-test CFD analysis for this mixer showed that the "regions of high temperature" associated with incomplete mixing of the hot flow within the lobes was not present.   However the ATM had developed a different flow pattern with concentric isothermal regions, which became known at Pratt & Whitney as the "ring of fire".   The CFD analysis of the ATM is shown on Figure 7.3.7.

In 1994, both noise and aero (i.e., Laser Doppler Velocimetry (LDV)) testing was conducted in the NASA Lewis Research Center Nozzle Acoustic Test Rig (NATR) for a splitter, 12-lobe mixer, 20-lobe mixer, and the ATM. The CFD analysis of both the baseline 12-lobe mixer and 20-lobe mixer compared favorably with the measured LDV data, as can be seen from Figures 8.2.7 and 8.2.8, respectively. The results of the CFD analysis for the mixers were then used as input to NASA Lewis's MGB (Mani et al.[9]) acoustic analogy code. The results of MGB were then compared to the actual measured noise data. The comparison was not favorable, which led to parametric studies of the MGB code, and also calibration by using noise data from the simpler splitter configuration.

In 1996, CFD was used to design a new 24-lobe mixer, which as with the 20-lobe mixer was a parametric version of the 12-lobe mixer with a higher lobe count. Pre-test CFD analysis showed that the 24-lobe mixer had a reduced peak jet velocity relative to the 20-lobe mixer, and therefore was expected to be quieter. CFD analysis also showed that a lower peak exhaust velocity for the 20-lobe mixer could be achieved if every other lobe were cutback (i.e., scarfed).

Noise and aero testing was once again conducted at NASA's NATR facility. Since LDV data acquisition was time consuming, it was decided to obtain total pressure and total temperature traverse measurements in the exhaust duct, and in the jet plume. Noise testing was conducted for all mixers that were tested in 1994 as well as the new 24-lobe mixer, and the modified 20-lobe mixer. Noise testing was conducted on the 20-lobe mixer with zero scarf, and then every other lobe was cutback 12 degrees. The result was a mixer with an alternating scarf angle of 0 and 12 degrees. See Figures 4.2.1.1 to 4.2.6.1 for a picture of all the mixers tested.

In addition to noise testing of different mixers, testing was also conducted with various changes in the flow path both upstream and downstream of the mixer. The changes upstream consisted of the incorporation of simulated engine probes to determine their impact on the performance of the mixers, (see Figure 4.4.1 for a picture of the probes). Changes downstream consisted of an enhanced mixing device concept called vortex generators, which were essentially low-profile triangular shaped wedges that were attached to the tailplug (see Figure 4.3.1.1). Testing was also conducted with a scale-model version of a device called a "muffler", that has proven to reduce combustion noise in JT8D-200 series engine testing. This device is a Helmholtz resonator that is tuned for low frequency combustion noise. Refer to Figure 4.5.1 for a picture of the muffler. The intent of this test was to determine if the muffler could cause an adverse effect on the mixing process downstream of the mixer.

Examination of the 1996 acoustic EPNL data (Section 7.1) indicates that *the ATM mixer was the best mixer design and that it achieved a 1.8 EPNdB reduction over the baseline 12-lobe configuration.* Of interest was the observation that the static performance ($M_\infty=0.0$) of all the mixers were essentially the same. This is most likely due to the importance of the low frequency jet noise, which dominates the spectra at the static (0 Mach number) condition. However in flight, the low frequency jet noise is reduced, and as a result the higher frequency "mixing noise" becomes the dominant source. The acoustic data also indicated that the muffler with the ATM had essentially no effect on the noise results. However geometry perturbations of scalloping, scarfing and vortex generators increased the noise approximately 0.5 EPNdB, and the effects of engine probes increased the noise by approximately 1 EPNdB and 2 EPNdB, with the 12-lobe mixer, and the ATM, respectively. Also, the ATM with unheated fan flow was approximately 1 EPNdB higher than the ATM with heated fan flow.

At the same time, examination of the measured aerodynamic data shows the existence of a residual-mixing region downstream of the common-flow nozzle exit plane. This mixing region produces high frequency noise, which dominates the EPNL calculations. A detailed discussion of this residual mixing region downstream of the nozzle exit plane can be found in reference 26.

The computational studies performed in this program used the P&W NASTAR Navier-Stokes analysis and the MGB acoustic analogy code developed by NASA-NYMA.
Aerodynamic analyses were performed and favorable comparisons with measured LDV and traverse data were obtained for the mean axial velocity, the turbulent kinetic energy and the total temperature fields downstream of the nozzle exit plane for both the splitter and mixer configurations. The NASTAR analysis predicted accurately the basic flowfield patterns as well as the detailed levels and gradients.

The MGB analysis, used in conjunction with the NASTAR Navier-Stokes flow solver, has been successfully applied to predict the acoustic characteristics of a multistream axisymmetric nozzle. From these calculations, one can note that:

- MGB provides reasonable acoustical signature predictions for axisymmetric multistream nozzles,
- MGB provides reasonable acoustical signature predictions of scaling effects, e.g. size and observer distance,
- MGB is a useful analytical tool for assessing turbulence modeling and input boundary condition effects, and that sensitivities of order 2 to 4 dB were noted.

While calibrations with experimental data were good, it is believed that the CFD/MGB analysis approach is best suited for predicting qualitative trends rather than absolute levels. Similar comparisons performed for three-dimensional forced mixer nozzles were less successful. While the analyses predicted the general shift in directivity pattern from the axisymmetric splitter nozzle, they were unable to successfully discriminate between different lobed mixer configurations. This appears to be largely due to the inability of the circumferential averaging procedure for CAA to represent the 3D problem, rather than the accuracy limitations of the CFD analysis.

2.0   INTRODUCTION

Community sensitivity to aircraft noise has intensified over the years. As a result, ever increasing noise stringency and regulations have been mandated by the FAA under FAR 36, Stage 3 noise limits. This mandate specifies noise limits as a function of aircraft takeoff gross weight in terms of EPNL for three conditions: approach, takeoff, and sideline during takeoff. The aircraft engine industry responded to the more stringent noise limits by introducing noise reduction design features into aircraft engines. The biggest advance in noise reduction was the introduction of high-bypass ratio engines. These engines have much lower exhaust velocities than low-bypass ratio engines and therefore lower jet noise. This is due to the fact that jet noise decreases rapidly as jet exhaust velocity decreases. Therefore, in order to reduce noise of low-bypass ratio turbofan engines, it is necessary to reduce jet exhaust velocity. One very effective method to achieve this is the incorporation of an Internal Exhaust Gas Mixer (IEGM, called mixer from here on). This device, see Fig. 2.0.1, mixes high velocity core flow with lower velocity fan flow so that the peak exhaust velocity at the nozzle exit is reduced. As a result, the low frequency jet noise is reduced relative to a turbofan engine without a mixer.

Turbofan exhaust system mixer technology for jet noise reduction has been under development for approximately 30 years. Historically, this development has relied on extensive parametric testing, including both scale-model tests and full-scale engine tests. Testing was carried out to determine both noise and thrust performance, and this generally required separate tests in different facilities. Pratt & Whitney tested literally hundreds of configurations of mixers in the 1970's during development of mixers for both the JT8D and JT8D-200 series of engines. This development effort led to the low bypass ratio mixers that are in service today.

In the late 1980's, P&W's hushkit partners successfully used P&W designed mixers as the major element of hushkits for their JT8D engines. These hushkits were successfully used to obtain Supplemental Type Certificates that allowed over 95% of JT8D powered aircraft to meet Stage 3 noise limits. Pratt & Whitney is redesigning the mixer to further reduce jet noise and thereby allow the remaining JT8D powered aircraft to meet Stage 3 noise limits. Pratt & Whitney is also pursuing improvements to the mixer used for the JT8D-200 engine which powers the MD-80 aircraft. The JT8D-200 is essentially a re-fanned JT8D engine with approximately a 70% higher bypass ratio than the original JT8D. The JT8D-200 engine also incorporated a mixer when it was originally certified. As a result, the JT8D-200 is significantly quieter than the JT8D engine, and when entered into service on the MD-80 aircraft was certified to FAR 36 Stage 3 noise limits.

The regulatory environment in the 1990's is increasingly stringent, with noise reductions beyond FAR Part 36 Stage 3 being considered. Also, many airport authorities are imposing landing fees and other restrictions based on aircraft noise levels. Thus, there is a need for additional mixer technology for further reducing jet noise from low-bypass ratio turbofan engines. Furthermore, it is critical that development time and cost be reduced so that the new technology can be introduced in a timely fashion.

In 1993, NASA Lewis Research Center initiated a three year effort to research, design, and develop internal mixers for reducing the subsonic jet noise of both low-bypass ratio (approximately 1.7) and high-bypass ratio (approximately 6.0) turbofan engines. The goal of the program was to reduce the sideline noise during takeoff by at least 3 EPNdB relative to noise levels consistent with 1992 era technology, without producing significant drag penalties. This program was known as LET (Large Engine Technology) Task XXXVII, Subsonic Jet Noise Reduction NASA contract NAS3-26618.

An objective under this NASA contract is to assess design methods based on computational fluid dynamics (CFD) and computational aeroacoustics (CAA) codes that are capable of predicting both the far-field jet noise and performance impact of mixed nozzle exhaust systems. This capability will permit analytical evaluation of promising concepts and minimize reliance on costly and time consuming "cut and try" development methods. Under this contract, Pratt & Whitney elected to pursue jet noise reductions for low-bypass ratio turbofan engines, since the technology developed in this program would be applicable to both the hushkitted JT8D engines and also JT8D-200 powered MD-80 aircraft.

Under this contract, far-field noise and aerodynamic measurements of the jet were conducted on 1/7th scale-model exhaust systems at the NASA Lewis Research Center Nozzle Acoustic Test Rig (NATR) facility, in 1994 and 1996. Testing was conducted for a splitter (non-mixed) exhaust system, and for multiple mixed-flow exhaust system configurations. Figure 2.0.2 is a schematic of both a splitter and a typical lobe mixed exhaust system installed in the NATR test facility.

In the fall of 1994 far-field noise measurements were obtained for a total of five exhaust nozzle configurations; the splitter (no mixer), a 12-lobe, a 20-lobe mixer plus two versions of the 16-lobe ATM (with, and without lobe scallops). Figure 4.2.2 is a side view schematic of a typical mixer showing a scallop (i.e., lobe cut out). The 12-lobe mixer was a scale-model version of the mixer currently in service in the JT8D-200 engines that power the MD-80 aircraft, and hence is the baseline mixer. The 20-lobe mixer was designed to be a parametric variation on only lobe count relative to the 12-lobe mixer. The ATM was the first attempt by P&W to design a mixer by using CFD with the objective of obtaining the most uniform exit velocity profile possible based on the assumption that this would produce the most noise reduction. See Figures 4.1.1 for a photo of the splitter (no mixer), and Figures 4.2.1.1 through 4.2.6.1 for photos of all the mixers tested, including a 24-lobe mixer, which was tested in 1996 and will be discussed shortly. The noise data were obtained over a range of simulated engine power conditions from takeoff to approach and for two conditions of simulated flight speed: static and 0.27 Mach number. The ATM, as well as all of the other models tested during this contract, with the exception of the 24-lobe mixer, were designed and built under Pratt & Whitney internal funding.

Also in 1994, LDV data were obtained for a total of four configurations; the splitter (no mixer), the 12 and 20-lobe mixers, and also the CFD designed 16-lobe Advanced Technology Mixer (ATM). Since the LDV tests were a time consuming process it was decided to obtain the LDV data at only one power condition. The point selected was power condition 8 (Table 3.1) at a flight Mach number of 0.10 in order to calibrate the contractor's CFD capability at a typical takeoff power condition for the JT8D-200 powered MD-80 aircraft. A higher Mach number was desired to match the sideline during takeoff acoustic certification condition (Mach 0.27), but was prevented due to excessive vibration of the LDV system. The measurements obtained above were used to compare Pratt & Whitney's CFD pre-test predictions to the LDV data. Upon good agreement, the CFD results were then used as input to NASA Lewis's MGB code, which was then compared to the measured noise data.

Prior to conducting tests at the NATR in 1996, two modifications were incorporated which had a substantial impact on the results of the testing and therefore need to be mentioned. The first difference was that in 1994 the fan flow was unheated, whereas in 1996 the NATR facility was modified to heat the fan flow, which allowed for a better simulation of full-scale engine conditions. The second difference between 1994 and 1996 testing was the location of both the core and fan charging station locations. The pressures and temperatures in the full-scale engine are measured at the interface of the engine exit and the entrance to the exhaust system (i.e., entrance to the mixer). Therefore it was desired to set the pressures and temperatures at the same locations for the model-scale testing. This axial location is marked with a vertical dashed line on Figure 5.3.1.1, and is labeled "desired" model charging station location. However, in 1994 due to lack of instrumentation, the pressures and temperatures of the core flow and the temperatures of the fan flow prior to the mixer entrance had to be estimated based on analysis of the upstream jet exit rig charging station data (station 113.5 of Figure 5.3.1.1). However, since there was a pressure probe (labeled PW) in the fan stream at the entrance to the mixer, the fan pressure was the only parameter that was not estimated. In 1996 a new model charging station (Figure 5.3.2.1) was designed and fabricated, thus eliminating the need to estimate temperature and pressure profiles going into the mixer. A further discussion of the charging station locations for 1994, and 1996 can be found in Sections 5.3.1 and 5.3.2, respectively.

In 1996 both noise and aerodynamic measurements were again obtained at NASA's NATR facility. Since all of the mixers that were tested for noise in 1994 were re-tested in 1996 with heated fan flow and due to the charging station differences, the analysis in this report emphasizes the noise data obtained in 1996. Far-field noise data and total pressure and temperature traverse measurements in the jet plume at four axial locations were obtained. These traverse measurements were made in lieu of LDV measurements, which would have required more time than was available. The traverse measurements were taken at power condition number eight (Table 3.2), with the tunnel Mach number set to 0.27, since this closely represented the takeoff flight noise certification condition for the MD-80 aircraft. Traverse measurements of four mixers were conducted; the 12, 20, ATM, and a new 24-lobe mixer.

Noise testing was conducted for all mixers that were tested in 1994 as well as the new 24-lobe mixer. Based on CFD analysis, the 24-lobe mixer showed a reduction in peak jet velocity relative to the 20-lobe mixer, and as a result the 24-lobe was expected to be quieter than the 20-lobe mixer. CFD analysis also showed that a lower peak velocity for the 20-lobe mixer could be achieved by cutting back every other lobe. The cutting back of lobes creates a scarf angle at the lobe exit as shown on Figure 4.2.2. Based on this analysis noise testing was first conducted on the 20-lobe mixer with zero scarf angle, and then every other lobe was cut back 12 degrees. The result was a mixer with an alternating scarf angle of 0 and 12 degrees. See Figure 4.2.3.1 for a picture showing a side view of the 20-lobe mixer with an alternating scarf angle of (0/12 degrees). See Figures 4.2.1.1 to 4.2.6.1 for pictures of all of the mixers tested in 1996, including the 24-lobe mixer.

In addition to noise testing of different mixers, testing was also conducted with various changes in the flow path both upstream and downstream of the mixer. The changes upstream consisted of the incorporation of simulated engine probes to determine their impact on the performance of the mixers, (see Figure 4.4.1 for a picture of the probes). Changes downstream consisted of an enhanced mixing device concept called vortex generators, which were essentially low-profile triangular shaped wedges that were attached to the tailplug (see Figure 4.3.1.1). The intent of the vortex generators was to promote additional mixing in the exhaust duct prior to the nozzle exit. Testing was also conducted with a scale-model version of a device called a "muffler", that has been proven to reduce combustion noise on the JT8D-200 engine models. This device is a Helmholtz resonator that is tuned for low frequency combustion noise. Refer to Figure 4.5.1 for a picture of the muffler. The intent of this test was to determine if the muffler could cause an adverse effect on the mixing process downstream of the mixer, and also if noise would be generated due to flow over the open slots. This concern was a raised based on full-scale engine testing with the muffler that had been conducted at P&W's facility prior to conducting the model tests.

3.0 TEST OBJECTIVES

NASA's overall test objectives for the LET Task XXXVII were to research, design and develop mixers for reducing the jet noise of aircraft powered by low by-pass ratio (approximately 1.7 BPR) engines and also aircraft powered by high by-pass ratio (approximately 6 BPR) engines without producing significant drag penalties. The goal was to reduce the sideline noise during takeoff by at least 3 EPNdB relative to their respective 1992 noise levels.

P&W's test objective, a subset of NASA's overall test objective, was to:

1) conduct LDV testing at NASA Lewis in order to calibrate the contractor's internal CFD design system (developed under P&W funding) and
2) enhance the MGB (theoretical jet noise prediction developed by Mani et al.[9]) capability that could be used for the design of improved mixers for low by-pass ratio engines in a timely and cost effective manner.

The ultimate goal is to assess design methods based on computational fluid dynamics (CFD) and computational aeroacoustics (CAA) codes that are capable of predicting both far-field jet noise and performance impact of mixed-flow exhaust systems. Pratt & Whitney's specific objective was to use the calibrated CFD and MGB codes to design and develop an advanced mixer to achieve a substantial jet noise reduction for Pratt & Whitney's low by-pass ratio JT8D-200 turbofan engine. This engine powers the MD-80 aircraft, which is currently certified to FAR 36 Stage 3 noise limits.

To achieve the objectives stated above, two phases of testing were conducted at NASA's NATR facility. The first phase was conducted in 1994 with unheated fan flow, and the second phase of testing was conducted in 1996 with heated fan flow.

3.1 1994 (PHASE I) TEST OBJECTIVES and TARGET TEST CONDITIONS (*unheated fan flow*)

The intent of the model-scale testing was to duplicate full-scale engine conditions as close as possible, therefore it was desired to heat both the core flow and the fan flow. However the NATR did not have the capability to heat the fan flow, and as a result the model-scale conditions were not an accurate simulation of the full-scale engine conditions. However testing was conducted with the following objectives:

1. *Establish a reference level of far-field jet noise for a mixed-flow exhaust system incorporating a 12-lobe mixer that is representative of the current JT8D-200 mixer.* The jet noise is defined in terms of its effective perceived noise level (EPNL) as derived from data measured by an array of far-field microphones. Data was obtained over a range of engine power conditions from takeoff to approach for two conditions of simulated flight speed; static and 0.27 Mach number.

2. *Obtain far-field jet noise for two additional mixer designs, a 20-lobe mixer and the Advanced Technology Mixer (ATM), which was designed using CFD under Pratt & Whitney internal funding.* These two mixers represented an initial design concept for reduced jet noise based on a more uniform velocity profile than the baseline 12-lobe mixer.

3. *Obtain far-field jet noise data for an axisymmetric splitter configuration at a more limited set of conditions than described above for the mixer configurations.* This case was included for purposes of CFD/CAA code calibration.

4. *Obtain detailed laser Doppler velocimetry (LDV) data in the exhaust duct and jet at one engine power condition for four nozzle configurations: the axisymmetric splitter; the reference 12-lobe mixer; the 20-lobe mixer and the ATM.* The LDV data include both mean velocities and turbulence intensities. These data were used to calibrate the CFD codes and associated Reynolds-averaged turbulence models, and to verify that the velocity field information required as input to the CAA code was being accurately computed.

TABLE 3.1:   1994 TARGET TEST CONDITIONS (***unheated fan flow***)

STATIC (Mn = 0.0) and FLIGHT (Mn = 0.27)					
POWER CONDITION	**TTcore T_0**	**PTcore P_0**	**TTfan T_0**	**PTfan P_0**	**FLIGHT CONDITION**
1	2.29	1.46	1.0	1.44	APPROACH
2	2.34	1.51	1.0	1.48	
3	2.36	1.54	1.0	1.50	
4	2.38	1.57	1.0	1.53	
5	2.43	1.62	1.0	1.57	
6	2.56	1.80	1.0	1.71	CUTBACK
7	2.63	1.88	1.0	1.78	
8	2.71	1.98	1.0	1.85	TAKEOFF
9	2.77	2.04	1.0	1.90	

3.1.1 FAR-FIELD NOISE MEASUREMENTS and FAR-FIELD NOISE DATA

The far-field noise measurements were acquired at two conditions of simulated flight speed; static and 0.27 Mach number. Simulated engine power conditions, ranging from approach to takeoff, are defined in Table 3.1. The pressures and temperatures in the full-scale engine are measured at the interface of the engine exit and the entrance to the exhaust system (i.e., entrance to the mixer). Therefore it was desired to set the pressures and temperatures at the same locations for the model-scale testing. The pressure ratios and the temperature ratios of

Table 3.1 are defined relative to the "desired" charging station location. This charging station location is discussed in detail in Section 5.3.1, and is shown on Figure 5.3.1.1. A complete noise test of a given exhaust system configuration consisted of acquiring the far-field noise data for all power conditions, first for static external condition and then again at the 0.27 external Mach number condition. The nozzle pressure and temperature ratios were set to the same values for both external flow conditions. The intent was to define the effects of forward flight on noise at constant exhaust mixed jet Mach number ($Vmix/C_0$).

The far-field noise data received from NASA was sound pressure level (SPL) at full-scale, 150-foot radius, for an acoustic standard day condition (i.e., 77 degrees F, 70% R.H.), with all of the corrections applied that are discussed in Section 6.0. The sound pressure level for both static (0.0 Mach number), and flight (0.27 Mach number) were supplied to Pratt & Whitney on 3.5-inch diskettes.

3.1.2 AERODYNAMIC DATA MEASUREMENTS (LDV) and LDV MEASURED DATA MATRIX

Since taking laser Doppler velocimetry (LDV) data was a time consuming process, and since the intent of the test was to obtain a detailed resolution of the velocity field, it was decided to obtain LDV data at only one power condition. The flow condition chosen to conduct all LDV testing was power condition 8 (Table 3.1) at a flight Mach number of 0.10. A Mach number of 0.27 was desired to match the sideline during takeoff acoustic certification condition for the JT8D-200 powered MD-80 aircraft, but was prevented due to excessive vibration of the LDV system. Data were obtained at the nozzle exit plane and several downstream locations, as far as 6(D) nozzle diameters. A summary of the LDV data obtained can be found in Table 3.1.2.1. A discussion of LDV testing can be found in Section 5.5.2, and a summary of the results can be found in Section 7.2. Also refer to Figure 5.5.2.1 for a picture of the LDV scan rig and NATR.

Table 3.1.2.1: LDV Measured Data Matrix

Date	Runs	Configuration	X/D	Comments
7/26/94	374-408	Splitter	0	
	409-457	Splitter	4	
	458-472	Splitter	2	
7/28/94	491-532	Splitter	0	Repeat
	533-566	Splitter	2	Repeat
7/29/94	567-691	20	0	
	692-774	20	1	
9/12/94	872-968	20	2	
	969-990	20	4	
9/13/94	991-1049	12	0	
	1050-1106	12	2	
9/19/94	1107-1168	12	4	
	1169-1188	12	6	
9/20/94	1189-1246	ATM	0	
	1247-1305	ATM	2	
	1306-1362	ATM	4	
	1363-1392	ATM	0	Repeat
9/21/94	1393-1450	ATM	6	
	1451-1489	ATM	1	Radial Surveys
9/26/94	1513-1548	ATM	Int	
		Splitter	Int	
9/28/94	1683-1716	12	Int	

3.2 1996 (PHASE II) TEST OBJECTIVES and TARGET TEST CONDITIONS (*heated fan flow*)

The intent of the model-scale testing was to duplicate full-scale engine conditions as close as possible, therefore it was desired to heat both the core flow and the fan flow. Prior to testing in 1996, the NATR was modified so that the fan flow could be heated. As a result the nozzle model conditions simulated the full-scale engine conditions. Testing was conducted with the following objectives:

1. *Establish far-field jet noise levels for the splitter, 12-lobe, 20-lobe, 24-lobe, and ATM mixers.* The data were obtained over a range of simulated engine power conditions from take-off to approach and for two conditions of simulated flight speed; static and 0.27 Mach number.

2. *Obtain jet noise data for the 20-lobe mixer with two different scarf angles at the same power conditions as above.*

3. *Obtain jet noise data for one configuration of an advanced mixing concept: Vortex Generators (VGs) at the same power conditions as above.* Here the VGs refer to low profile triangular shaped surfaces that are mounted on the tailplug.

4. *Obtain total pressure and temperature data in the exhaust duct and plume at one engine power condition for four configurations which, were chosen based on the results of the acoustic testing.* These configurations were the 12-lobe, 20-lobe 24-lobe, and the ATM. Data were acquired with external flow simulating a 0.27 Mach number flight condition.

TABLE 3.2:   1996 TARGET TEST CONDITIONS (*heated fan flow*)

STATIC (Mn = 0.0) and FLIGHT (Mn = 0.27)					
POWER CONDITION	TTcore T_0	PTcore P_0	TTfan T_0	PTfan P_0	FLIGHT CONDITION
1	2.29	1.46	1.16	1.44	APPROACH
2	2.34	1.51	1.17	1.48	
3	2.36	1.54	1.17	1.50	
4	2.38	1.57	1.18	1.53	
5	2.43	1.62	1.19	1.57	
6	2.56	1.80	1.22	1.71	CUTBACK
7	2.63	1.88	1.24	1.78	
8	2.71	1.98	1.26	1.85	TAKEOFF
9	2.77	2.04	1.27	1.90	

3.2.1   FAR-FIELD NOISE MEASUREMENTS and FAR-FIELD NOISE DATA

Far-field noise measurements were acquired at two conditions of simulated flight speed; static and 0.27 Mach number. Simulated engine power conditions, ranging from approach to takeoff, are defined in Table 3.2. The pressure ratios shown in Table 3.2 are defined relative to the reference charging station for the exhaust system. Prior to this test, a new model charging station was designed and fabricated eliminating the need to estimate temperature and pressure profiles going into the mixer as was done for 1994 testing. Section 5.3.2 discusses the charging station location in some detail, and Figure 5.3.2.1 shows the location of the charging station. A complete noise test of a given exhaust system configuration consisted of acquiring the far-field noise data for all power conditions, first for static external conditions and then again at the 0.27 external Mach number condition. The nozzle pressure and temperature ratios were set to the same values for both external flow conditions. The intent was to define the effects of forward flight on noise at constant exhaust mixed jet Mach number ($Vmix/C_0$).

The far-field noise data received from NASA was sound pressure level (SPL) at full-scale, 150-foot radius, for an acoustic standard day condition (i.e., 77 degrees F, 70% R.H.), with all of the corrections applied that are discussed in Section 6.0. The sound pressure level for both static (0.0 Mach number), and flight (0.27 Mach number) were supplied to Pratt & Whitney on 3.5-inch diskettes.

3.2.2 AERODYNAMIC DATA MEASUREMENTS (Flow Field) with CHARGING STATION CONDITIONS FOR TEMPERATURE and PRESSURE TRAVERSES

The diagnostic aerodynamic data of main interest are the total pressure and total temperature traverse measurements in the jet exhaust. These measurements were made in lieu of LDV measurements, which required more time than was available for the test. The measurements were taken at power condition number 8 (Table 3.2), with the tunnel Mach number set to 0.27, since this closely represents the sideline during takeoff flight noise certification condition for the JT8D-200 powered MD-80 aircraft. A summary of the downstream axial locations and charging station conditions for the temperature and pressure traverses can be found in Table 3.2.2.1. A discussion of the temperature and pressure traverse can be found in Section 5.5.3, and a discussion of the results in Section 7.3. Also refer to Figure 5.5.3.1 for a view of the traverse planes downstream of the nozzle exit, and traverse density across the exhaust jet.

Table 3.2.2.1: Charging Station Conditions for Temperature and Pressure Traverses

Case	X Loc.	Runs	Pt/Pa Core Tt/Ta Core	Pt/Pa Fan Tt/Ta Fan	Mcore Mfan
12-lobe **Pa=14.14 Ta=65F**	1.0"	1014	2.035 2.802	1.896 1.275	3.64 6.49
	2.5"	1013	2.030 2.801	1.889 1.272	3.62 6.48
	5.0"	1012	2.033 2.787	1.886 1.270	3.59 6.48
	10.0"	1011	2.039 2.774	1.898 1.281	3.42 6.49
20-lobe **Pa=14.27 Ta=45F**	1.0"	964	2.039 2.805	1.879 1.280	3.71 6.53
	2.5"	965	2.044 2.811	1.888 1.286	3.72 6.59
NO DATA	5.0"				
NO DATA	10.0"				
24-lobe **Pa=14.27 Ta=45F**	1.0"	994	2.043 2.782	1.907 1.009	3.20 7.11
	2.5"	993	2.038 2.770	1.905 1.009	3.43 7.12
	5.0"	992	2.035 2.778	1.902 1.009	3.50 7.11
	10.0"	988	2.042 2.792	1.892 1.274	3.45 6.51
ATM **Pa=14.07 Ta=59F**	1.0"	949	2.055 2.809	1.894 1.289	3.52 6.39
	2.5"	951	2.041 2.775	1.888 1.278	3.58 6.47
	5.0"	952	2.043 2.783	1.886 1.282	3.53 6.47
	10.0"	954	2.045 2.786	1.891 1.289	3.55 6.51

4.0   DESCRIPTION OF MODELS TESTED

A total of four 1/7th scale-model internal mixers and a splitter configuration were fabricated by Pratt & Whitney and tested at NASA's NATR facility in 1994 and 1996. In addition to testing various exhaust nozzle configurations, the effect of simulated engine probes, and muffler (tuned for full-scale combustor noise) were tested. Also tested were an enhanced mixing device concept called Vortex Generators, which were mounted on the tailplug. The intent of these devices were to promote additional mixing in the exhaust duct, prior to exiting the nozzle. Section 4.1 through 4.5 discusses the configurations tested in more detail.

4.1   SPLITTER EXHAUST NOZZLE CONFIGURATION

The splitter is a simple body of revolution part. Its trailing edge is located at approximately the same axial station as those of the mixers, and is designed to run at the same by-pass ratio as the mixer configurations.   Figure 2.0.2 shows a schematic of a splitter, and a typical lobe mixer. A picture of the splitter can be found on Figure 4.1.1, along with the tailcone/tailplug hardware. This axisymmetric splitter was tested for noise in 1994 (unheated fan flow), and also in 1996 (heated fan flow). This configuration was tested for purposes of both CFD and CAA code calibration.

4.2   MIXED EXHAUST NOZZLE CONFIGURATIONS and GEOMETRIC PARAMETERS

In 1994 (with unheated fan flow), both noise and aerodynamic (i.e., LDV) data were obtained for three mixed exhaust nozzle configurations. The three mixer designs tested were the 12-lobe (baseline), 20-lobe, and the Advanced Technology Mixer (ATM). The ATM was tested first without lobe scallops, and then with lobe scallops. Figure 4.2.2 is a schematic view of a typical mixer showing an example of a lobe scallop. In 1996 (with heated fan flow), both noise and aerodynamic (i.e., total temperature and total pressure traverse) data were obtained for a total of five mixed exhaust configurations. Three of the five mixers that were tested in 1994 with unheated fan flow were also tested in 1996 with heated fan flow. Two additional mixed configurations were tested in 1996. These were a new 24-lobe mixer, and a modification to the 20-lobe. The modification was the introduction of an alternating scarf angle of (0/12 degrees). Figure 4.2.2 is a schematic view of a typical mixer showing the scarf angle. Based on pre-test CFD analysis it was determined that both the 24-lobe and the 20-lobe mixer with alternating scarf angle were both shown to have a reduced peak jet velocity relative to the 20-lobe mixer with zero scarf angle. Each mixer configuration is discussed in more detail below. The mixed exhaust nozzle geometric parameters are defined on Figure 4.2.1, and the full-scale geometric parameter values for all four mixers are supplied in Table 4.2. All of the mixers, with the exception of the 24-lobe mixer, were designed and fabricated under Pratt & Whitney internal funding.

Table 4.2 FULL-SCALE MIXED EXHAUST NOZZLE GEOMETRIC PARAMETERS
(Units in Inches)

Parameter	12-Lobe	20-Lobe	24-Lobe	ATM
Core flow area	615	615	615	615
Fan flow area	1105	1105	1105	1105
Nozzle exit area (A8)	1098	1098	1098	1098
Lobe length, L	18.6	18.6	18.6	18.6
Lobe height, h	11.7	11.7	11.7	11.7
Lobe radius, R	22.1	22.1	22.1	---
Sublobe valley radius (ATM), R1	---	---	---	18.5
Sublobe crest radius (ATM), R2	---	---	---	22.1
Max lobe width, Wmax	4.5	2.6	2.0	4.7
Min lobe width, Wmin	2.4	2.2	1.4	2.3
Valley angle, θ_v	22	22	22	22
Max depth of scallop, D	5.2	5.3	5.2	5.2
Flowpath height, H	25.4	25.4	25.4	25.4
Plug radius, Rp	9.6	9.6	9.6	9.6

4.2.1   12-LOBE (*BASELINE*) MIXER

The MD-80 aircraft, which is powered by Pratt & Whitney JT8D-200 series engines, was certified to stage 3 noise limits in 1979. The JT8D-200 has a by-pass ratio of approximately 1.7, and has an internal 12-lobe mixer to reduce the jet noise generated by this engine model. This mixer is representative of mid-1980 low-BPR mixer technology, and therefore was the baseline mixer for this entire test program. The mixer trailing edge has a zero scarf angle, and the lobes are scalloped. Pictures of the 12-lobe (Baseline) mixer can be found on Figure 4.2.1.1.

4.2.2   20-LOBE MIXER

This mixer was designed to be a parametric variation on lobe count relative to the 12-lobe mixer. The scarf angle, scallop, lobe peak and valley trough lines are identical to that of the 12-lobe mixer. Pictures of the 20-lobe mixer, with zero scarf angle can be found on Figure 4.2.2.1.

4.2.3   20-LOBE MIXER WITH ALTERNATING SCARF ANGLE (0/12 degrees)

This mixer is the same as was described in Section 4.2.2, with the addition of an alternating scarf angle of 0 and 12 degrees. CFD analysis showed that the peak exhaust velocity was reduced relative to the 20-lobe mixer with zero scarf angle, and therefore was expected to be quieter. Figure 4.2.3.1 is a photo of the side view showing the alternating scarf angle.

4.2.4 24-LOBE MIXER

This mixer was designed to be a parametric variation on lobe count relative to the 12-lobe mixer. The scarf angle, scallop, lobe peak and valley trough lines are identical to that of the 12-lobe mixer. Pre-test CFD analysis of this mixer indicated that the peak exhaust velocity was reduced relative to the 20-lobe mixer with zero scarf angle (Section 4.2.2). Figure 4.2.4.1 is a photo of the 24-lobe mixer.

4.2.5 ADVANCED TECHNOLOGY MIXER (ATM)

A CFD design study was carried out in the early part of 1994 to generate an additional candidate mixer for the model testing conducted at NASA's NATR. This study was a P&W funded effort, separate from the NASA contract. Results of calculations for the existing 12- and 20-lobe mixers showed that a "region of high temperature" or high velocity region persisted downstream of each lobe peak. The effect of scallops were shown to better mix out the flow in the mid span region, but the "region of high temperature" was essentially unaffected. The double lobe mixer concept was developed to attack this "region of high temperature" that persists downstream of the lobe peak. The initial design has 16 primary lobes, and the outer portion of each primary lobe bifurcates into two smaller secondary lobes separated by a small fan air chute (i.e., mini-chute), which lets cold air into the former "region of high temperature". Figure 4.2.5.1 is a photo of the ATM, without lobe scallops. The ATM similar to the 12-lobe mixer has a zero scarf angle.

4.2.6 ADVANCED TECHNOLOGY MIXER WITH LOBE SCALLOPS

Section 4.2.5 discusses the evolution of the Advanced Technology Mixer design, which also applies here, as well as the incorporation of lobe scallops.

4.3 MIXING ENHANCING DEVICE/CONCEPT

4.3.1 VORTEX GENERATORS (VGs)

The model primary tailplug was fitted with small low profile triangular shaped wedges in an attempt to further mix out the flow. Figure 4.3.1.1 shows a schematic view of these devices, and also shows their location on the tailplug. These devices were designated Vortex Generators (VGs) and were tested with the 20-lobe mixer. Analysis has shown that there was deficit in the radial velocity profile in the region just downstream of the mixer, which could be eliminated or reduced by the use of these Vortex Generators.

4.4 SIMULATED ENGINE PROBES

Prior to conducting model testing at NASA in 1996, P&W was concerned that the 8 full-scale engine probes were having a negative impact on the noise reduction of the mixer, and there was also a concern raised that the probes could generate a tone. As a result eight 1/7th scale-model probes were built and tested. Figure 4.4.1 shows a picture of the upstream simulated engine probes that were tested.

4.5   MUFFLER (For Full-Scale Engine Combustor Noise)

Pratt & Whitney had determined from full-scale engine noise testing in the mid 1980s that combustion noise was an important source in the JT8D-200 series engines spectral data. It was also determined that the full noise reduction benefit of the 12-lobe mixer could not be realized unless the combustion noise could be reduced. As a result a muffler (essentially a Helmholtz resonator tuned for 315 Hz-400 Hz) was designed and built by Pratt & Whitney. Similar to the engine probes of Section 4.4, there was a concern that the muffler, which is located immediately downstream of the mixer exit, could have a negative impact on the noise reduction features of the internal mixers. A photo of the muffler is shown on Figure 4.5.1.

5.0   TEST FACILITY AND TEST METHODS

In 1994, and 1996 both noise and aerodynamic measurements were obtained at NASA Lewis Research Center's Aeroacoustic Propulsion Laboratory (APL). A picture of the APL is shown on Figure 5.0.1. The APL consists of the Nozzle Acoustic Test Rig (NATR) and the 65-foot radius Anechoic Hemispherical Dome. Far-field acoustic data were measured using a 50-foot radius microphone array centered at the test nozzle exit plane. A detailed description of the test facility, test procedures, acoustic data acquisition and data reduction can be found in References 1, and 27.

5.1   NOZZLE ACOUSTIC TEST RIG (NATR)

The NATR consists of the 53-inch diameter free-jet duct section and the Jet Exit Rig (JER). The free-jet is driven by an annular air ejector system that entrains ambient air through a plenum and a transition bellmouth section and expels the air through a 53-inch inner diameter free-jet duct with a centerline height of 120-inches. The system can produce free-jet Mach numbers up to 0.3. A contraction nozzle, with a 7° contraction angle was installed at the exit plane of the 53" free-jet duct for all testing. The contraction nozzle was used to accelerate the airflow and thereby reduce the external boundary layer on the JER. The JER is the structure through which airflows are delivered to the core and fan nozzles via connections to the facility's compressed air supply systems. Figure 5.1.3 shows a schematic view of the Jet Exit Rig (JER). The core nozzle airflow is heated by a combustor using hydrogen as fuel. The fan nozzle airflow is heated by electric heaters (available for 1996 phase of testing only). Exhaust gases from the free-jet and jet rig are expelled through the 43-ft high by 55-ft wide exhaust door downstream of the jet rig. A 60-inch diameter exhaust fan in the top of the dome provides air circulation. Figure 5.0.2 shows a picture of the NATR and the acoustic anechoic test arena. Figure 5.1.1 shows a schematic view of the model assembly attached to the JER with key axial stations identified and also shows the JER charging instrumentation at station 113.5. Figure 5.1.2 shows the model external flowpath with contraction nozzle, and the NATR with model assembly attached.

5.2   ANECHOIC TEST AREA

The anechoic test arena is a 65-ft radius hemispherical dome. The walls of the dome and half the floor area are treated with acoustic wedges. The untreated half of the floor, occupied by the Power Lift Rig (PLR), has an acoustically treated wall installed near the NATR exit plane and extending aft along the untreated floor to shield unwanted sound reflections from the untreated floor area and other test equipment. The floor area in front of the test nozzle was treated with wedges prior to actual acoustic data acquisition. Microphones for the acoustic data acquisition are located along a 50-ft radius arc centered at the exit plane of the test nozzle. These microphones are mounted on 10-ft poles bolted to the treated floor. The angle locations for the microphones are from 50 to 160 degrees at intervals of every 5 degrees. Figure 5.0.2 shows a picture of the 50-ft radius microphone array, and the anechoic test area.

5.3   FACILITY INSTRUMENTATION

The NATR/JER instrumentation provides data on test variables such as free-jet Mach number, fan nozzle pressure ratio, core nozzle pressure ratio, fan flow temperature, core flow temperature, and airflow rates for the core and fan nozzles. The facility is not configured for nozzle thrust measurements. Four (4) total pressure/temperature rakes are installed at the charging station (i.e., 113.5) of the fan and core ducts of the JER, as shown on Figure 5.1.1. The four radial rakes are spaced 90 degrees apart, and each rake has five (5) total pressure and five (5) total temperature sensors. The instrumentation system can display all twenty individual values or an averaged value for the total pressure and temperature. Flow venturi located in the compressed air supply lines give the flow rates of the core and fan streams.

5.3.1   EXHAUST NOZZLE CHARGING STATION LOCATION (1994)

The pressures and temperatures in the full-scale engine are measured at the interface of the engine exit and the entrance to the exhaust system (i.e., entrance to the mixer). Therefore it is desired to set the pressures and temperatures for model-scale testing at the same respective location. Figure 5.3.1.1 shows this location as the "Desired" charging station. Since there were no pressure or temperature probes in the primary stream or temperature probes in the fan stream at the "Desired" location, the values had to be estimated based on measurements obtained at the upstream jet exit rig charging station (i.e., 113.5). This was accomplished by applying an approximated pressure and temperature drop to the primary stream pressure and temperature values obtained at the JER charging station (i.e., 113.5). The temperature and pressure drop between the JER charging station and the "Desired" charging station was estimated prior to the start of the test. The fan temperatures at the "Desired" charging station also had to be approximated by applying a slight increase in temperature (due to conduction from the primary stream) to the values obtained at the JER charging station. Similar to the primary stream, the temperature increase of the fan stream between station 113.5 and the "Desired" charging station was estimated prior to the start of the test.   Therefore, the pressures and temperatures set at station 113.5 for the primary stream were slightly higher than the values shown in Table 3.1. The fan temperature at the "Desired" charging station location was estimated to be slightly higher than the values shown in Table 3.1. Since there were P&W supplied pressure probes at the "Desired" charging station, the fan pressures did not have to be estimated, and therefore were set to the values shown in Table 3.1.

5.3.2   EXHAUST NOZZLE CHARGING STATION LOCATION (1996)

The pressures and temperatures in the full-scale engine are measured at the interface of the engine exit and the entrance to the exhaust system (i.e., entrance to the mixer). Therefore it is desired to set the pressures and temperatures for model-scale testing at the same respective location. In 1996, a model charging station (located at the mixer entrance) was designed and fabricated which eliminated the need to estimate temperature and pressure profiles going into the mixer, as was done in 1994. Therefore the pressures and temperature values at the entrance of the mixer were set to the values as shown in Table 3.2. The charging station locations are shown on Figure 5.3.2.1, and are labeled A-A and B-B for the primary, and bypass streams, respectively.

5.4   ACOUSTICS TEST MATRIX

The target pressure and temperature ratios for the model test (Table 3.2) were defined based on full-scale engine conditions of the low by-pass ratio (1.7) JT8D-200 turbofan engine. This engine incorporates a 12-lobe (baseline) mixer, and is certified on the MD-80 aircraft. The target test conditions for the model are defined relative to a charging station located at the mixer entrance, as shown on figure 5.3.2.1. This charging station location was selected since the pressures and temperatures of the full-scale engine are measured at the same respective axial location. Far-field noise measurements were obtained for engine conditions ranging from approach to takeoff power, for two conditions of simulated flight speed; static and 0.27 Mach number. The pressure and temperature ratios were set to the same values for both external flow conditions; static and simulated flight. The intent is to define the effects of forward flight on noise at constant exhaust mixed jet Mach number ($Vmix/C_0$).

.   5.5   TEST METHODS

NASA Lewis was responsible for the acquisition and the reduction of all of the acoustic data. Refer to Section 6.0 for a discussion on the data acquisition and reduction procedures used by NASA. Full-scale, 150-foot radius corrected Sound Pressure Level (SPL) data was supplied to Pratt & Whitney on 3.5-inch diskettes.

5.5.1   ACOUSTIC TESTING

To assess the noise reduction potential of the various mixer designs, it is required to establish a reference level of far-field jet noise for a mixed-flow exhaust system incorporating the 12-lobe (baseline) mixer. The jet noise is defined in terms of its Effective Perceived Noise Level (EPNL) as derived from data measured by an array of far-field microphones. Data is obtained over a range of engine power conditions, from approach to takeoff, and for two conditions of simulated flight speed; static and 0.27 Mach number. The range of engine powers at a simulated flight speed of 0.27 Mach number will allow for an EPNL comparison of all candidate mixer designs relative to the 12-lobe mixer at the three noise certification conditions. A complete noise test of a given exhaust system configuration consisted of acquiring far-field noise data for all power conditions, first for static external condition and then again at the 0.27 external Mach number condition. The nozzle pressure and temperature ratios were set to the same values for both external flow conditions. The intent was to define the effects of forward flight on noise at constant exhaust mixed jet Mach number ($Vmix/C_0$).

5.5.2   LDV TESTING

The LDV test requirements were to obtain a set of highly accurate, highly detailed flow field data for calibrating CFD design codes. The output of these CFD codes is used as input to CAA codes, which then estimate the noise produced from a nozzle operating at a specified condition. The key flow field features of interest are the shear layers at the interface between the primary and secondary flow streams, and the shear layers between the nozzle exhaust jet and the free-jet flow. Noise is created in these shear layers and it is necessary for the CFD codes to accurately predict the mean velocity gradients and the turbulence intensities within

these layers in order for the CAA codes to accurately predict the acoustics. Therefore, the data requirements for the LDV testing were: 1) to accurately resolve the shear layers in terms of mean velocity fields, 2) define how rapidly the core and bypass flows mix-out, and 3) provide quantitative turbulence intensity levels within the exhaust duct and the near-field jet.

Given the data requirements, the following were considered in the development of the LDV system:

- The nozzle exhaust flow was expected to be at a very high velocity. Preliminary CFD calculations indicated that in the case of the reference splitter configuration, where the mixing between the core and bypass flows is relatively limited, velocities approaching 1900 ft/sec (579 m/sec) could be expected. The LDV system optics and signal processing electronics would have to be chosen such that this high velocity could be measured.
- High flow accelerations would occur. The highest accelerations were expected just downstream of the nozzle exit, where the exhaust flow expands to ambient pressure. The LDV seed material would have to be small enough to follow the flow accelerations with negligible lag. The LDV system receiving optics would have to be able to "see" these small particles.
- The flow exiting the mixer could be thought of as circumferentially periodic but not axisymmetric. Therefore it would be necessary to map the flow within a pie-slice shaped sector extending circumferentially over at least one half of a lobe.
- The LDV laser and optical components would have to be located outside the jet flow created by the 53-inch (1.35-M) diameter NATR. Otherwise, the impingement of the flow might vibrate the laser and/or misalign the LDV system optics. Vibration could misalign the mirrors within the laser resulting in a decrease in laser beam power.
- Three separate flows - the nozzle core, the nozzle bypass, and the free-jet - are being mixed within the nozzle exhaust plume. In order for the LDV to accurately measure the time-averaged, mean velocity flow field within the plume, it would be necessary to seed each of these flows separately.
- To simulate actual turbofan engine operating conditions, the primary flow would be heated to a total temperature of 1440 degrees Rankine during the LDV testing. A solid seed material with a melting point above this operating temperature would be required.

The above considerations led to the development of an orthogonal, three component, forward-scatter LDV system. This system is described in the following sections.

Traverse System: For an LDV system to generate adequate signals off of these submicron particles, it is best to place the receiving optics so that they collect the light scattered by the particles in the "forward" direction (i.e., place the receiving optics on the side of the probe volume opposite that of the lens used to cross the laser beams). This forward scatter arrangement is preferred since the submicron seed particles scatter light much more effectively in the forward direction. A major difficulty in employing a forward scatter arrangement involves the requirement that the receiving optics remain focused on the probe volume as the probe volume is moved to different locations in the flow field. The most reliable means of doing this is to traverse both sets of optics in unison using a single traversing system. A photograph of the scan rig developed for the APL is shown in Figure

5.5.2.1. The scan rig is operated remotely from the LDV control room. A detailed description of the LDV system can be found in Reference 5. Both the seeder and scan rig were removed for acoustic testing.

Seeding: There were two requirements for the LDV seeding material. One, it had to have a melting point temperature above the 1440 degrees Rankine stagnation temperature of the core flow; and, two, it had to be in the size range of about 0.5 to 1.0 micron. This size range is preferred since these particles would be small enough to follow the flow, yet big enough to generate adequate Doppler signals. There are a number of metal oxide powders, which are sold as satisfying these criteria, including alumina and titanium dioxide. Unfortunately, even though product specifications may indicate that a powder is commercially available within a desired size range, interparticle forces cause the particles to agglomerate to the point that when they arrive from the manufacturer, most of the particles are too big to adequately follow a rapidly accelerating flow.

For the LDV test in the APL, it was decided to use a method of seeding with metal oxide particles. With this method, rather than using a dry powder, the metal oxide is suspended in a liquid. While in solution the agglomerated particles are broken apart using a sonicator and/or a laboratory blender. The evaporation of the liquid droplets leaves behind a dry aerosol of seed particles of the desired size. By continuously spraying the solution into the flow, a continuous supply of seed particles is maintained. In this test, alumina seed particles were introduced into three separate flows - the primary model flow, the secondary model flow, and the external free-jet. The alumina particles were relatively monodisperse with a mean diameter of 0.7 micron and a standard deviation of 0.2 micron. Two different seed solutions were created - a 5% by weight alumina in water solution for the internal water flows and a 1% by weight alumina in water solution for the free-jet.

Data Post Processing: Post-test data processing consisted primarily of two functions: 1) discarding outliers in the velocity histograms and 2) correcting for velocity bias. The new processors, which employ frequency domain techniques such as the 3107 FDP, provide better signal detection, noise rejection, and improved accuracy relative to the older counter processors.   In the nozzle test data, there were some histograms, which showed measurements, which were obviously not generated by particles passing through the probe volume.   As an added measure to ensure that all such bad data were eliminated, each histogram was replotted after the test, and the outliers were discarded as needed.

Velocity biasing was recognized as a potential problem since the flow in the nozzle exhaust plume results from the mixing of three separate flows - the nozzle core (primary), the nozzle bypass (secondary), and the free-jet. Velocity biasing occurs whenever there is a correlation between data rate and velocity. In this test, the three different flow streams were seeded in an effort to eliminate velocity biasing.   Nevertheless, the data were corrected using a velocity bias correction method developed by Meyers and Edwards.

5.5.3 NOZZLE DOWNSTREAM FLOW PLUME SURVEY TESTING (TOTAL TEMPERATURES & PRESSURES)

Diagnostic aerodynamic measurements of the total pressure and total temperature downstream of selected mixer nozzle configurations have been made in lieu of LDV measurements. Previous experience, gained during earlier elements of this program, has demonstrated that LDV is a time consuming and costly diagnostic technique. In addition, setup and calibration times have been unreasonably high. The surveys were conducted along the jet centerline and at several lateral horizontal positions for several axial distances downstream of the jet. The plume survey rake assembly itself contains four (4) rakes. The left outboard rake is spaced approximately 4.28-inches from the centerline of the rake assembly and this rake contains 41 total pressure sensors. The left inboard rake is 1.28-inches from the rake assembly centerline and this rake contains 41 total temperature sensors. The next two rakes (i.e., the right outboard and inboard rakes) contain static pressure sensors only. Typically, traversing the rake assembly in 0.25-inches lateral increments generated a plume survey. The pressure and temperature probes were laterally offset to avoid interference effects. This orientation provided a complete, unreplicated view of the exhaust flow field at locations X =1.0, 2.5, 5.0 and 10.0 inches downstream of the nozzle exit plane. A view of the traverse planes and traverse density (across the exhaust jet) is shown on Fig. 5.5.3.1.

6.0   ACOUSTIC DATA ACQUISITION AND REDUCTION PROCEDURES

NASA Lewis Research Center processed the raw acoustic data and applies corrections for:

- microphone pistophone calibrations,
- actuator frequency responses,
- free-field and grid cap frequency responses,
- analogy filter roll-off,
- free-jet shear layer refraction corrections,
- atmospheric attenuation at test day condition over test distance corrections,
- spherical spreading attenuation corrections, and
- scaling of the data to full-scale (scale factor of 7) and 150-ft radius.

(For test points simulating flight conditions, the free-jet background noise were subtracted from the measured acoustic data before corrections were applied). Figure 6.0.1 shows a flowchart of how the acoustic data is processed.

The acoustic and aerodynamic performance (mass flow rates, nozzle discharge coefficients) data along with test condition (total temperatures, total pressures and calculated jet velocities and ideal net thrust) information were supplied to Pratt & Whitney by the NASA Lewis Research Center. The acoustic data points were supplied on 3.5-inch diskettes, and the aerodynamic data points were generally supplied in excel spreadsheets. Each data point for all configurations were identified with a unique escort number.

6.1   150-Ft RADIUS (FULL-SCALE) SOUND PRESSURE LEVEL SPECTRAL DATA

The acoustic data supplied to Pratt & Whitney were corrected 1/3-octave band Sound Pressure Level (SPL) spectral data scaled up to a 7-scale factor and projected to a 150-ft radius distance at the acoustic standard day condition (i.e., 77 deg. F and 70 % relative humidity). Refer to Section 6.0 for a discussion of all the corrections that are applied to the raw acoustic data.

6.2   1500-Ft ALTITUDE/1476-Ft SIDELINE (FULL-SCALE) LEVEL FLYOVER SPECTRAL DATA AND CALCULATED EFFECTIVE PERCEIVED NOISE LEVELS (EPNdB)

The data of Section 6.1 was flown through Pratt & Whitney's flyover prediction deck to calculate the Effective Perceived Noise Levels. The data was flown for a level flight path at an altitude of 1500-foot, and a sideline distance of 1476-feet. This was to simulate the sideline during takeoff noise certification condition for the MD-80 aircraft. The calculated EPNL values are supplied in two formats, tabular and comparison plots. Tables A-1 through A-8, in the appendix supply the calculated EPNL values for all of the configurations tested. Figures 7.1.1.1 to 7.1.1.15 (also in the appendix) supply comparison plots of EPNL versus mixed jet Mach number for all of the configurations tested. Mixed jet Mach number used here is defined as the ratio of the fully expanded mixed velocity (fps) at the nozzle exit divided by the speed of sound calculated from the test day ambient temperature (i.e., V_m/C_0).

7.0   SUMMARY OF TEST RESULTS

7.1   ACOUSTIC SUMMARY FOR ALL TASK 37 CONFIGURATIONS

Tables A-1 through A-8 lists mass flow rates, charging station pressure ratios (i.e., test conditions), and calculated jet velocities supplied by NASA along with Pratt & Whitney's calculated Effective Perceived Noise Levels (EPNLs) for a level flyover at 1500-foot altitude and sideline distance of 1476-feet. The EPNLs were calculated from the corrected, full-scale, 150-foot radius, standard acoustic day 1/3 octave band sound pressure level (SPL) data supplied by NASA on 3.5-inch diskettes. Refer to Section 6.0 for a discussion of all the corrections and adjustments that are applied to the acoustic data.   All the EPNL values supplied in Tables A-1 thru A-8, and all of the comparison plots supplied in Section 7, are for a 1500-foot altitude, and 1476-foot sideline. Also all of the comparison plots of Sections 7.1.1, 7.1.2, 7.1.3, and 7.1.4 are all at a simulated flight speed of 0.27 Mach number, unless otherwise noted on the plot.

Tables A-1 and A-2 contain data from testing conducted in 1994 only, and as a result all test points were with cold (i.e., unheated) fan flow. Table A-1 is for a static (0.0 Mach number) condition, whereas Table A-2 is for a simulated flight condition of 0.27 Mach number. Tables A-3 through A-8 contain data from testing conducted only in 1996, for all configurations. Some of the configurations (like the ATM, for example) were tested with both heated and unheated fan flow, to determine the effect of fan temperature on the noise results.   Table A-3 is for static condition and contains all of the configurations tested, whereas Tables A-4 through A-8 are for a simulated flight condition of 0.27 Mach number. Due to the large amount of information at the simulated flight condition, all of the performance and noise data for each mixer or splitter is supplied in its entirety in its own table. For example Table A-4 contains only splitter data, and Table A-5 contains only 12-lobe mixer results.

7.1.1   EPNL VERSUS MIXED JET MACH NUMBER COMPARISON PLOTS

Figures 7.1.1.1 through 7.1.1.15 are all plots of acoustic data obtained in 1996 with heated fan, except Figure 7.1.1.10 which presents data obtained in 1994 with an unheated fan. Figures 7.1.1.1 through 7.1.1.15 (except 7.1.1.(2, 4, 6 or 8) are plots of mixed jet Mach number versus level flyover EPNL at 1500-foot altitude and 1476-foot sideline distance for various configuration comparisons. Mixed jet Mach number used here is defined as the ratio of the fully expanded mixed velocity (fps) at the nozzle exit divided by the speed of sound calculated based on the test day ambient temperature (i.e., V_m/C_0).   The mixed jet Mach number parameter was used since it reduces EPNL variations due to the daily fluctuations of the ambient temperature. Figures 7.1.1.2, 4, 6 and 8 are plots of mixed jet Mach number versus delta EPNL generated from level flyover EPNL values at 1500-foot altitude and 1476-foot sideline distance for multiple configurations. All of the plots are at a simulated flight speed of 0.27 Mach number, unless otherwise noted, and all have heated fan flow with the exception of Figure 7.1.1.10 since the effect of lobe scallops on the ATM was only tested in 1994. The mixed jet Mach number equivalent to a full power takeoff condition for the JT8D-200-powered MD-80 aircraft is approximately 1.21, and 1.10 at takeoff with cutback power.

Figure 7.1.1.1 and 7.1.1.2 show the benefit of the 12-lobe (baseline) mixer for this program relative to a splitter configuration. The 12-lobe mixer achieves as much as 6 EPNL reduction at high mixed jet Mach numbers, and decreases with a decrease in mixed jet Mach number.

Figure 7.1.1.3 is a comparison of all the mixers tested, and Figure 7.1.1.4 shows the delta EPNL benefit for all mixers relative to the baseline 12-lobe mixer. This figure seems to indicate that noise reduction of mixers increases with an increase in mixer lobe count, since the ATM has 16 major lobes with 16 mini-lobes the ATM could be thought of as having 32-lobes. From Figure 7.1.1.4 the ATM benefit relative to the 12-lobe baseline mixer is approximately 1.8 EPNL at a simulated flight speed of 0.27 Mach number. However from Figures 7.1.1.5 and 7.1.1.7 it is observed that for the static (0 Mn) condition all of the mixers are essentially equal to the 12-lobe baseline mixer. The majority of the 20-lobe, 24-lobe and ATM noise reductions relative to the 12-lobe mixer appear for a simulated flight speed of 0.27 Mach number, and minimal reduction (if any) is seen at the static condition.

Figure 7.1.1.9 and 7.1.1.10 show that the incorporation of scarf cut angles, and lobe scallops (i.e., lobe cutouts) have a small detrimental impact on the noise reduction characteristics of a specific mixer design. Figures 7.1.1.13 and 7.1.1.14, also show that both the vortex generators and muffler had very little impact on the EPNL results, for the 20-lobe and ATM, respectively. Figure 7.1.1.14 actually shows a slight increase due to the incorporation of the vortex generators with the 20-lobe mixer.

Figure 7.1.1.11 and 7.1.1.12 show that the simulated engine probes increased the EPNL values for both the 12-lobe and ATM. As will be shown later (from the spectral data) a tone was induced most likely due to vortex shedding off of the probes. Figure 7.1.1.15 shows the difference in noise between a mixer with hot fan flow and the same mixer with unheated fan flow. The ATM with unheated fan flow has higher noise levels than the ATM with heated fan flow.

7.1.2   PNL VERSUS ANGLE COMPARISON PLOTS

PNL versus angle comparison plots of configurations can be found on Figure 7.1.2.1 through 7.1.2.11, for both a typical MD-80 takeoff, and cutback power. The PNL curves will not be discussed unless there was a reasonable reduction in EPNL values. Figure 7.1.2.1a and 7.1.2.1b, show a large PNL reduction for the 12-lobe mixer relative to the splitter configuration, especially at the peak PNL angles, and aft toward 160 degrees.

Figures 7.1.2.2a and 7.1.2.2b, show that the ATM had the largest PNL noise reduction relative to the baseline 12-lobe mixer at almost all angles, including the angle of peak PNL. However, at far aft angles the ATM as well as the 20-lobe and 24-lobe mixers show minimal noise reductions relative to the baseline 12-lobe mixer.

Figure 7.1.2.3 shows a larger reduction in the PNL directivity in flight for the ATM relative to the 12-lobe mixer, than is seen at the static (0 Mn) condition. This benefit of flight is seen at almost all of the angles, with the exception of the far aft angles (i.e., 130 and aft) in which case the ATM does not appear to show a PNL reduction relative to the 12-lobe mixer. From Figure 7.1.2.4 it can be seen that both the 20 and 24-lobe mixers show only a slight PNL reduction relative to the 12-lobe mixer, for both flight and static conditions. This figure also shows that the noise reduction benefit of both the 20 and 24-lobe mixers relative to the 12-lobe mixer is slightly larger in flight than at the static (0 Mn) condition. Similar to the results of the EPNL comparison, the effect of flight primarily benefits the ATM relative to the 12-lobe mixer.

Figure 7.1.2.11 shows that the PNL directivity is increased by approximately 1 dB for the ATM with unheated fan flow versus the ATM with heated fan flow, for approximately all angles.

7.1.3   SPL VERSUS FREQUENCY COMPARISON PLOTS

Similar to the PNL directivity plots, a spectra comparison will be discussed here, only if the reduction was not insignificant.

Figures 7.1.3.1 through 7.1.3.22 show spectral comparisons for the configurations tested at both cutback power (condition 5), and takeoff power (condition 8), at 4 angle locations, of 60, 90, 115 (usually peak pnl), and 150 degrees. Figure 7.1.3.1 and 7.1.3.2 show a substantial low frequency reduction for the 12-lobe (baseline) mixer relative to a splitter configuration. The spectra at 150 degrees show the biggest reduction for the 12-lobe mixer. It is also observed that the 12-lobe mixer has higher spectral values between 1000 Hz, and 3000 Hz. This is no surprise since mixers do generate some internal mixing noise due to the mixing of the fan and core shear layers, it is also believed that some of the high frequency noise increase is not all due to internal mixing noise.

Reference 26 concludes that some of the high frequency noise generated with a mixer is not all internal, but that there is a contribution of unknown quantity due to some residual mixing at the exit plane of the nozzle. This conclusion was reached by looking at the effect of simulated flight Mach number on the measured model spectra. The effect of Mach number showed the high frequency noise decreased somewhat, and therefore had to partially be generated outside of the nozzle exit, since pure internal mixing noise would not decrease with an increase in flight Mach number.

Figures 7.1.3.3 and 7.1.3.4 are comparison plots of all the mixers relative to the 12-lobe (baseline) mixer for the simulated flight condition of 0.27 Mach number. From these figures it can be readily seen why both the EPNL and PNL values are reduced for higher lobe count mixers, since they show that as mixer lobe count increases, there is an improvement (i.e., reduction) at high (internal mixing noise) frequencies. This is most noticeable at the angle of peak PNL value, which is at 115 degrees.

Figures 7.1.3.5 through 7.1.3.8 show the effect of flight on all the mixers relative to the 12-lobe mixer. From the EPNL plots of Section 7.1.1 it was concluded that almost all of the noise reduction for the higher lobe count mixers relative to the 12-lobe mixer was primarily observed at flight (0.27 Mn) condition. This can be observed in the spectra of Figures 7.1.3.5 and 7.1.3.6, since the ATM appears to show a larger difference in high frequency noise between the static and simulated flight condition, than does the 12-lobe (baseline) mixer. As expected, from Figure 7.1.3.13 through 7.1.3.16 there appears to be a tone shed from the simulated engine probes at approximately a frequency of 800 Hz, and it is most noticeable at low power (i.e., cutback).

Figure 7.1.3.21 and 7.1.3.22 show the impact of heated fan flow versus un-heated fan flow for the ATM mixer. The un-heated fan flow spectra shows an increase relative to heated fan flow at high frequencies. It might very well be due to a larger velocity difference between the fan and core streams when the fan stream is un-heated, which thus causes an increase in the internal mixing noise generated by the mixing process.

7.1.4   NOY WEIGHTING VERSUS FREQUENCY COMPARISON PLOTS

Figures 7.1.4.1 and 7.1.4.2 show that the peak annoyance is reduced as the number of lobes is increased. In fact the peak annoyance for the 12-lobe mixer occurs at approximately 2000 Hz at the angle of Peak PNL (i.e., 115 degrees), and also at 150 degrees. The ATM reduces the Sound Pressure Level (SPL) at 2,000 Hz by such a large amount, the peak annoyance occurs at approximately 500 Hz for the ATM at 115, and 150 degrees, instead of at 2,000 Hz. This annoyance shift equates to a PNL benefit and therefore an EPNL benefit for the ATM relative to the 12-lobe (baseline) mixer.

7.2   LDV RESULTS SUMMARY

LDV testing was carried out on the splitter and mixer configurations to quantify velocity differences and patterns at the nozzle exit and in the plume. Internal velocities were measured at one location as well. All of the LDV data was taken at a high power point corresponding to a primary nozzle pressure ratio of about 2.0. Free stream Mach number was set to 0.1. A higher Mach number was desired to match the sideline acoustic condition (Mach 0.27), but was prevented by excessive vibration of the LDV system.

LDV data was obtained for the splitter, 12, 20, and ATM mixers. Table are available that show the corresponding axial locations and run numbers for these configurations. Axial locations are normalized to the nozzle diameter (5.376-inches). One location is located inside the tailpipe. This was made possible by cutting a hole through the tailpipe and inserting a quartz insert into it so that the lasers can pass through. The scans were done as far back as six nozzle diameters. A schematic of the LDV data plane relative to the nozzle is shown in Figures 7.2.1 and 7.2.2.

The scan plane at each axial location for the mixer configurations consist of approximately 50 points, arranged in a polar type grid. Scans consisted of either one or two lobes (circumferential extent) of data. This data includes axial (u) and vertical (v) velocity components, as well as the fluctuating velocities, u' and v'. Although a three component LDV system was used, only two were working at the time. Color velocity contours of selected configurations are shown in Fig. 7.2.3. The plot shows the LDV measured axial velocity contours for the 12, 20, and ATM lobe mixers at locations, X/D = 0, 2, and 4 downstream of nozzle exit plane. Comparisons of the LDV measured results with CFD predictions will be presented in Section 8.2.

7.3   TOTAL PRESSURE AND TOTAL TEMPERATURE TRAVERSE DATA

Results of the mean flow traverses are presented on Figs. 7.3.1 to 7.3.4. In all cases, color contour data is presented for the full exhaust at locations X =1.0, 2.5, 5.0, and 10.0 inches downstream of the nozzle exit plane. While total temperature traverses are shown for 12, 20, 24, and ATM lobe mixers, total pressure traverses were taken only for the 12-lobe mixer. The total temperature data shows the expected repeated kidney-shaped patterns typical of lobed mixer flowfields, with increased mixedness occurring with increased lobe count. The ATM mixer however produces a different flow pattern, known colloquially as the "ring of fire" and does not appear to be better mixed than the higher lobe count standard mixers.

Figures 7.3.5 to 7.3.6 shows total temperature traverse comparisons between the measured data and CFD (NASTAR, Section 8.2) predictions at locations X = 1.0, 2.5, 5.0, and 10.0 inches downstream of the nozzle exit plane for the 12-lobe mixer configuration. While the CFD calculations have been performed on a substantially denser grid than the experiment, these results have been interpolated onto the experimental grid and then plotted. The agreement in level and pattern is quite good. Figure 7.3.7 shows an equivalent total temperature comparisons at locations X = 5.0, and 10.0 inches downstream of the nozzle exit plane for the ATM configuration. In this case the pattern agreement is good, but the predicted results are hotter than the measured data.

8.0   ANALYSIS OF SELECTED CONFIGURATIONS

The aim of the following research study is to determine if advanced CFD & CAA computational techniques can be used to provide a more direct analysis of the jet noise characteristics of advanced exhaust nozzle systems. The viscous flow analysis used in this study is the NASTAR code, described in Section 8.1. Jet noise characteristics are assessed from a variety of predicted flowfield-based parameters. Analytically-based acoustic signature assessments are performed using NASA Lewis Research Center's (LeRC) modified version of the FAA MGB analysis[9]. This study will calibrate these analyses for axisymmetric multistream nozzles as well as assess the applicability of the analyses to 3-dimensional forced mixer nozzles.

8.1   ANALYSIS METHODS

NASTAR Navier-Stokes Analysis: The viscous flow analysis used was the NASTAR code, which solves the Reynolds-averaged form of the governing equations for steady, three-dimensional flows including the effects of turbulence and heat release due to chemical reaction. The code is based on the method due to Rhie[6]. Essentially, NASTAR represents a significant extension of the pressure-correction methodology used in the TEACH family of codes[7]. The governing equations are approximated using a finite-volume method. The discretized continuity and momentum equations are used to derive a pressure-correction equation that is used in place of the continuity equation. Rhie's method provides a single-cell, general curvilinear coordinate procedure that is applicable for Mach numbers ranging from incompressible flow to hypersonic flow. The results described in the current study were obtained using the two equation (**k-ε**) model for turbulence due to Jones and Launder[8].

The algorithm used in NASTAR provides for a controlled amount of numerical damping based on the local cell Reynolds number to promote numerical stability. Various measures were used to determine whether the computation was converged sufficiently. As with most CFD codes, NASTAR provides the user with periodic reports of the level of residual errors that represent the extent to which the discrete form of the governing equations are in balance. In addition to the residual history, selected integral measures were also monitored as the iteration proceeded. For example, the bypass ratio, BPR (the ratio of bypass to core mass flow rates at the mixer exit) was computed and was seen to approach an asymptotic value indicating that the iteration had essentially converged. NASTAR evaluates residual errors as well as selected integral measures. These measures can be used to assess convergence characteristics, aerodynamic performance and jet noise penalties, e.g. contours of stagnation temperature (T_O) at the mixing duct/nozzle exit plane, profiles of axial velocity (U), downstream of the mixer and at the nozzle exit plane, and mixedness $\eta(x)$ defined as

$$(1) \qquad \eta = 100.\left[1.0 - \frac{\int \rho u |T_{ox} - T_{om}| \, dA}{\int \rho u |T_{oi} - T_{om}| \, dA}\right]$$

where the subscripts **x** refers to the local axial plane, **i** to the initial axial plane in the mixing duct, and **m** to the fully mixed out plane. Experience shows that each nozzle case required approximately 5000 iterations to achieve "convergence."

The primary measure for jet noise reduction, however, has been that lower jet noise corresponded to reduced peak velocity and temperature profiles at the exit plane of the exhaust nozzle. In the next section we will consider a computationally based aeroacoustic (CBA) analysis aimed at directly predicting noise spectra (SPL) and acoustic signatures (OASPL, PNL).

MGB Acoustics Analysis: The direct computation of an engine exhaust sound field by solving the unsteady-flow form of the Navier-Stokes equations (computational aeroacoustics: CAA) is currently not feasible. An alternative approach based on a unified aerodynamics/ acoustics prediction analysis has been developed by Mani et al.[9] and is called the MGB analysis. Mani followed Lighthill's original assumption that the turbulent fluctuations produced in the mixing regions of the jet are the primary source of noise generation. The MGB solution technique is described in two sections: (1) source/spectrum modeling and (2) sound/ flow interaction.

In the first part, the aerodynamic predictions from a flowfield analysis are used to model the source strength and its spectrum. In the original version, this analysis was based on the semi-empirical Reichardt model. Khavaran[10, 11] has recently developed an improved model that incorporates a steady-state Navier-Stokes analysis to determine the mean flow aerodynamics together with **k** (turbulent kinetic energy) and **ε** (turbulent dissipation rate) turbulence parameters to define the eddy scales. The acoustics solution applies Lighthill's acoustic anal-ogy. The source terms in the acoustics equation are determined by applying Ribner's model (for which the correlation function is a linear combination of second-order tensors) assuming isotropic turbulence. While the original analysis applied Davies empirical model (based on the mean shear, $\partial U/\partial r$) for the turbulent eddy scales, the current analysis assumes a scaling based on **k/ε**, a *turbulent* time scale. The source and spectrum tensor (**I**) is proportional to $\mathbf{k}^{7/2}$ and includes Doppler shift and convective Mach number effects. The Doppler effect provides a relationship between the source frequency (**Ω**) and the observed frequency (**f**).

Lighthill's acoustic analogy approach does not incorporate the effect of the surrounding mean flow on the sound radiated by convected multipole sources. Pressure fluctuations propagate through regions of nonuniform velocity and temperature before reaching the observer point. Thus, the location of the source within the jet determines the amount of radiated sound. The mean flow affects the refraction of the radiated sound and provides an additional convective amplification factor.

In the second part of the MGB analysis, Mani & Balsa's formulation for the sound / flow interaction for axisymmetric geometries is adopted; i.e., the turbulent properties of the jet are coupled with its acoustic radiation. The mean square pressure in the far-field is an integrated effect of (1) a factor related to the source intensity and frequency and (2) a series of directivity factors, which are functions of the flow and convective Mach numbers.

Consistent with acoustical modeling practice, these Mach numbers are defined with reference to the *freestream* speed of sound. The acoustical signature, or sound pressure level (SPL), for an axisymmetric jet, is expressed in terms of the mean square pressure field,

(2)
$$SPL = 10 \log_{10} \left| \frac{\bar{p}^2}{p_{ref}^2} \right| = 10 \log_{10} \left[\int \Lambda f(a_{ij}) \, dV \right]$$

where Λ is a factor related to the source intensity and frequency, and the a_{ij}'s are directivity factors expressed in terms of the polar observation angle (θ), the local sound speed, and flight and convective Mach numbers through a shielding function. The mean square of the pressure field at a point in space, due to all sources, can be approximately given as

(3)
$$\bar{p}^2 \approx \left(\frac{1}{4\pi R} \right)^2 \left| (\omega \tau_0)^4 e^{-(\Omega \tau_0)^2/8} \right| \left[\rho_\infty^2 k^{7/2} \Delta V \right] \bullet \left| \frac{(1-M \sin\theta)^4 a_\infty^6}{(1-M_c \sin\theta)^2 a^6} \right| \left[\frac{1}{(1+M_\infty \sin\theta)} \right] \beta$$

where the source intensity spectrum and flow shielding factors are defined as follows,

(4)
$$I(\Omega) \approx \rho_\infty k^{7/2} (\Omega \tau_0)^4 \Delta V$$

(5)
$$\beta = \exp \left| -2(\frac{\Omega}{a_\infty}) \int \left| g^2(r,\theta,M_c,M) \right|^{1/2} dr \right|$$

and other key parameters are defined as follows:

$$M = \frac{U}{a_\infty}, \quad M_j = \frac{U_j}{a_\infty},$$

$$M_c = 0.5(M - M_\infty) + \beta_c (M_j - M_\infty)$$

$$\tau_0 = \left(\frac{k}{\varepsilon} \right) \left(\frac{1}{\alpha} \right) = characteristic\ time\ delay$$

$$\Omega = 2\pi \omega \left[(1 - M_c \sin\theta)^2 + \alpha_T \frac{k^{1/2}}{a_\infty} \right]$$

The parameters, α, α_T and β_c, are user-specified constants that are empirically determined. The angle, θ, is measured from the jet centerline starting from the inlet or upstream direction. More frequently, however, SPL is converted into a weighted average, such as OASPL (overall sound pressure level). OASPL integrates SPL at a given measurement location/orientation over all frequencies.

8.2   AERODYNAMIC STUDIES[12]

8.2.1   COMPUTATIONAL MODEL

The computational volume for the CFD calculations is illustrated schematically in Fig. 8.2.1. The inflow boundary is at a station upstream of the mixer. The outflow boundary is on the order of 10 to 17 diameters downstream of the nozzle exit. It is assumed that the mixer flowfield is perfectly periodic, so that the circumferential extent of the computational volume is one–half of a lobe. The inflow boundary conditions required for the CFD calculations are total pressure, total temperature, meridional flow angle (assumed zero here), turbulence kinetic energy (**k**), and turbulence dissipation (**ε**) as functions of radius for each of the three streams. In the jet exit rig, total pressures and total temperatures are measured just downstream of the flow-conditioning module, where the profiles should be flat. Due to the significant length of duct between the jet exit rig instrumentation station and the downstream CFD inflow station, the above profiles are needed at the downstream station reflecting losses in the bypass and primary ducts.

To meet the above requirement, a total pressure rake was installed in the bypass duct just aft of station 161.35. Time and budget constraints prevented a more extensive instrumentation array at this location. To get the detailed profiles at this station, a pre–test CFD calculation was done for each duct, from the jet exit rig instrumentation downstream to the CFD inflow station. The analysis included both viscous and thermal effects. By knowing what the approximate total pressure and temperature losses are in the ducts, test conditions could be set using the jet exit rig instrumentation to match full-scale engine exhaust system operating conditions. Fig. 8.2.2 shows the predicted profiles for a high power point along with the flat input profile at the JER instrumentation station.

The calculations were performed in two stages. Initially, a calculation (CFD1) was completed from the upstream charging station to a station where the lobed mixer would begin in a three-dimensional flow case. The results of these calculation provided inlet profiles for all subsequent aerodynamic calculations. These latter calculations (CFD2) were performed from the mixer inlet station, through the nozzle exit plane, to a plane approximately 17 nozzle diameters downstream of the nozzle exit. The forced mixer calculations were performed on a computational domain that extended 12D downstream, with some axisymmetric calculations extending the domain to 20D. Based on an observation concerning the impact of turbulence level on the OASPL acoustical signature, parametric studies varying the inlet turbulence profile were conducted. Two types of calculations were performed. In the first type, levels of freestream turbulence and an improved wall boundary condition were imposed to achieve a "best" match with the measured downstream level of turbulence energy. This type of "best" calculation used a single-block Cartesian grid of 400 by 133 (53,200) points (Fig. 8.2.3). A second approach was also pursued, whereby the measured U′ data was used to define a turbulent kinetic energy profile at the X/D = -0.8 station. A single-block Cartesian grid of 254 by 167 (42,418) points was used for these "experimentally" started calculations.

The generation of lobed mixer grids involved a multi-step process: determination of the surface geometry, generation of 2-D slices at constant axial planes, generation 2-D grids using an expert system, knowledge-based analysis[13, 14] and stacking the 2-D grids to form a final 3-D grid. Single blocked-structured grids were generated with internal surfaces defined using cell types for the cells internal to solid sections that indicate no flow is present. This feature is a generalization of the IBLANK concept used in codes accepting grid files in PLOT3D format. Each case considered a half-lobe geometry, assuming symmetry planes in the azimuthal direction. A typical grid used about 185,000 points (71 axial, 75 radial, 35 azimuthal). Specific cells on the lobe surface were identified as flow-through cells, creating a stair-step description of the scallop. Figure 8.2.3 illustrates a typical axial (crest-cut) and cross-sectional grid and the cells for modeling the effects of scalloping (cutouts) and scarfing (cutback) case. The axial extent of the computational domain was approximately 10 nozzle diameters downstream of the exit plane. The radial extent of the domain was 5 nozzle diameters.

The 2D grids were simply stacked to form the required 3D grid. Finally, the 3D grid was passed through the fifth process, which checks metrics associated with the 3D grid, such as skewness, aspect ratio, twist, and area distributions. Any problems found with the 3D grid were remedied by identifying the cause, updating the knowledge base for axial positions in the affected range, and regenerating the 2D grids locally. The new 2D grids were then re–stacked and the condition tests were re–run. The shaded scallop region constitutes an area in which grid nodes are not flagged as a solid boundary.

While the solver used is capable of utilizing both single–block and block–structured grids, all of the results obtained to date have used single–block topologies. Solid regions were excluded from the domain by using a generalization of the IBLANK concept commonly found in solvers operating with grids in PLOT3D format. For the three–dimensional cases described herein for which comparisons were made with data acquired downstream of the nozzle exit, the computational domain extended approximately ten nozzle diameters downstream of the nozzle exit. In the circumferential (lobe–to–lobe) direction, the domain extended from the plane of symmetry through the peak of a lobe to the plane of symmetry through the valley. The computational grid consisted of 1.05 million grid nodes. Approximately 425,000 nodes were used to describe the flow within the nozzle and about 460,000 nodes were used to represent the flow downstream of the nozzle exit; the remaining nodes were placed external to and upstream of the nozzle exit. The case was run using 20 Sun Sparc20 CPU's and required about 300 hours of run time.

8.2.2   AXISYMMETRIC SPLITTER STUDIES

A reference splitter configuration was added to the test program because the currently available CAA codes can only handle axisymmetric geometries. CFD results for the mixer configurations have to be manipulated into a axisymmetric field prior to being used as input into a CAA code.

Grids for the axisymmetric splitter cases were generated using the P&W Nozzle Design and Analysis System[15]. This software rapidly creates single–blocked Cartesian grids for multi–stream duct/nozzle configurations, initializes the flowfield, and runs the NASTAR code. Figure 8.2.4 shows a typical grid. There are 400 axial, 133 radial, and 3 circumferential grid points for a total of 159,600 nodes. The domain extends 17 nozzle diameters in the downstream direction and 16 nozzle diameters radially. The cases were run on seven Sun Sparc20 CPU's using P&W's PROWESS program for parallel CFD calculations on distributed workstations[16]. Convergence was obtained at about 6000 iterations, which required about 7 hours of elapsed time.

All LDV data was taken at a high power point corresponding to a primary nozzle pressure ratio of about 2.0. Free stream Mach number was 0.10. A higher Mach number was desired to match the sideline acoustic condition ($M_\infty = 0.27$), but was prevented by excessive vibration of the LDV system. Table 8.2.2.1 shows a summary of the test conditions for each configuration, taken at the CFD inflow station.

Table 8.2.2.1: LDV Test Conditions

Configuration	Primary			Bypass		
	Pt*	Tt*	W	Pt*	Tt*	W
	(psia)	(deg R)	(lbm/s)	(psia)	(deg R)	(lbm/s)
Splitter	27.82	1442	3.63	26.24	528	7.56
12-lobe mixer	28.03	1454	3.55	26.24	536	7.28
20-lobe mixer	27.99	1444	3.55	26.24	544	7.13
	*based on pre-test CFD analysis					

Several approaches were used to initialize the CFD calculation. The first simply used the **k** and ε profiles predicted by the upstream duct calculation previously described. Comparisons between computed and measured axial velocity (U) and the fluctuation velocity components (u',v') at one internal tailpipe location and three locations across the plume are shown in Fig. 8.2.5. Good agreement is noted for the mean axial velocity component with slight undermixing relative to the measured data. Comparisons to the measured turbulence data indicate a significant underprediction. It should be noted that the **k-ε** model assumes isotropic turbulence and that the turbulent velocity components are calculated from the **k** (turbulent kinetic energy) distribution. In addition, a comparison between data obtained within a low velocity plume of a round conical nozzle using a hot wire probe and this LDV system showed the LDV to generally measure higher turbulent velocities.

Figure 8.2.6 shows how the shear layers from the splitter and nozzle lip form and explains the shape of the fluctuating velocity profiles shown in Fig. 8.2.5. Note that the geometry and flowfield have been stretched in the vertical direction for this depiction. Since the goal of this study is to provide input to a CAA code for jet noise prediction, the effect of an error in predicted turbulence intensity on sound pressure level (SPL) will be investigated in the next subsection.

By increasing the primary stream inflow **k** profile by a factor of four and the bypass stream inflow **k** profile by a factor of two, a better comparison to the data was obtained for the fluctuating velocities at X/D= –0.8 and X/D=0.05.   There was however only slight improvement at the two downstream LDV locations. Furthermore, the peak turbulence levels predicted within the shear layers did not increase to any great extent. These curves are labeled **best turb. profile** on Fig. 8.2.5. Comparisons of the U predictions show a slightly higher level of downstream mixing.

An alternative strategy was also pursued, whereby the measured u' data was used to define a turbulent kinetic energy profile at the X/D= –0.8 station. A new CFD grid was generated that began at this location, and initialized using the total temperature and pressure profiles predicted by the previous case at this location. The v' and w' components were defined as 0.7 of u', based on the data taken at X/D=.05, which show that v'/u' varies from 0.6 to 0.8. This is consistent with data from other published work that shows v'/u' in shear layers typically varies[17] from 0.5 to 0.8. A value of **k** was then calculated based on the measured u' component, and the calculated v' and w' components. The resultant calculations, plotted as **exp. turb. profile** in Fig. 8.2.5, show substantially higher levels of downstream turbulence. The effect on the predicted mean velocity profile is evident, with a higher level of mixing along the plume centerline.

The CFD results presented for both mixer and splitter cases were obtained using a turbulent Prandtl number, Pr_t, of 0.9, which is the standard default value for the NASTAR code. Previous studies suggest that the turbulent Prandtl number, which relates the diffusion of momentum to the diffusion of heat, is about 0.7 for heated axisymmetric jets[18]. The effect of this parameter was investigated by repeating the splitter analysis with the lower value of Pr_t. The results showed a slightly higher spreading of the temperature profile within the plume and a negligible effect on the mean and fluctuating velocity field.

8.2.3   FORCED MIXER STUDIES

A pacing item in performing CFD analyses is obtaining a computational grid that exhibits little skewness, has suitable grid clustering to resolve boundary layers and other flow features of interest, and is rapidly generated. The generation of the 3D computational grid for the JT8D lobe mixer cases considered here involved a five step process. The first step was the determination of the surface geometry from the surface description point files using an internally developed code that provides the geometry as two–dimensional slices at selected axial locations. In the second step, the two–dimensional curves for the surface definition were fitted with splines so as to provide an analytical description of the surface slices. The third process involved the determination of the 2D grid for each axial position. This process was accomplished using the expert system, knowledge–based code developed by J.F. Dannenhoffer (Refs. 13, 14). The power of this block–structured grid generation technique is that only boundary definitions are needed; grid smoothing and stretching are functionally controlled by the user instead of only manually controlled by the user; and a knowledge base is maintained that can be used for additional or alternative axial cuts. Due to the power of this tool, it is possibly to generate quickly all 2D axial grids, since the knowledge base

incorporates a stack language that allows the user to "program" the required inputs, (e.g. viscous layer stretching parameters) as a function of axial position. Grid clustering was applied along the centerbody, mixer, and duct walls to capture boundary–layer effects. In the experimental program, mean and fluctuating velocity components were measured at several axial locations downstream of the nozzle exit with the 12–lobe and 20–lobe mixers installed. In this section, comparisons are made between the measured mean and fluctuating values of axial velocity with CFD results at selected stations. The initialized turbulence profile used was the **best turb. profile** (increased **k** values) described in the splitter section. The data were acquired at each cross section at several radial and azimuthal locations. In terms of CFD grid resolution, the measurement "grid" was relatively coarse. Therefore, the CFD results show greater detail than that shown by the measurements and care must be exercised in interpreting the relative differences in computed and measured values. For purposes of display, the CFD results have been limited in radial extent to that used at each measuring station, and have been reflected about the plane of symmetry through the peak. The circumferential extent of the LDV data is 1 lobe for the 12–lobe mixer and two lobes for the 20–lobe mixer.

Consideration is given first to comparisons for the 12–lobe mixer. The first set of plots in Fig. 8.2.7 presents the measured and computed axial velocity contours at X/D=0.05 downstream of the nozzle exit. As will be observed in subsequent results as well, some asymmetry is seen in the data. It is thought that at the nozzle exit station, this is due to an asymmetry in the model itself. It appears that the asymmetry in the measurements at the downstream locations is the result of a progressive shifting of the model relative to the scan rig during the data acquisition process (see Ref. 5). Generally, the CFD results exhibit less mixing than is measured, as can be seen by comparing the maximum contour levels. Comparisons for the 12–lobe case at X/D = 2 show that both the data and the CFD prediction indicate that the flow field is essentially axisymmetric, an interesting result, with less mixing being exhibited by the CFD prediction. Similarly, at X/D = 4, less mixing is observed in the CFD results.

Measured and CFD results were also obtained for the 20–lobe mixer and these are shown in Fig. 8.2.8 for X/D =0.05, 1 and 2, downstream of the nozzle exit. As in the 12–lobe mixer results, the 20–lobe CFD results show approximately the same level and distribution as seen in the data. The level of mixing exhibited in the CFD results is somewhat less. Again, the flow is essentially axisymmetric within two nozzle diameter downstream of the exit plane.

Figure 8.2.9 shows the mixer turbulence data compared to the CFD results for both the 12 and 20–lobe configurations. The view is along a radial line through the lobe peak. Overall agreement between the data an analysis is good and appears to be better than the level of agreement for the splitter cases. However, additional calculations for the 12–lobe case show that the level of agreement is also sensitive to the assumed values for inlet turbulence parameters (**k** and **ε**). No systematic variation of inlet turbulence parameters was conducted due to the lack of sufficient data internal to the nozzle with which to adjust the inlet profiles for the mixer cases. Furthermore, due to the larger contact area of the shear layers for the 20–lobe configuration, it is possible that the 20–lobe results are less sensitive to changes in inlet turbulence parameters. In any case, the results indicate the necessity of obtaining reasonable

estimates of the inlet turbulence quantities. Also the significant differences between the measured u' and v' values suggest that a nonisotropic turbulence model may be required.

Table 8.2.3.1 Calculated Mixedness Parameter

Nozzle Type	η (%)
Splitter	11.9
12-Lobe mixer	70.5
20-lobe mixer	74.9

These results confirmed that lobed-mixer nozzles have lower exit plane axial velocities than are found in splitter nozzles. The table above illustrates this in terms of an improved mixedness of the exit flow using a lobed mixer nozzle. The table also illustrates the effect of increased mixedness with increased lobe number. One should note that all calculations cited in the table below were performed for the same operating point. In addition, the mixer calculations were made for mixers without scalloping.

8.3   ACOUSTIC ANALYSES[19]

Based on the above aerodynamic calculations and comparisons with data, parametric studies have been performed to investigate whether certain CFD modeling factors will have a major impact on any noise analysis calibrations

8.3.1   AXISYMMETRIC SPLITTER STUDIES

Turbulence Initialization Issues: NASTAR comparisons of the fluctuating velocity components (u′, v′) with LDV measured data, cited in Ref. 12, have identified the effect of using different starting profiles for the turbulence variables.   These comparisons were performed at the forward flight condition of $M_\infty = 0.1$, where aerodynamic not acoustic data was measured.   Comparisons of NASTAR-MGB predictions of OASPL for model-scale conditions operating at the LDV test point indicate an approximately 2-3 dB difference between the different initialization approaches, see Fig. 8.3.1. Approximately 0.5 dB can be accounted for by comparing the peak values of **k** in the near-field shear layer, using:

$$\text{SPL error} = 10\log_{10}(k_{\text{exp profile}}/k_{\text{base profile}})^{7/2} \qquad (6)$$

The larger turbulence levels observed in the experiment do, as expected, produce the higher acoustic signature.

Compressibility Issues: Since the model for generation of jet noise depends strongly on the computed turbulence intensity and dissipation rate, it is expected that the predicted acoustical signature is dependent on the turbulence model used by the Navier-Stokes solver.   Of particular concern is whether compressibility effects have a strong influence on the MGB predicted acoustical signature.   It is important to note that when the convective (aerodynamic) Mach number approaches unity, the jet spreading rate decreases appreciably.

The so-called "Langley" curve[20], representing several planar shear layer data sources, illustrates this effect. Recently, turbulence model sensitivity studies were performed using the new MGB code and UTRC's UTNS[21] Navier-Stokes code. The test case was Yamamoto's underexpanded convergent nozzle[22] (case 114). The Reynolds number of the jet, based on exit flow conditions and the nozzle diameter, is about 1.4×10^6, therefore the flow can be considered fully turbulent. The effect of different turbulence models was evaluated[23] for the standard **k-ε** model, the compressibility-corrected Sarkar **k-ε** model[20], and the RNG **k-ε** model[23]. Approximately 2 dB shift due to compressibility effects was noted.

Defining an approximate convective Mach number for axisymmetric jet flows as follows,

$$M_c = \frac{(U_{cl} - U_\infty)}{(a_{cl} + a_\infty)} \tag{7}$$

then, the maximum value of $\mathbf{M}_c$ for the Yamamoto case is about 0.78. At this level, the spreading rate is reduced from its incompressible value by about 30 %. In the current splitter case, $\mathbf{M}_c$ is approximately 0.55 in the potential core and decreases downstream in the plume. Correspondingly, the centerline Mach number is barely sonic in the potential core and also decreases downstream in the plume. At this level $\mathbf{M}_c$ the effect of compressibility reduces the jet spreading rate by less than 5%, and the standard **k, ε** model should be adequate for all splitter and lobed mixer cases as far as the compressibility effects are concerned.

While compressibility effects should be expected to have little impact on the acoustic signature, Fig. 8.3.2 compares the MGB predictions using assorted turbulence models in the NASTAR flow solver. The flowfield results indicate little difference in the near-field of the jet, however the predictions confirms results previously observed by Choi et al[23], where **k-ε** predictions mix out more rapidly, while using the Sarkar compressibility correction reduces the effective spreading rate. One should also note that the mixing rate of hot jets can be significantly impacted by thermal diffusion effects ($Pr_t \neq 1$). All predictions cited in the text do not account for this effect.

MGB Calibration: Baseline acoustical predictions obtained using NASTAR and MGB for the case corresponding to sideline during takeoff noise operation, are shown in Figs. 8.3.3 and 8.3.4. Figures 8.3.3 and 8.3.4 show a comparison of the predicted OASPL and an aftlooking-spectra for a model scale geometry at 50-ft arc distance. The OASPL levels, especially for the rearward looking orientation (primary noise source), show good agreement with data. The effect of inlet turbulence profile does not appear to have a significant effect on the exhaust signature. The predicted spectra also show good agreement with measured peak levels, however a predicted dip in the 4k-12k Hz range is not seen in the experimental data. This result was also observed in predictions using the NPARC Navier-Stokes analysis, (obtained from NASA Lewis Research Center).

Model-to-Engine Scaling: A majority of jet noise data, as in this program, has been acquired at small scale. Full-scale, or engine-size, data are typically extrapolated from the small-scale data bases. When jet noise mechanisms are dominant, semi-empirical equations are used. By assuming equal jet velocity, temperature and environmental conditions, corrections can be made for jet size, observer distance, and acoustic frequency[20,21], i.e.,

$$
(8) \qquad SPL_{fs} - SPL_{ss} = 10\log_{10}\left[\frac{D_{fs}}{D_{ss}}\right]^2 - 10\log_{10}\left[\frac{R_{fs}}{R_{ss}}\right]^2 + 10\log_{10}\left[\frac{\Delta f_{fs}}{\Delta f_{ss}}\right]
$$

where, D is the diameter of the exhaust nozzle, R is the distance from the jet exhaust to the observer, and f is the acoustic frequency. The subscripts *fs* and *ss* refer to full-scale (engine) and small-scale (model) conditions, respectively. The first term in the above equation is based on the assumption that acoustic power increases directly with the source area. The second term relates acoustic power decay to an inverse-square law. The third term, a correction for filter bandwidth assuming the data were acquired in third-octave bands, is not always used. Manifest in this equation is the assumption that the same physical phenomena that are dominant at large scale are also dominant at small scale. For example, the scaling of jet frequencies is based on the observation that the dominant large-scale turbulence-induced noise occurs at constant Strouhal number ($St=fD/U_j$), even for a large range of Reynolds numbers. Thus, the frequency shift with scale for equal velocity jets can be expressed as follows

$$
(9) \qquad f_{fs} = f_{ss}\frac{\left[\dfrac{StU_j}{D}\right]_{fs}}{\left[\dfrac{StU_j}{D}\right]_{ss}} = f_{ss}\left[\frac{D_{ss}}{D_{fs}}\right]
$$

Therefore, by keeping the acoustic wavelength to jet diameter ratio constant, jet noise directivity patterns are assumed to be maintained.

Scaling studies have been performed using NASTAR and MGB for a configuration at a power corresponding to the sideline during takeoff noise operation point. Three calculations were performed to compare with the measured data, (1) a model scale CFD and MGB calculation, (2) a model scale CFD and a engine scaled MGB, and (3) an full size (engine) CFD calculation with its corresponding MGB calculation. The model-scale calculations were evaluated at 50-foot arc distance. This calculation was also scaled to full-scale engine conditions at a 150-ft arc distance. The last calculation was a CFD analysis of a full-scale engine nozzle evaluated at 150-foot distance. In the second analysis, the flowfield was assumed to be unchanged (no Reynolds number effect) so that the geometry could be directly scaled by a factor of 7.0, the ratio of full-scale to model-scale size. The model test data was also rescaled to engine size at 150-foot distance using a NASA LeRC procedure. Figures 8.3.5 and 8.3.6 illustrate the comparison. The CFD results indicate little Re effect in the rescaling calculations (about 1 dB). One can also note from the spectra results of Fig. 8.3.6

the expected spectra shift to lower frequencies (band numbers) with increased configuration size.

Forward Flight Effects: Extensive data in the open literature have demonstrated that a reduced flight velocity results in an increased acoustical signature. Acoustic data taken at the $M_\infty=0.27$ and at a static or no forward flight condition confirm this observation. Flowfield calculations for these conditions were attempted however, numerical instabilities at the static condition were encountered. Instead, flow calculations were obtained for the forward flight conditions of $M_\infty = 0.1$, where aerodynamic (LDV) data was obtained. MGB calculations are shown in Fig. 8.3.7. The OASPL predictions confirm experimental observations and show the expected increase in OASPL levels with decreased flight Mach number.

8.3.2 FORCED MIXER STUDIES

Three-dimensional calculations for 12 and 20-lobe mixer nozzles have been performed using the initialization procedures cited above. The 3-D CFD flowfield solution was then adapted to the axisymmetric MGB analysis. An equivalent axisymmetric flowfield was developed by circumferentially mass-averaging the 3-D flowfield in the manner suggested by Mani[9]. This approach was assumed adequate since the NASTAR predictions indicate that the flowfield rapidly approaches an axisymmetric pattern in the external plume. OASPL spectra comparisons with experimental data for the 12 and 20-lobe mixer nozzles are shown in Fig. 8.3.8. While the analysis is in general agreement with the data, the analysis incorrectly predicts a higher noise level for the 20-lobe mixer nozzle.

A closer look at the axisymmetric averaging approach is now presented. Figure 8.3.9 coplots the axisymmetric splitter velocity profile with the circumferentially averaged 12 and 20-lobe mixer velocity profiles. The mixer nozzles (both 12- and 20-lobe) reduce the peak velocity from 1500 fps to 1100 fps, however the 20-lobe mixer has a higher velocity level inboard of the peak. This helps explain the anomalous MGB noise prediction results shown in Fig. 8.3.8. A closer look at the exit plane velocity field for both mixer nozzles is shown on Fig. 8.3.10. Clearly the 12-lobe nozzle has peak velocities in excess of 1300 fps while the 20-lobed nozzle's peak velocity is less than 1200 fps. The linear averaging process therefore produces the erroneous profiles seen in Fig. 8.3.9. In hindsight, an averaging procedure that weights the velocity nonlinearly like Lighthill theory is probably necessary.

Additional insight to the mixing/noise generation process can be gained by examining the internal and external turbulent kinetic energy (k) field. Equation (4) indicates that the noise source intensity is dependent on **k**, i.e., higher **k** produces more noise. From the exit plane contours shown on Fig. 8.3.11, one can see that the maximum values of **k** are produced by the shear layers along the lobe sidewalls (linear averaging would not account for this) and is much larger than generated by the splitter. On the other hand, Fig. 8.3.12 indicates that the largest **k** regions occur in the exhaust plume and that the splitter and mixer nozzles appear to have the same **k** levels. The vertical scale in Fig. 8.3.12 has been enlarged by a factor of two to improve the display. Although the nozzle wall is not displayed, the splitter and nozzle wall shear layers are clearly visible. In the crest-cut mixer view shown on Fig. 8.3.12, only the nozzle shear layer is seen. Both configurations however have relatively the same turbulence intensity in the external plume.

Finally, by displaying the axial contribution to OASPL for a given viewing angle (Fig. 8.3.13), one can examine the cumulative noise contribution at the 120 degree viewing angle for the axisymmetric splitter and for the 12-lobe mixer. Since the 3D-mixer calculation was somewhat limited, a restarted, axisymmetric extended domain calculation was performed and is also displayed. First, one can verify Goldstein's observation that the majority of the noise occurs within 10 nozzle diameters of the exit plane for axisymmetric jets. Furthermore, one can see that the improved mixedness of the lobed mixer flow produces little additional noise downstream of the exit plane.

9.0   SUMMARY OF RESULTS AND CONCLUSIONS

P&W has completed a three-year research, design and development effort aimed at using and improving internal mixers as a means for reducing subsonic jet noise for low bypass ratio turbofan engines. The goal of the program was:

- to reduce sideline noise by 3 EPNdB relative to noise levels consistent with 1992 mixer technology.

Secondary goals were:

- to generate a detailed aerodynamic and acoustic data base and,
- to verify the ability of the state-of-the-art aerodynamic and acoustic modeling tools to predict the measured phenomena.

In order to accomplish the above goals, P&W designed and built a total of four $1/7^{th}$ scale-model internal mixers, as well as a non-mixed axisymmetric splitter configuration. These models were tested at NASA's NATR facility between 1994, and 1996. One of the mixers was a scale-model of the 12-lobe mixer that was certified with the JT8D-200 engine, which powers the MD-80 aircraft. This mixer served as the baseline mixer for the program. Another baseline configuration, an axisymmetric splitter, was designed and tested as being ideal for the code validation task. The other three mixers were designed by using CFD (Computational Fluid Dynamics) based on the design concept that a jet noise reduction relative to the baseline mixer would be achieved by obtaining a more uniform velocity profile. Two of the four mixers tested, the 20-lobe and 24-lobe, were of a conventional design. Both of these mixers were essentially the same as the 12-lobe mixer, with the exception of higher lobe count. The third mixer, designed under P&W auspices, is a unique double-lobe configuration and was designated the Advanced Technology Mixer (ATM).

During the experimental phase of this program, acoustic spectra, mean flow properties and turbulence profiles were acquired. The experimental program investigated the acoustic performance of four different mixers and a baseline splitter. The geometry perturbations also considered the effects of numerous geometrical variations of the mixers, e.g. scalloping, scarfing, engine probes, vortex generators, etc. on the acoustic and aerodynamic performance of the exhaust nozzle. Examination of the acoustic EPNL data indicates that *the ATM mixer was the best mixer design and that it achieved a 1.8dB reduction over the baseline 12-lobe configuration*. Of interest was the observation that the static performance ($M_\infty=0.0$) of all the mixers were essentially the same. This is most likely due to the importance of the low frequency jet noise, which dominates the spectra at the static (0 Mach number) condition. However in flight, the low frequency jet noise is reduced, and as a result the higher frequency "mixing noise" becomes the dominant source. The acoustic data also indicated that the muffler with the ATM had essentially no effect on the noise results. However geometry perturbations of scalloping, scarfing and vortex generators increased the noise approximately 0.5 EPNdB, and the effects of engine probes increased the noise by approximately 1 EPNdB and 2 EPNdB, with the 12-lobe mixer, and the ATM, respectively. Also, the ATM with unheated fan flow was approximately 1 EPNdB higher than the ATM with heated fan flow.

At the same time, examination of the measured aerodynamic data shows the existence of a residual-mixing region downstream of the common-flow nozzle exit plane. This mixing region produces high frequency noise which dominates the EPNL calculations. The aerodynamic data for the conventional mixers has the easily recognized repeated kidney-shaped temperature pattern representing incomplete mixing of the hot flow within the lobes. In contrast, the ATM produces a different flow pattern with concentric isothermal regions, known colloquially as the "ring of fire".

The computational studies performed in this program used the P&W NASTAR Navier-Stokes analysis and the NASA-NYMA MGB acoustic analogy code. Aerodynamic analyses were performed and favorable comparisons with measured LDV and traverse data were obtained for the mean axial velocity, the turbulent kinetic energy and the total temperature fields downstream of the nozzle exit plane for both the splitter and mixer configurations. The NASTAR analysis predicted accurately the basic flowfield patterns as well as the detailed levels and gradients.

The MGB analysis, used in conjunction with the NASTAR Navier-Stokes flow solver, has been successfully applied to predict the acoustic characteristics of a multistream axisymmetric nozzle. From these calculations, one can note that:

- MGB provides reasonable acoustical signature predictions for axisymmetric multistream nozzles,
- MGB provides reasonable acoustical signature predictions of scaling effects, e.g. size and observer distance,
- MGB is a useful analytical tool for assessing turbulence modeling and input boundary condition effects, and that sensitivities of order 2 to 4 dB were noted.

While calibrations with experimental data were good, it is believed that the CFD/MGB analysis approach is best suited for predicting qualitative trends rather than absolute levels. Similar comparisons performed for three-dimensional forced mixer nozzles were less successful. While the analyses predicted the general shift in directivity pattern from the axisymmetric splitter nozzle, they were unable to successfully discriminate between different lobed mixer configurations. This appears to be largely due to the inability of the circumferential averaging procedure to represent the 3D problem, rather than the accuracy limitations of the CFD analysis.

10.0   REFERENCES

1. NASA Nozzle Acoustic Test Rig (NATR) Operational Manual

2. Lord, W. K., Montuori, P., Zysman, S. H., "Subsonic Jet Noise Reduction 1994 Mixer Model Test at NASA Lewis Objectives and Test Plan", June 15, 1994.

3. Montuori, P. M., Zysman, S. H., "Subsonic Jet Noise Reduction 1996 Phase II Mixer Model Test at NASA Lewis Objectives and Test Plan", December 1995.

4. Waitz, I.A., et al., "Course on Gas Turbine Engine Performance" given at the UTC Leadership Center, Farmington, Connecticut, on January 5-9, 1998.

5. Podboy, G. G., Bridges, J., Saiyed, N. H., & Krupar, M., "Laser Doppler Velocimeter System for Subsonic Jet Mixer Nozzle Testing at the NASA Lewis Aeroacoustic Propulsion Lab," AIAA 95-2787, 31st AIAA/ASME/ SAE/ASME Joint Propulsion Conference, San Diego CA, July 1995.

6. Rhie, C. M. & Chow, W. L., "Numerical Study of the Turbulent Flow Past an Airfoil with Trailing Edge Separation," AIAA J., Vol. 21, No. 11, November 1983, pp. 1525–1532

7. Patankar, S. V., "Numerical Heat Transfer and Fluid Flow," Hemisphere Publishing, (New York), 1980.

8. Jones, W. P. and Launder, B. E., "The Prediction of Laminarization With a Two–Equation Model of Turbulence," Int. Journal of Heat and Mass Transfer, Vol. 15, 1972, pp. 301.

9. Mani, R., Balsa, T. E., Gliebe, P. R., et al., "High Velocity Jet Noise Source Location and Reduction: Task 2-Theoretical Developments and Basic Experiments," Federal Aviation Administration, FAA-RD-76-79-II, May 1978.

10. Khavaran, A., Krejsa, E. A., and Kim, C. M., "Computation of Supersonic Jet Mixing Noise for an Axisymmetric CD Nozzle Using k-e Turbulence Model," AIAA–92–0500, AIAA 30th Aerospace Sciences Meeting, Reno, NV, 1992.

11. Khavaran, A., Krejsa, E. A., and Kim, C. M., "Computation of Supersonic Jet Mixing Noise for an Axisymmetric CD Nozzle," Journal of Aircraft, Vol. 31, No. 3, 1994, p. 603.

12. Zysman, S. H., Chiappetta, L. M., Saiyed, N. H., & Podboy, G. G., "Flowfield Measurements and Analysis of a 1/7-Scale Mixed Flow Exhaust System Model," AIAA 95-2744, 31st AIAA/ASME/SAE/ASME Joint Propulsion Conference, San Diego CA, July 1995.

13. Dannenhoffer, J. F., III, "Computer–Aided Block–Structuring Through the Use of Optimization and Expert System Techniques," AIAA 91–1585, AIAA 10th Computational Fluid Dynamics Conference, Honolulu, HI, June 1991.

14. Dannenhoffer, J. F., III, "A Block–Structuring Technique for General Geometries," AIAA 91–0145, AIAA 29th Aerospace Sciences Meeting, Reno, NV, January 1991.

15. Malecki, R. E. and Lord, W. K., "A 2–D Duct/Nozzle Navier–Stokes Analysis System for Use by Designers," AIAA 95–2624, AIAA 31st Joint Propulsion Conference, San Diego, CA, July 1995.

16. Fischberg, C., Rhie, C., Zacharias, R., DesSureault, T., "Using Hundreds of Workstations for Production Running of Parallel CFD Applications," presented at "Parallel CFD '95," Pasadena, CA, June 27, 1995.

17. Chevray, R., and Tutu, N. K., "Intermittency and Preferential Transport of Heat in a Round Jet," Journal of Fluid Mechanics vol. 88, part 1, 1978, pp. 137.

18. Schetz, J. A., "Foundations of Boundary Layer Theory for Momentum, Heat, and Mass Transfer," Prentice–Hall, Inc., 1984, p. 228.

19. Barber, T. J., Chiappetta, L. M., and Zysman, S., "An Assessment of Jet Noise Analysis Codes for Multistream Axisymmetric & Forced Mixer Nozzles," AIAA Paper No. 96-0750, AIAA 34th Aerospace Sciences Meeting, Reno, NV, 1996, also AIAA Journal for Propulsion and Power, Vol. 13, No. 6, 1997, pp. 737-744.

20. Sarkar, S., Erlebacher, G., Hussaini, M. Y., and Kreiss, H. O., "The Analysis and Modeling of Dilatational Terms in Compressible Turbulence," J. Fluid Mechanics, Vol. 227, 1991, pp. 473-493.

21. Choi, D., Weeratunga, S. and Knight, C.J., "A Numerical Method for Navier-Stokes Equations with Finite Rate Chemistry," AIAA-89-1857, AIAA 20th Fluid Dynamics, Plasma Dynamics and Lasers Conference, June 1989, Buffalo, NY.

22. Yamamoto, K., Brausch, J. F., et al., "Experimental Investigation of Shock-Cell Noise Reduction for Single Stream Nozzles in Simulated Flight, Comprehensive Data Report, Vols. 1-3," NASA CR-168234, 1984.

23. Choi, D., Sabnis, J. S. and Barber, T. J., "Application of an RNG k-ε Model to Compressible Turbulent Shear Layers," UTRC Report 93-25, June 1993, also AIAA 94-0188, 32nd Aerospace Sciences Meeting, Reno NV, 1994.

24. Soderman, P. T., "On the Scaling of Small-Scale Jet Noise to Large Scale," DGLR/AIAA 92-02-109, DGLR/AIAA 14th Aeroacoustics Conference, Aachen, Germany, 1992, p. 663.

25. Simonich, J., "Hush Kit Directional Microphone Acoustic Test," UTRC Report 90-30, August 17, 1990.

26. Saiyed, N.H., Bridges, J.E., Krejsa, E.A., "Core and Fan Streams' Mixing Noise Outside the Nozzle for Subsonic Jet Engines with Internal Mixers," AIAA 96-1667, May 6-8, 1996.

27. Castner, R.S. "The Nozzle Acoustic Test Rig: An Acoustic and Aerodynamic Free-Jet Facility," AIAA 94-2565, June 20-23, 1994.

11.0   APPENDIX
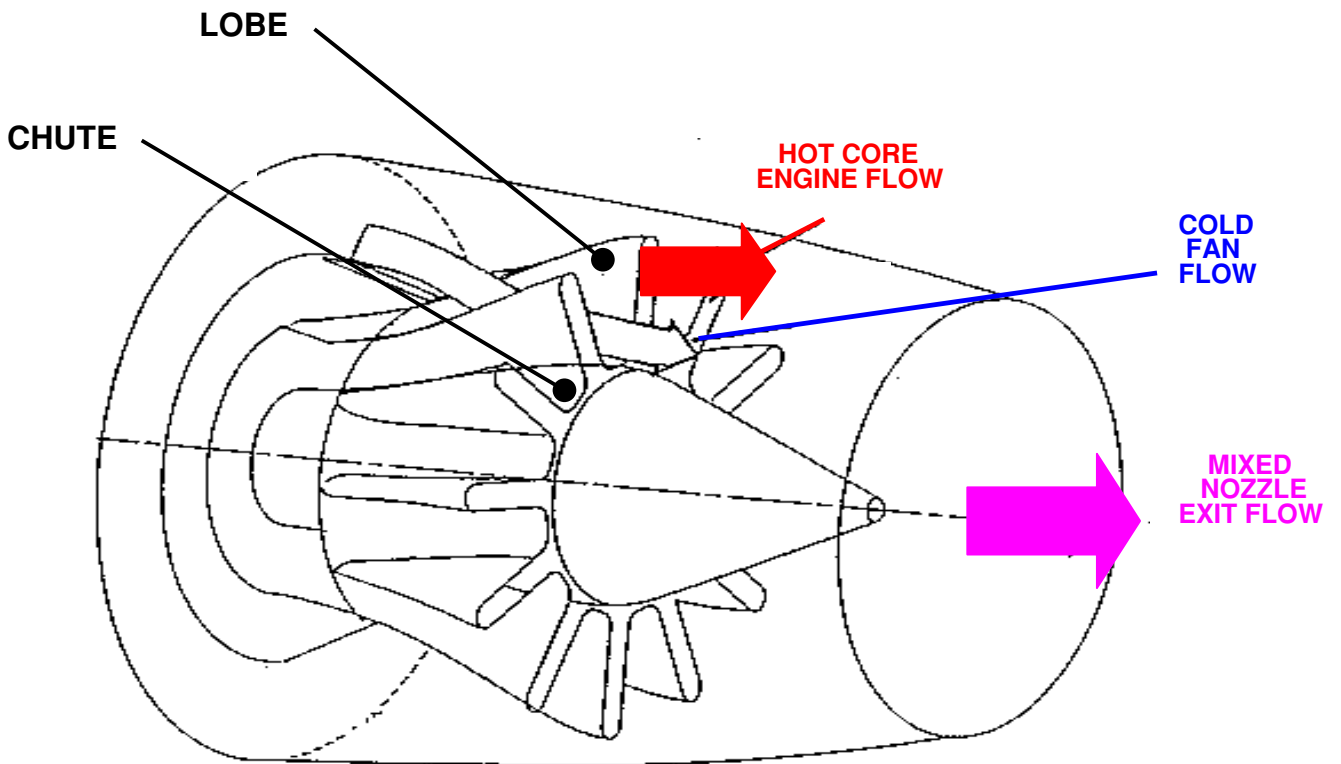
Figure 2.0.1: Typical Lobe Forced Mixer Exhaust Geometry
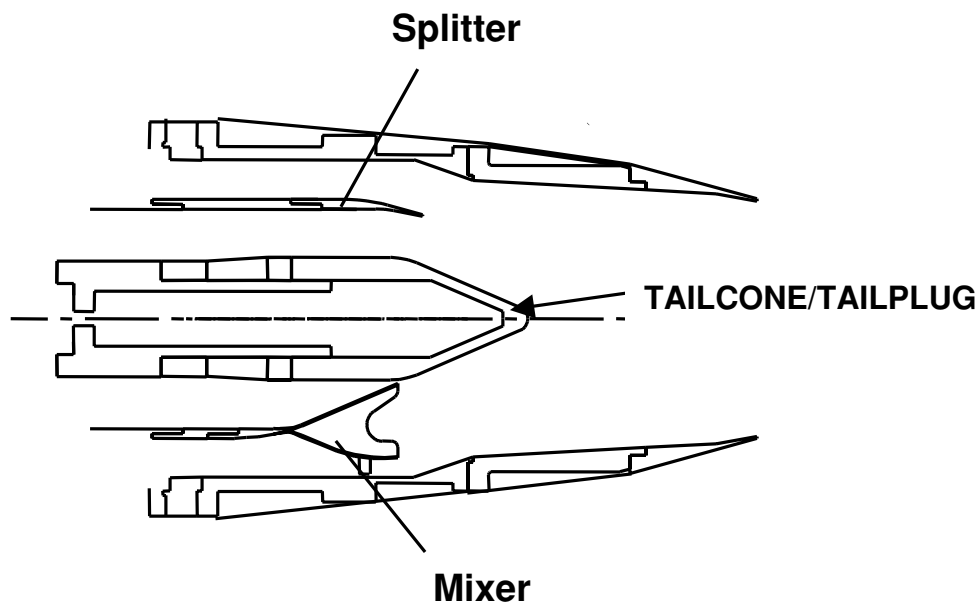
Figure 2.0.2: Schematic of Splitter and Typical Lobe Mixer Exhaust System

BASIC PROFILE

SPLITTER

12-LOBE

(BASELINE)

20-LOBE

MINI-CHUTE
(Additional Fan Air)

16
PRIMARY
LOBES

Double-Lobe

ADVANCED TECHNOLOGY
DOUBLE-LOBE

24-LOBE

SECTION A-A
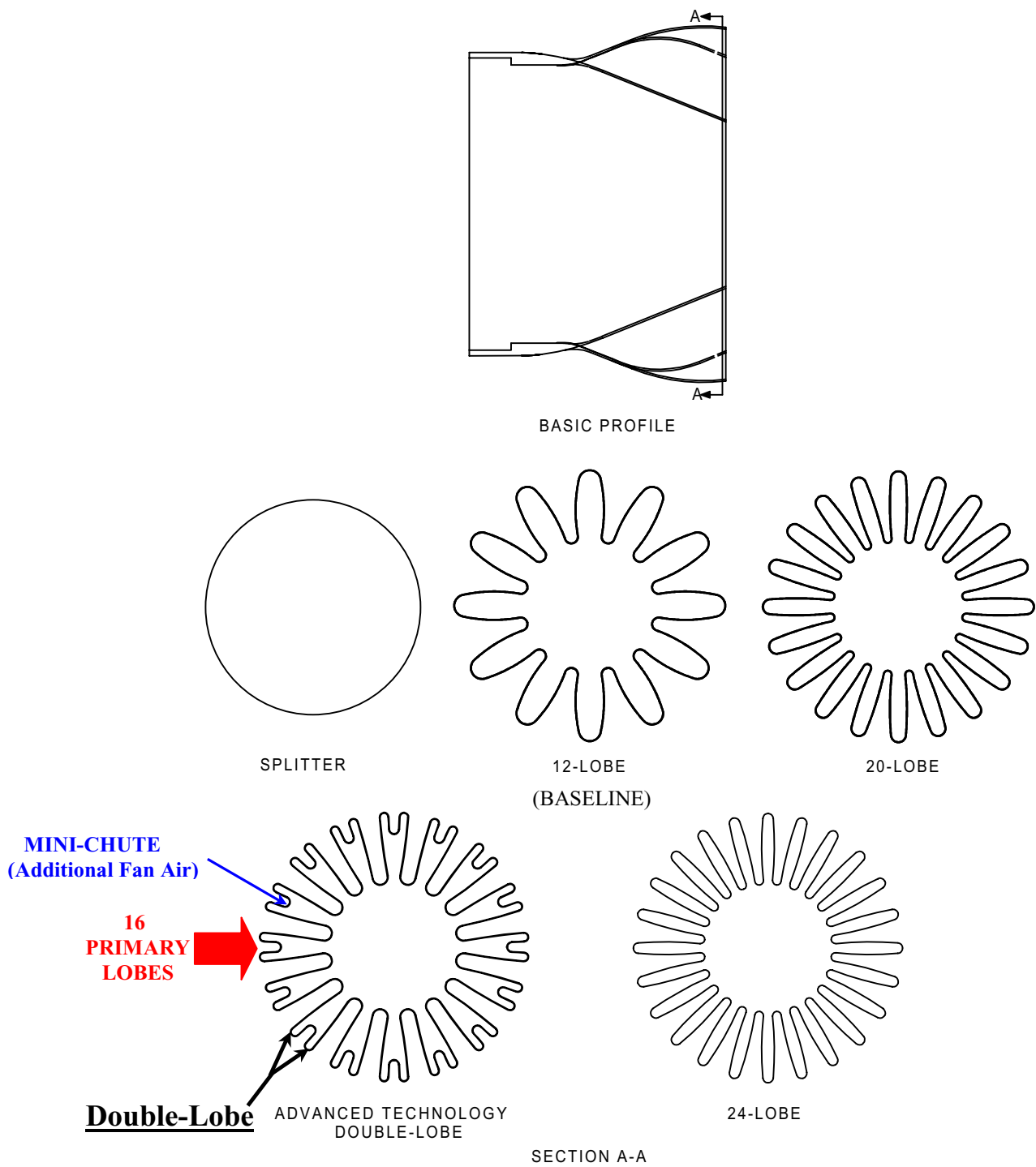
Figure 4.0.1: Trailing Edge view of Splitter and Mixers

Figure 4.1.1: Picture of Splitter with Tailcone/Tailplug
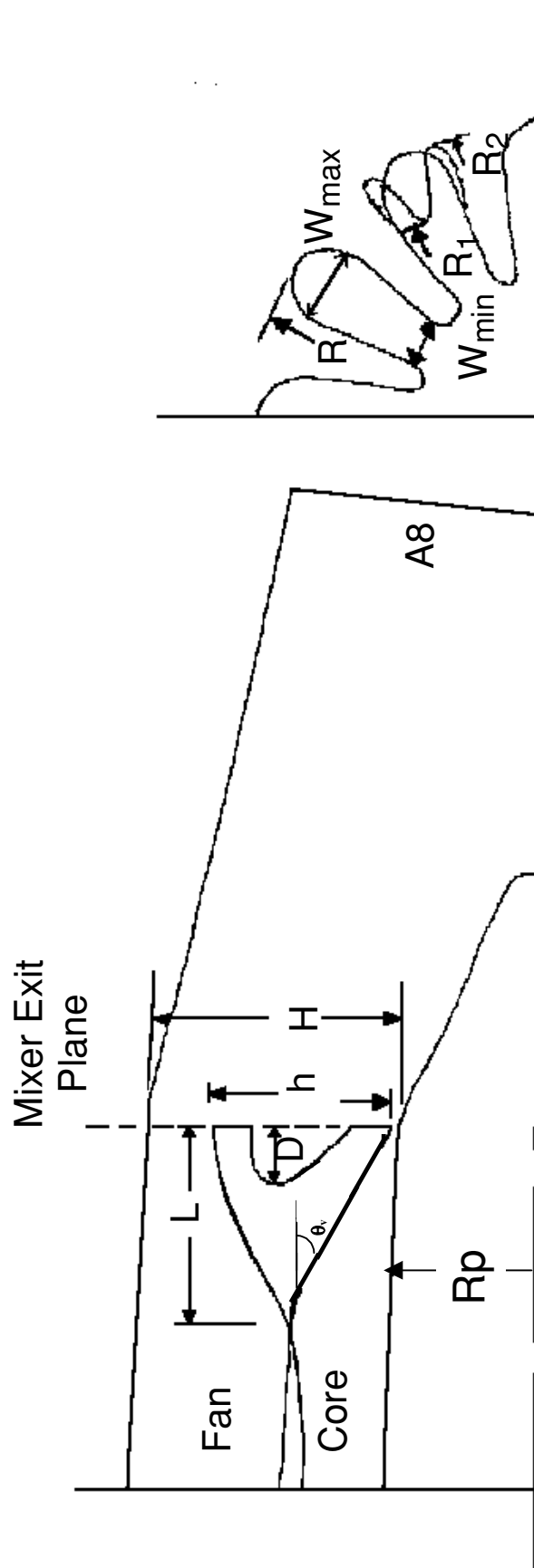
Figure 4.2.1: Mixed Exhaust Nozzle Geometric Parameters
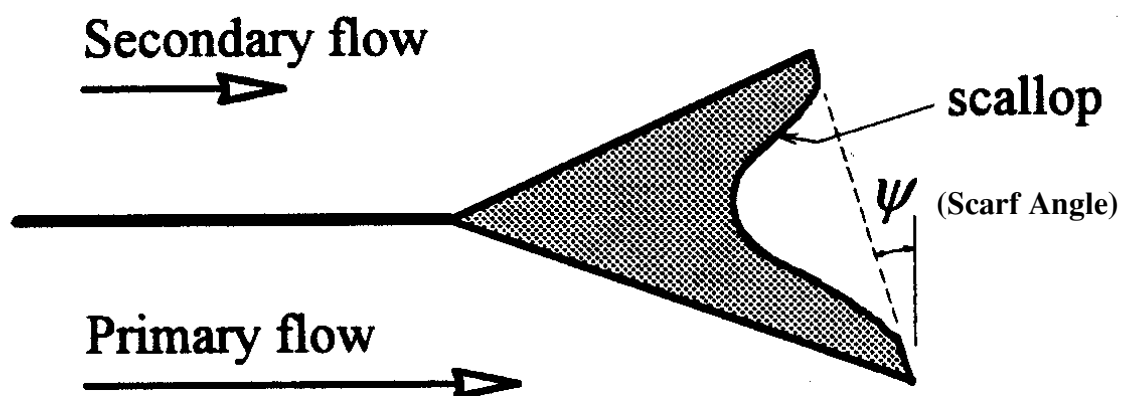
Figure 4.2.2: Typical Lobe Mixer with Scallop and Scarf Angle Defined
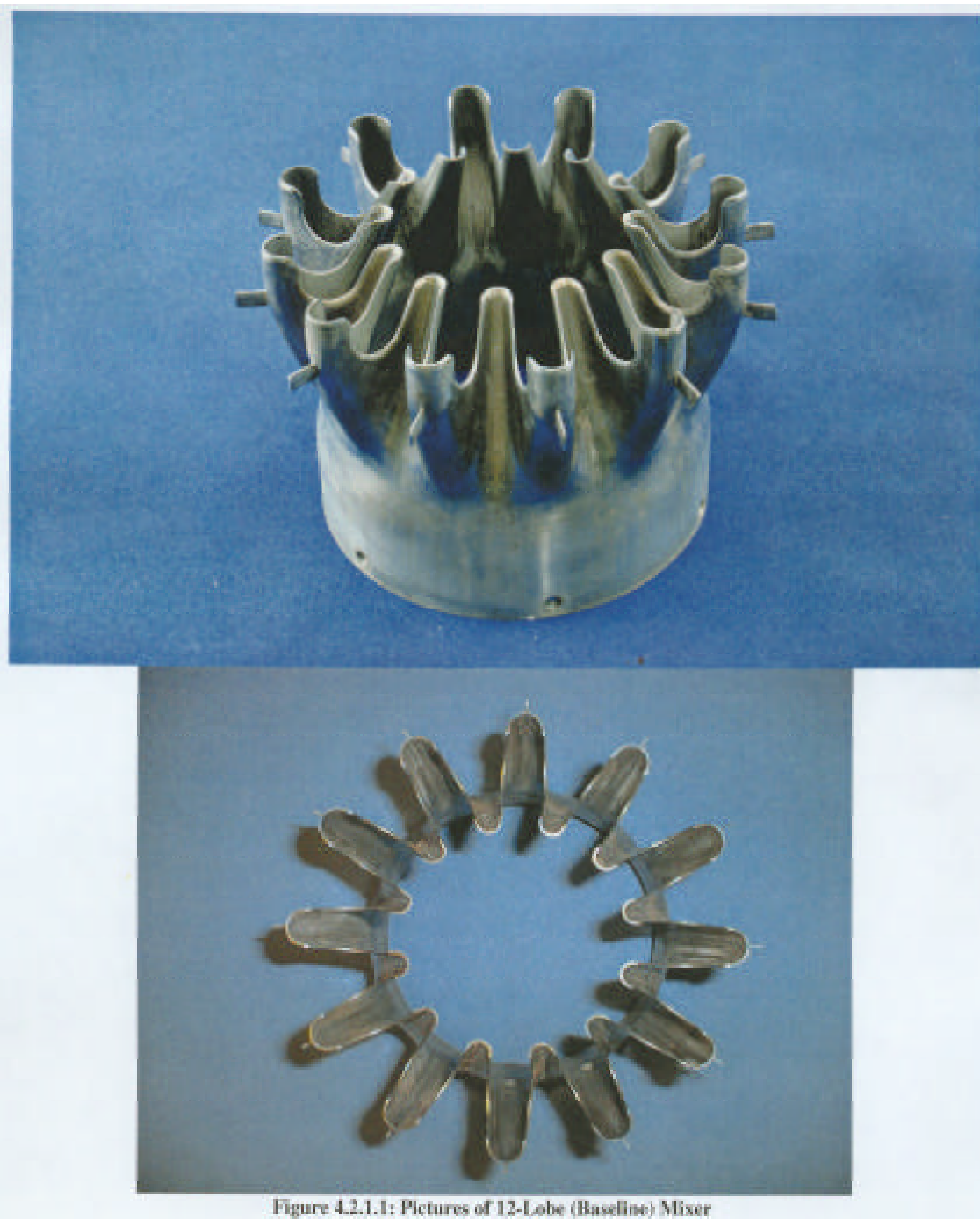
Figure 4.2.1.1: Pictures of 12-Lobe (Baseline) Mixer
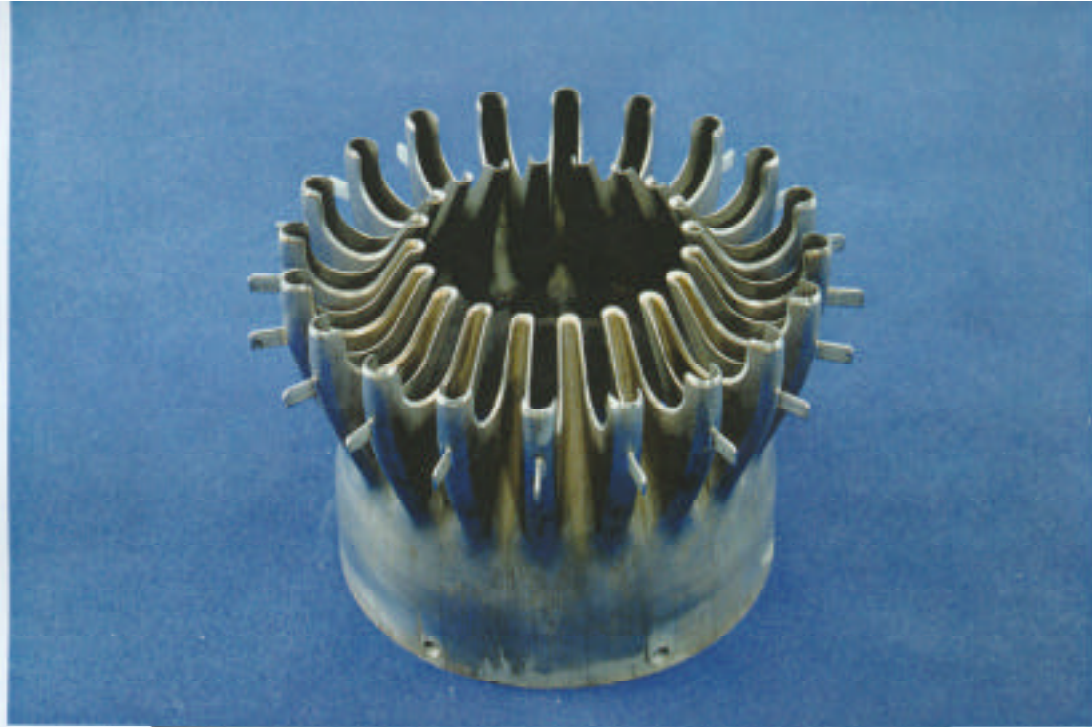
Figure 4.2.2.1: Pictures of 20-Lobe Mixer
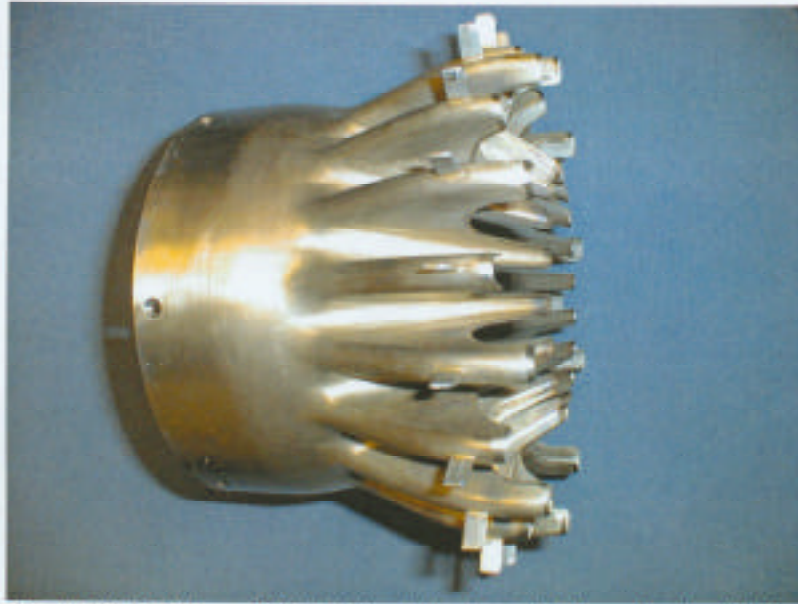
Figure 4.2.3.1: Picture of 20-Lobe Mixer (side view) with Alternating Scarf Angle (0/12 degrees)

Figure 4.2.4.1: Picture of 24-Lobe Mixer

Figure 4.2.5.1: Picture of Advanced Technology Mixer (ATM) <u>Without Lobe Scallops</u>

Figure 4.2.6.1: Picture of Advanced Technology Mixer (ATM) <u>With Lobe Scallops</u>
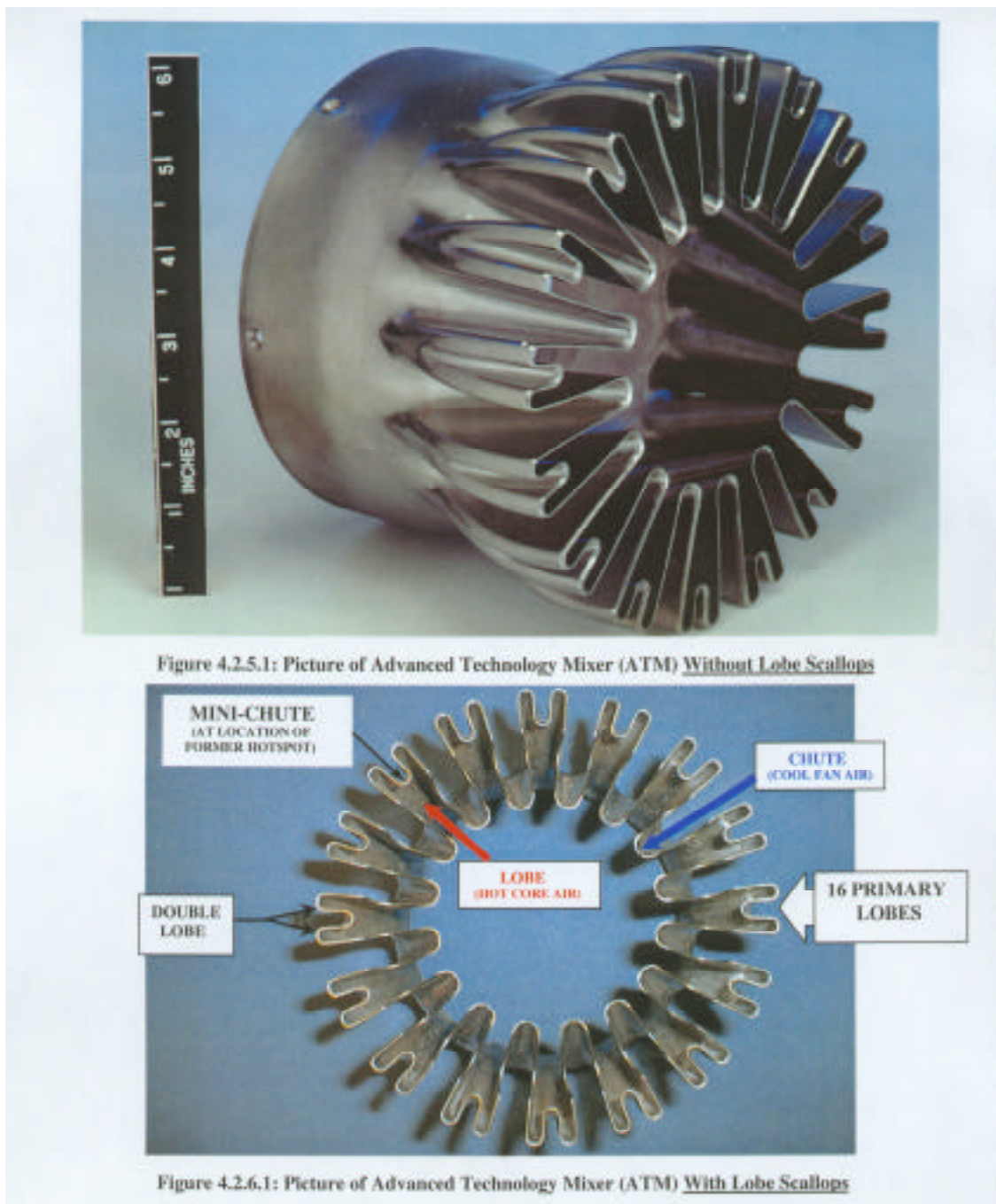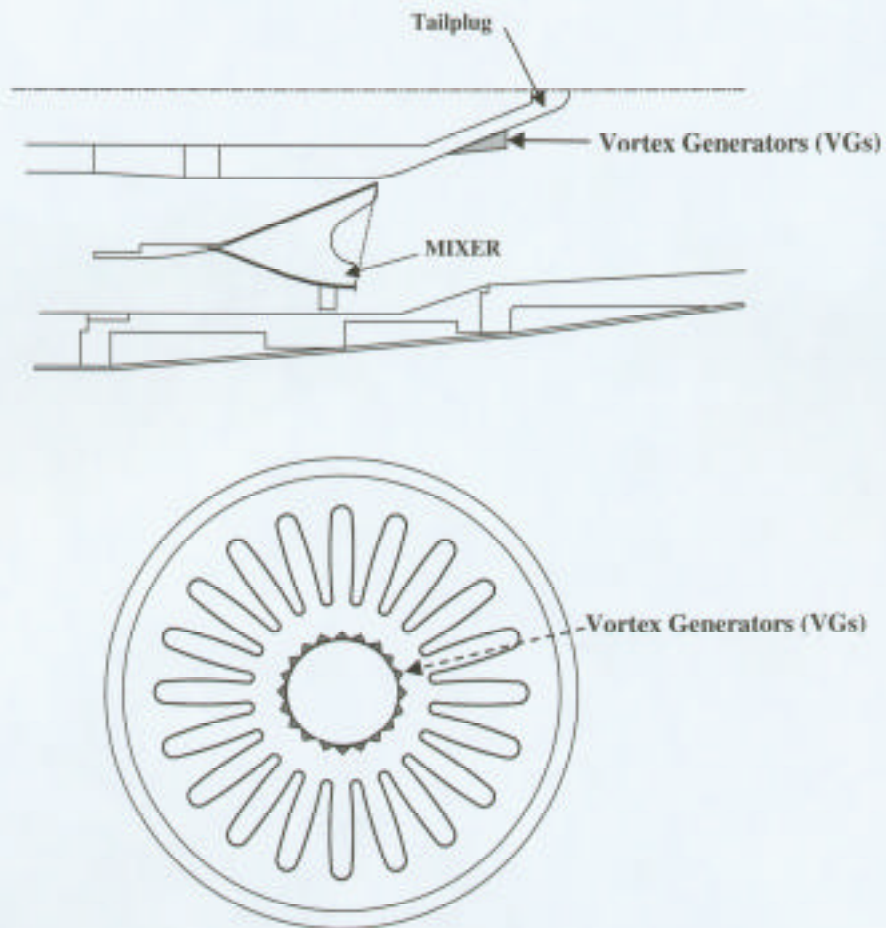
Figure 4.3.1.1: Location of Vortex Generators (VGs)

Figure 4.4.1: Picture of 12-Lobe Mixer with Simulated Engine Probes (Upstream)

Figure 4.5.1: Picture of Solid and Muffler Tailcone/Tailplug

Figure 5.0.1: Picture of APL Dome
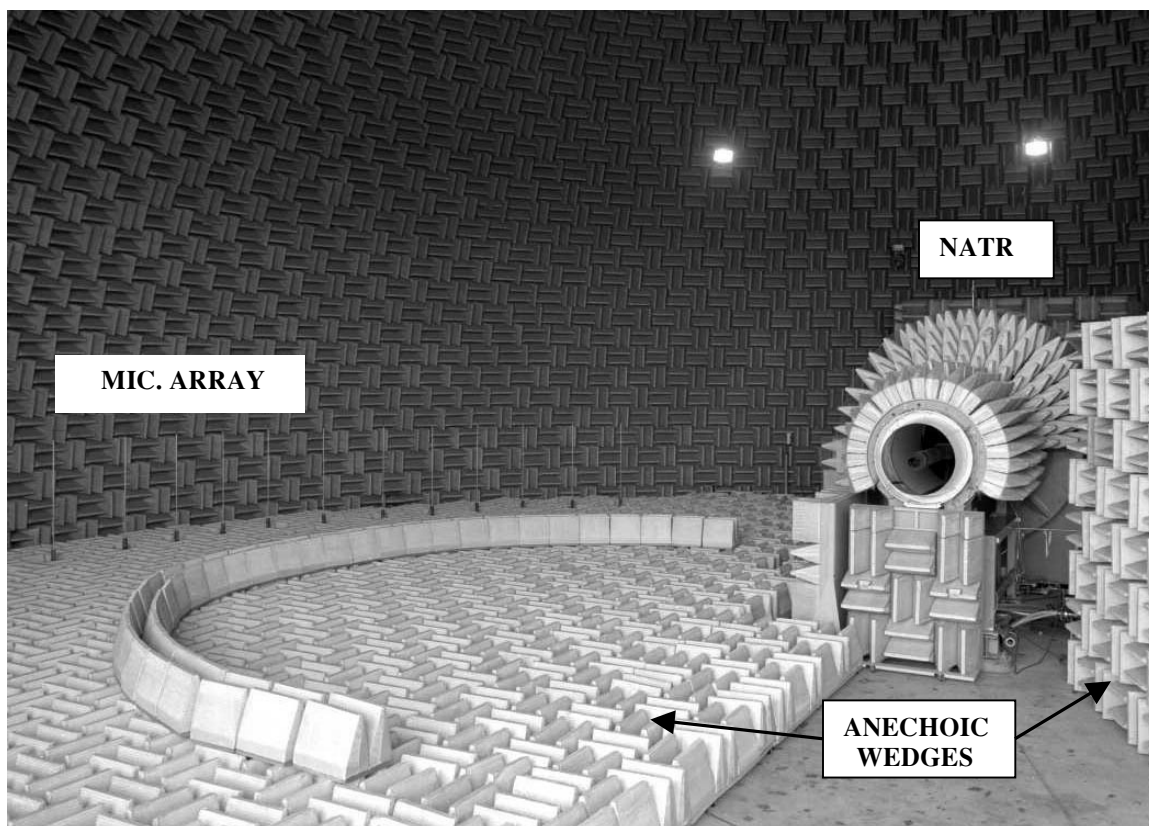
Figure 5.0.2: Picture of NATR, Anechoic Test Area, and Microphone Array Location

SECTION A-A
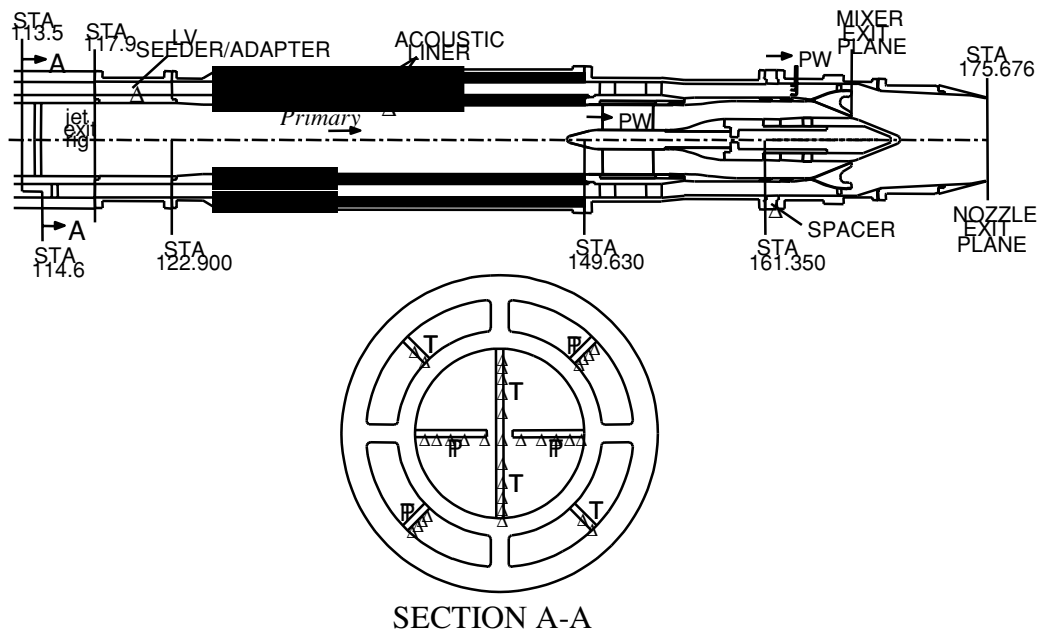
Figure 5.1.1: Model Internal Flowpath
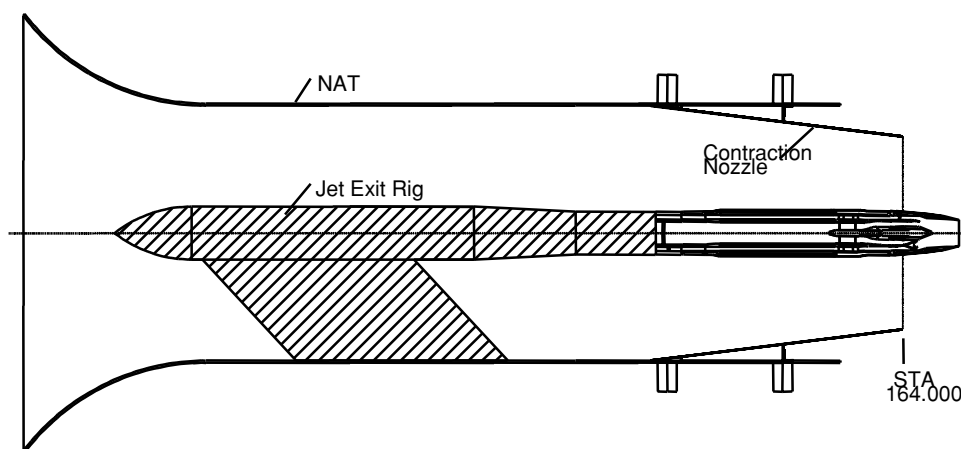
Figure 5.1.2: NATR / Model External Flowpath

Customer attach point

Flow conditioning module

Core flow combustor

Geometry transition

Force balance

Support strut
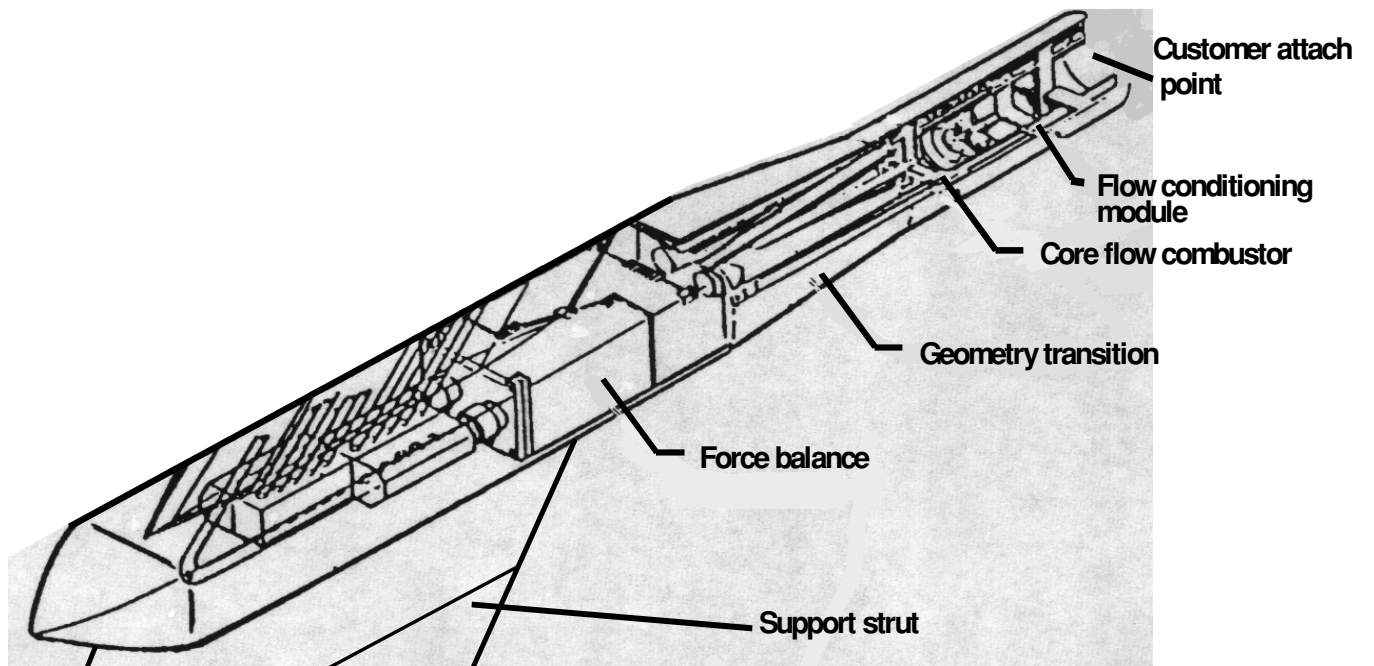
Figure 5.1.3: Schematic of Jet Exit Rig (JER)

"DESIRED" CHARGING STATION

STA 113.5 STA 117.9 LV SEEDER/ADAPTER ACOUSTIC LINER MIXER EXIT PLANE STA 175.676

A

PW

jet exit rig

Primary

PW

A

STA 114.6 STA 122.900 STA 149.630 STA 161.350 SPACER NOZZLE EXIT PLANE

SECTION A-A
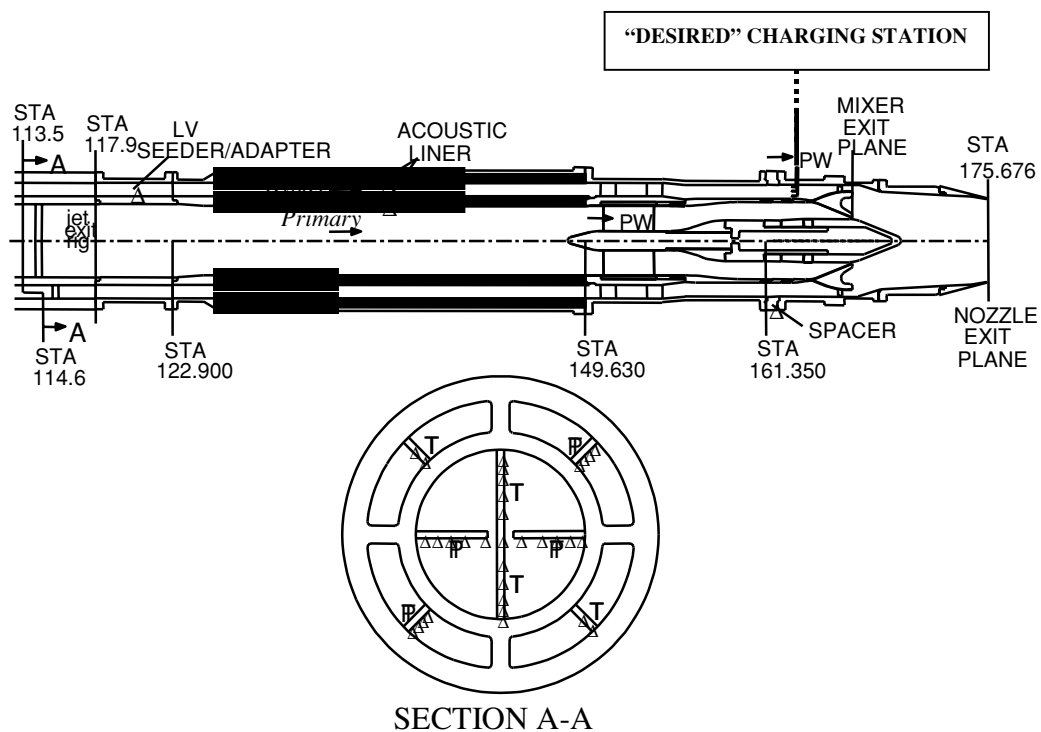
Figure 5.3.1.1: 1994 Charging Station Locations: Actual and "Desired"

STA 113.5 STA 117.9 LV SEEDER/ADAPTER ACOUSTIC LINER B-B MIXER EXIT PLANE STA 175.676

A

PW

jet exit rig

Primary

PW

A

STA 114.6 ST 122.900 STA 149.630 STA 161.350 SPACER NOZZLE EXIT PLANE

A-A

SECTION A-A (PRIMARY)   SECTION B-B (BYPASS)
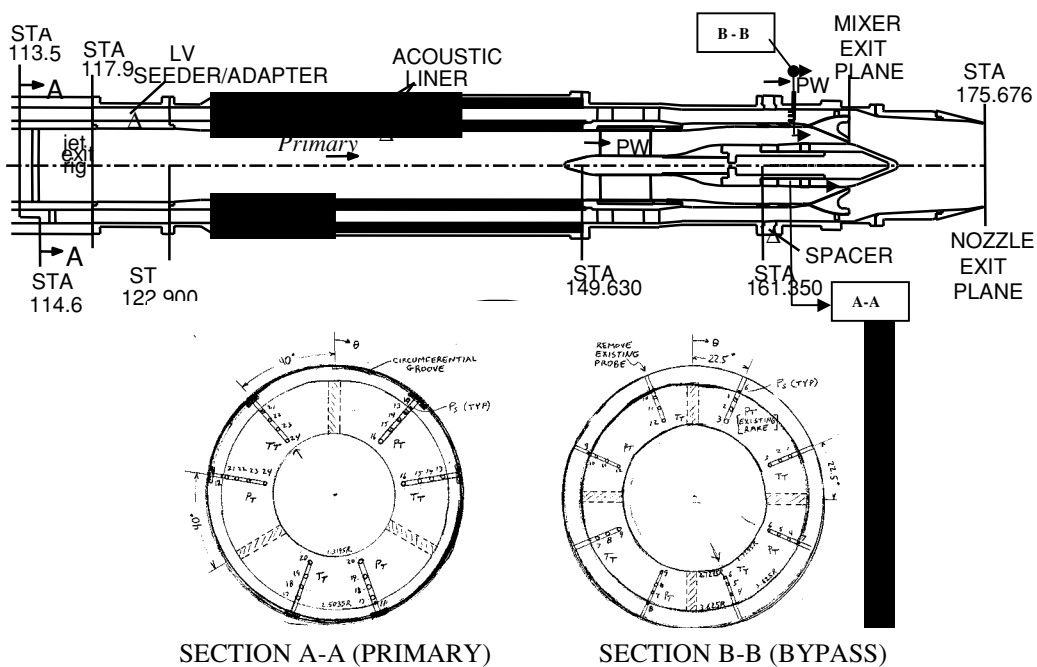
Figure 5.3.2.1: 1996 Charging Station Location
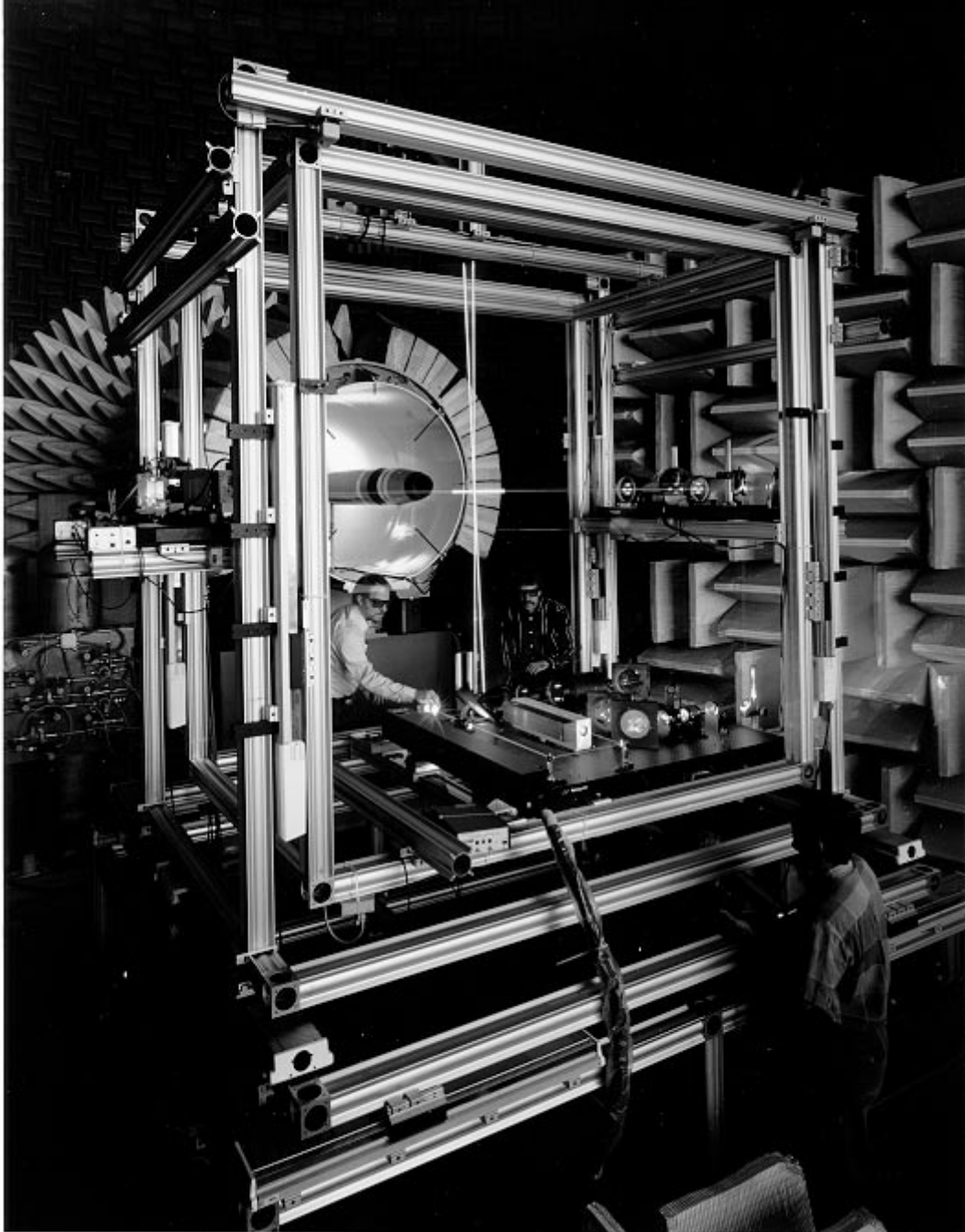
Figure 5.5.2.1: Picture of LDV Scan Rig / NATR
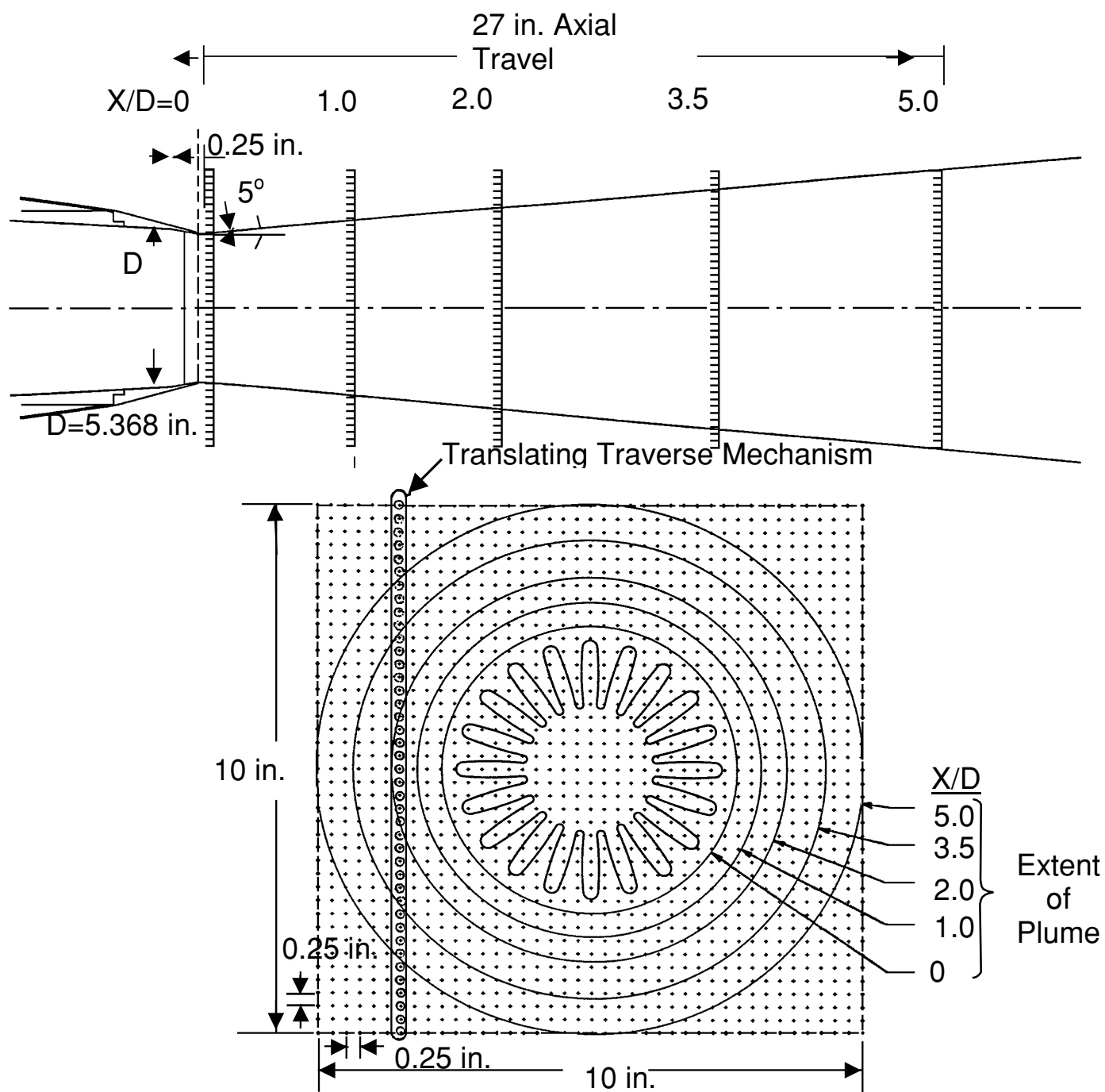
Figure 5.5.3.1: Total Temperature and Pressure Traversing Acquisition System and Orientation

NASA LeRC Acoustic Data Processing Scheme

| Digitize sound signals | → | Digital tape archives |

| Convert to units of pressure using calibration coefficients obtained via pistonphone | ← | Test and model conditions from facility computer |

| Compute averaged narrowband spectra, convert to narrowband SPL |

| Correct for microphone actuator frequency response | ← | B&K certified electrostatic calibration |

| (I) Correct for microphone free-field and grid cap response | ← | B&K provided grid response |

| Correct for analog filter roll-off | → IEEE compliant 1/3 octave → | Data output status: as measured | II |

| Correct for freejet shear layer refraction | → IEEE compliant 1/3 octave → | Data output status: corrected | (IV) |

| Remove atmospheric attenuation at test day conditions over test distance | | (III) |

| Remove spherical spreading attenuation from test distance to a 1 foot arc | → | Archive narrowband spectra for customer-specific processing |

| Impose spherical spreading attenuation from 1 foot arc to 150 foot arc |

| Change scaling of data to full-scale (frequency & amplitude) | IEEE compliant 1/3 octave → | Data output status: 1 foot, lossless |

| Apply Doppler shift for sideline flyover by adjusting frequency |

| Instate atmospheric attenuation at FAA Standard Day conditions over distance to 1500 foot sideline |

| Instate spherical spreading attenuation from 1 foot arc to 1500 foot sideline | | (V) |

| IEEE compliant 1/3 octave | → Noy weighting, summation, and tone correction → | Data output: PNLT vs angle |

| (V) | Summation of PNLT plus duration correction → | Data output: EPNLT |

| | | (V) |

Figure 6.0.1: NASA LeRC Acoustic Data Processing Scheme

Figure 7.1.1.1: EPNL vs Mixed Jet Mach Number for Splitter and 12-Lobe Mixer
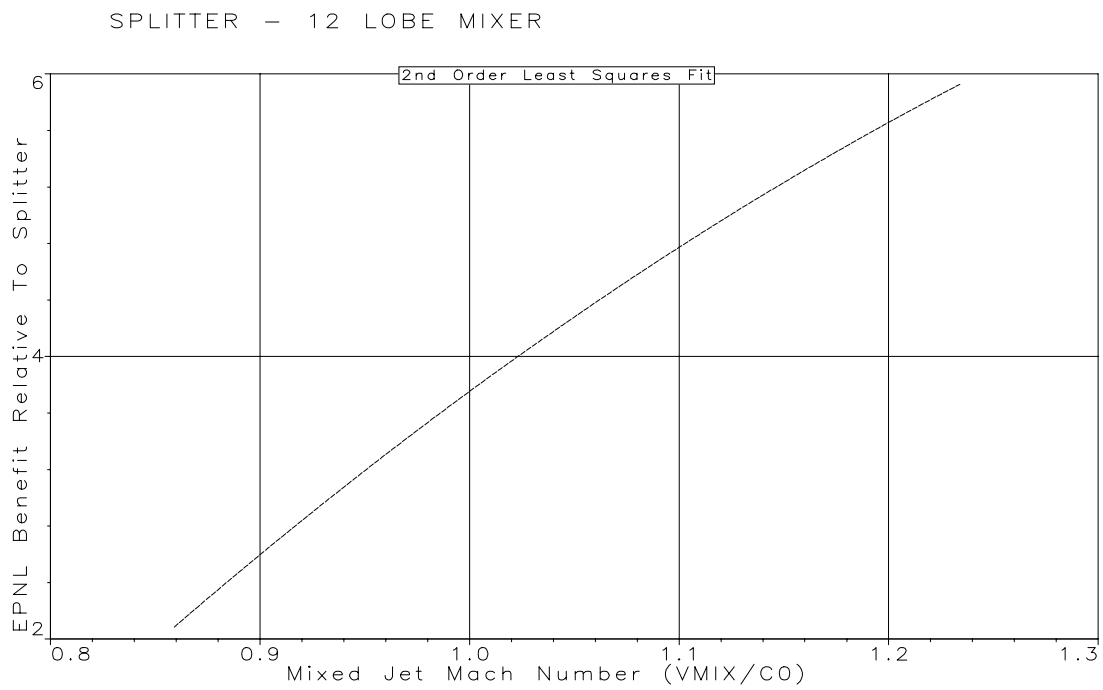
Figure 7.1.1.2: Delta EPNL Reduction vs Mixed Jet Mach Number for 12-Lobe Mixer Relative to Splitter
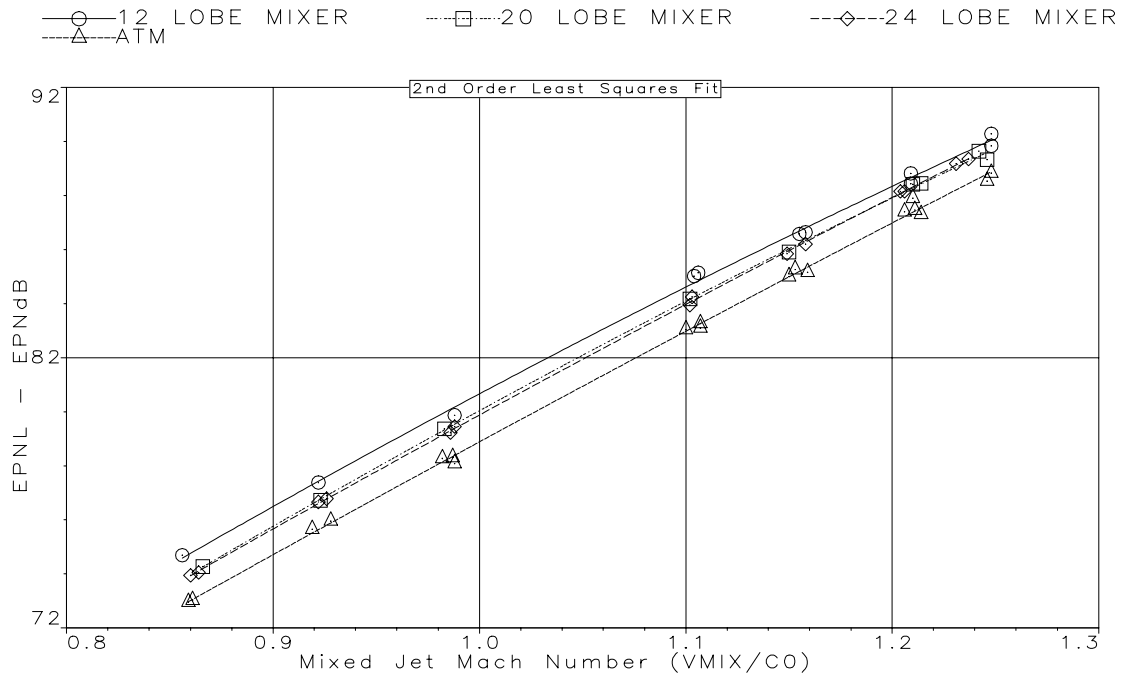
Figure 7.1.1.3: EPNL vs Mixed Jet Mach Number for All Mixers (12, 20, 24, and ATM)
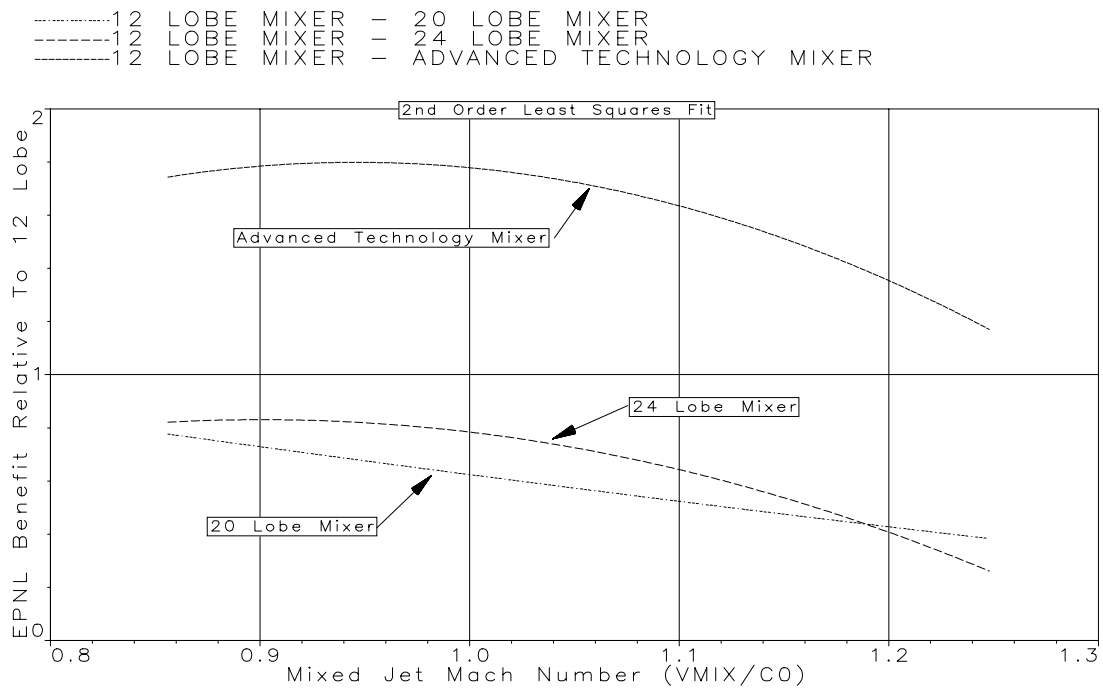
Figure 7.1.1.4: Delta EPNL Reduction vs Mixed Jet Mach Number for 20, 24, and ATM Relative to the Baseline 12-Lobe mixer
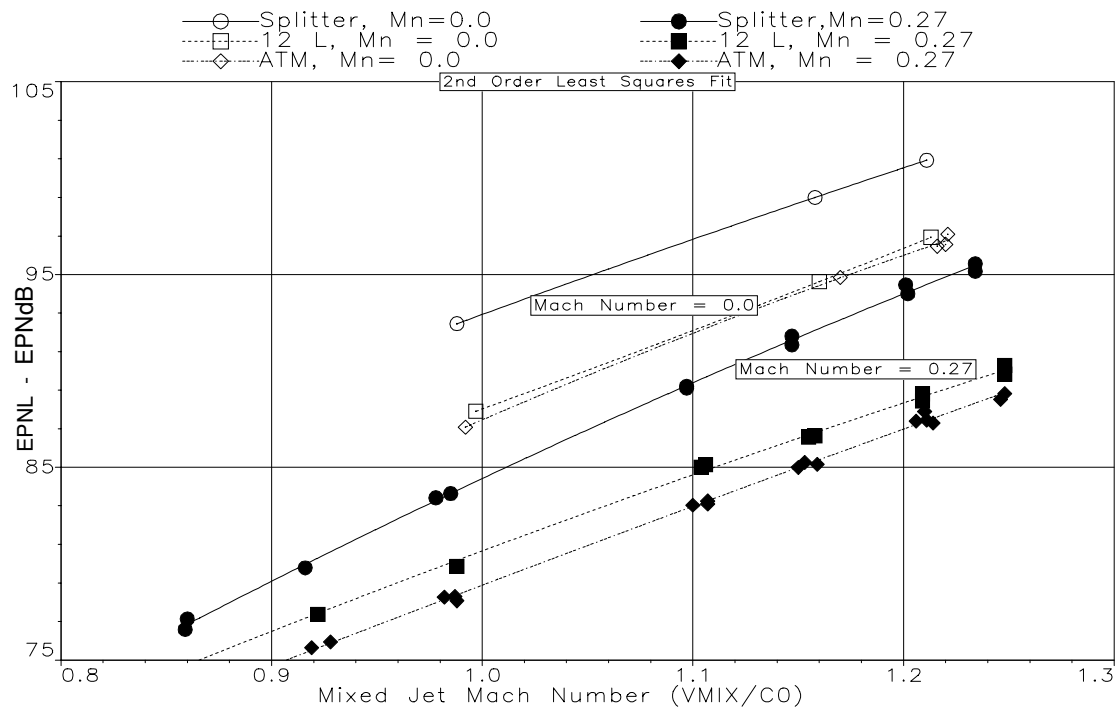
Figure 7.1.1.5: EPNL vs Mixed Jet Mach Number : Effect of Flight on Splitter, 12-Lobe, and ATM
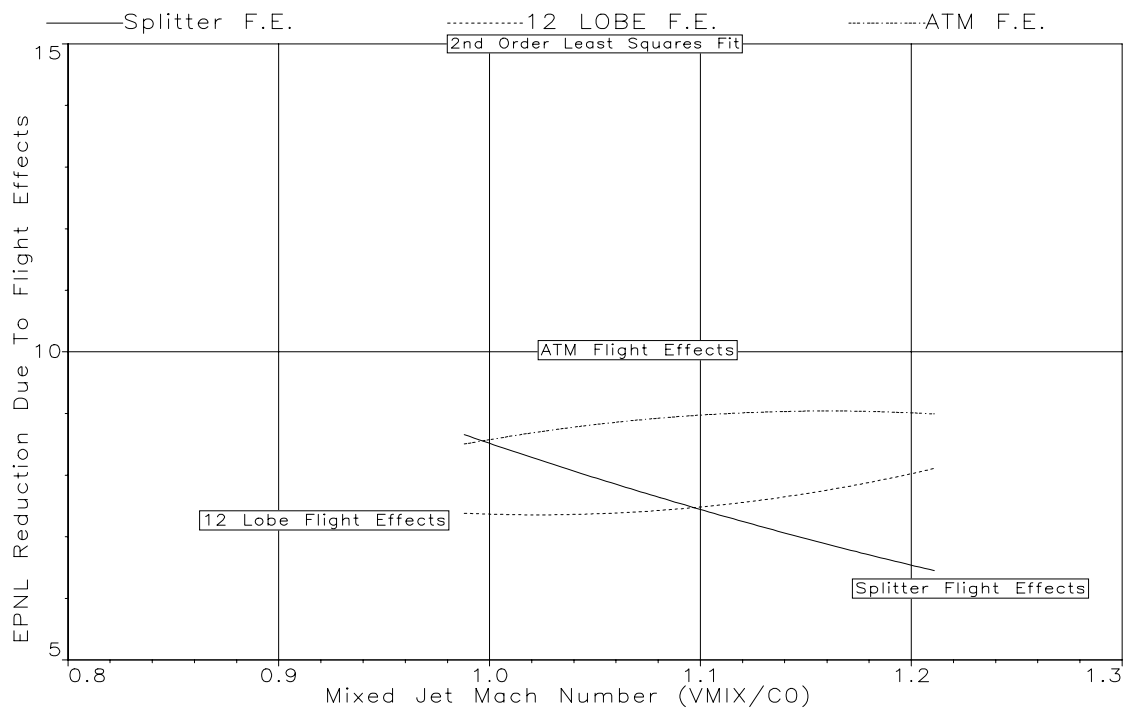
Figure 7.1.1.6: Delta EPNL vs Mixed Jet Mach Number : Effect of Flight on Splitter, 12-Lobe, and ATM
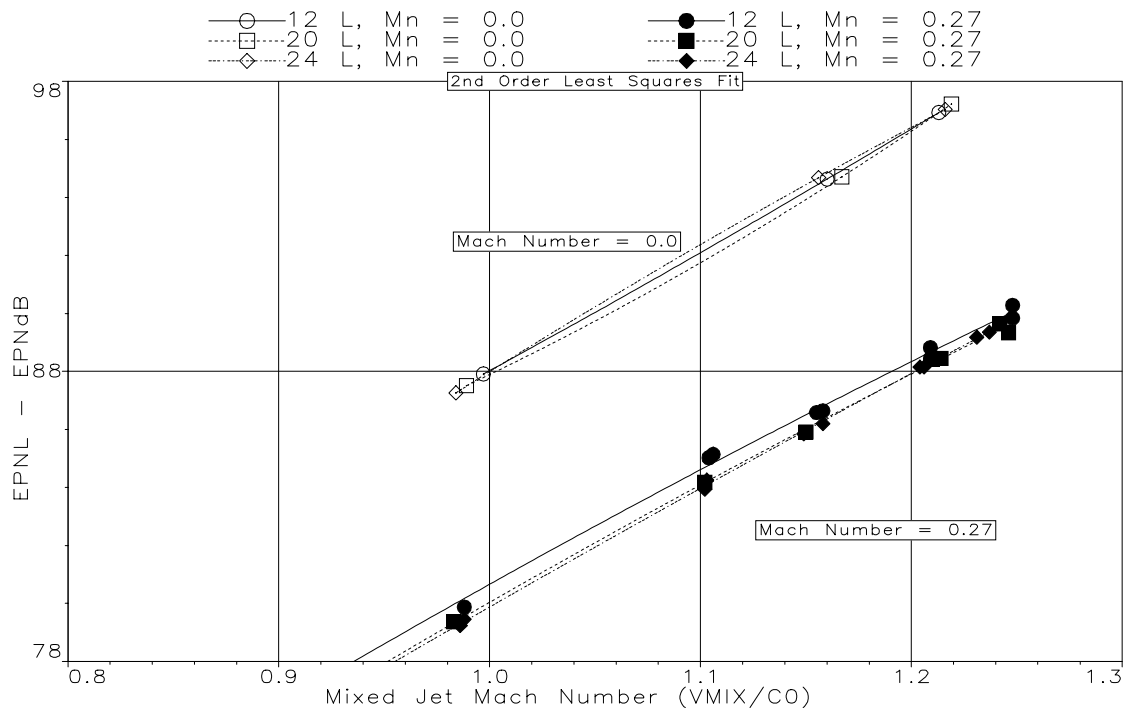
Figure 7.1.1.7: EPNL vs Mixed Jet Mach Number : Effect of Flight on 12, 20, and 24-Lobe Mixers
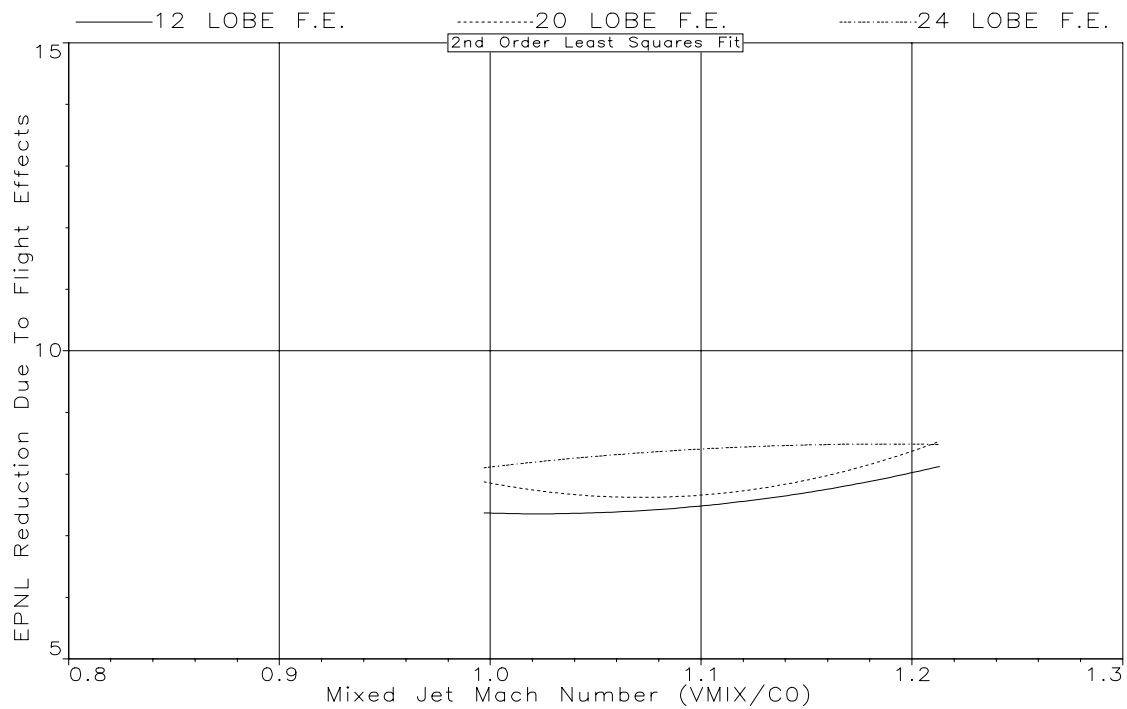
Figure 7.1.1.8: Delta EPNL vs Mixed Jet Mach Number : Effect of Flight on 12, 20, and 24-Lobe Mixers
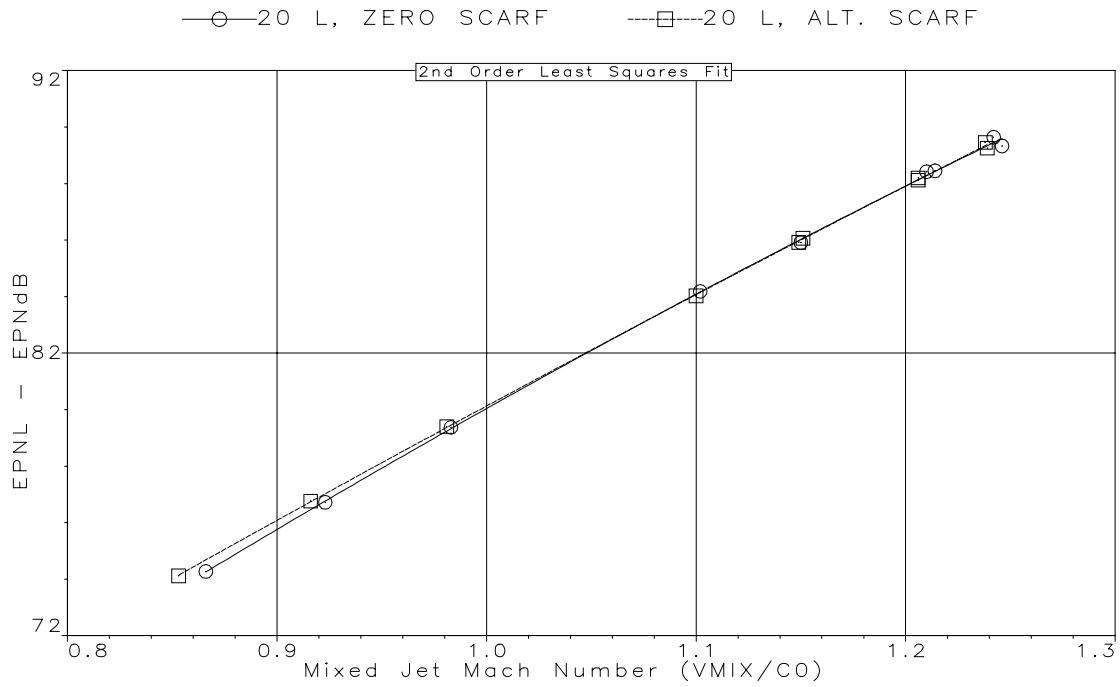
Figure 7.1.1.9: EPNL vs Mixed Jet Mach Number Comparison of Zero and Alternating Scarf Angle (0/12 deg.) on 20-Lobe Mixer
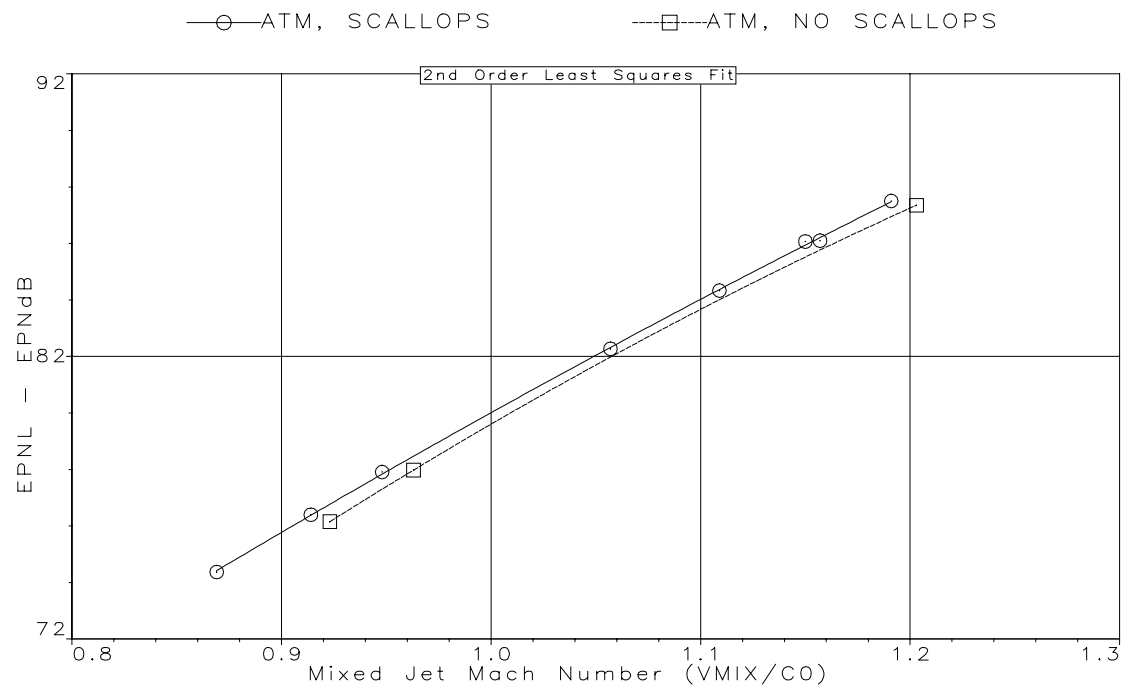
Figure 7.1.1.10: EPNL vs Mixed Jet Mach Number : Effect of Lobe Scallops on ATM (UnheatedFan)
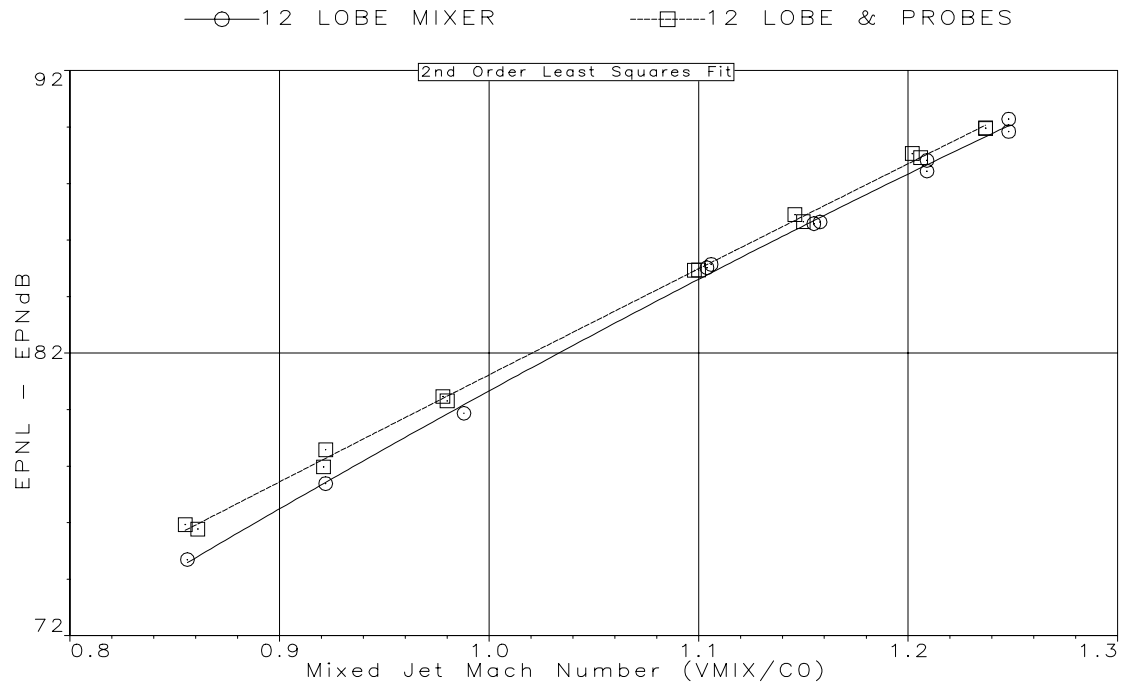
Figure 7.1.1.11: EPNL vs Mixed Jet Mach Number : Effect of Simulated Engine Probes with Baseline 12-Lobe Mixer
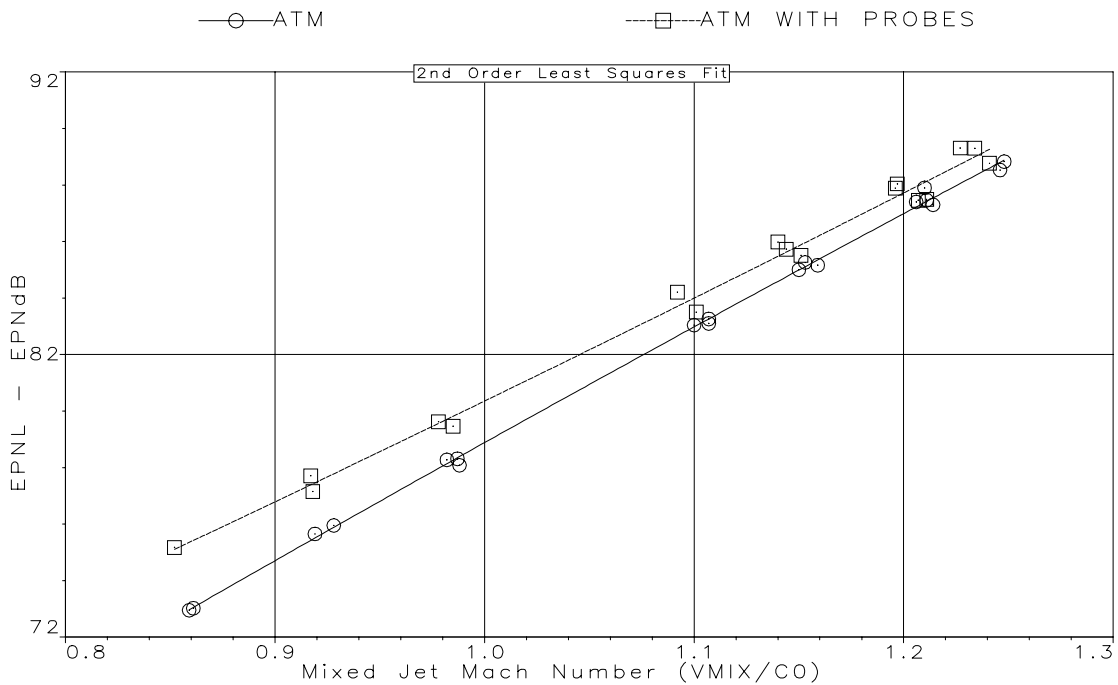
Figure 7.1.1.12: EPNL vs Mixed Jet Mach Number : Effect of Simulated Engine Probes with ATM
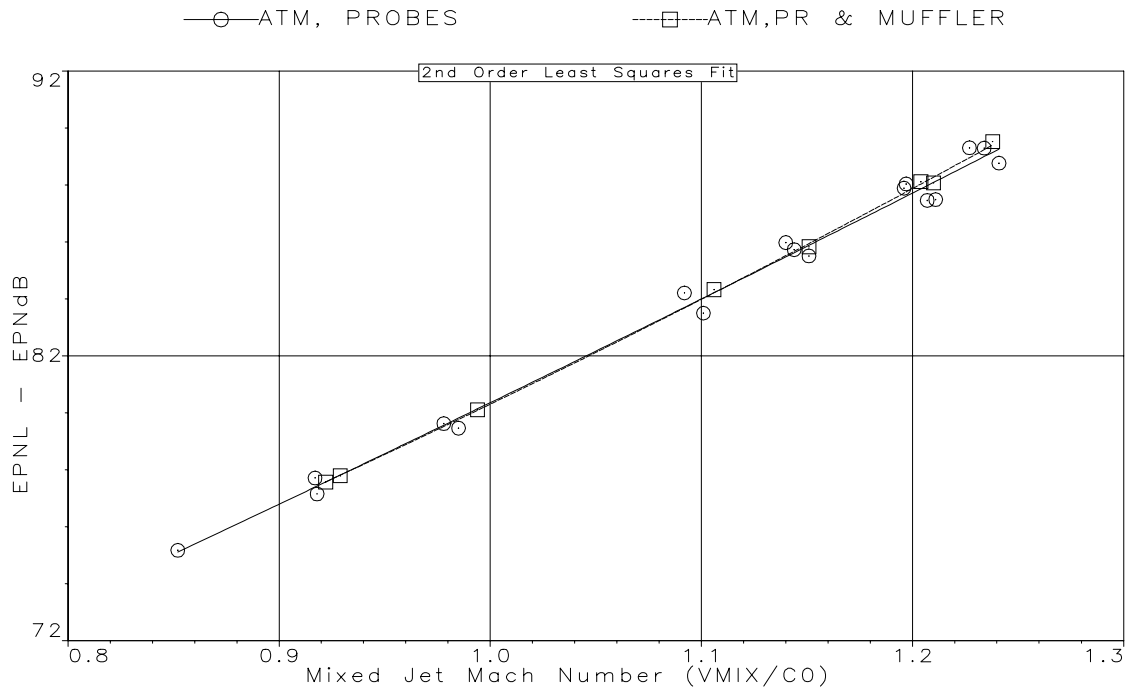
Figure 7.1.1.13: EPNL vs Mixed Jet Mach Number : Effect of Muffler with ATM
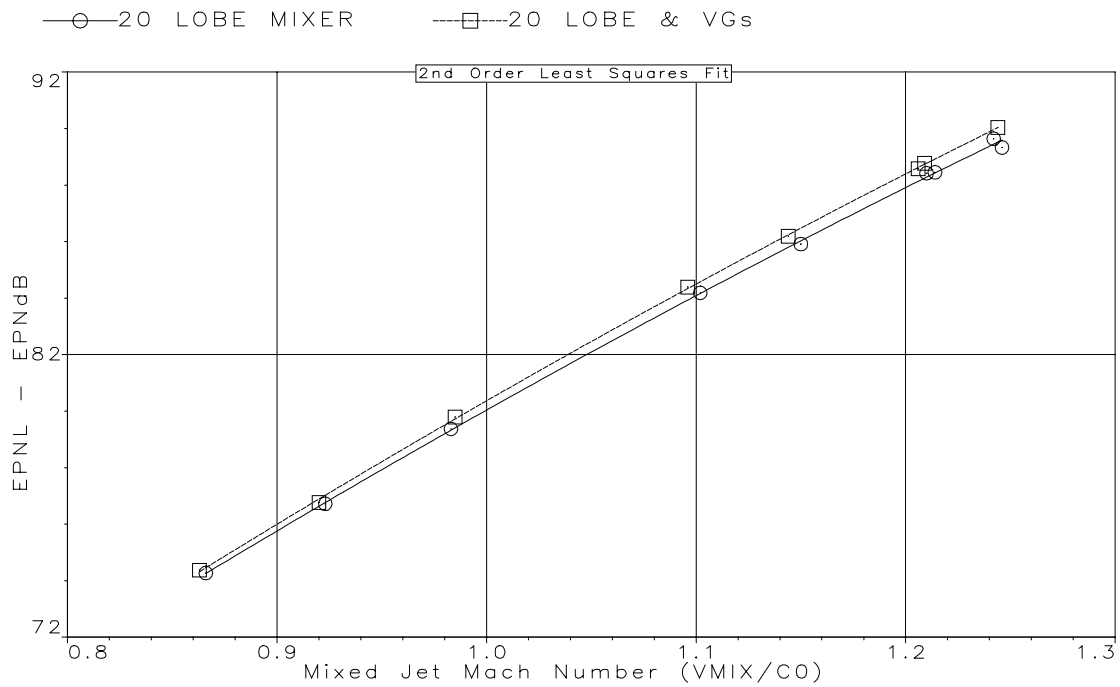
Figure 7.1.1.14: EPNL vs Mixed Jet Mach Number : Effect of Vortex Generators with 20-Lobe Mixer

Figure 7.1.1.15: EPNL vs Mixed Jet Mach Number : Effect of Fan Temperature with ATM

(a) Cutback Power
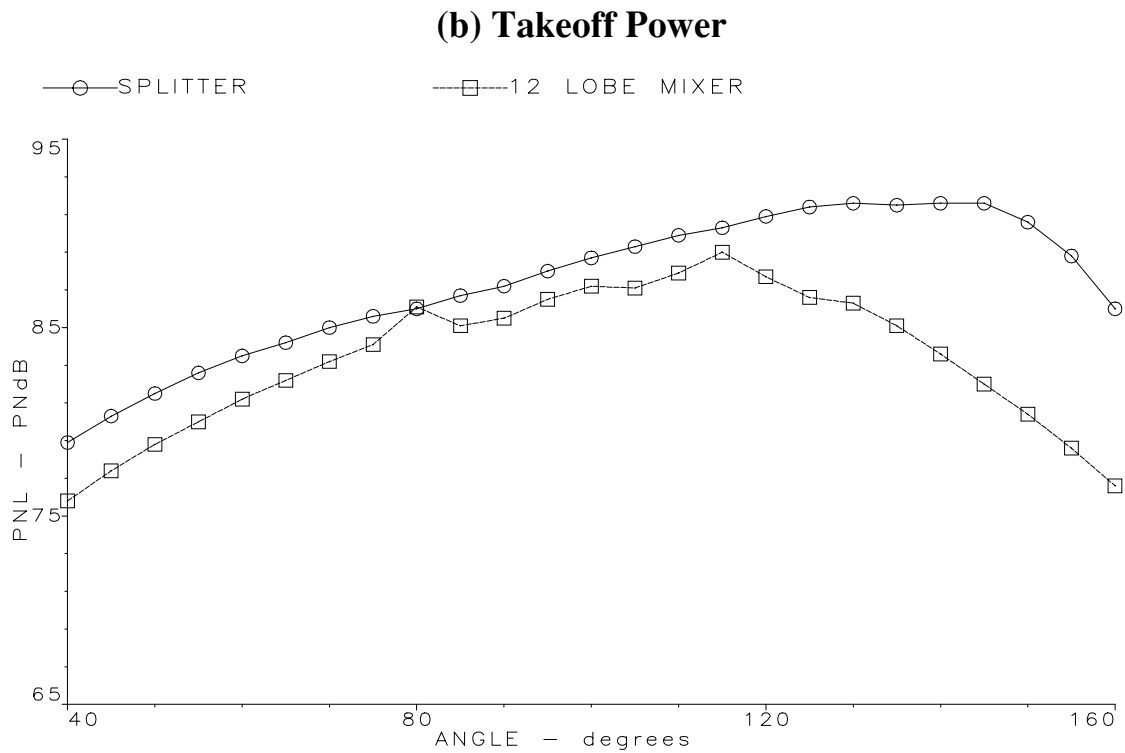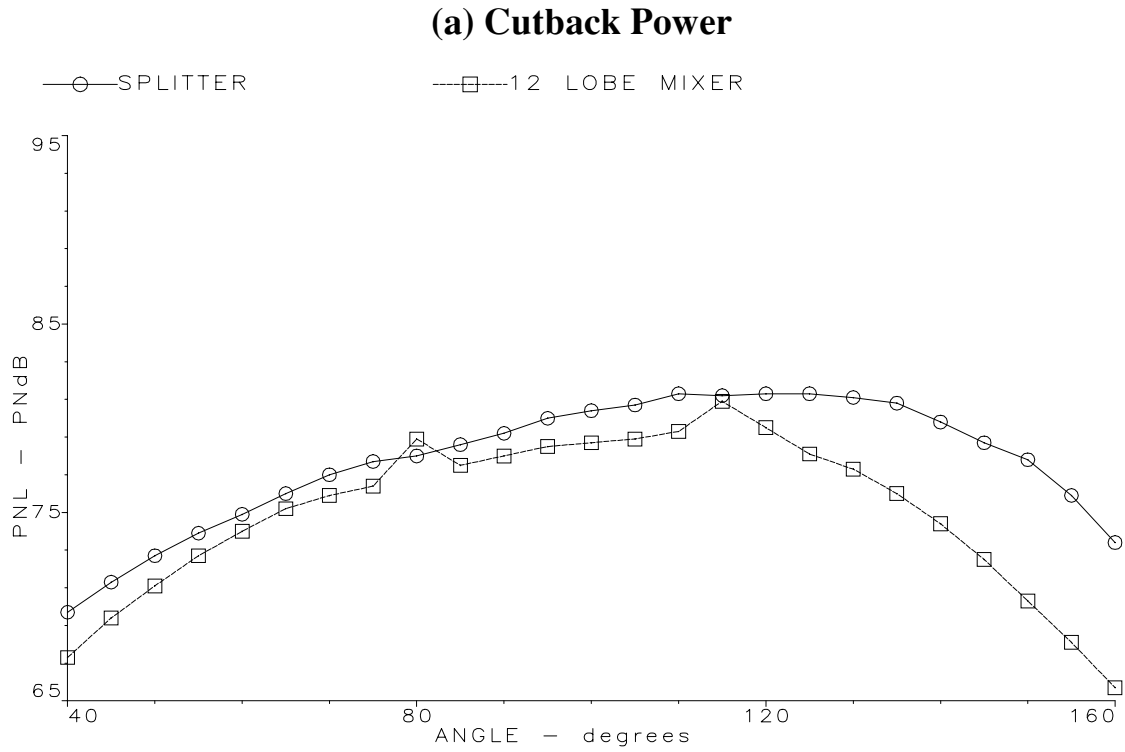
(b) Takeoff Power

Figure 7.1.2.1: PNL vs Angle Comparison of the Splitter and 12-Lobe Mixer at (a) Cutback Power (Cond. 5) and (b) Takeoff Power (Cond. 8)

(a) Cutback Power
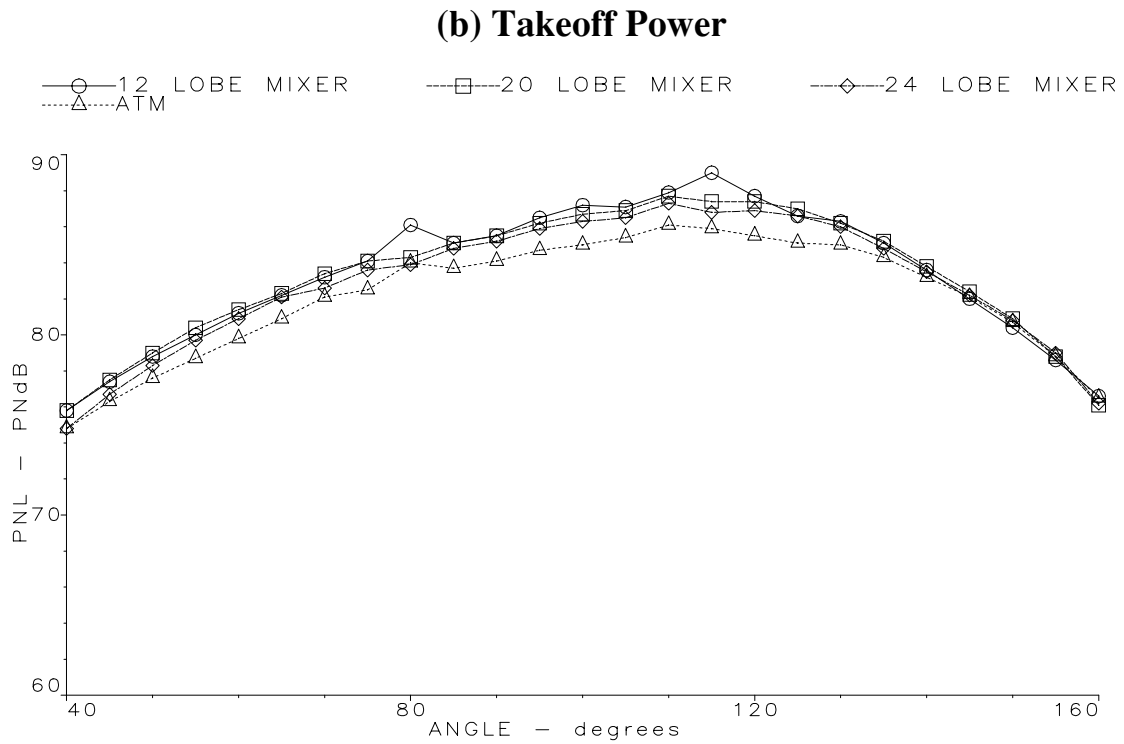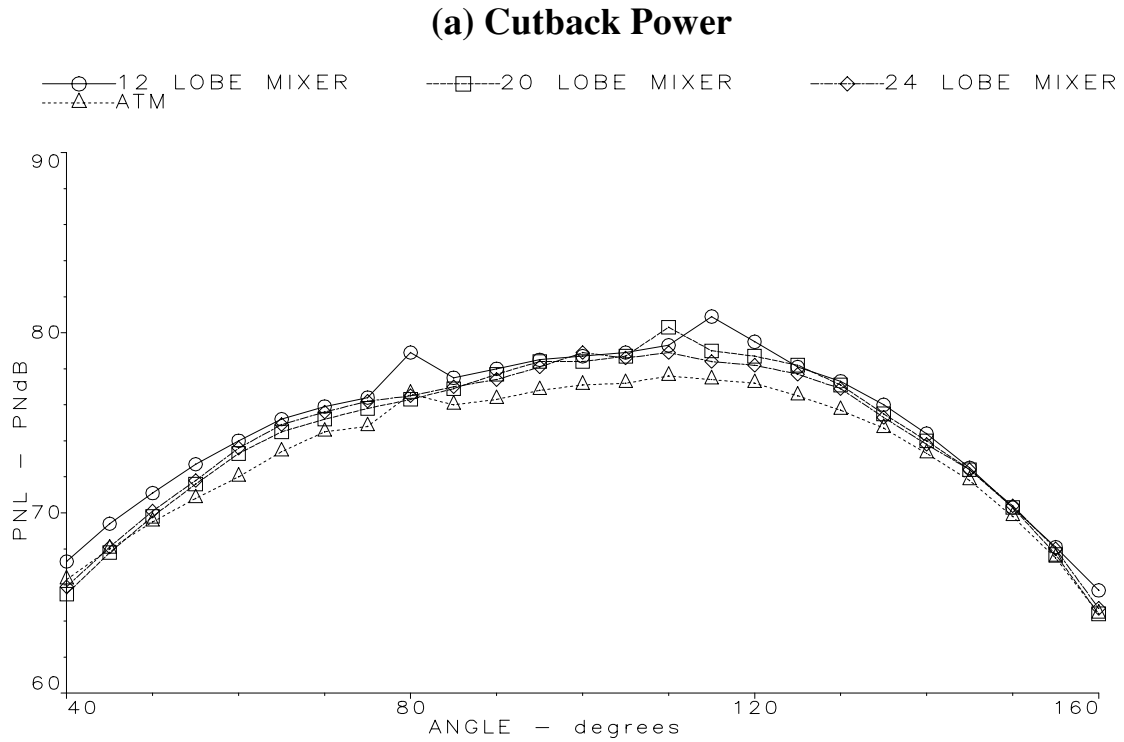
(b) Takeoff Power

Figure 7.1.2.2: PNL vs Angle Comparison of all Mixers (12, 20, 24, and ATM) at (a) Cutback Power (Cond. 5) and (b) Takeoff Power (Cond. 8)

(a) Cutback Power
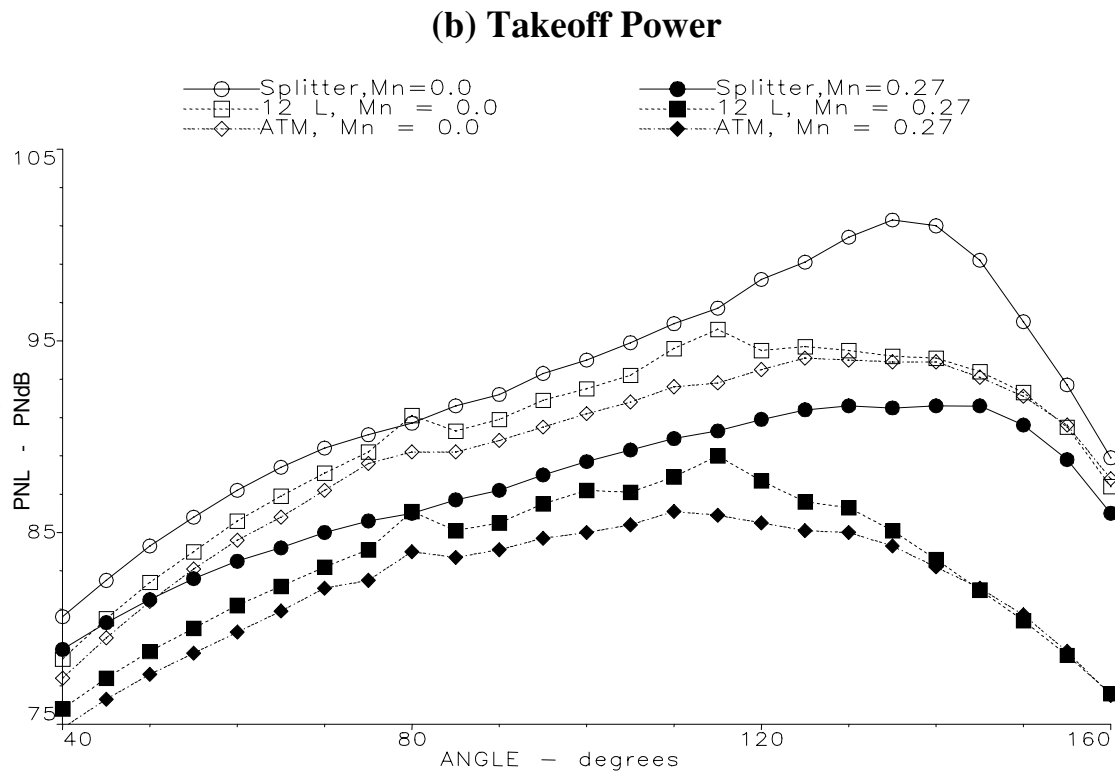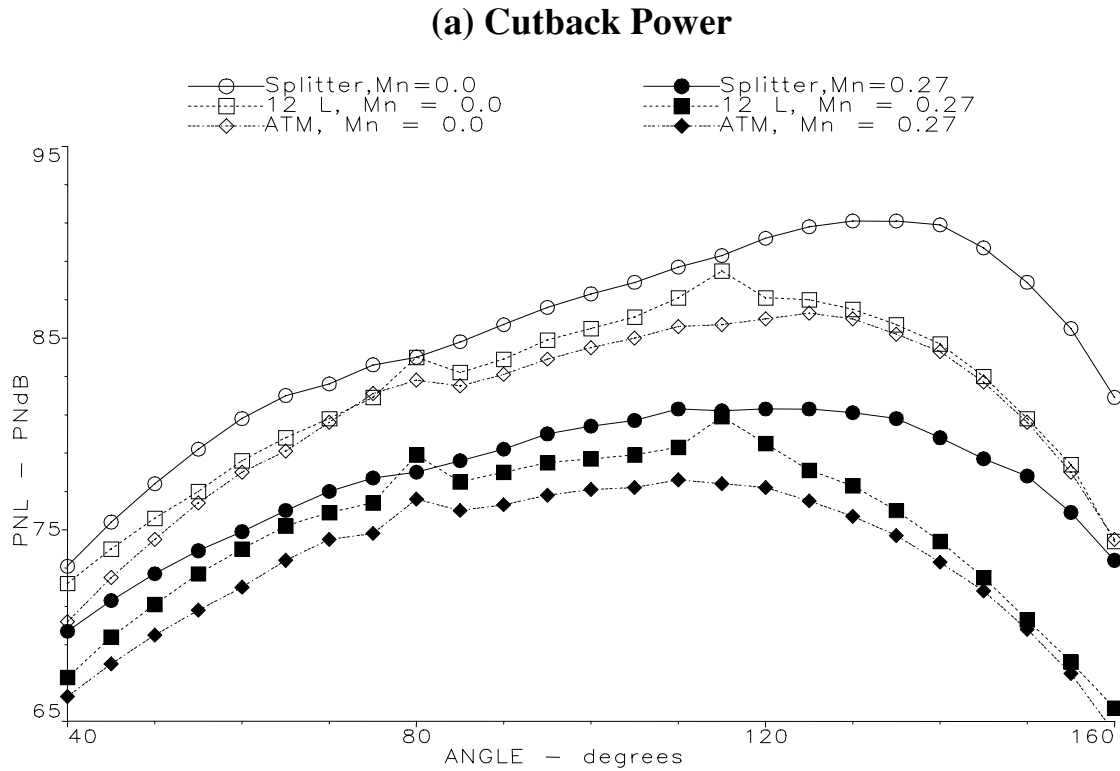
(b) Takeoff Power

Figure 7.1.2.3: PNL vs Angle at (a) Cutback Power (Cond. 5) and (b) Takeoff Power (Cond. 8) : Effect of Flight on Splitter, 12-Lobe Mixer, and ATM

(a) Cutback Power
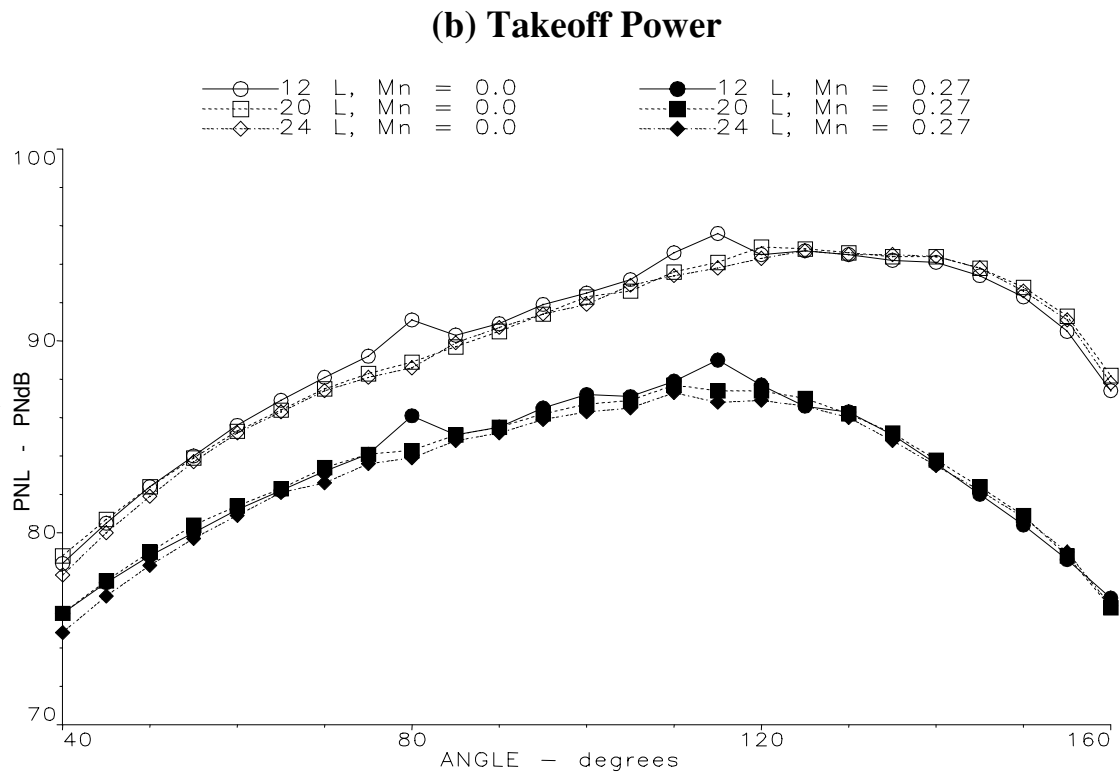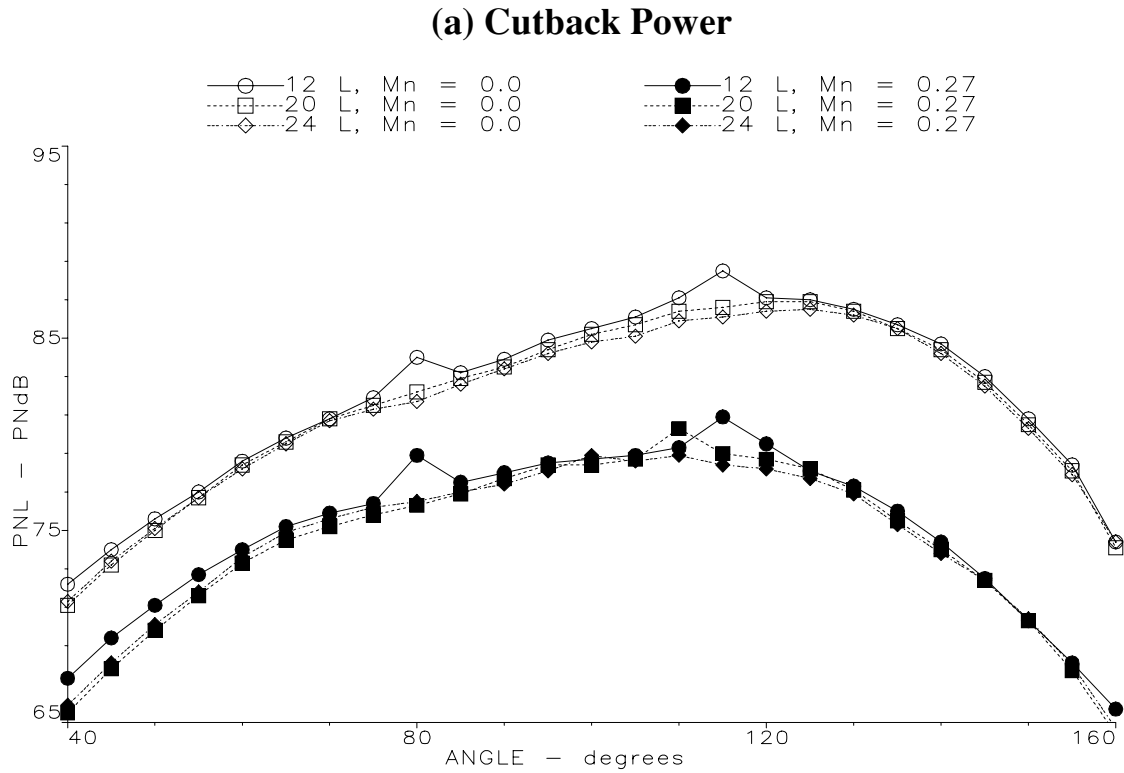
(b) Takeoff Power

Figure 7.1.2.4: PNL vs Angle at (a) Cutback Power (Cond. 5) and (b) Takeoff Power (Cond. 8) : Effect of Flight on 12, 20, and 24-Lobe Mixers

(a) Cutback Power
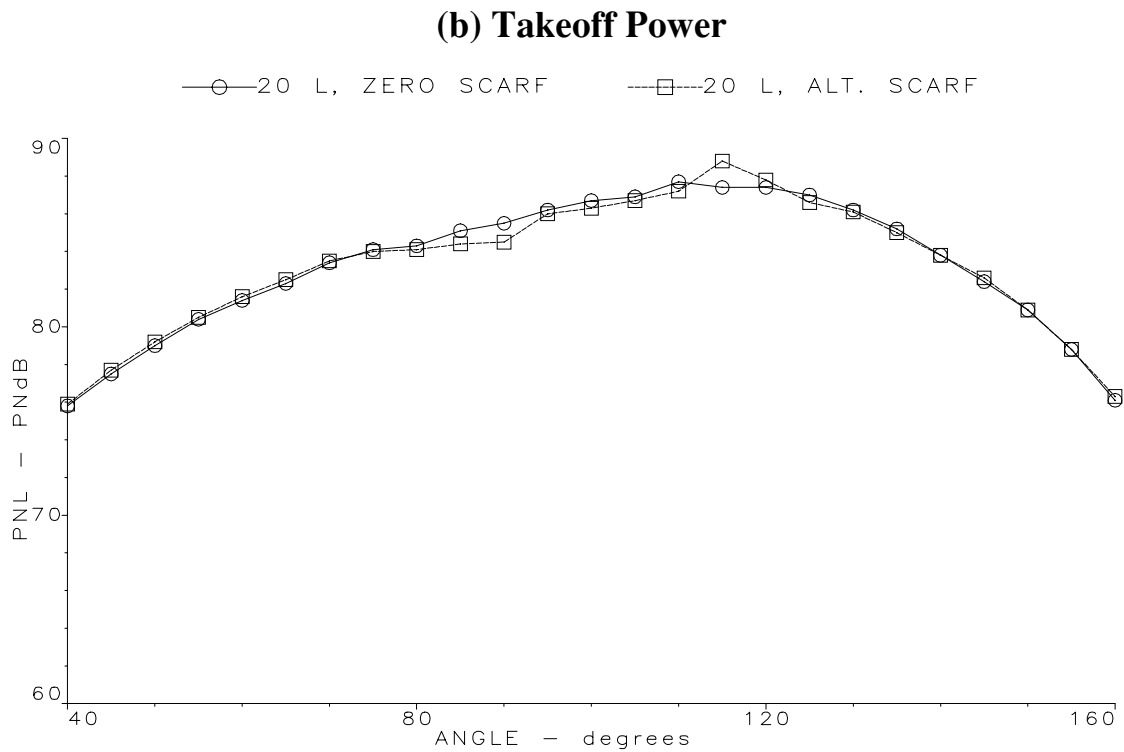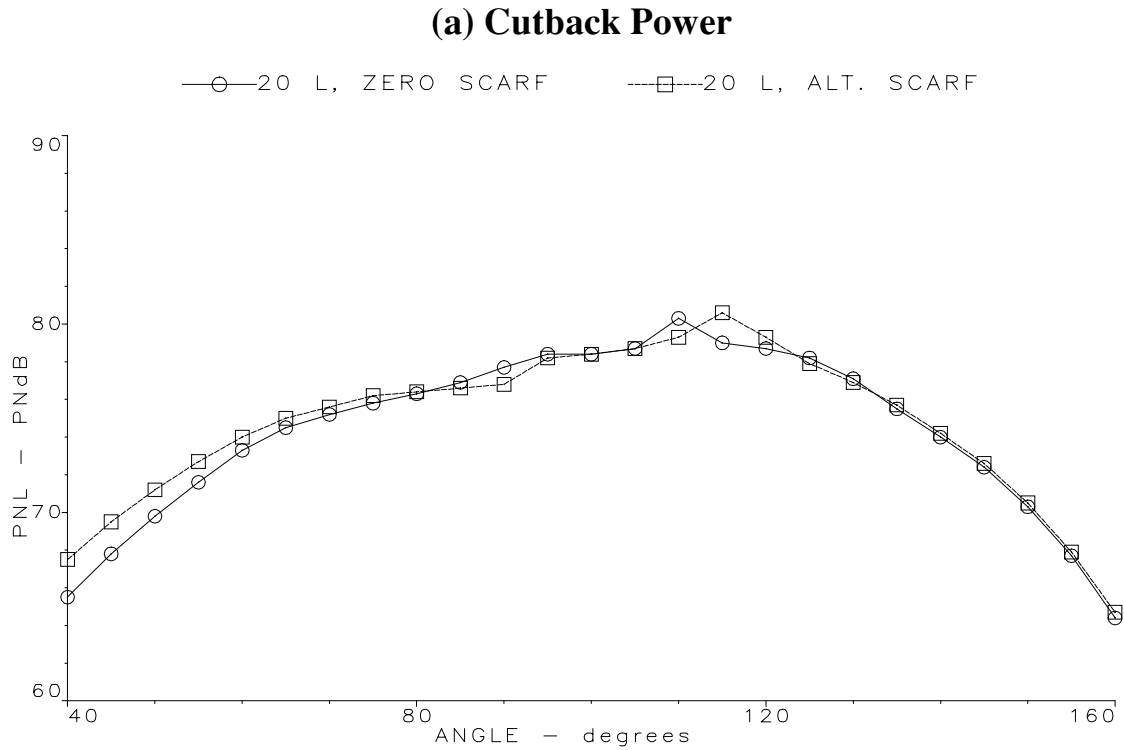
(b) Takeoff Power

Figure 7.1.2.5: PNL vs Angle Comparison of Zero and Alternating Scarf Angle (0/12 deg.) on 20-Lobe Mixer at (a) Cutback Power (Cond. 5) and (b) Takeoff Power (Cond. 8)

(a) Cutback Power
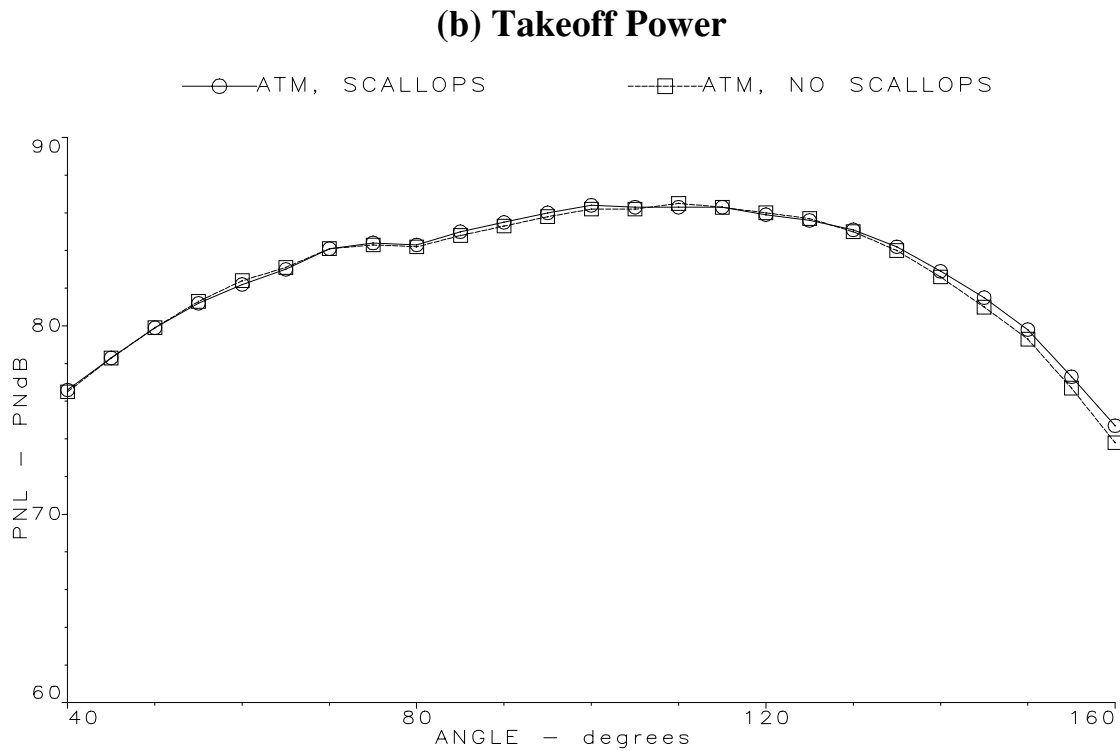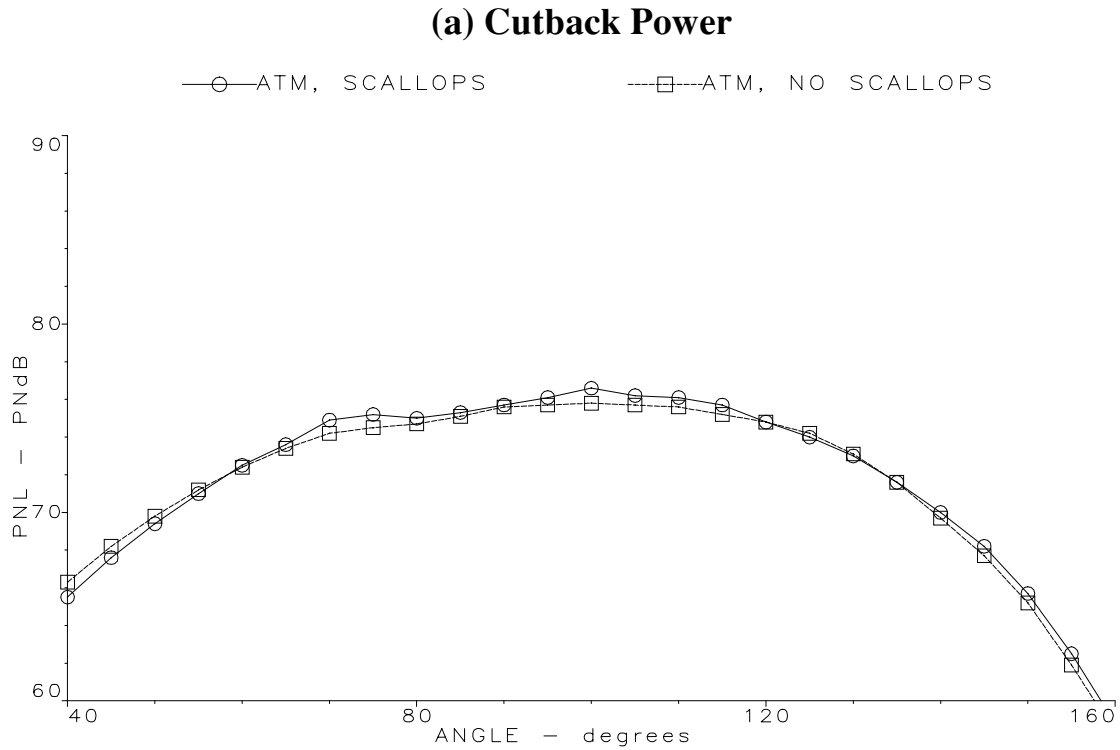
(b) Takeoff Power

**Figure 7.1.2.6: PNL vs Angle at (a) Cutback Power (Cond. 5) and (b) Takeoff Power (Cond. 8) :
Effect of Lobe Scallops on ATM**

(a) Cutback Power
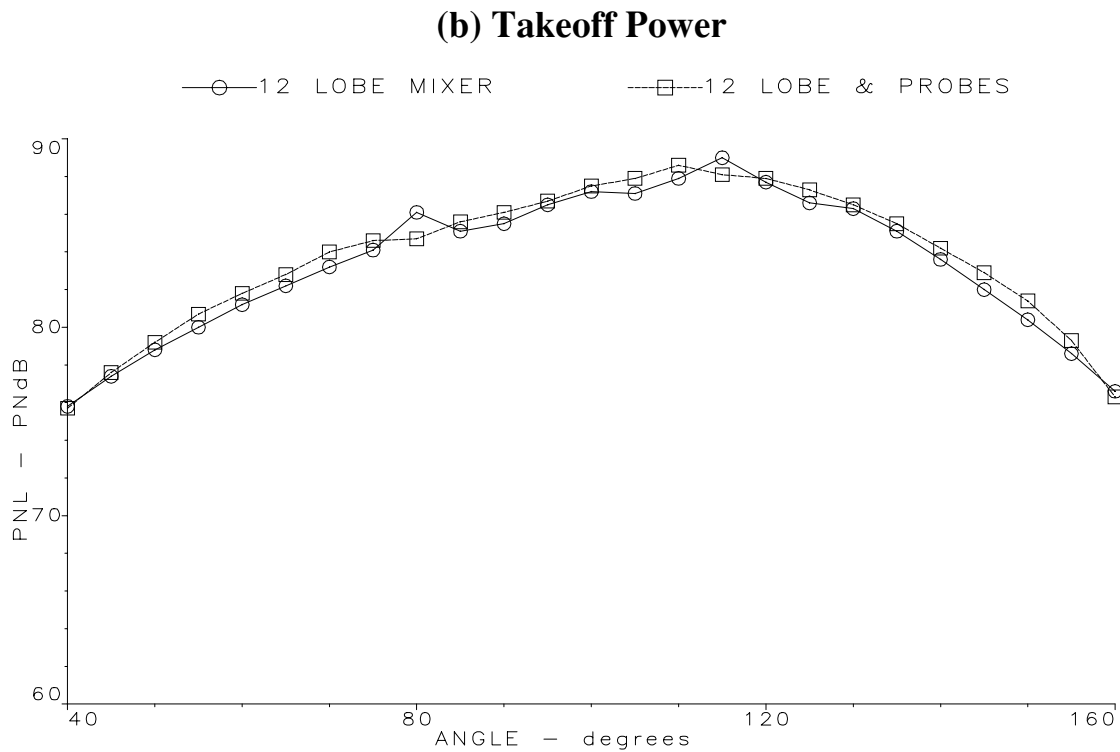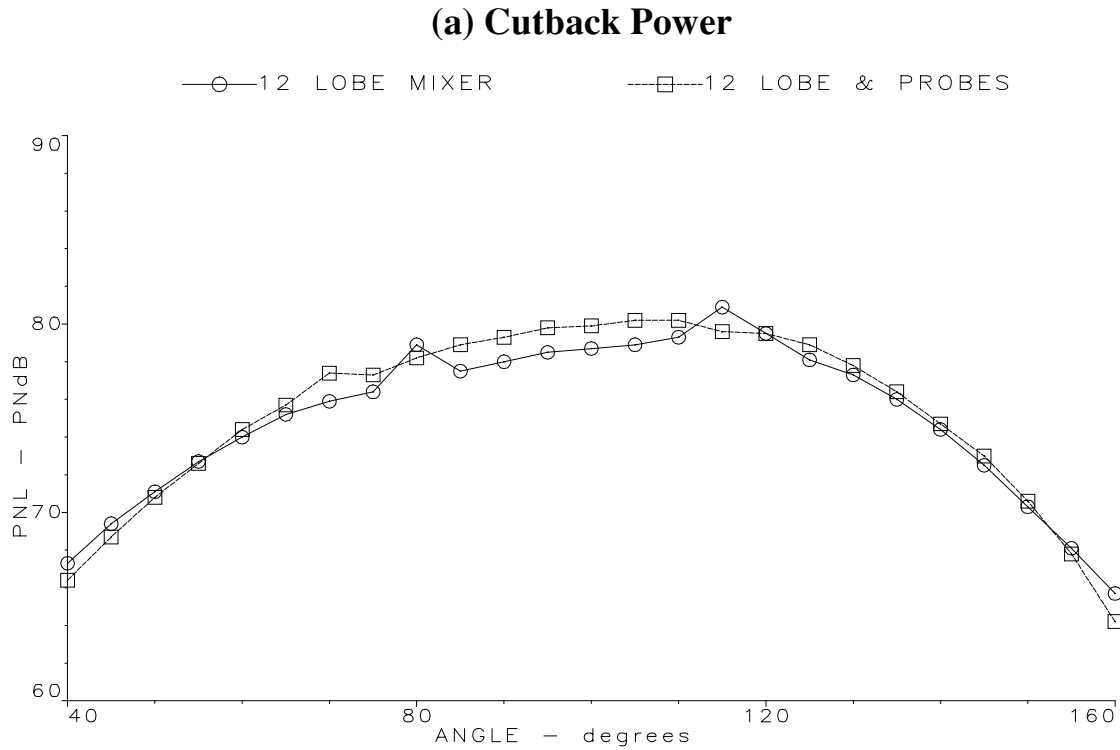
(b) Takeoff Power

Figure 7.1.2.7: PNL vs Angle at (a) Cutback Power (Cond. 5) and (b) Takeoff Power (Cond. 8) :
Effect of Simulated Engine Probes with 12-Lobe Mixer

(a) Cutback Power
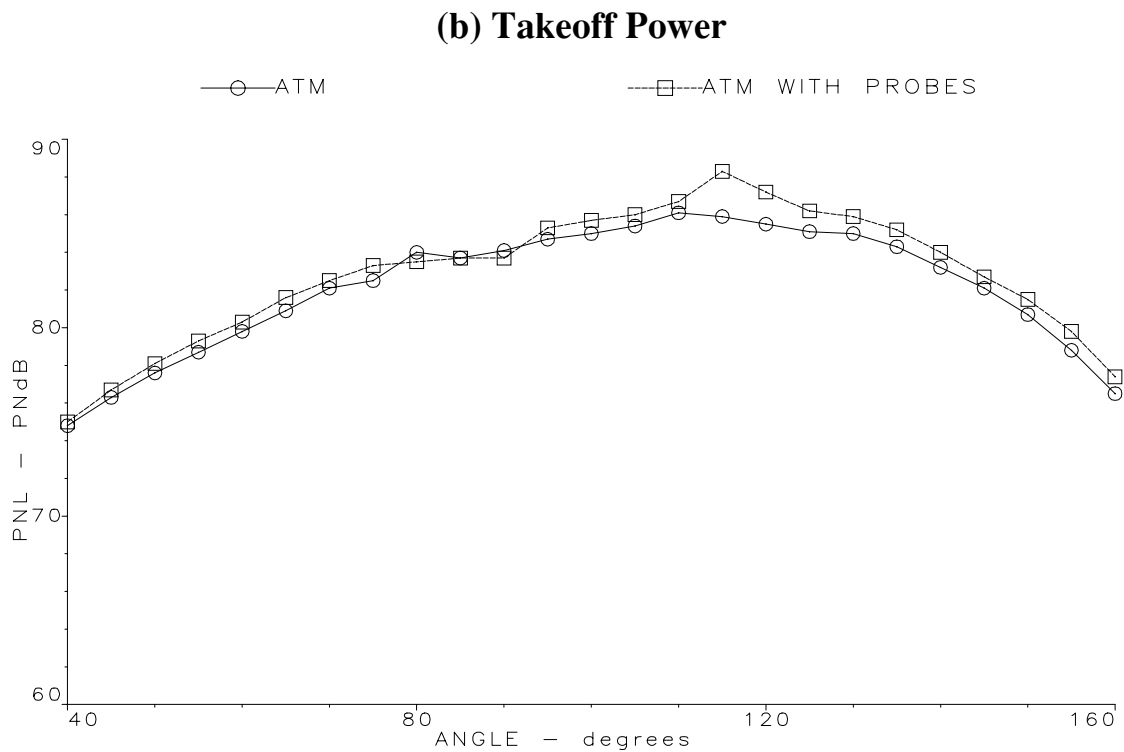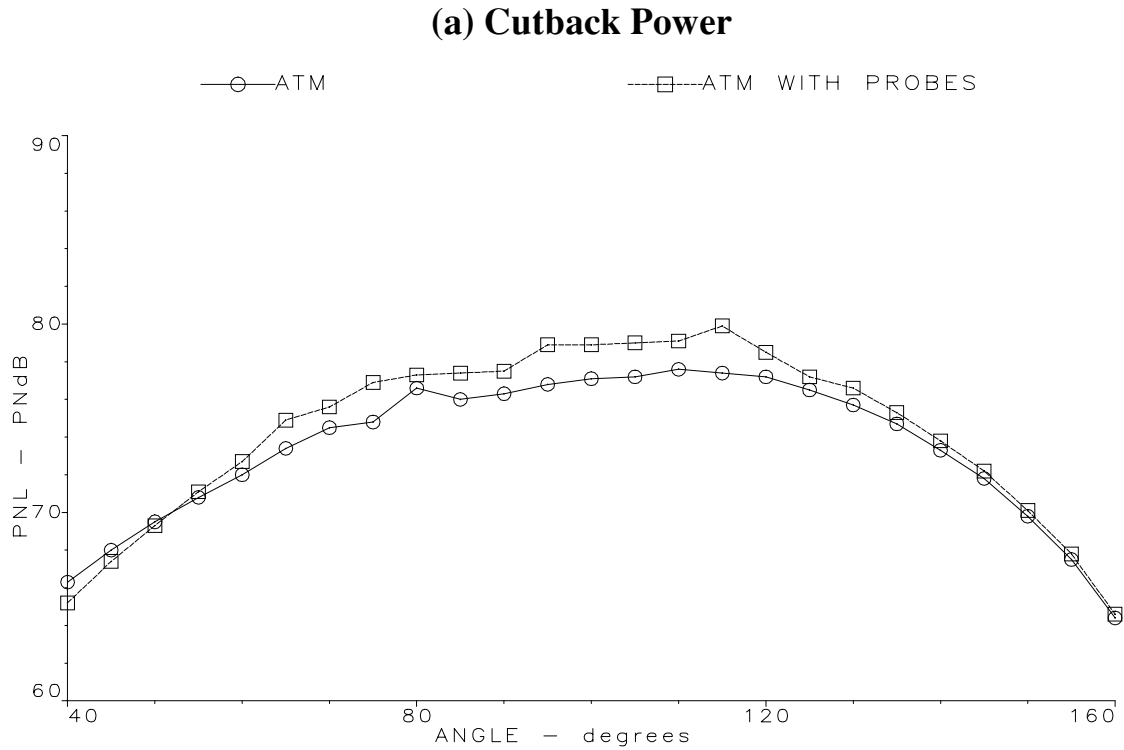
(b) Takeoff Power

Figure 7.1.2.8: PNL vs Angle at (a) Cutback Power (Cond. 5) and (b) Takeoff Power (Cond. 8) : Effect of Simulated Engine Probes with ATM

(a) Cutback Power
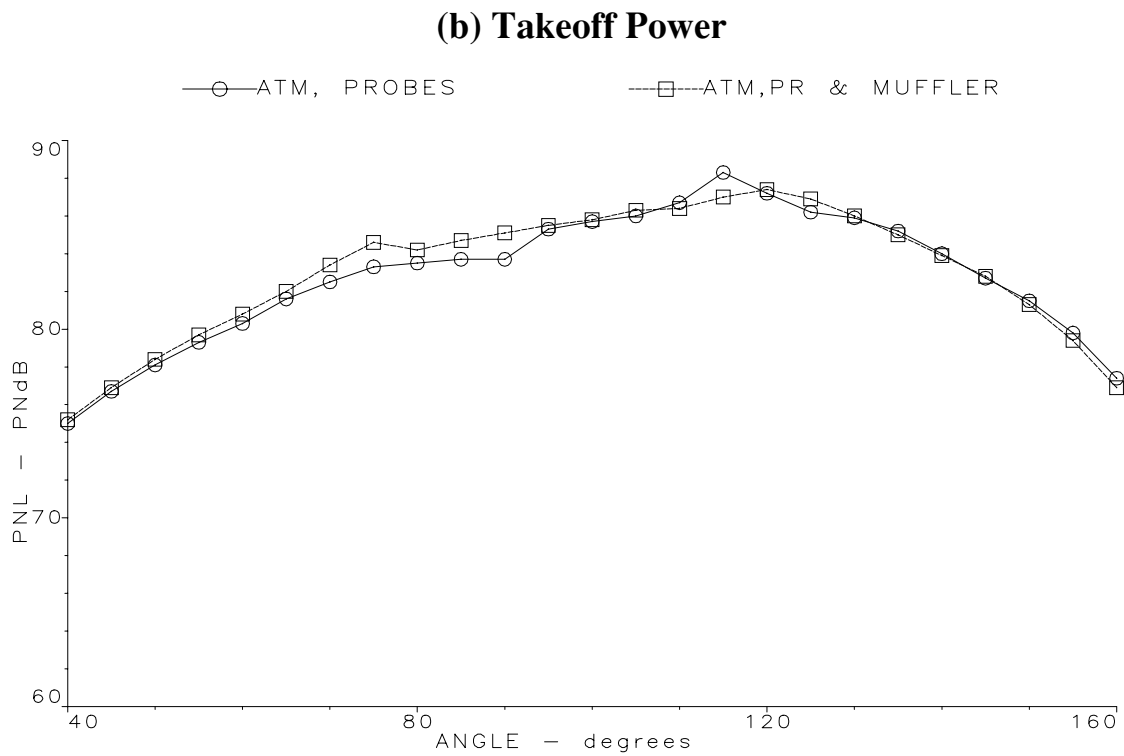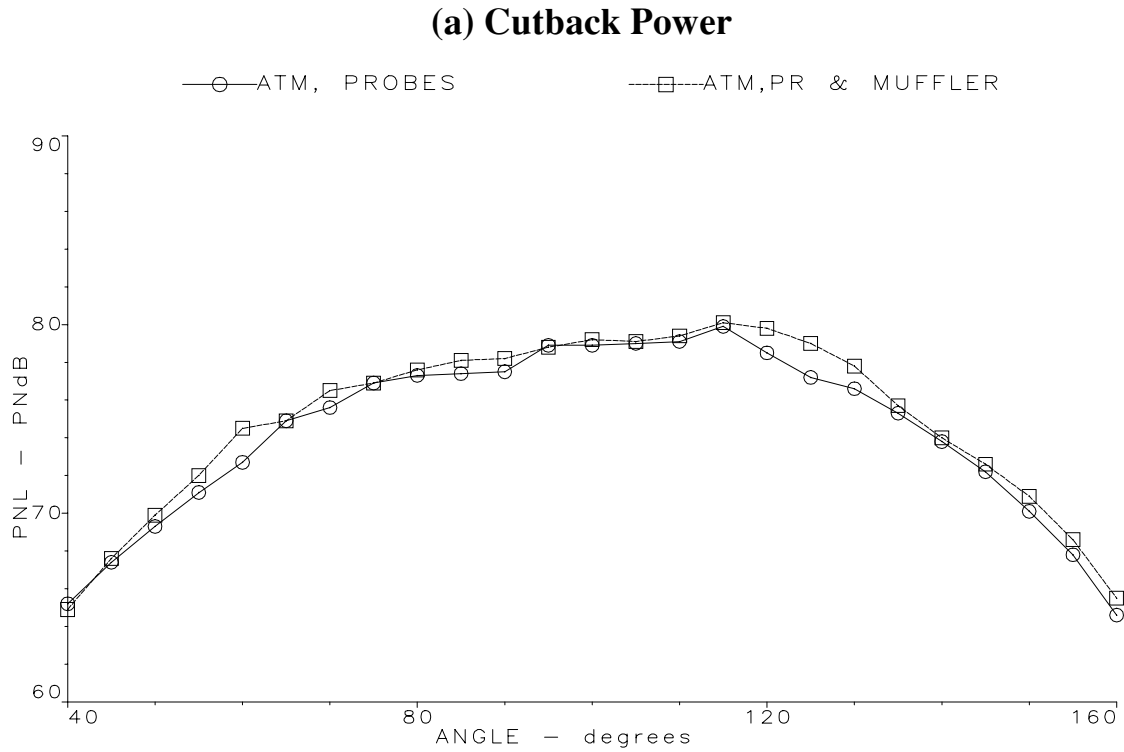
(b) Takeoff Power

Figure 7.1.2.9: PNL vs Angle at (a) Cutback Power (Cond. 5) and (b) Takeoff Power (Cond. 8) : Effect of Muffler with ATM

(a) Cutback Power
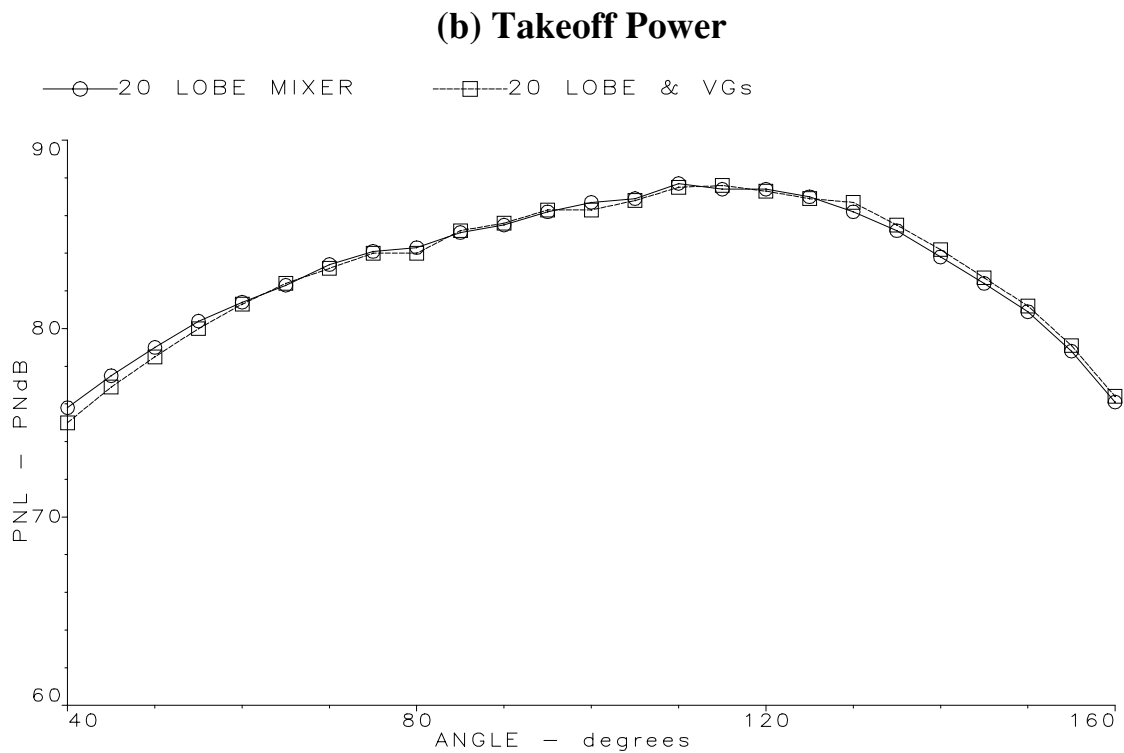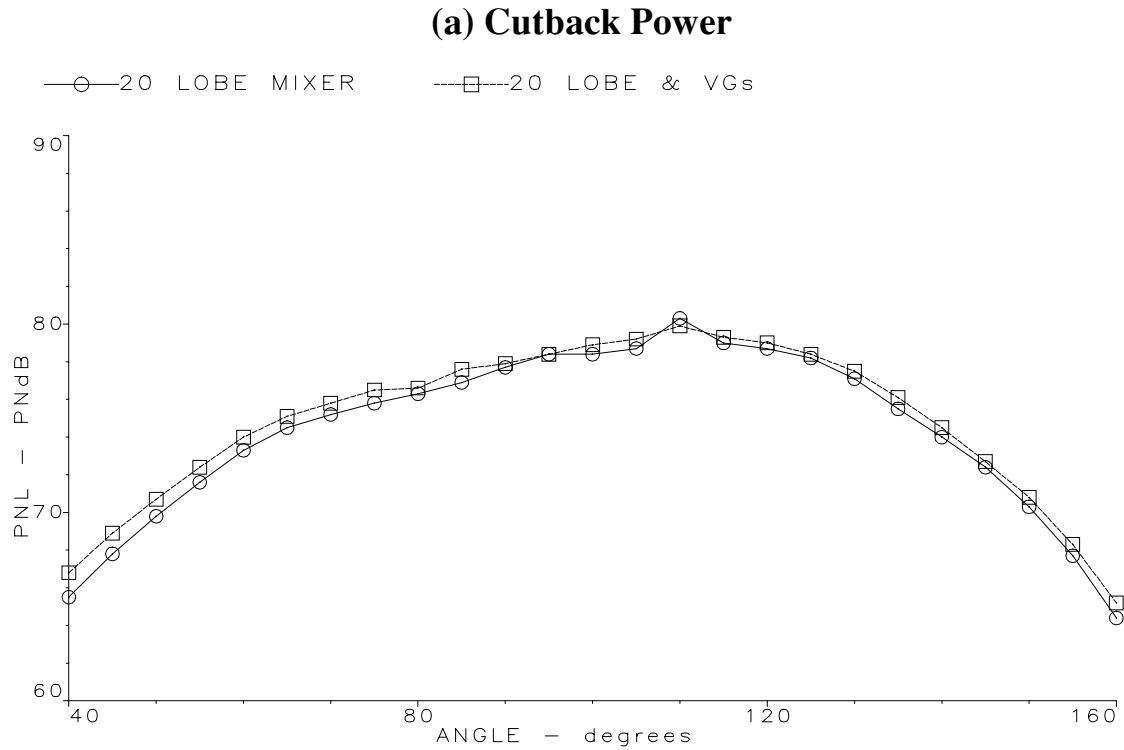
(b) Takeoff Power

**Figure 7.1.2.10: PNL vs Angle at (a) Cutback Power (Cond. 5) and (b) Takeoff Power (Cond. 8) :
Effect of Vortex Generators with 20-Lobe Mixer**

(a) Cutback Power
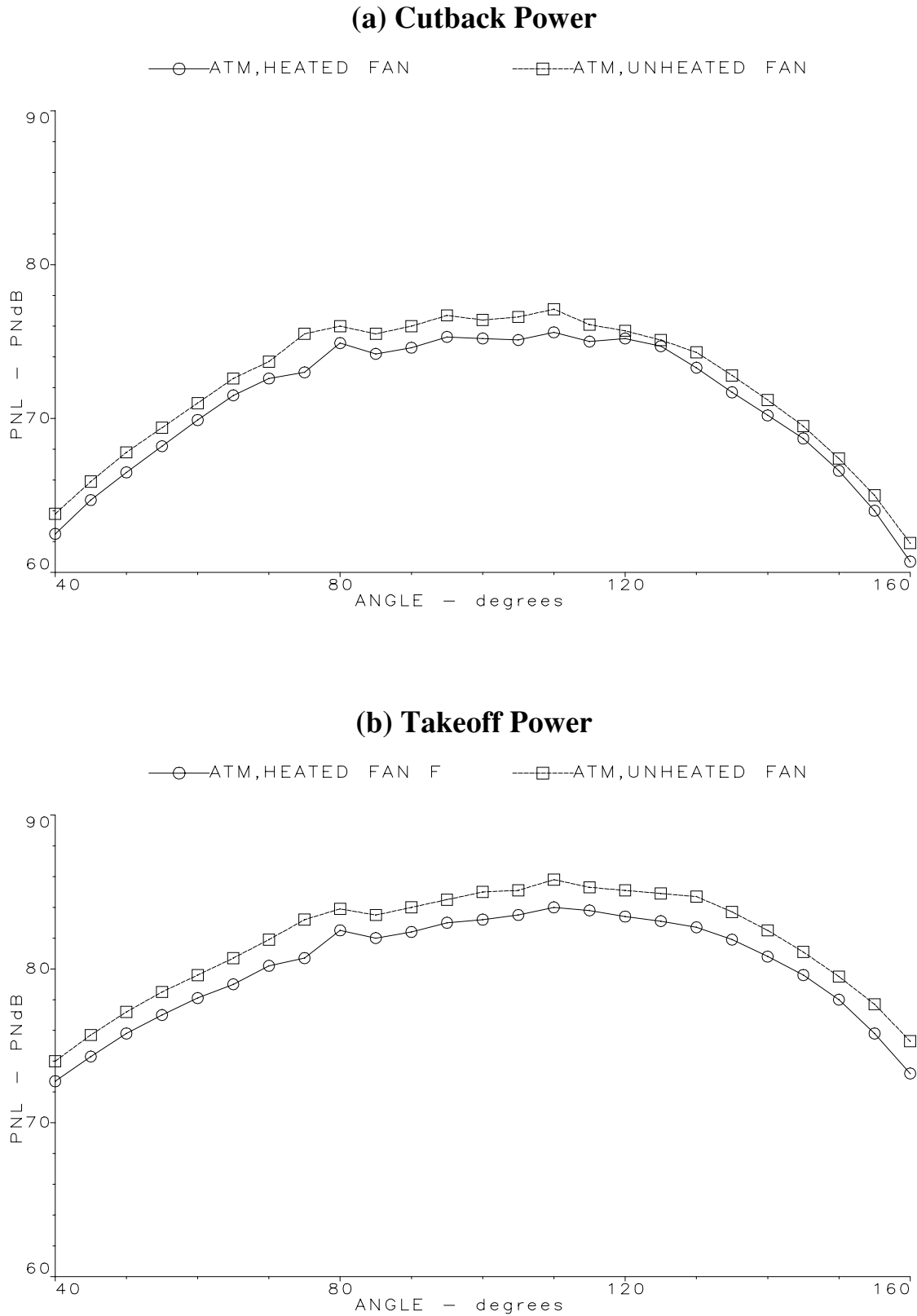
(b) Takeoff Power

Figure 7.1.2.11: PNL vs Angle at (a) Cutback Power (Cond. 5) and (b) Takeoff Power (Cond. 8) :
Effect of Fan Temperature with ATM
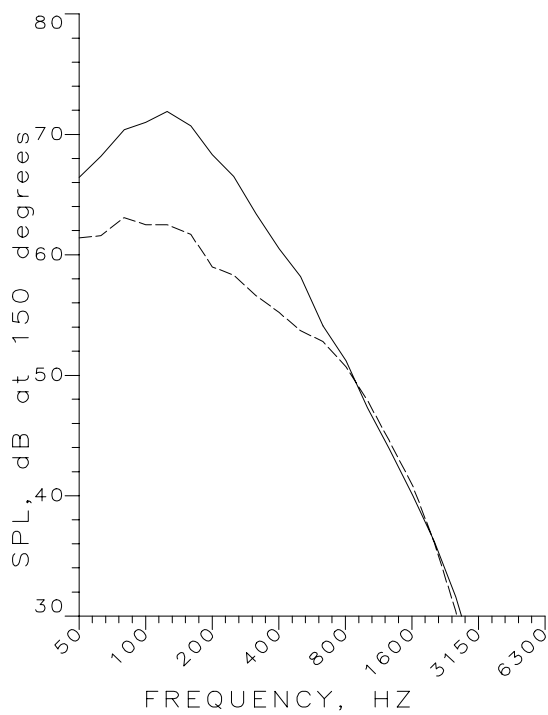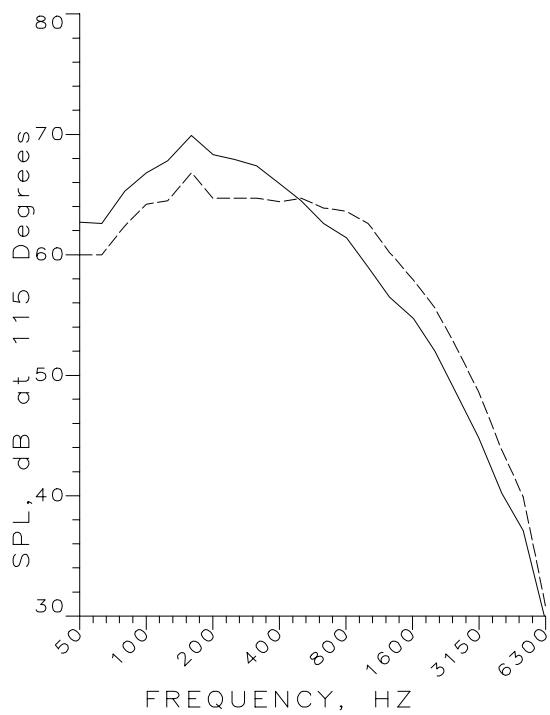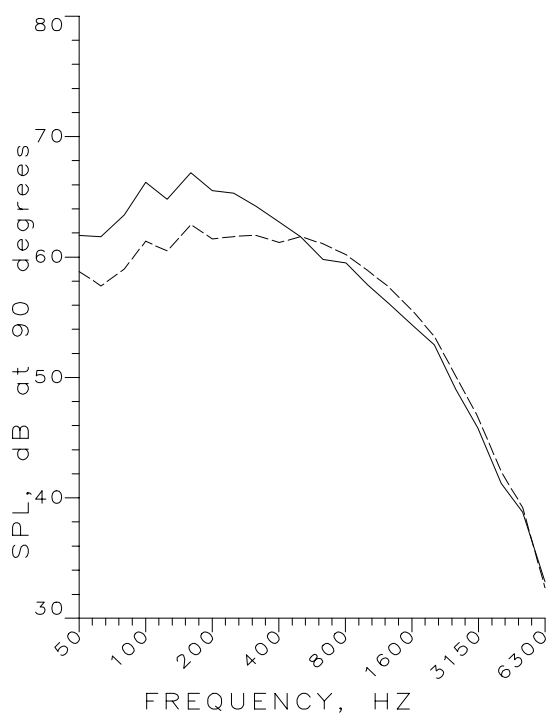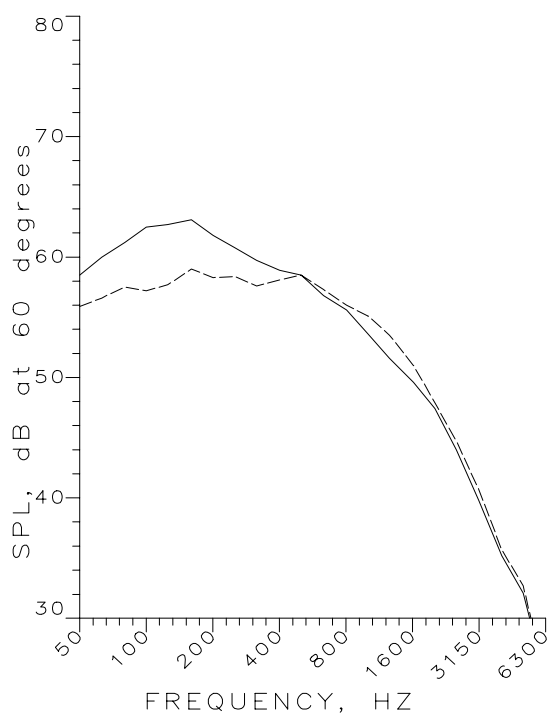
Figure 7.1.3.1: SPL vs Frequency Comparison of Splitter and 12-Lobe Mixer for Angles 60, 90, 115, and 150 degrees at Cutback Power (Condition 5)
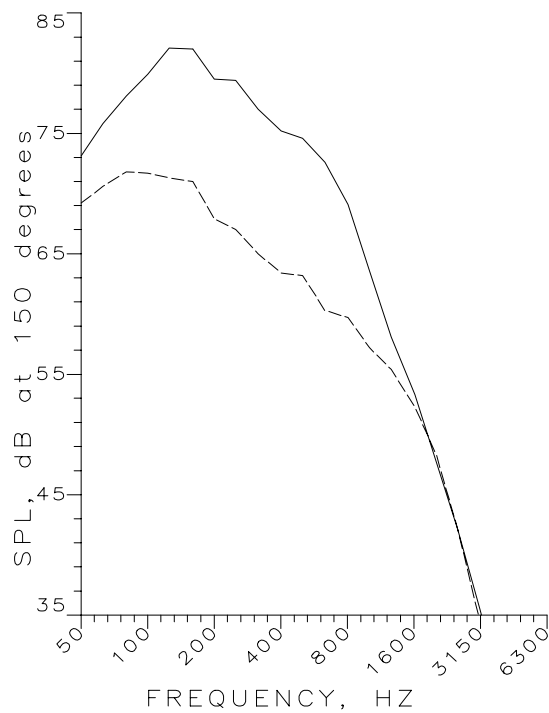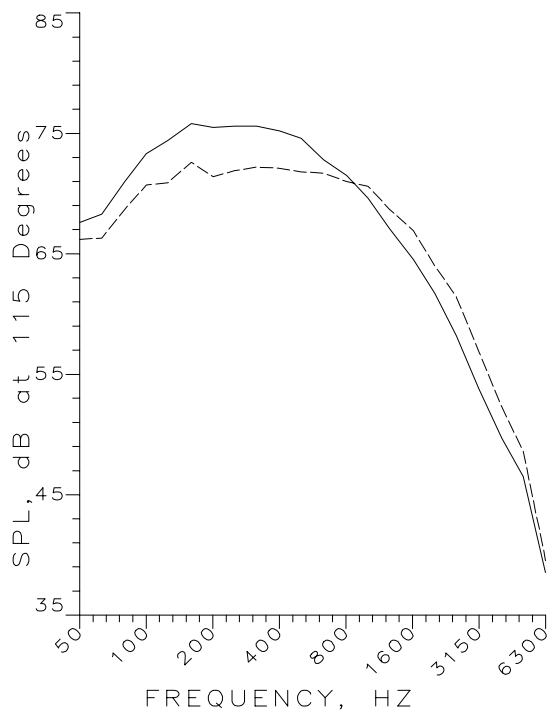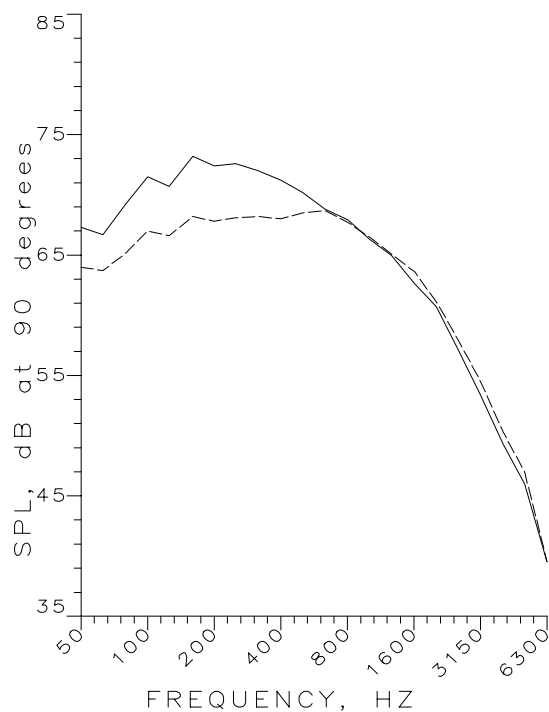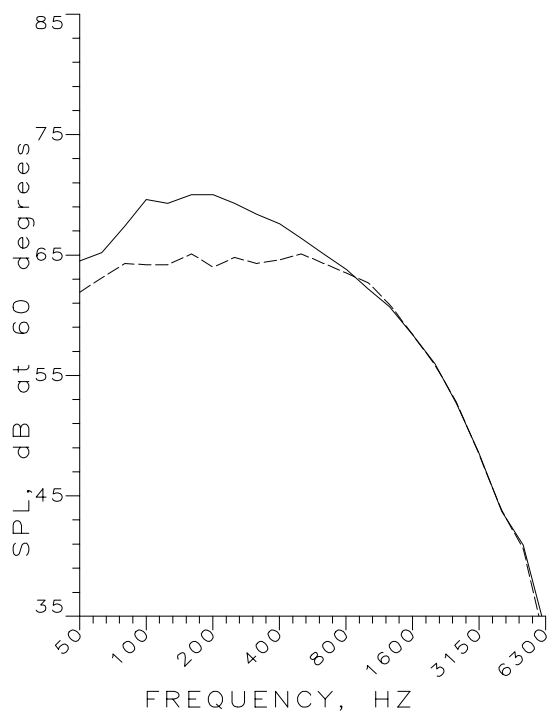
Figure 7.1.3.2: SPL vs Frequency Comparison of Splitter and 12-Lobe Mixer for Angles 60, 90, 115, and 150 degrees at Takeoff Power (Condition 8)
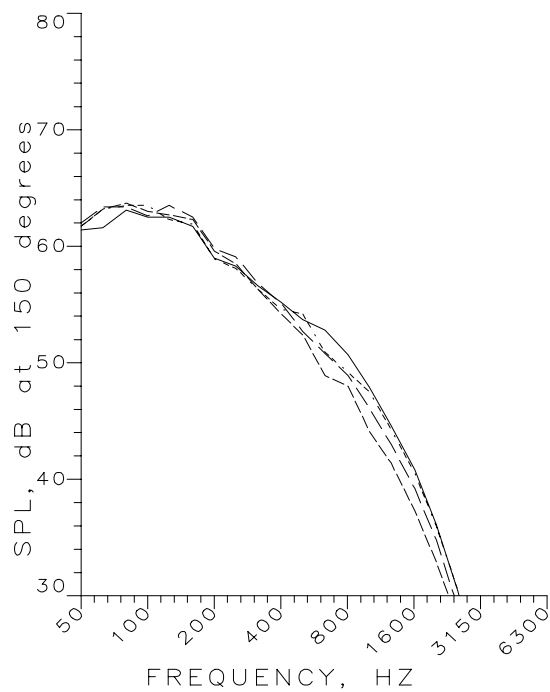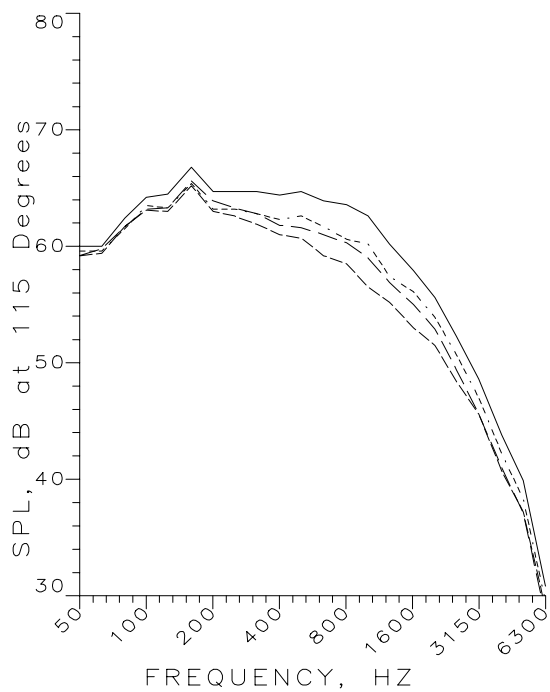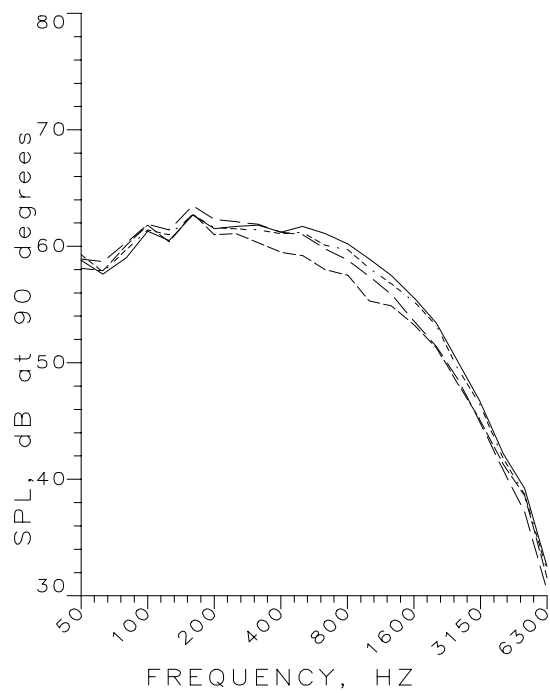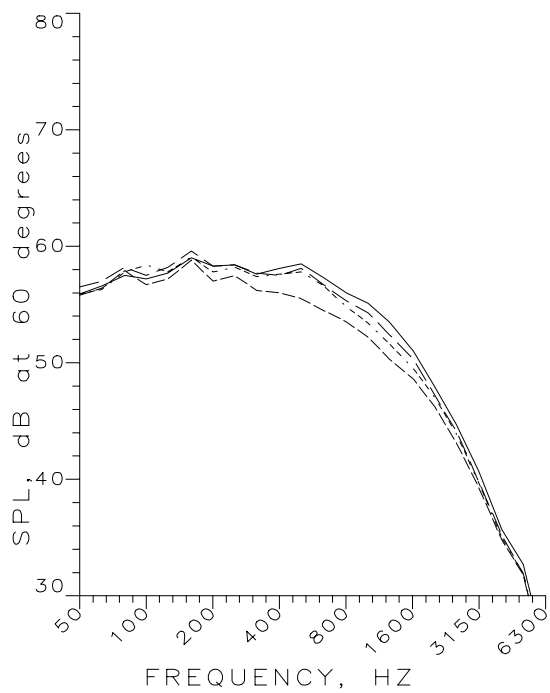
Figure 7.1.3.3: SPL vs Frequency Comparison of All Mixers (12, 20, 24-Lobe and ATM) for Angles 60, 90, 115, and 150 degrees at Cutback Power (Condition 5)
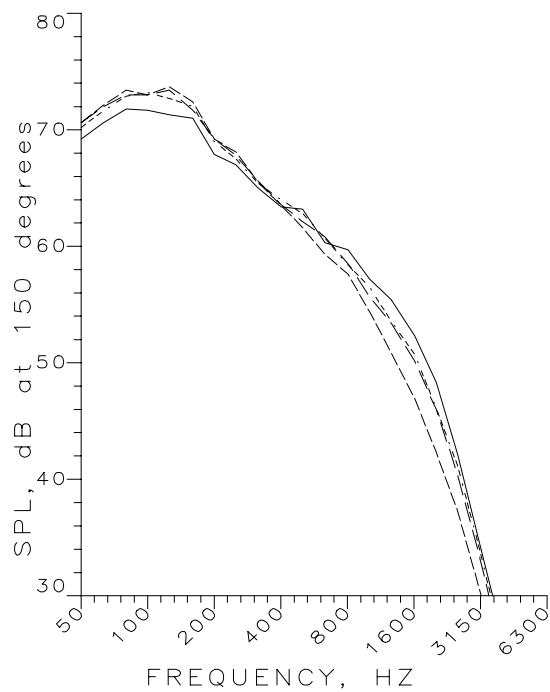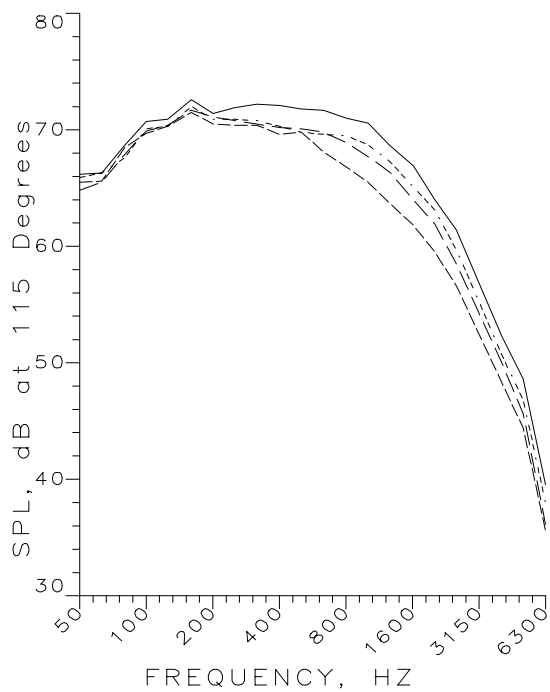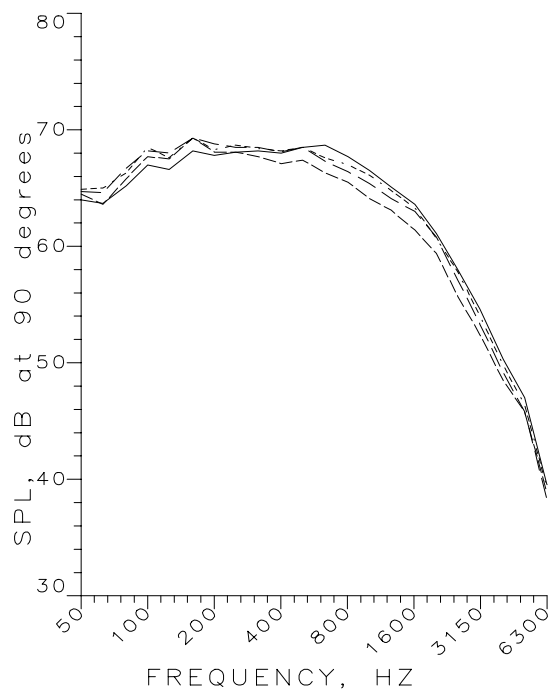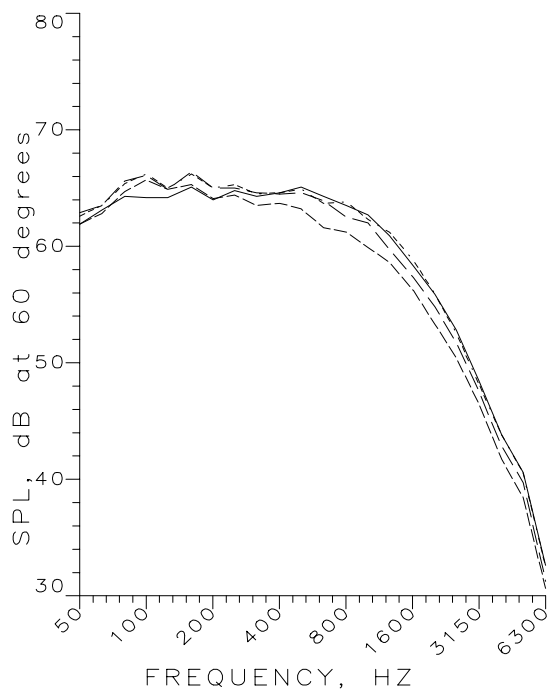
Figure 7.1.3.4: SPL vs Frequency Comparison of All Mixers (12, 20, 24-Lobe and ATM) for Angles 60, 90, 115, and 150 degrees at Takeoff Power (Condition 8)
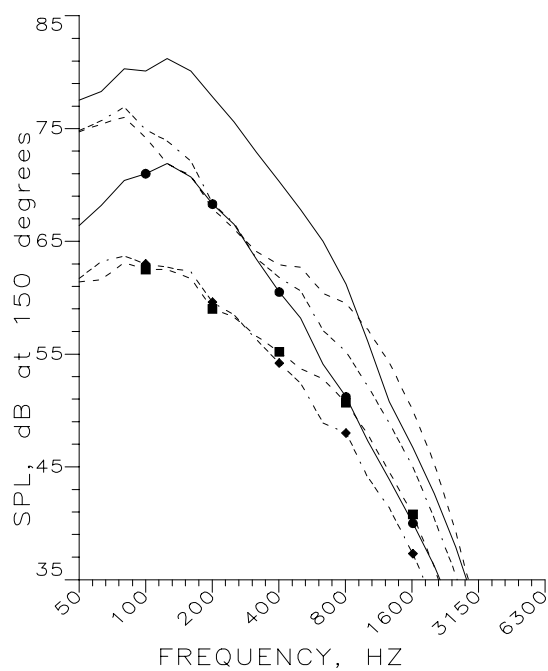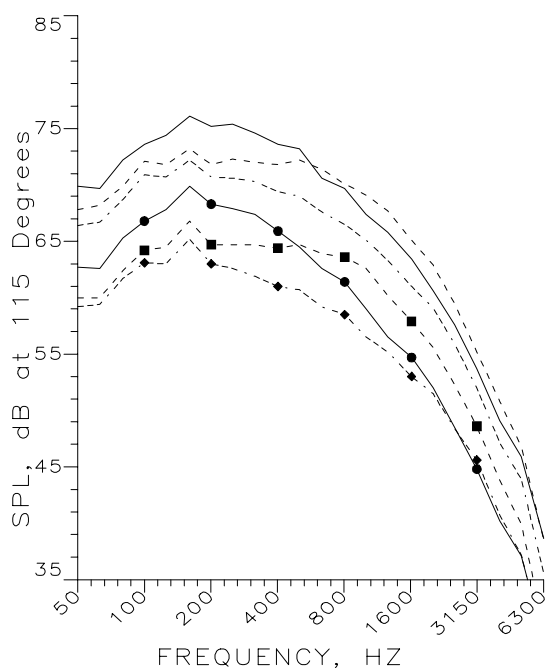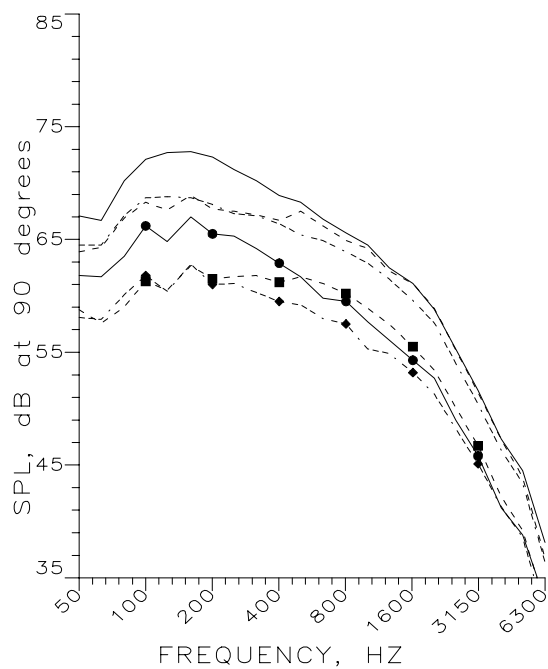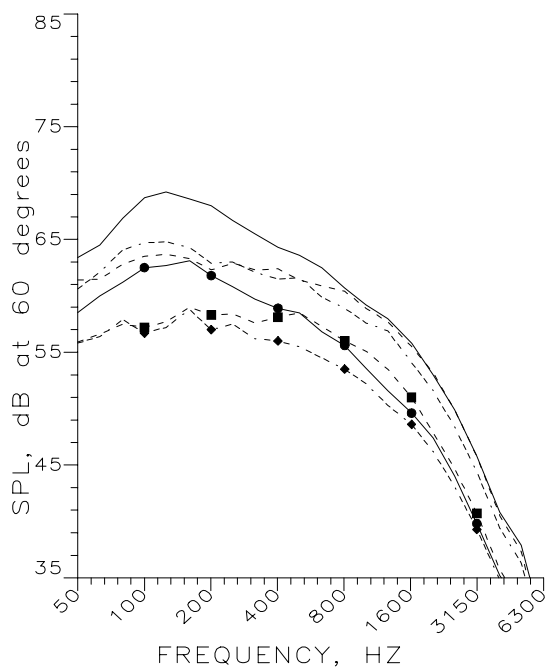
Figure 7.1.3.5: SPL vs Frequency Comparison of Static and Flight Conditions for Splitter, 12-Lobe, and ATM at Angles 60, 90, 115, and 150 degrees at Cutback Power (Cond. 5)
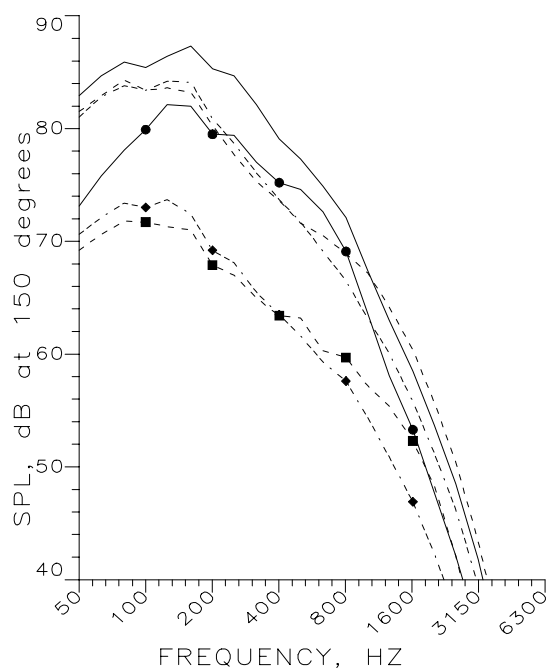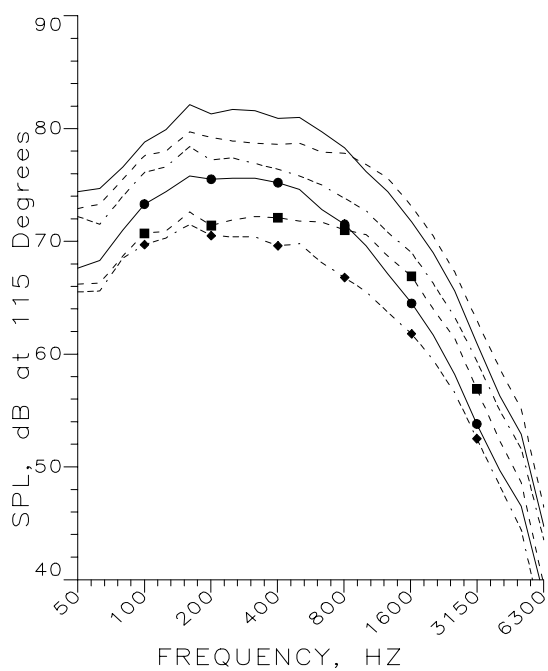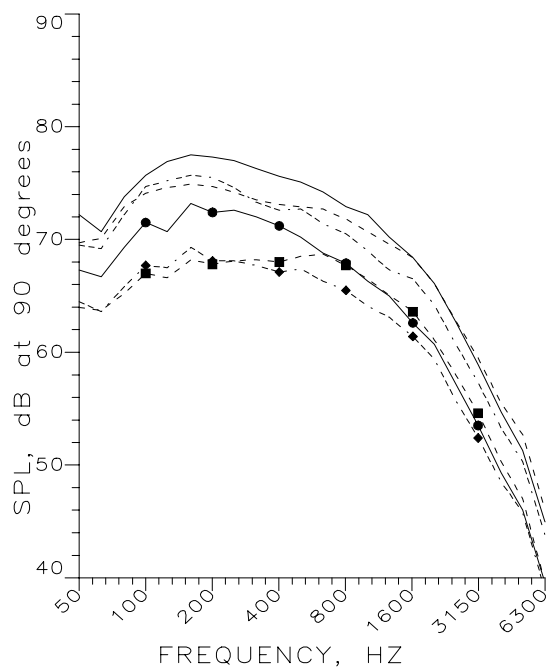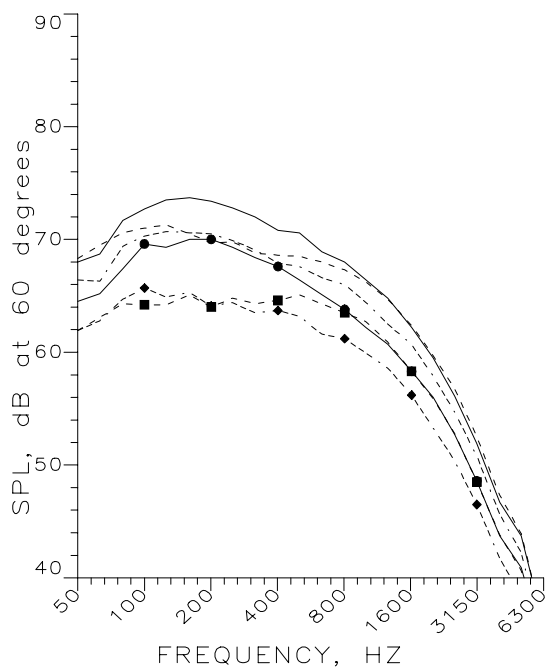
Figure 7.1.3.6: SPL vs Frequency Comparison of Static and Flight Conditions for Splitter, 12-Lobe, and ATM at Angles 60, 90, 115, and 150 degrees at Takeoff Power (Cond. 8)
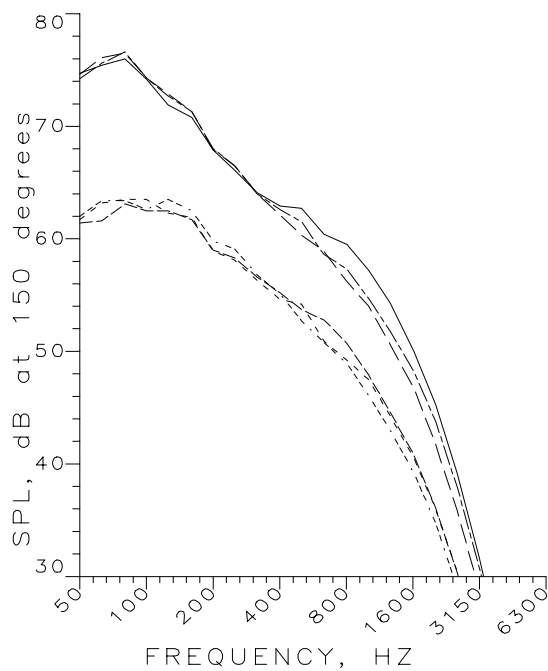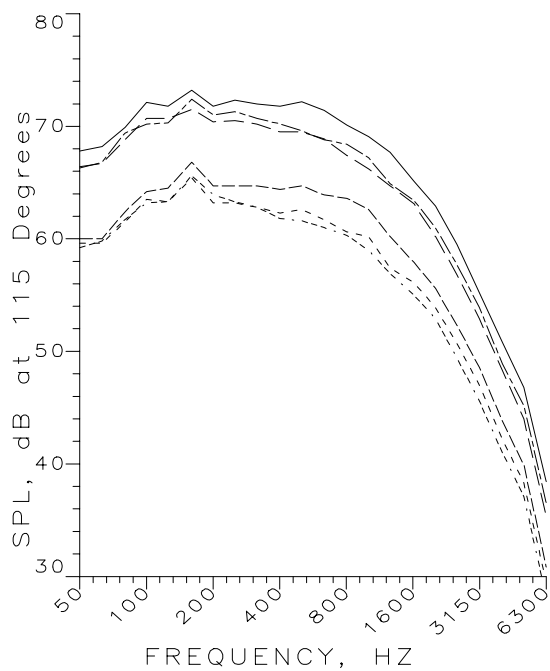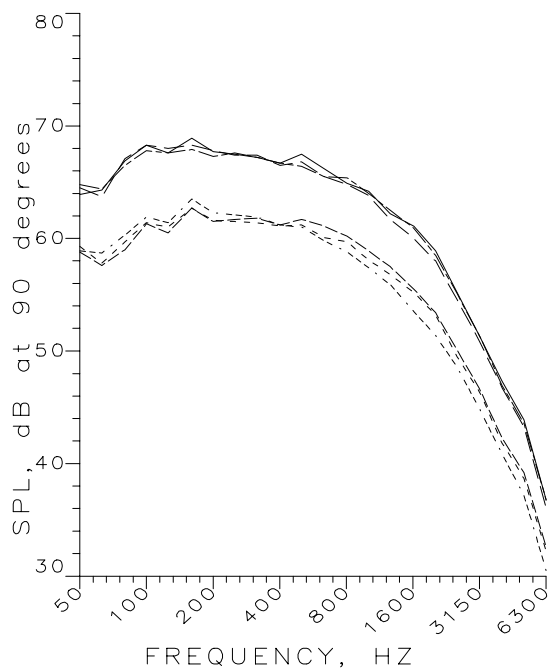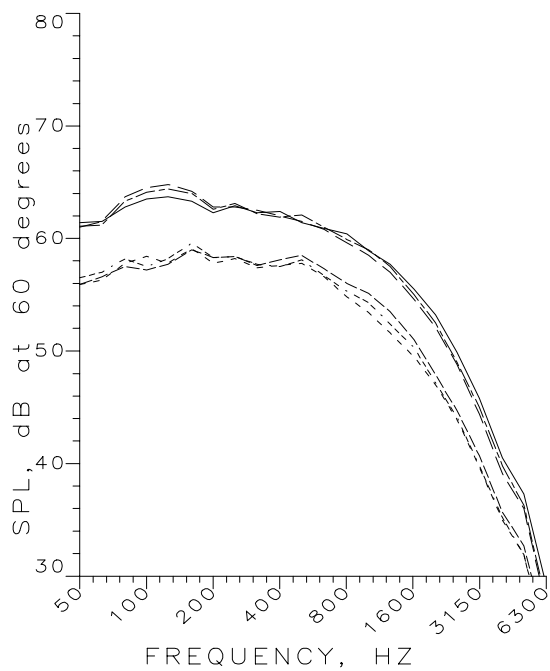
Figure 7.1.3.7: SPL vs Frequency Comparison of Static and Flight Conditions for 12, 20, & 24-Lobe at Angles 60, 90, 115, and 150 degrees at Cutback Power (Cond. 5)
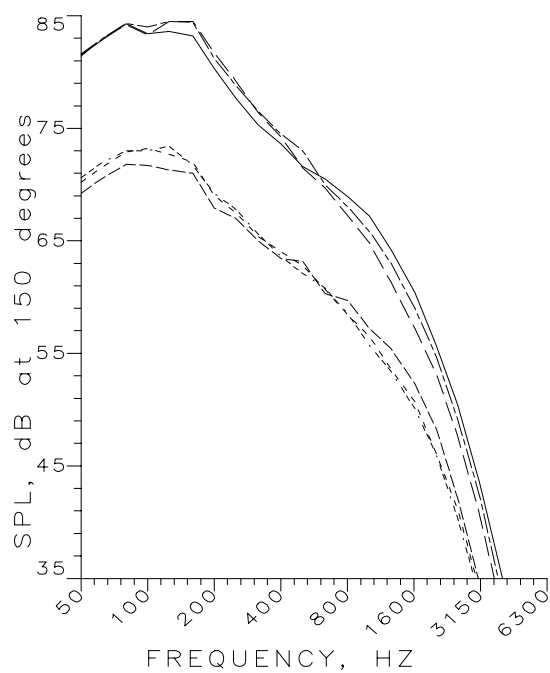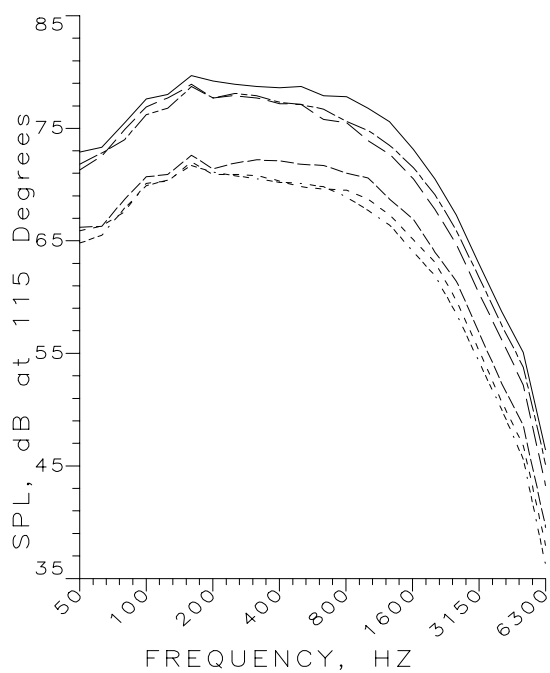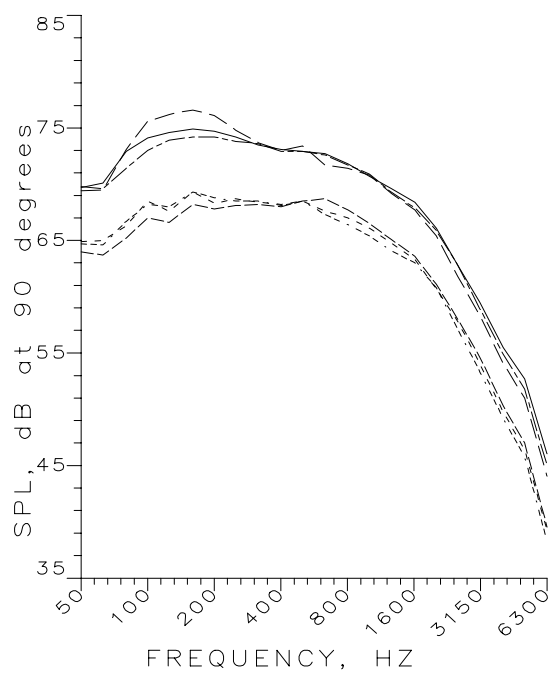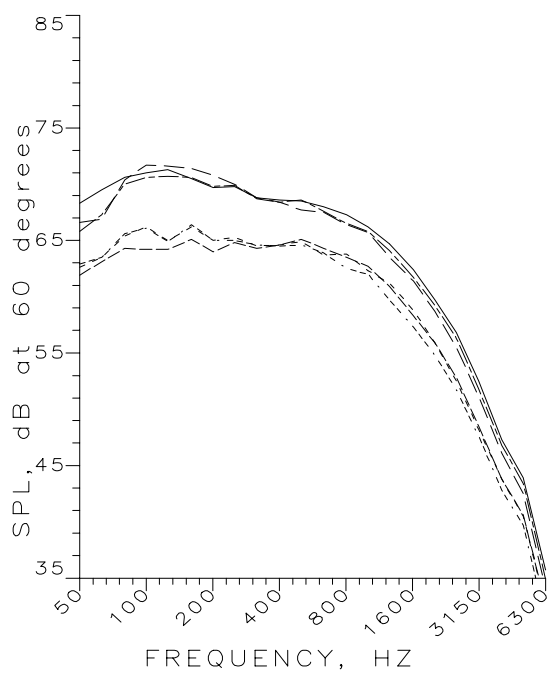
Figure 7.1.3.8: SPL vs Frequency Comparison of Static and Flight Conditions for 12, 20, & 24-Lobe at Angles 60, 90, 115, and 150 degrees at Takeoff Power (Cond. 8)
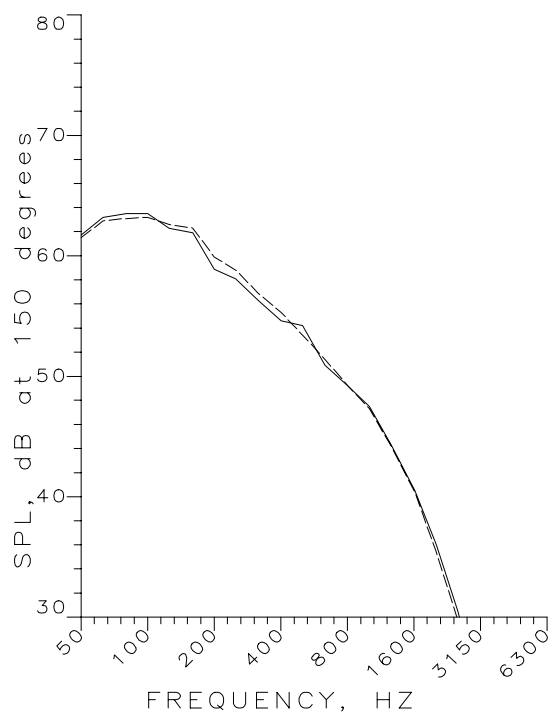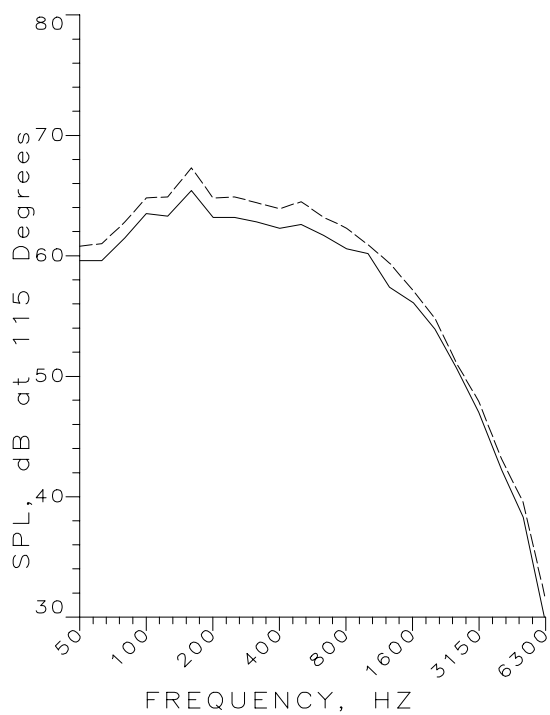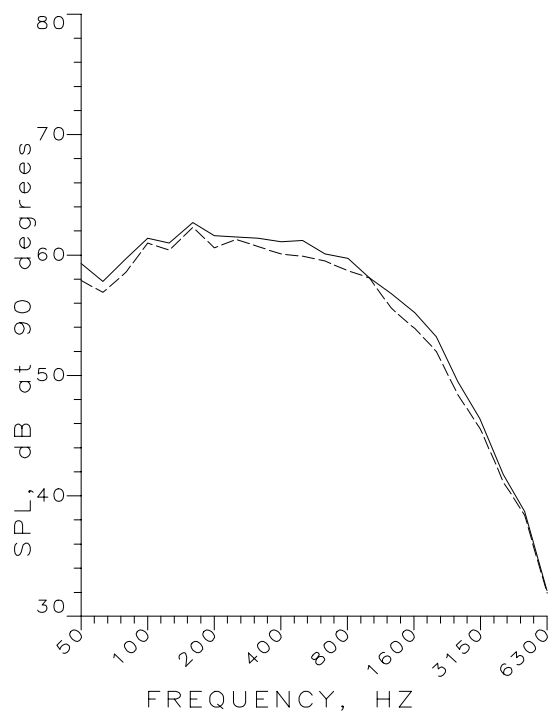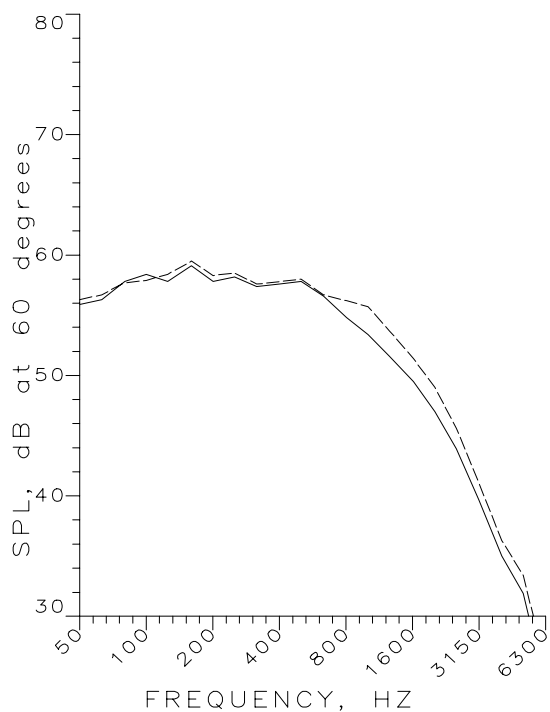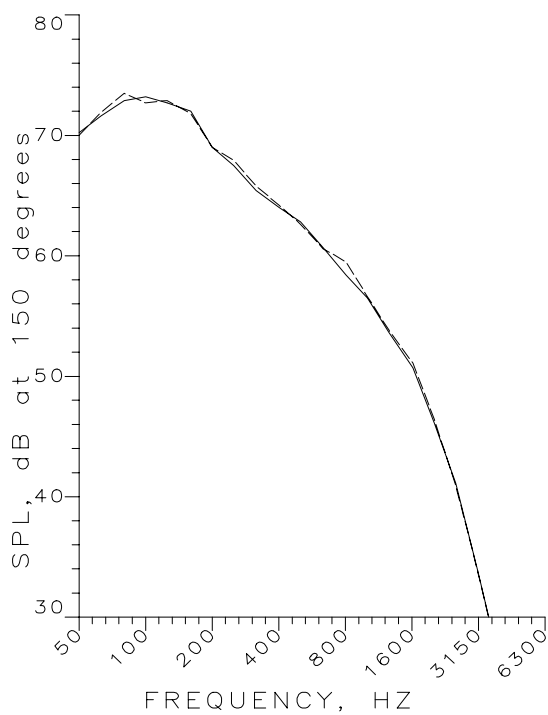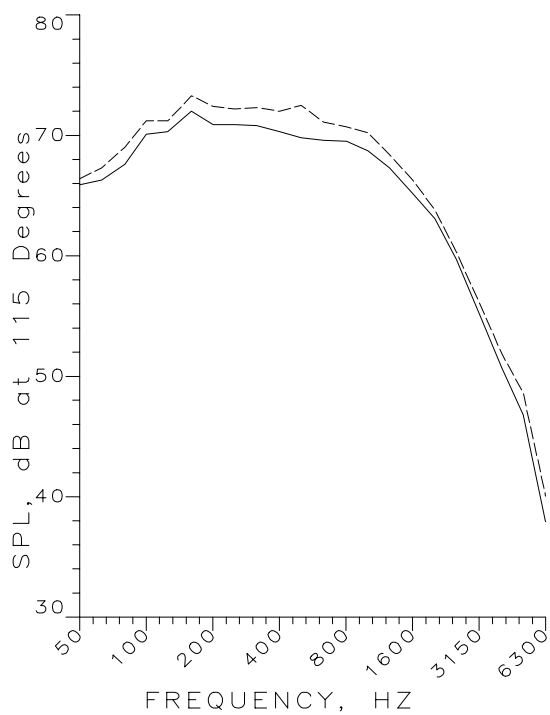
Figure 7.1.3.9: SPL vs Frequency Comparison of Zero and Alternating Scarf Angle (0/12 deg.) on the 20-Lobe Mixer for Angles 60,90, 115, and 150 degrees at Cutback Power (Condition 5)
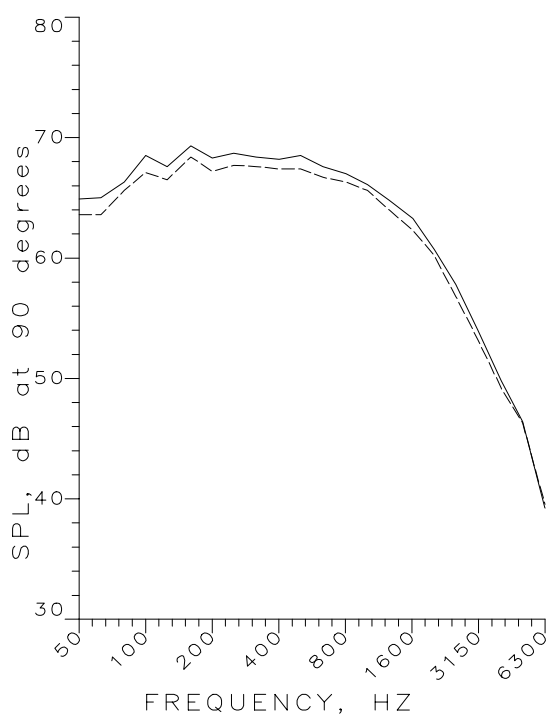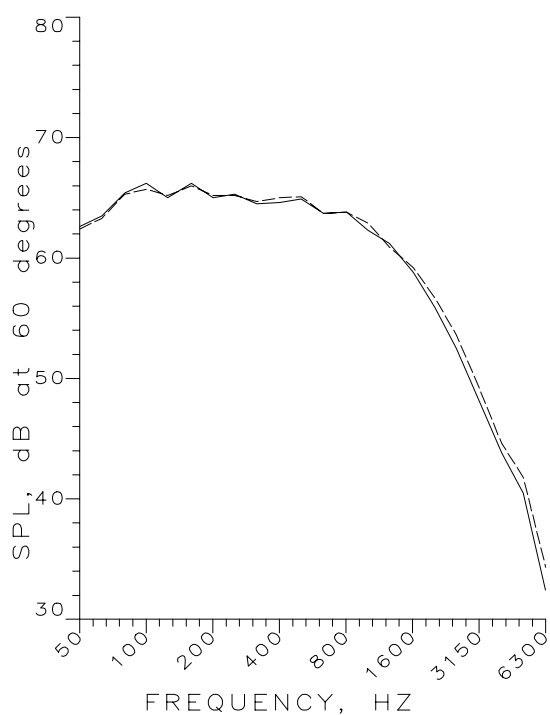
Figure 7.1.3.10: SPL vs Frequency Comparison of Zero and Alternating Scarf Angle (0/12 deg.) on the 20-Lobe Mixer for Angles 60,90, 115, and 150 degrees at Takeoff Power (Condition 8)
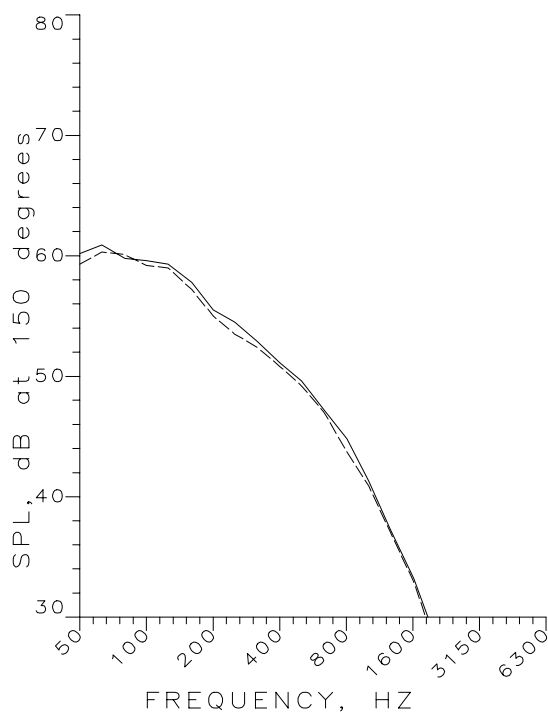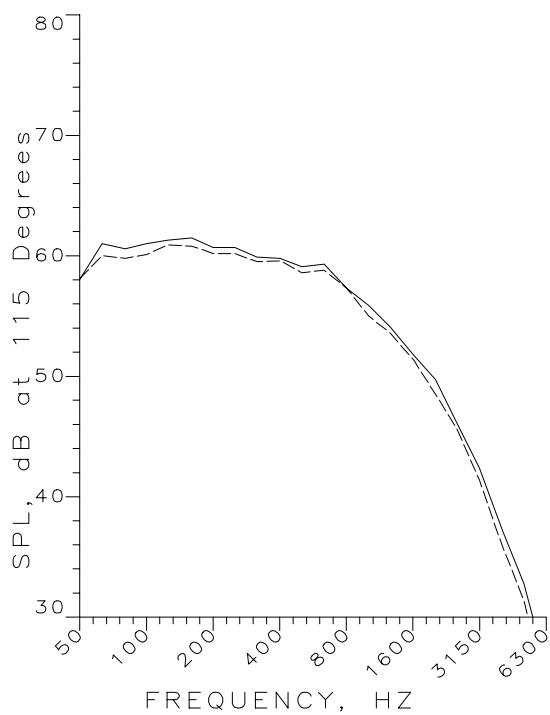
Figure 7.1.3.11: SPL vs Frequency Comparison of ATM With and Without Lobe Scallops for Angles 60, 90, 115, and 150 degrees at Cutback Power (Condition 5)

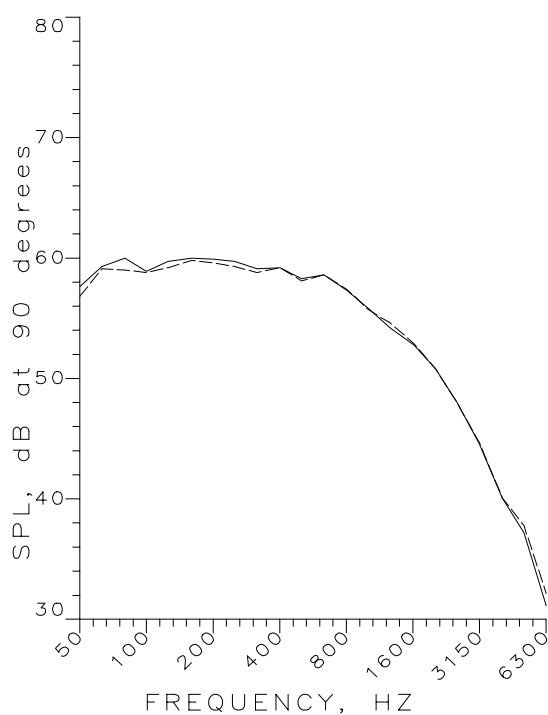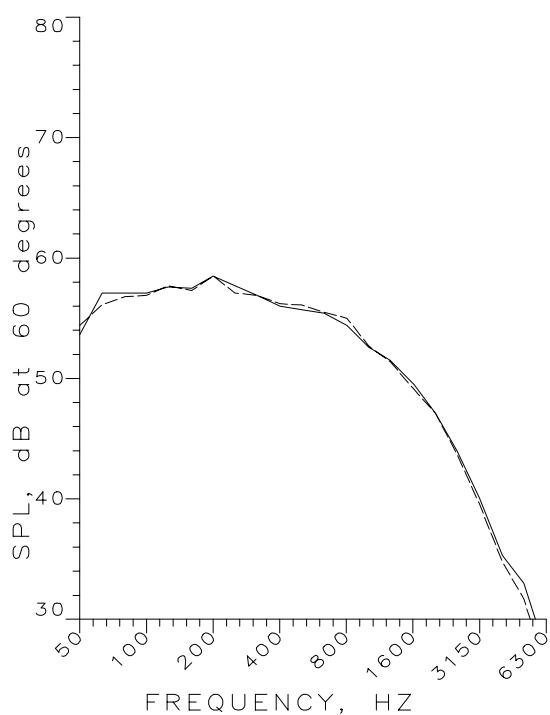**Figure 7.1.3.12: SPL vs Frequency Comparison of ATM With and Without Lobe Scallops for Angles 60,90, 115, and 150 degrees at Takeoff Power (Condition 8)**
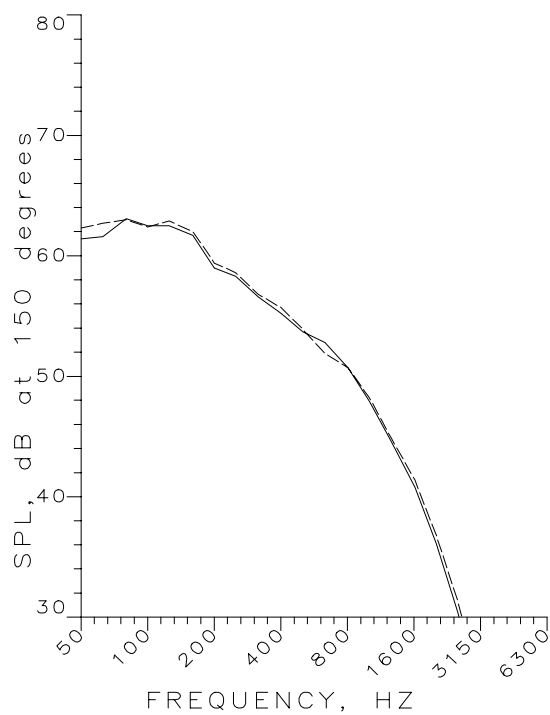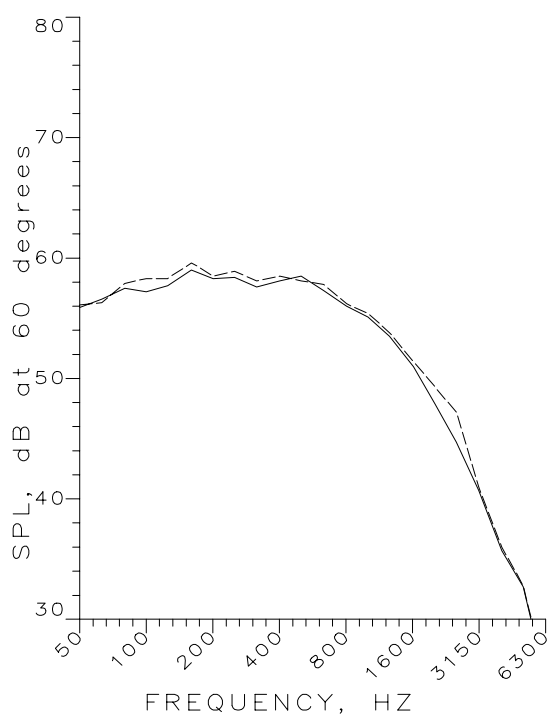
Figure 7.1.3.13: SPL vs Frequency Comparison of 12-Lobe Mixer Without and With Simulated Engine Probes for Angles 60, 90, 115, and 150 degrees at Cutback Power (Condition 5)
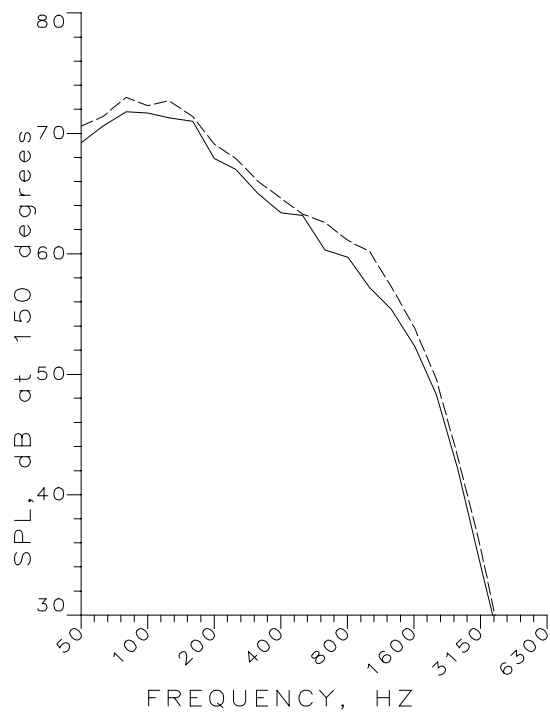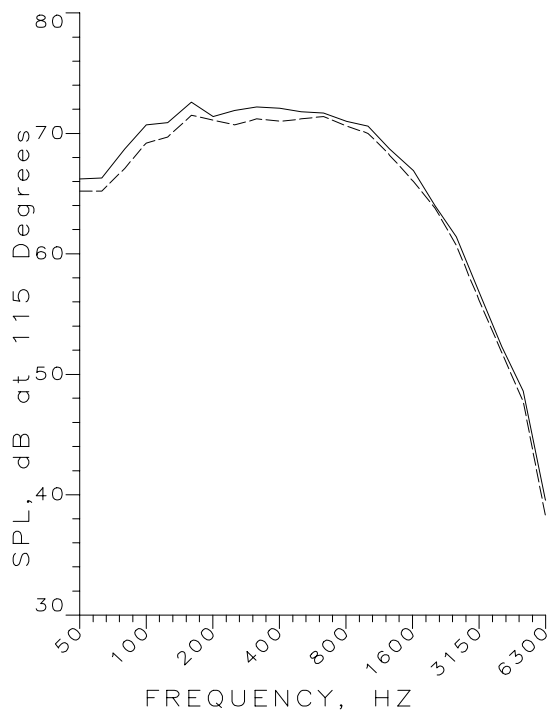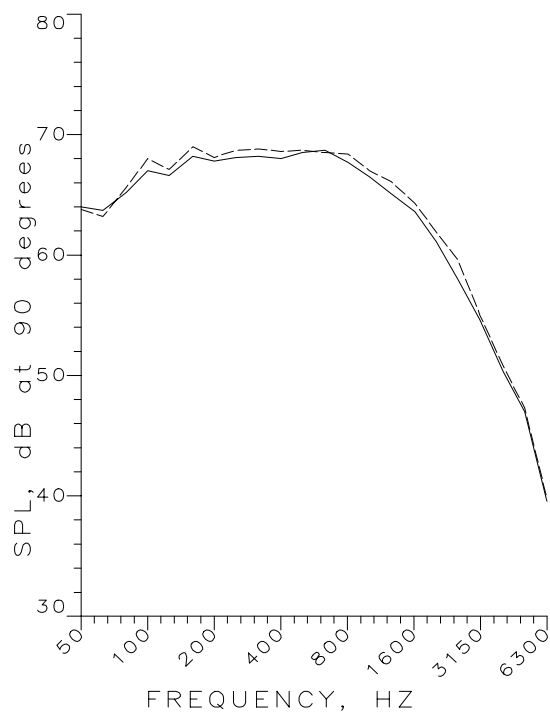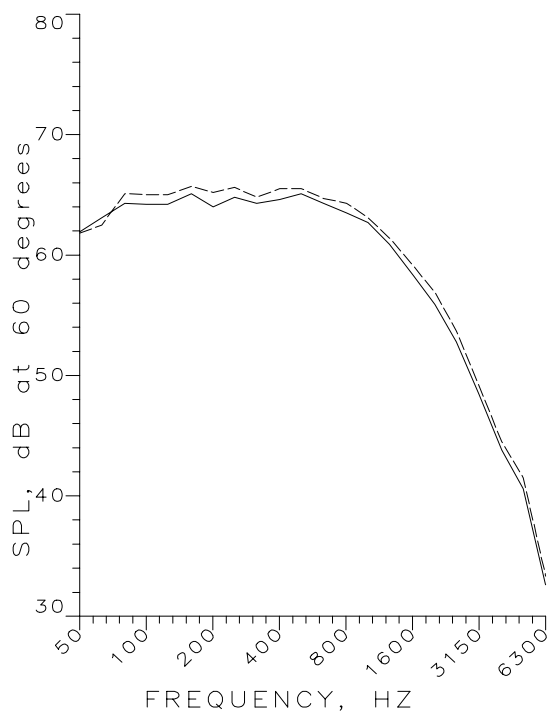
Figure 7.1.3.14: SPL vs Frequency Comparison of 12-Lobe Mixer Without and With Simulated Engine Probes for Angles 60, 90, 115, and 150 degrees at Takeoff Power (Condition 8)
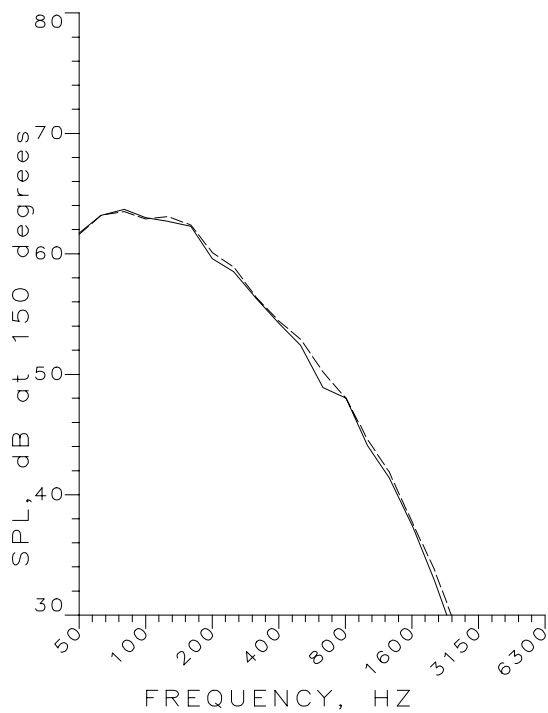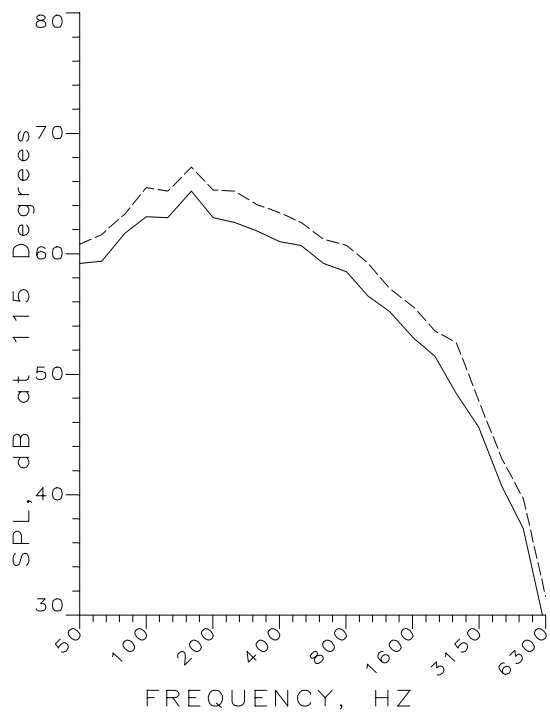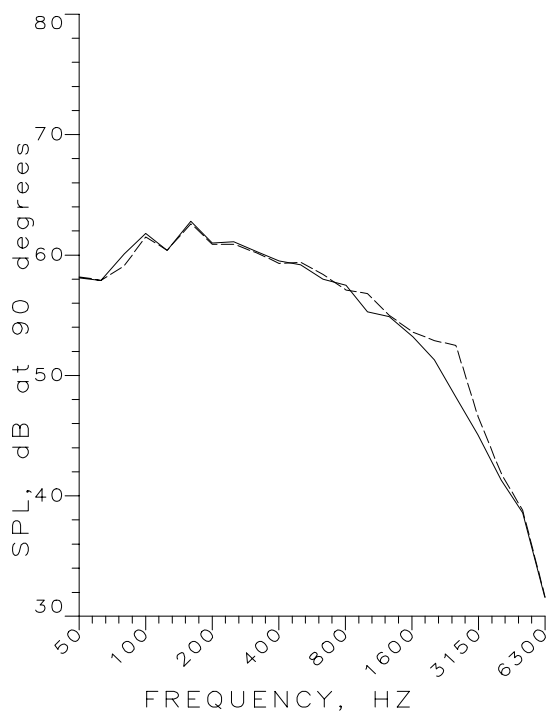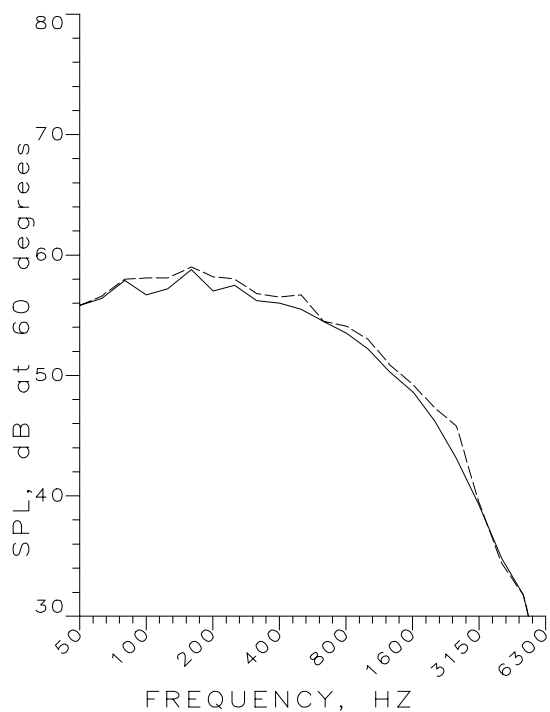
Figure 7.1.3.15: SPL vs Frequency Comparison of ATM Without & With Simulated Engine Probes for Angles 60, 90, 115, and 150 degrees at Cutback Power (Cond. 5)
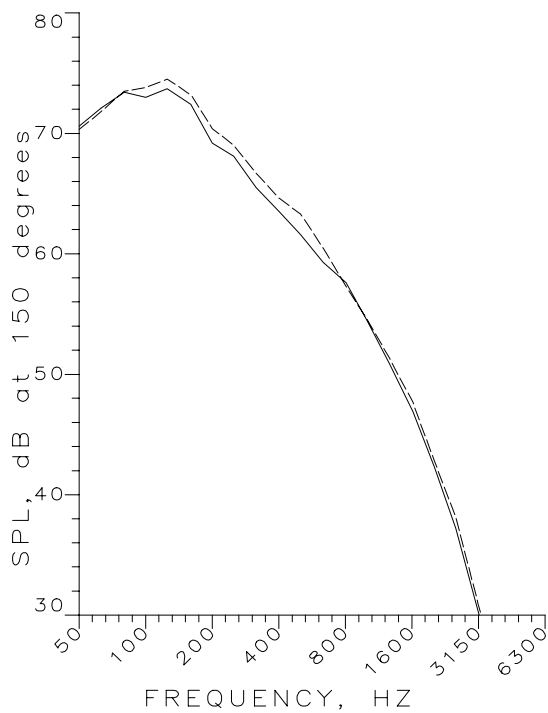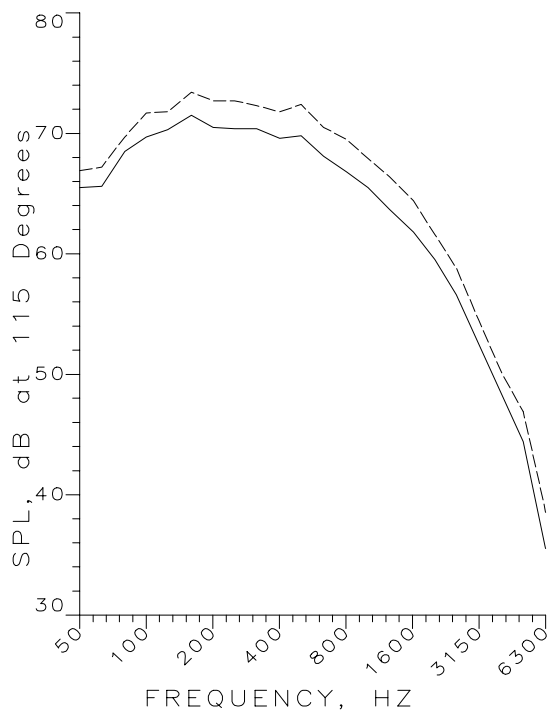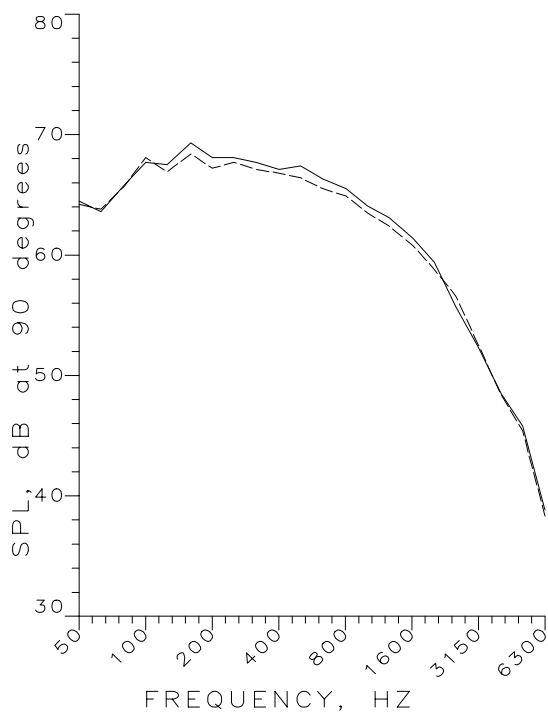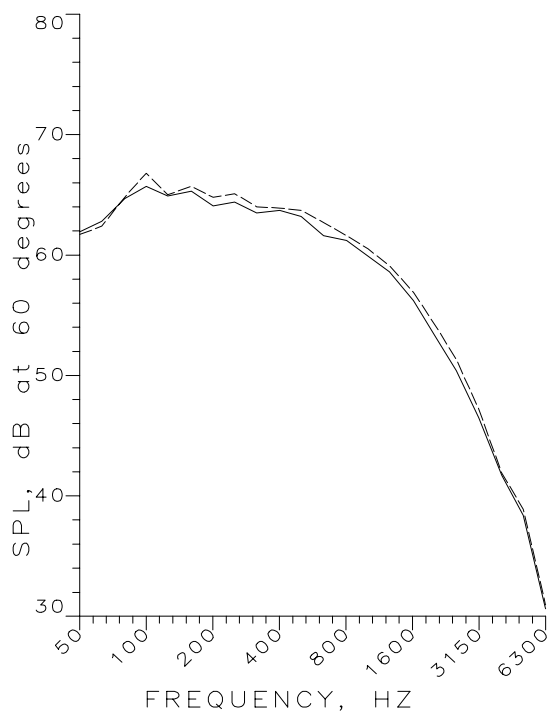
Figure 7.1.3.16: SPL vs Frequency Comparison of ATM Without & With Simulated Engine Probes for Angles 60, 90, 115, and 150 degrees at Takeoff Power (Cond. 8)
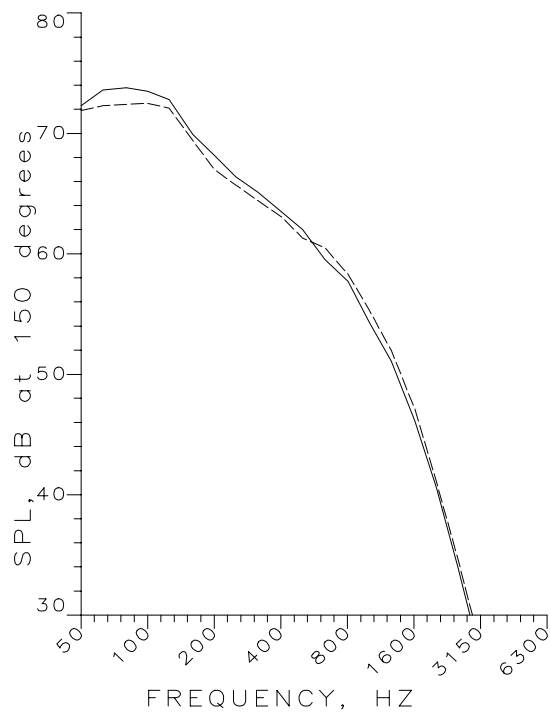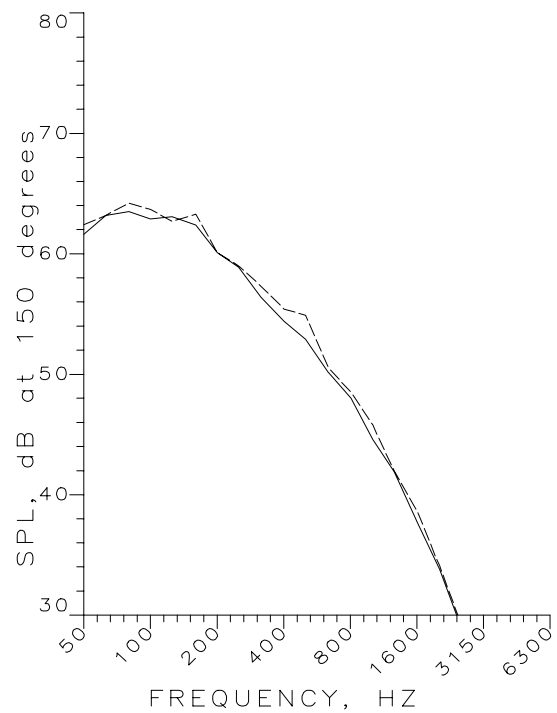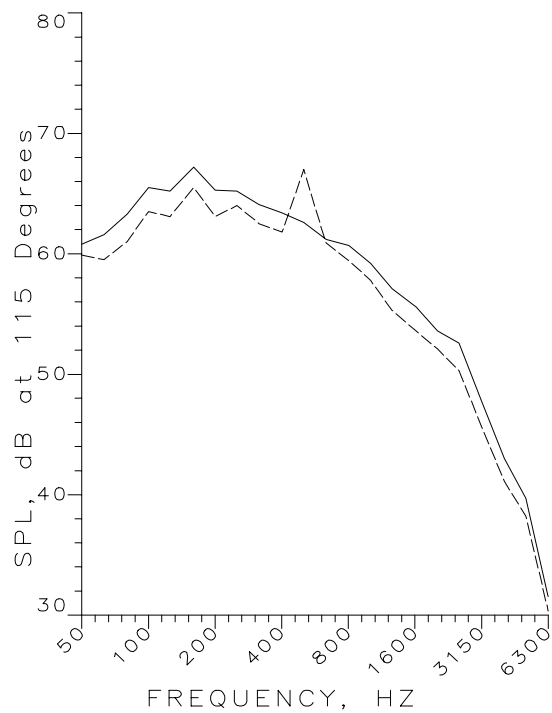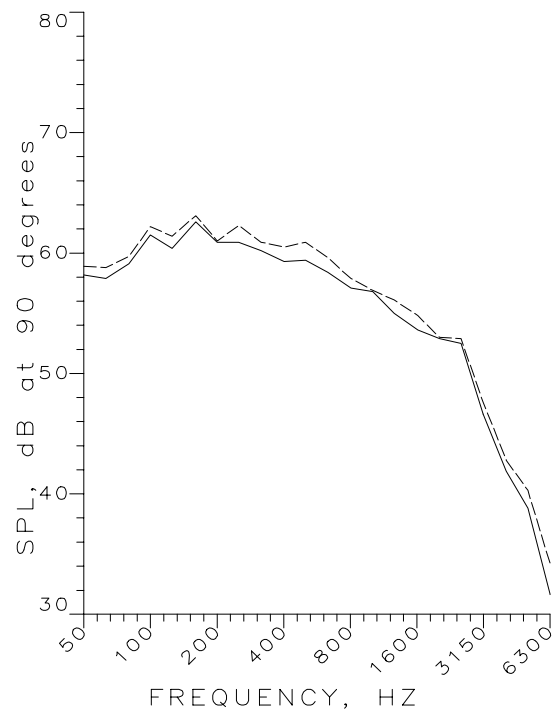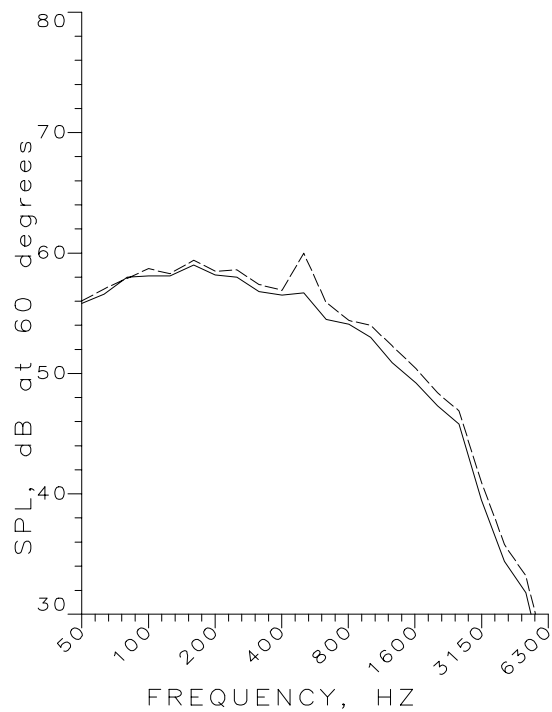
Figure 7.1.3.17: SPL vs Frequency Comparison of ATM Without and With Muffler for Angles 60, 90, 115, and 150 degrees at Cutback Power (Condition 5)
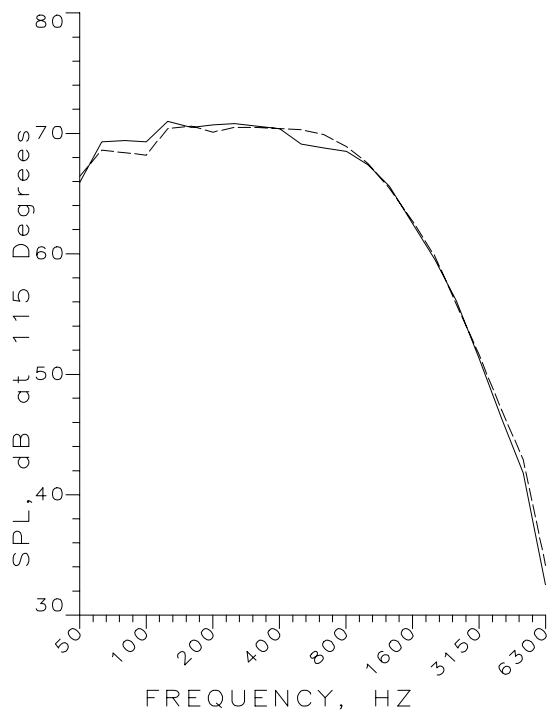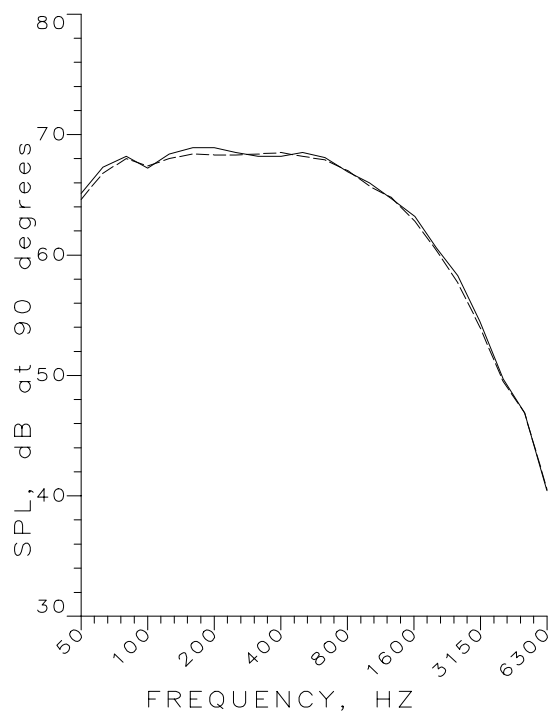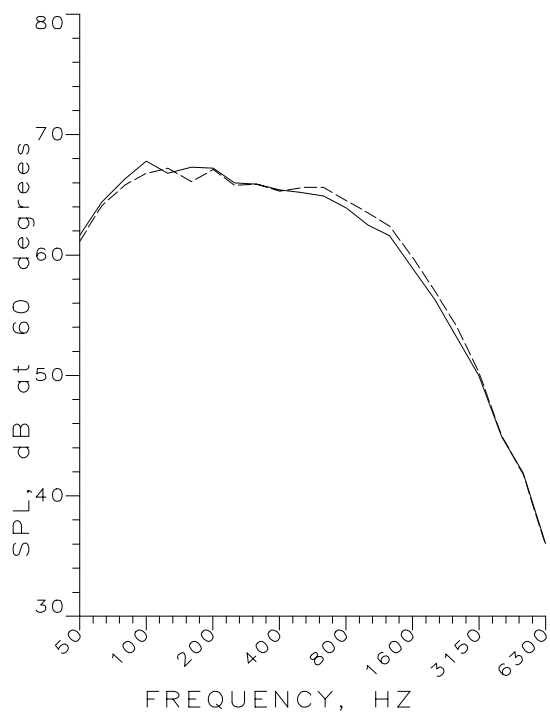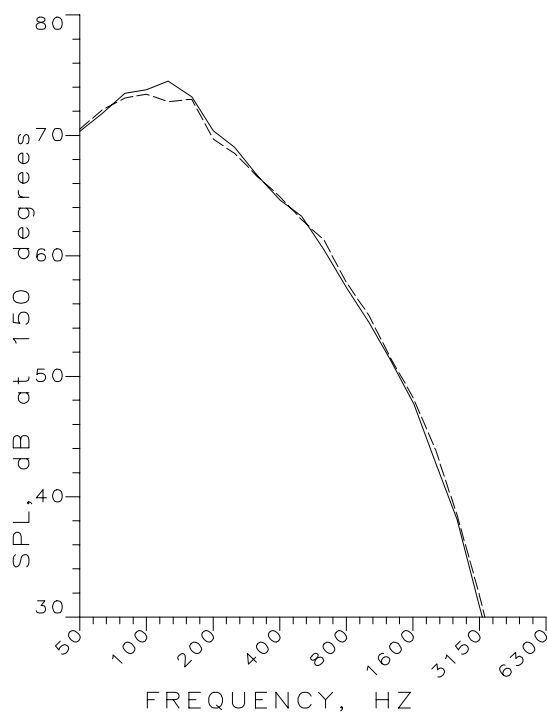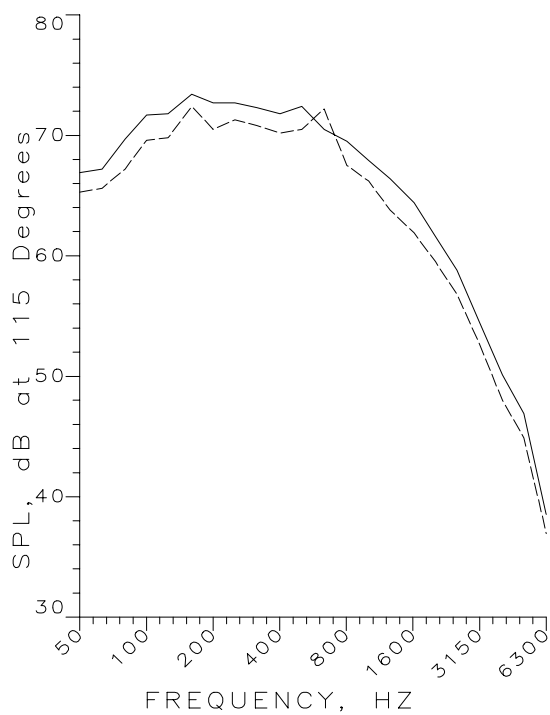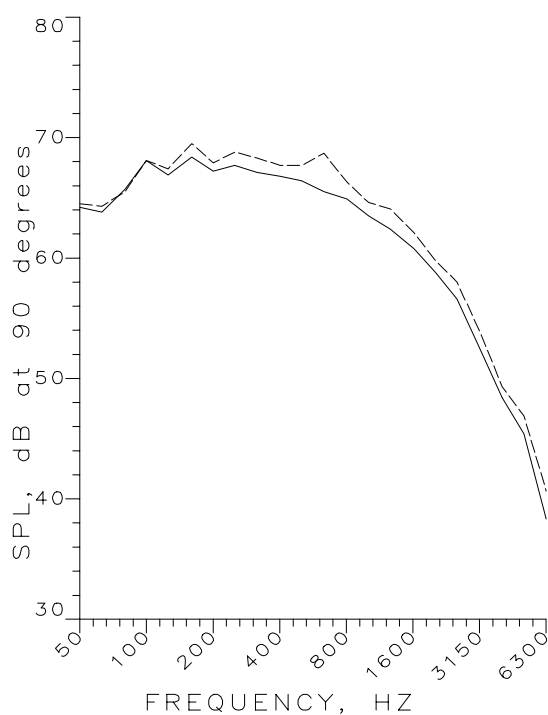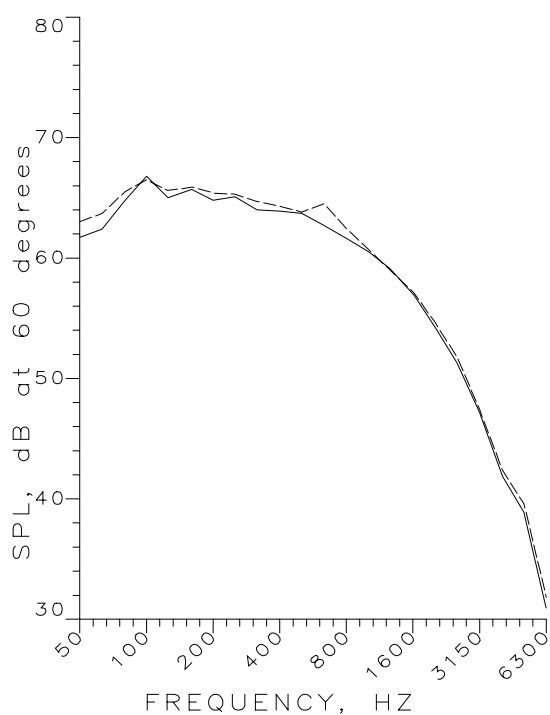
Figure 7.1.3.18: SPL vs Frequency Comparison of ATM Without and With Muffler for Angles 60, 90, 115, and 150 degrees at Takeoff Power (Condition 8)
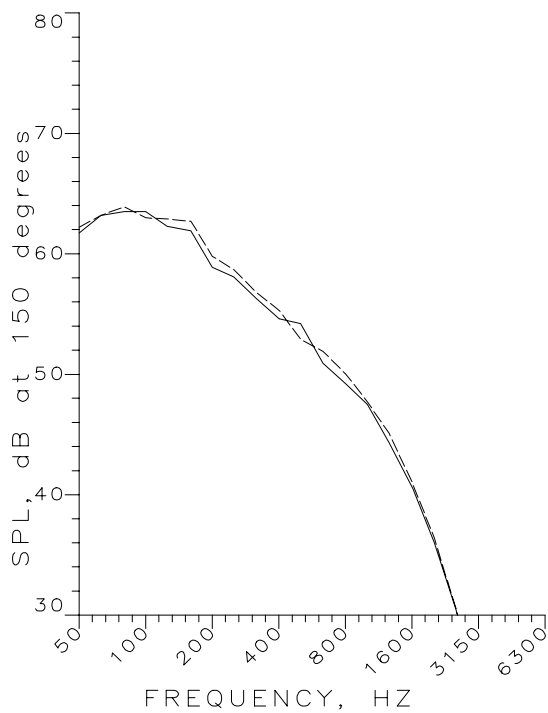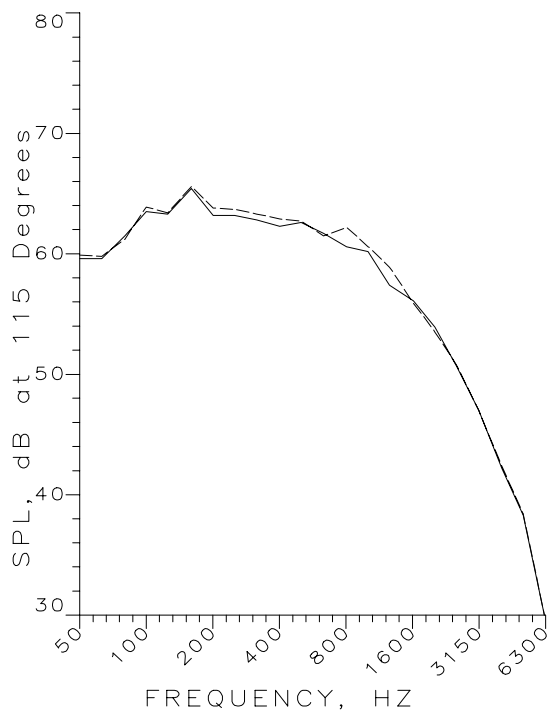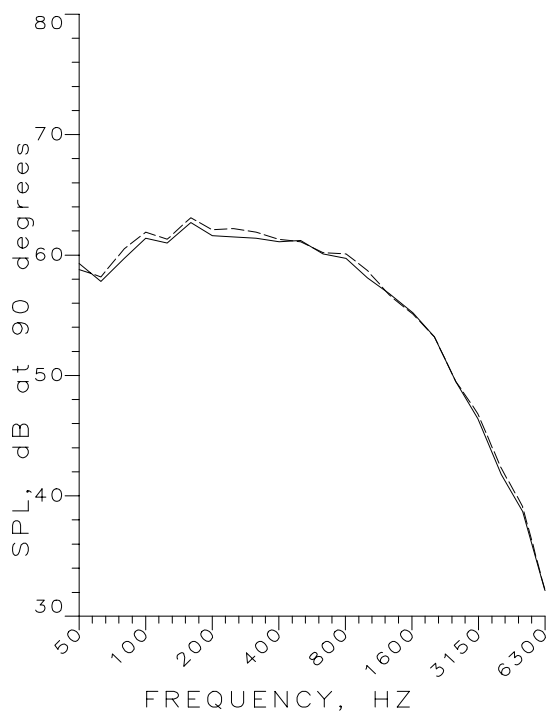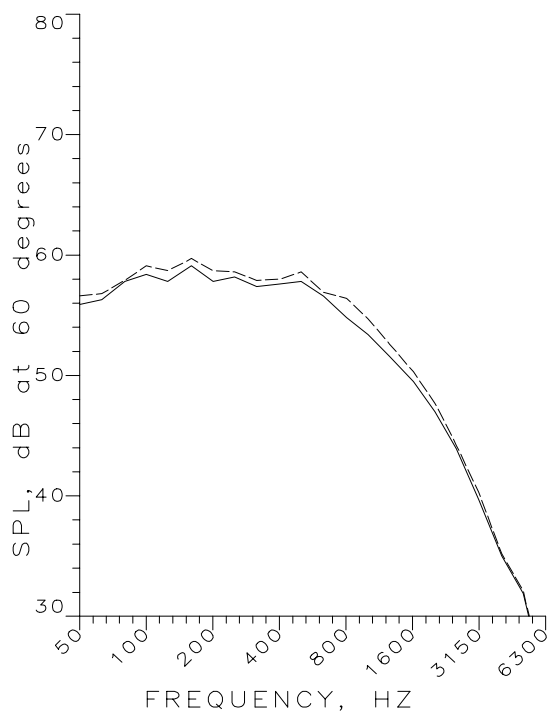
Figure 7.1.3.19: SPL vs Frequency Comparison of 20-Lobe Without and With Vortex Generators for Angles 60, 90, 115, and 150 degrees at Cutback Power (Condition 5)

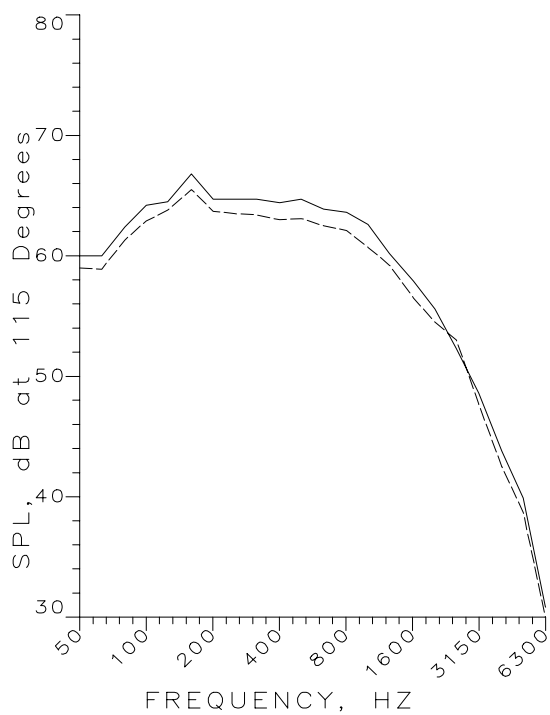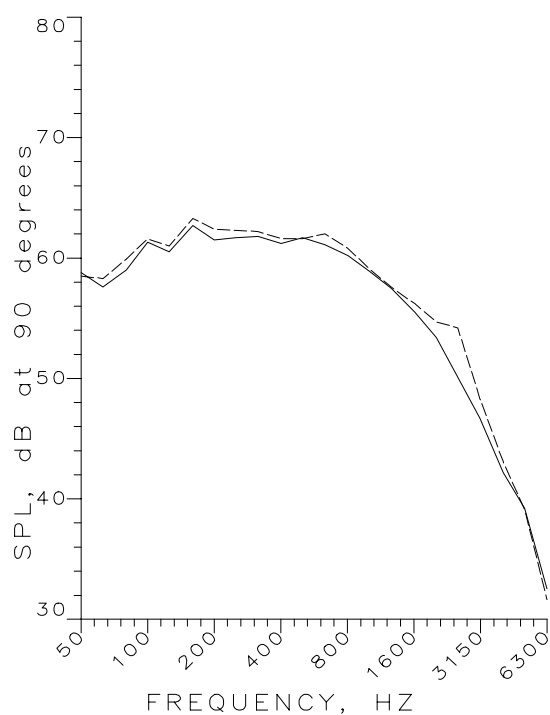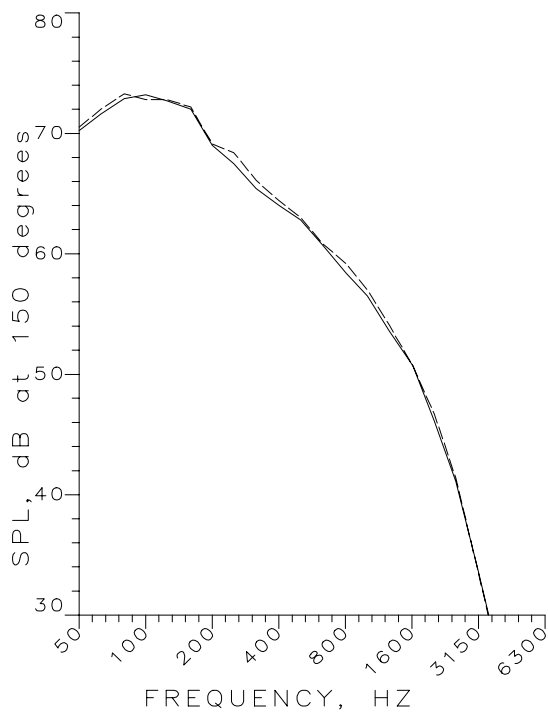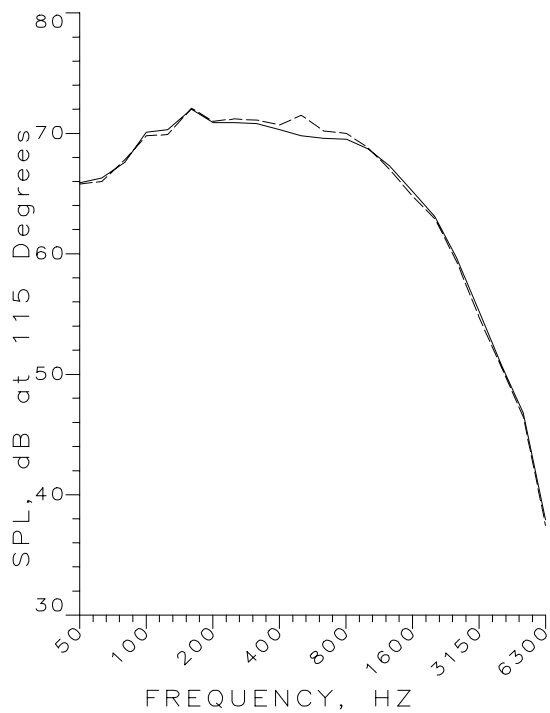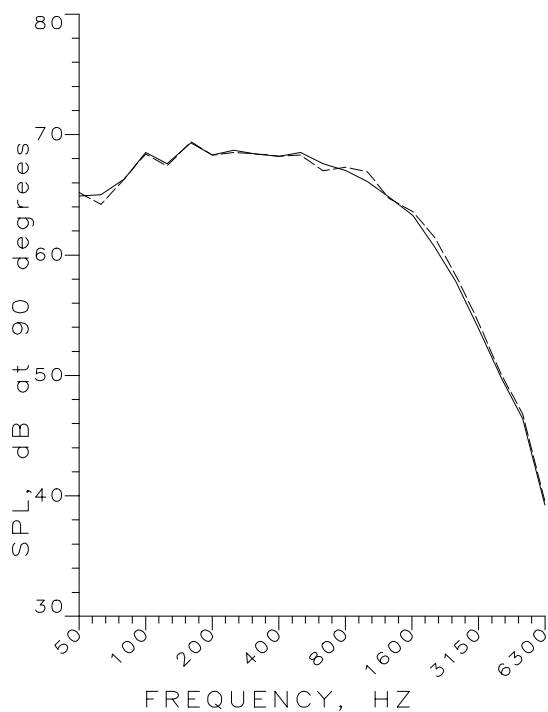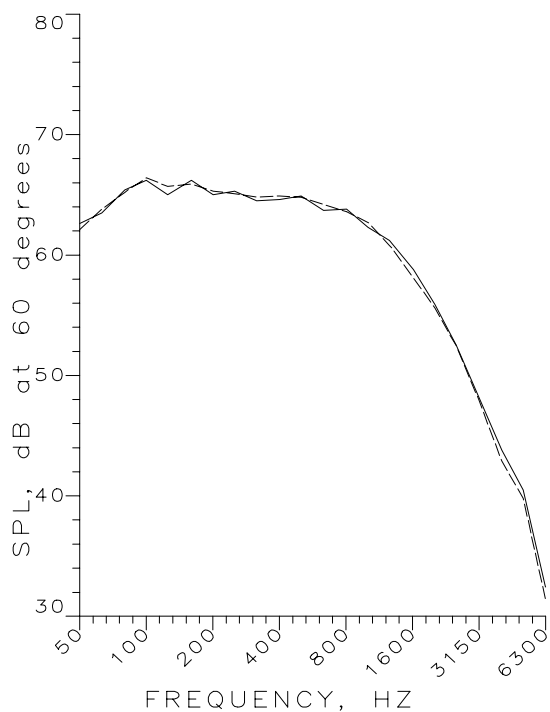**Figure 7.1.3.20: SPL vs Frequency Comparison of 20-Lobe Without and With Vortex Generators for Angles 60, 90, 115, and 150 degrees at Takeoff Power (Condition 8)**
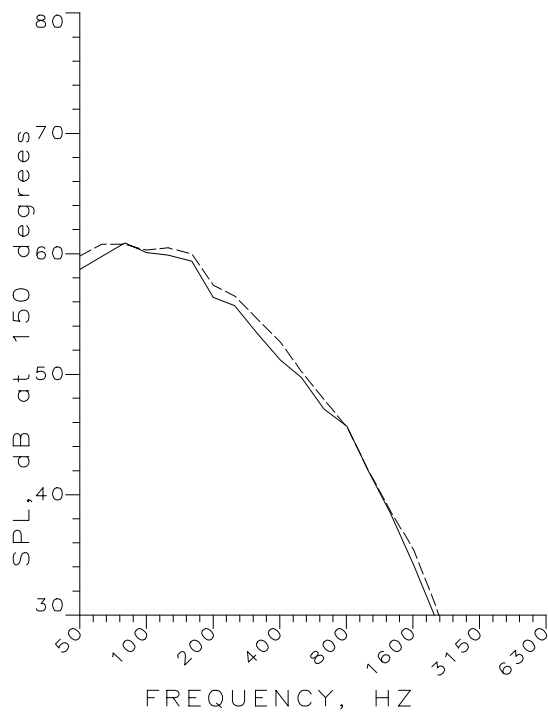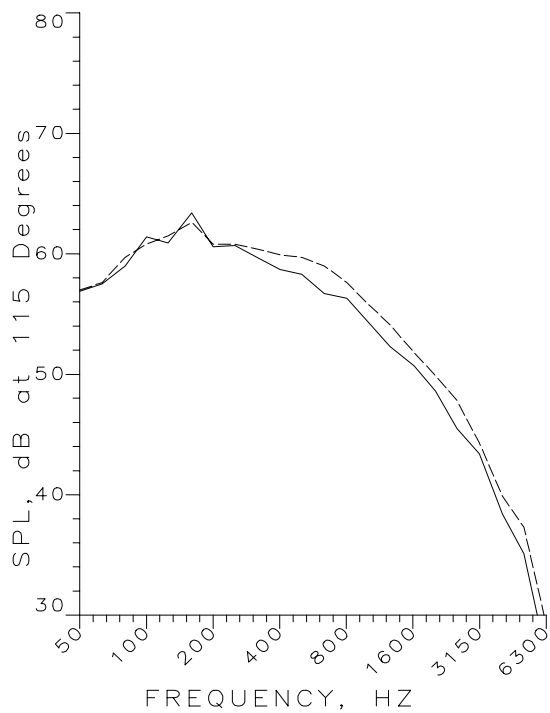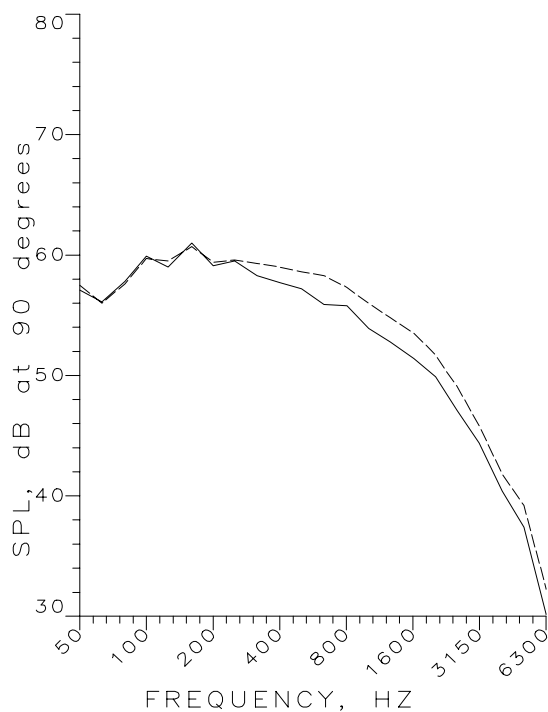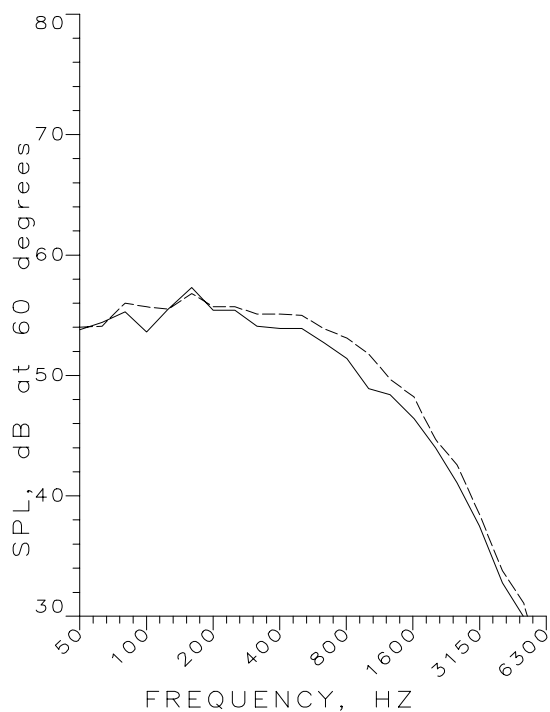
Figure 7.1.3.21: SPL vs Frequency Comparison of ATM With Heated and Unheated fan flow for Angles 60, 90, 115, and 150 degrees at Cutback Power (Condition 5)
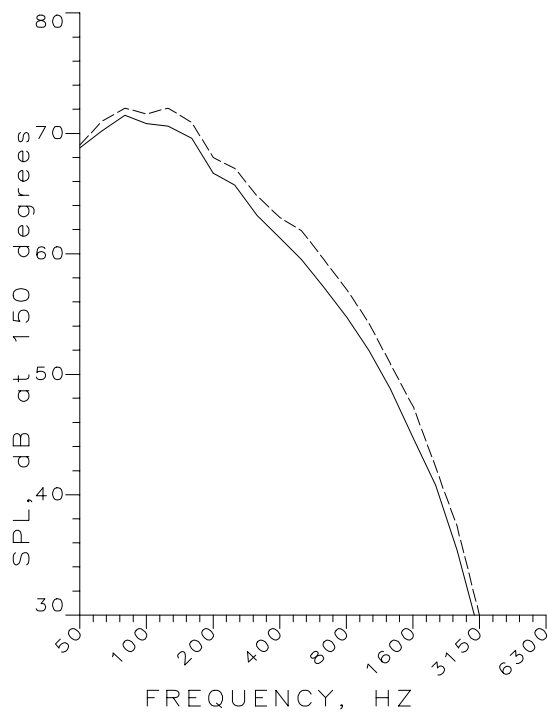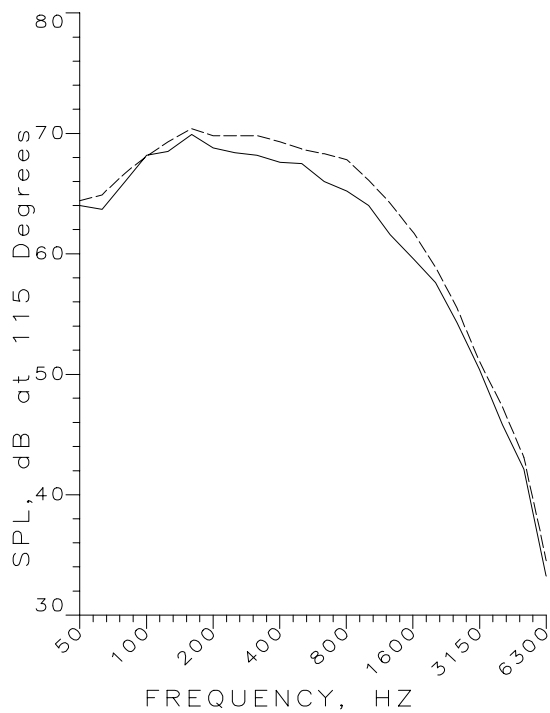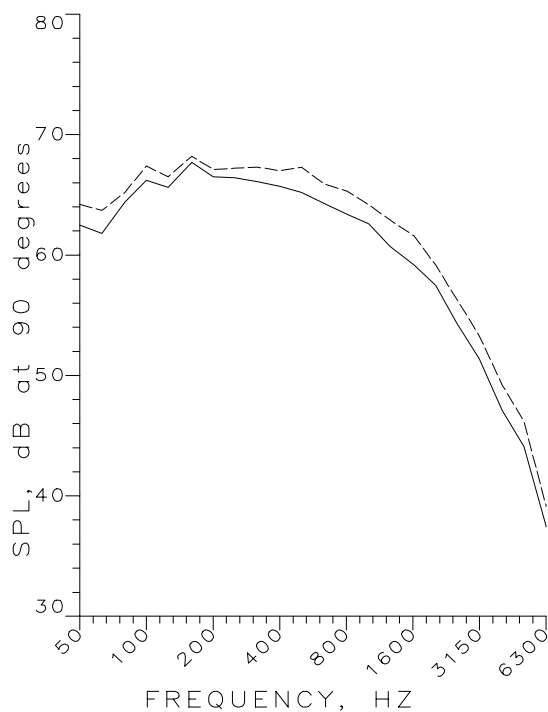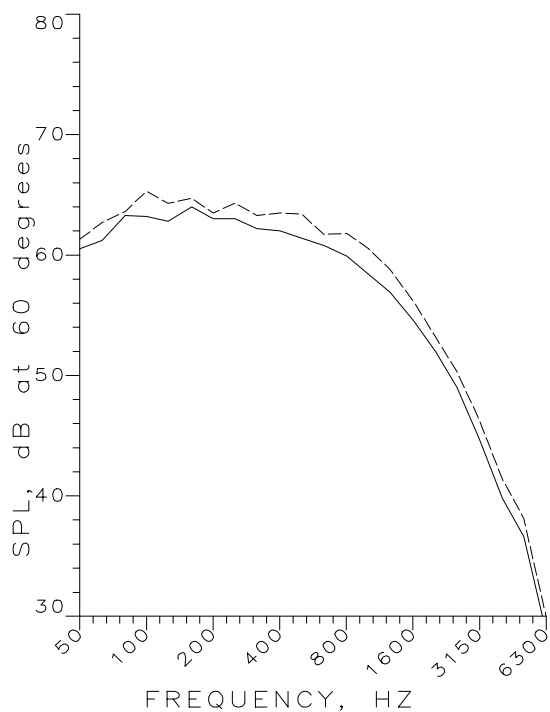
Figure 7.1.3.22: SPL vs Frequency Comparison of ATM With Heated and Unheated fan flow for Angles 60, 90, 115, and 150 degrees at Takeoff Power (Condition 8)
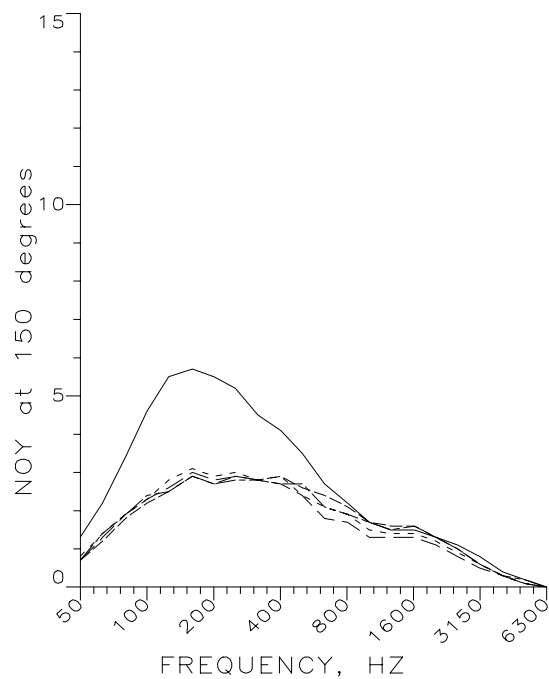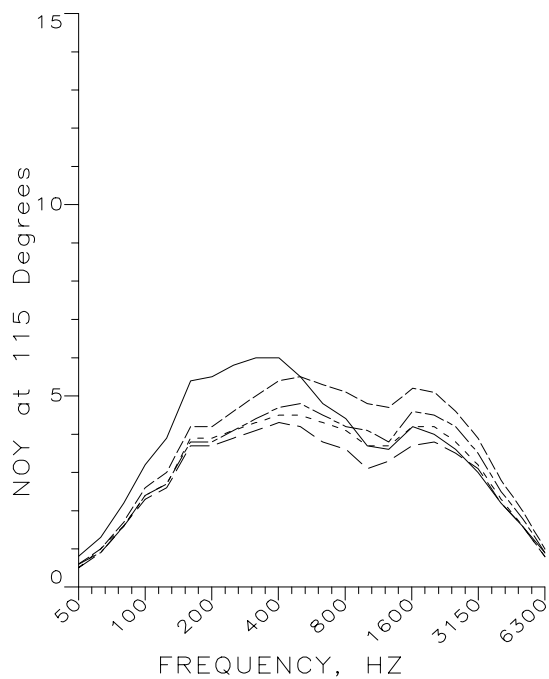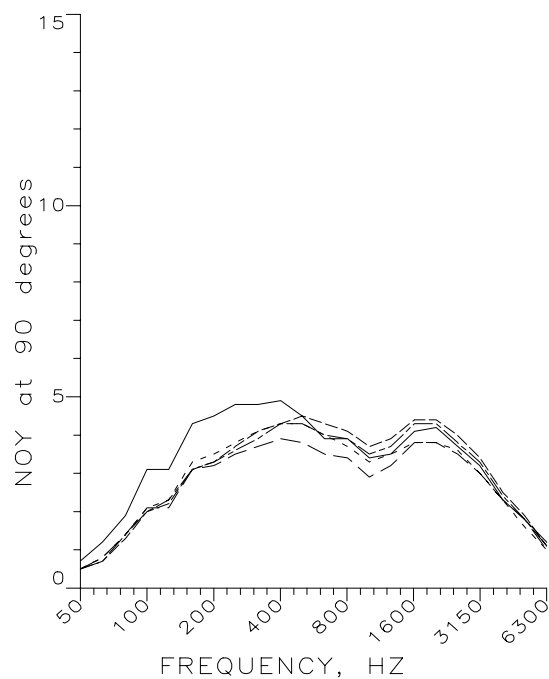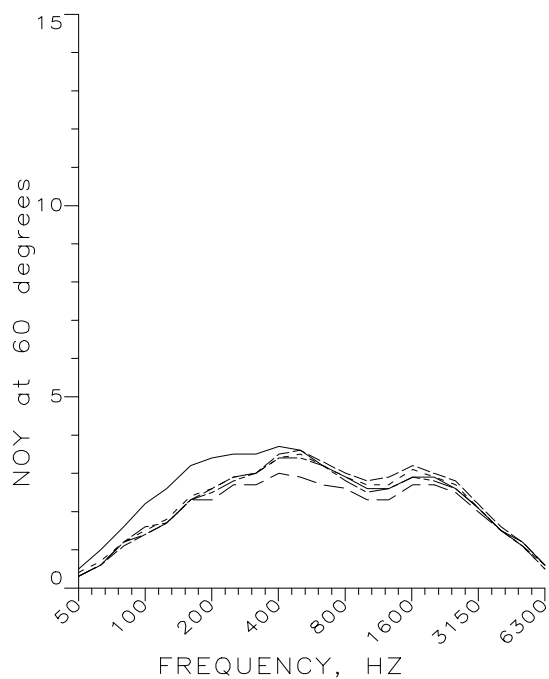
Figure 7.1.4.1: NOY Weighting vs Frequency Comparison of Splitter with all Mixers (12, 20, 24, and ATM) for Angles 60, 90, 115, and 150 degrees at Cutback Power (Cond. 5)
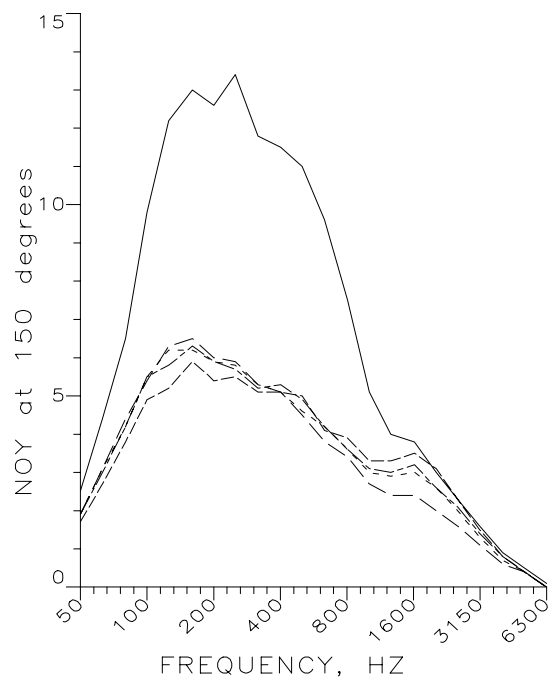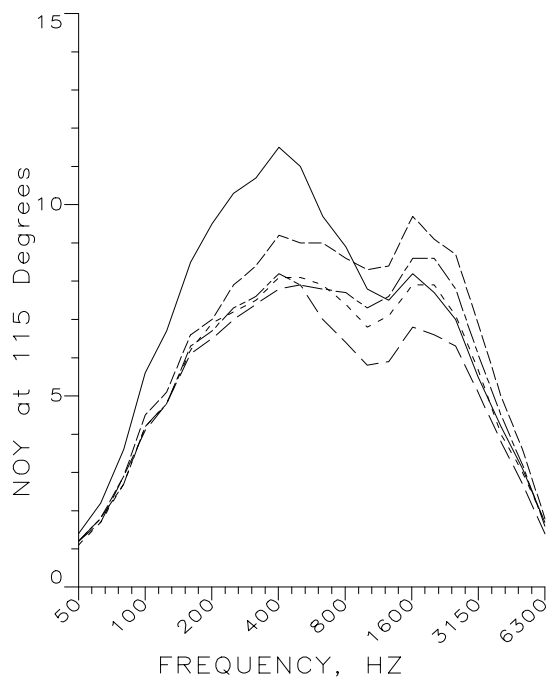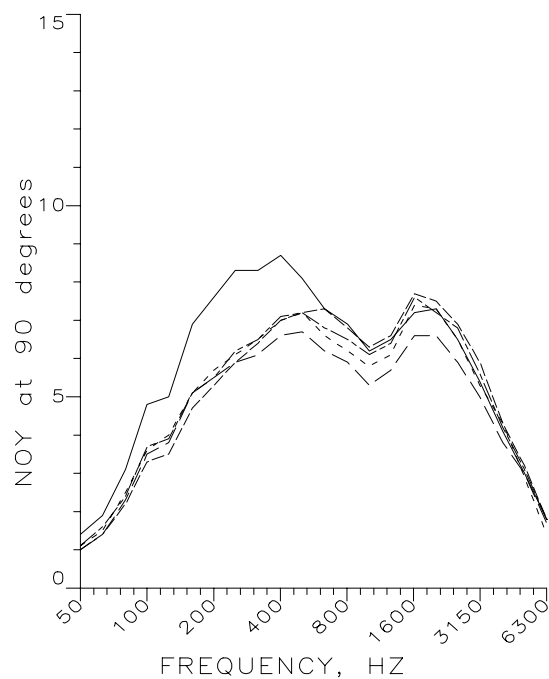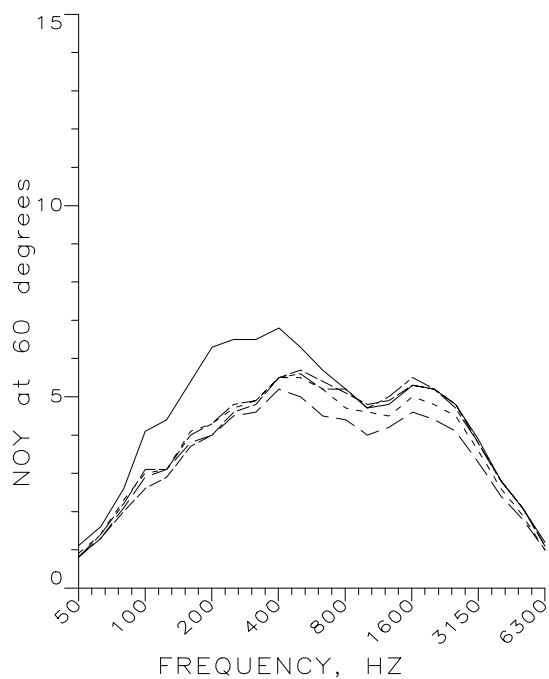
Figure 7.1.4.2: NOY Weighting vs Frequency Comparison of Splitter with all Mixers (12, 20, 24, and ATM) for Angles 60, 90, 115, and 150 degrees at Takeoff Power (Cond. 8)
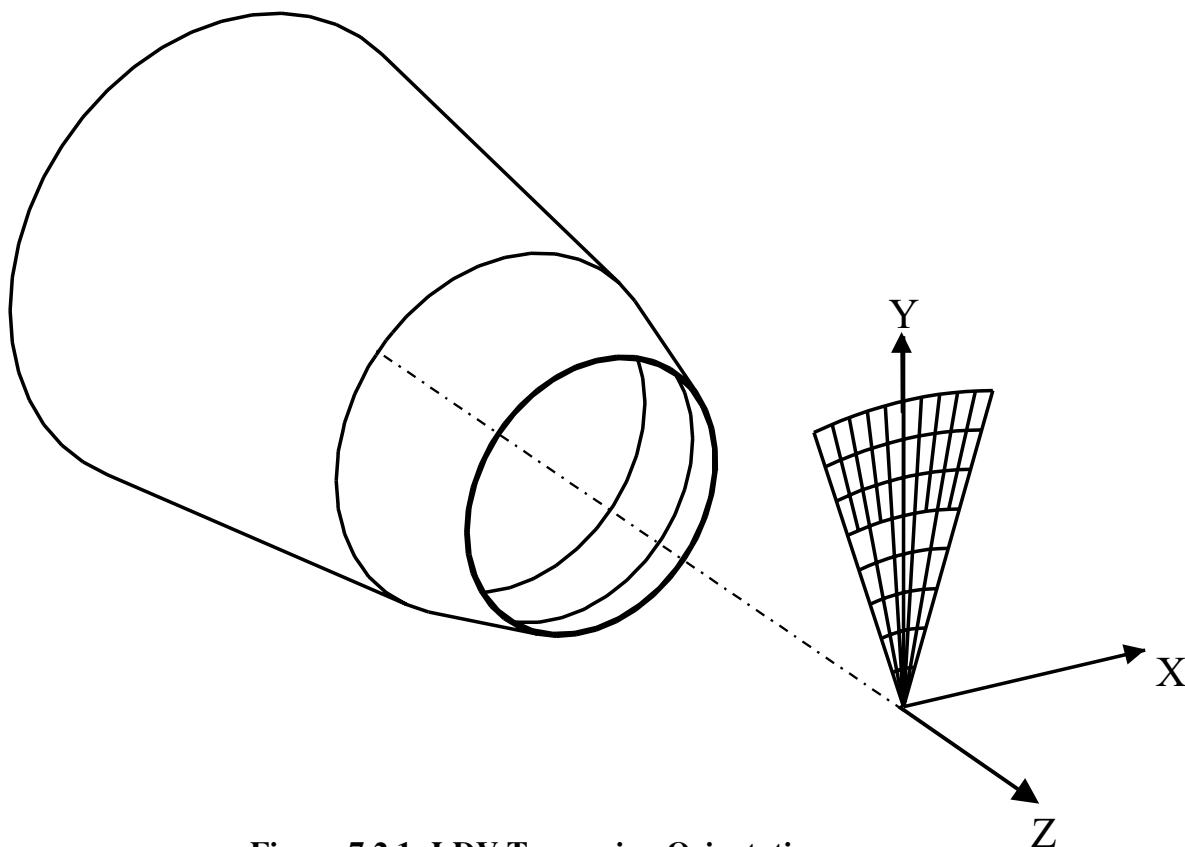
Figure 7.2.1: LDV Traversing Orientation
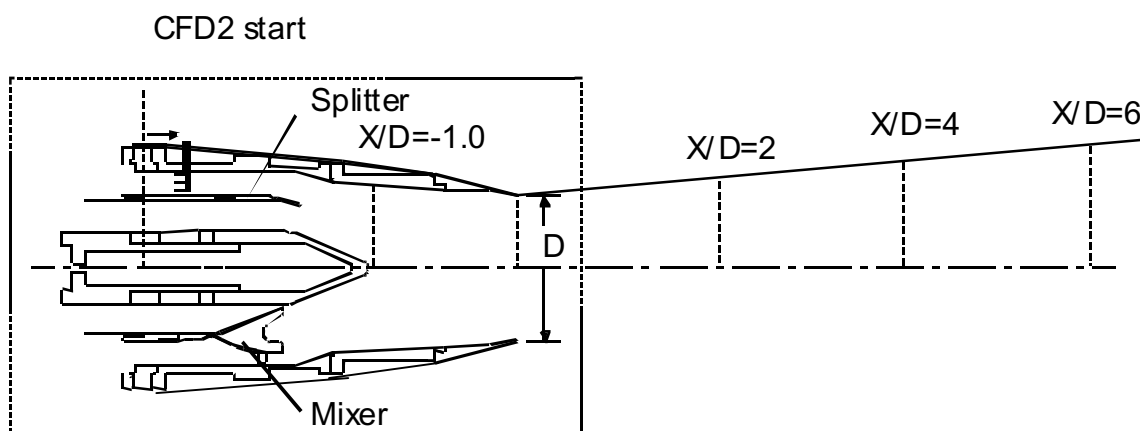
Figure 7.2.2: Schematic of exhaust nozzle installations in NASA NATR test facility

12-lobe mixer
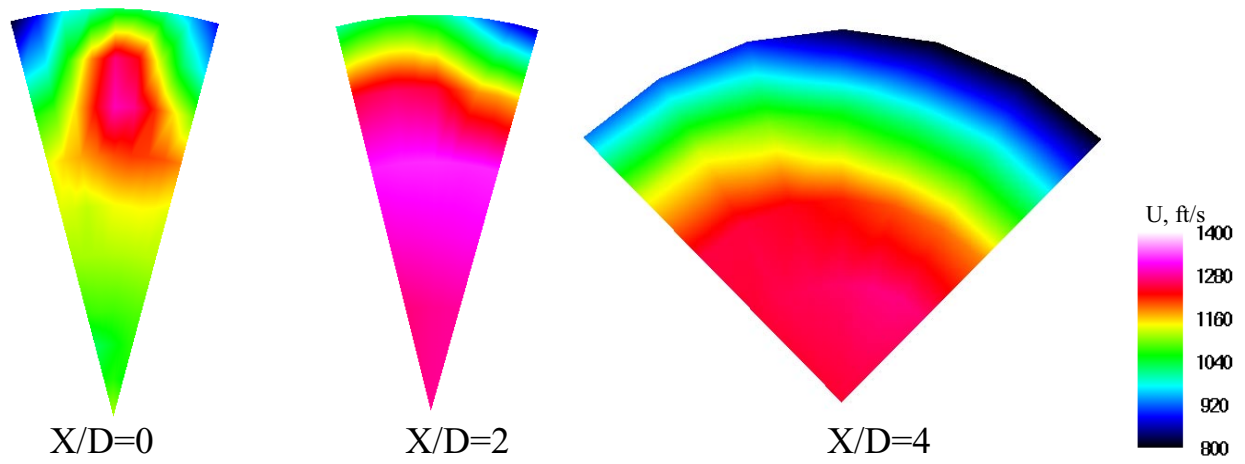
20-lobe mixer
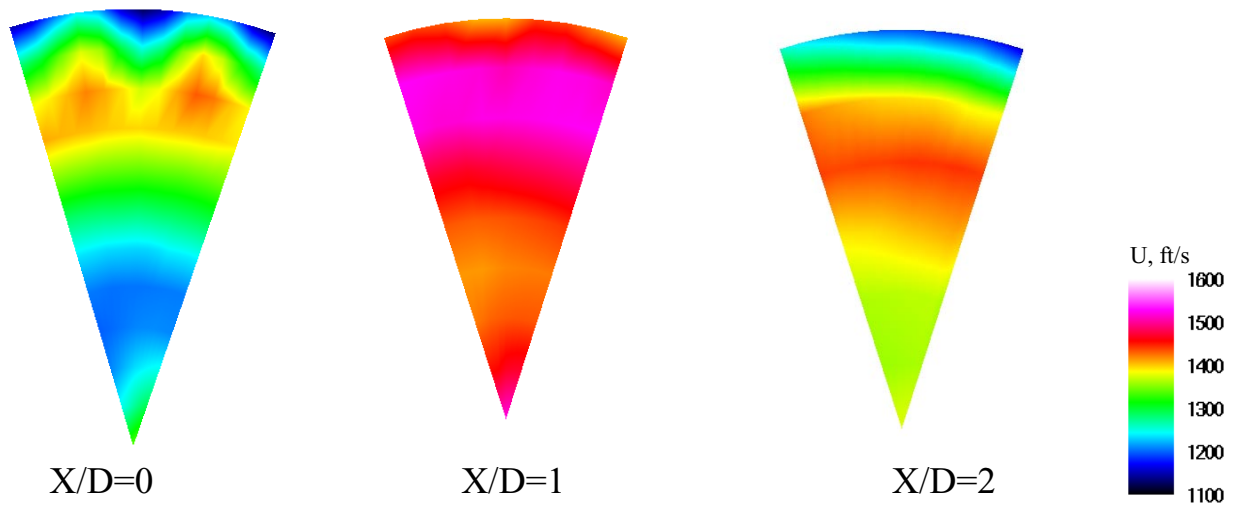
ATM
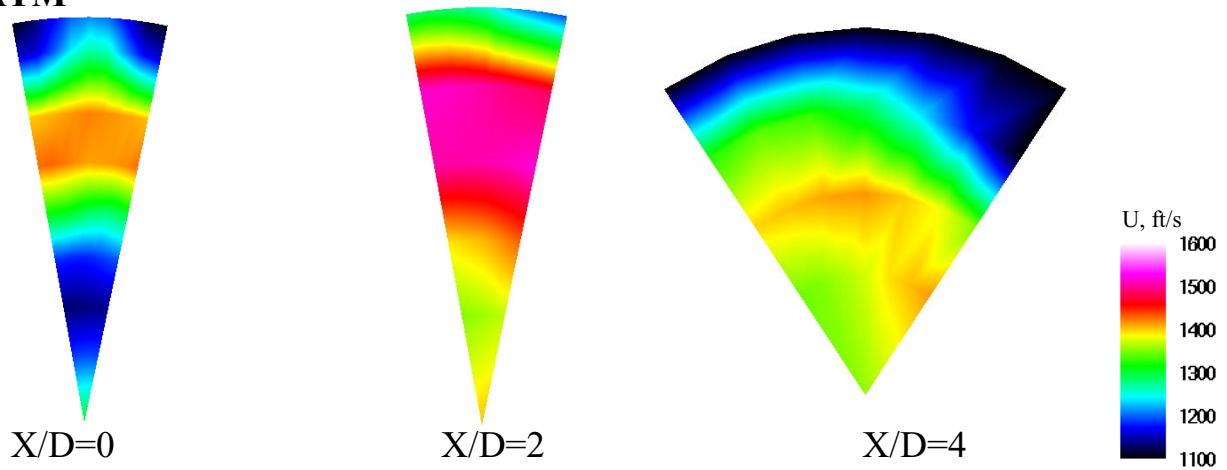
Figure 7.2.3: LDV Axial Velocity Contours Downstream of Nozzle Exit Plane for 12-, 20-, and ATM-Lobe Mixers at Locations, X/D = 0, 1, 2, and 4
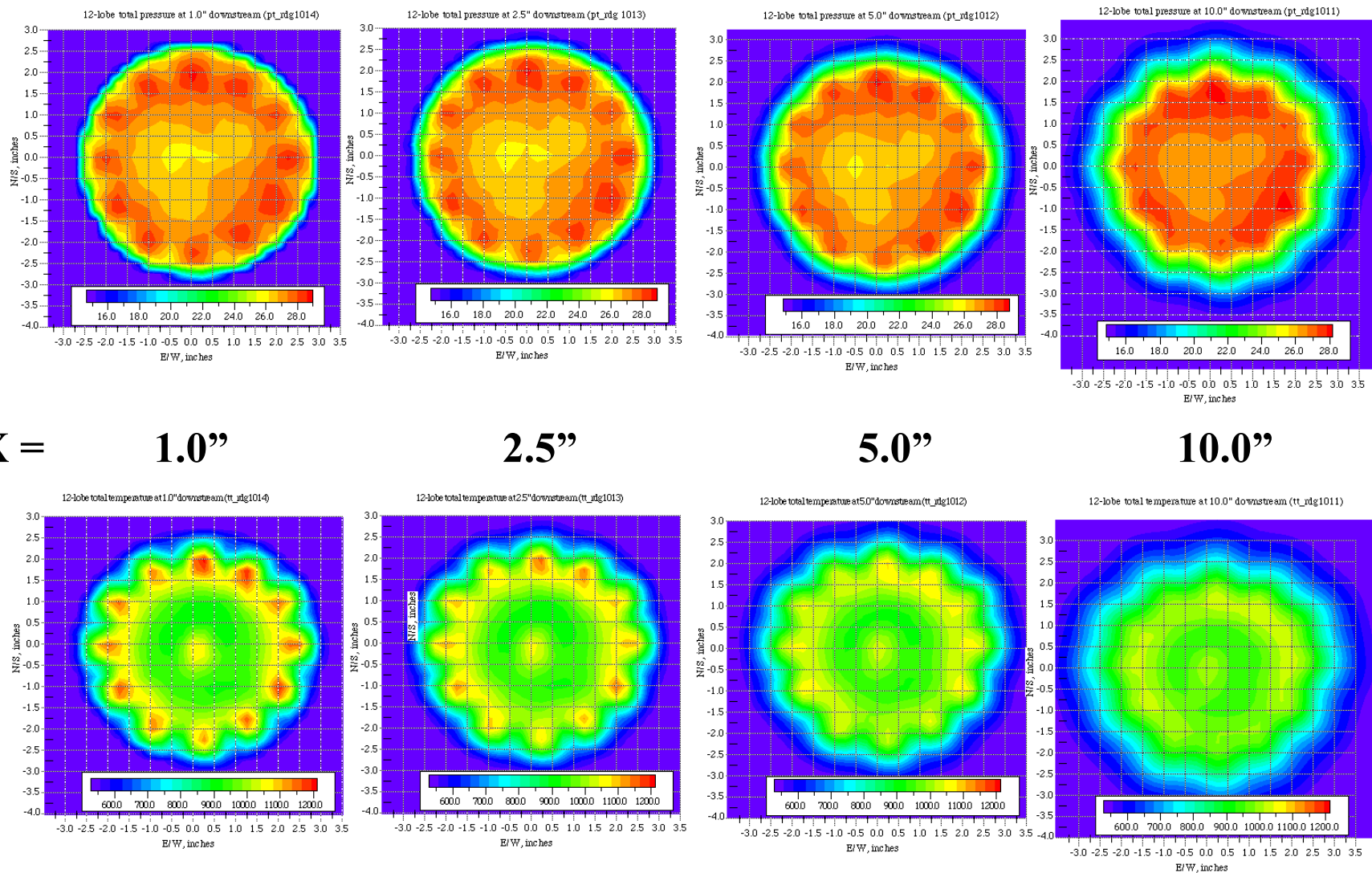
Figure 7.3.1: Total Pressure (psia) and Total Temperature (degrees R) Traverses at X = 1.0, 2.5, 5.0, and 10.0 Inches Downstream of the Nozzle Exit Plane for the 12-Lobe Mixer

X =   1.0"   2.5"   1.0"   2.5"
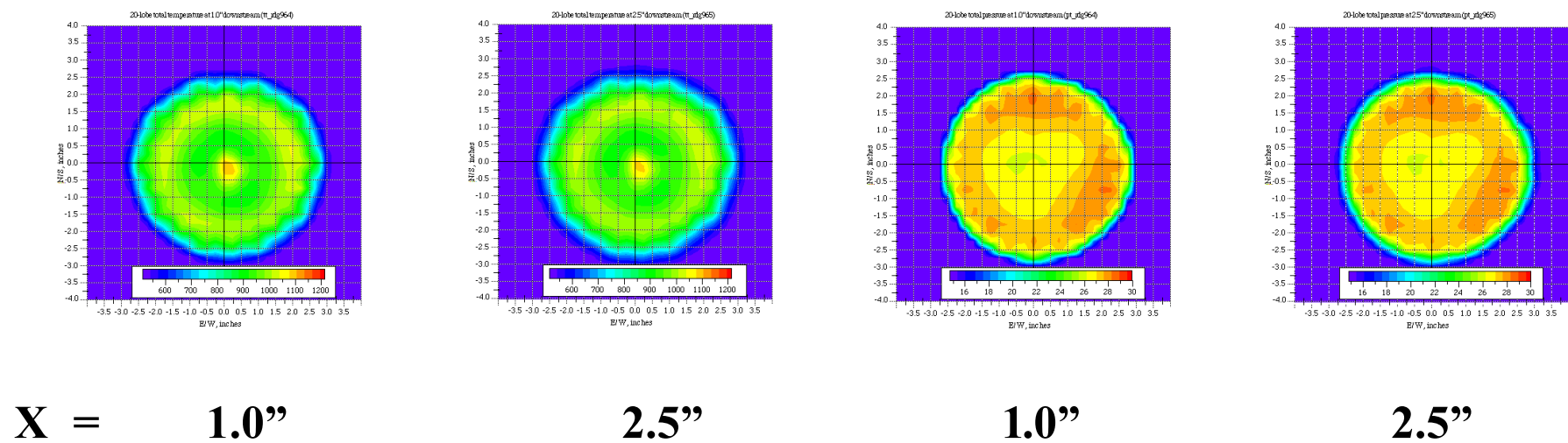
Figure 7.3.2: Total Temperature (degrees R) and Total Pressure (psia) Traverses at X = 1.0, and 2.5 Inches Downstream of the Nozzle Exit Plane for the 20-Lobe Mixer
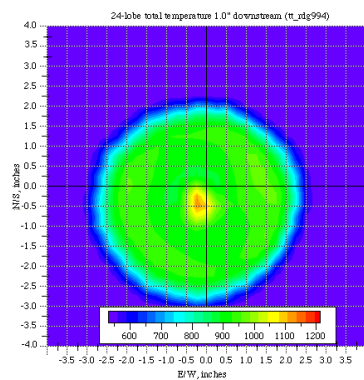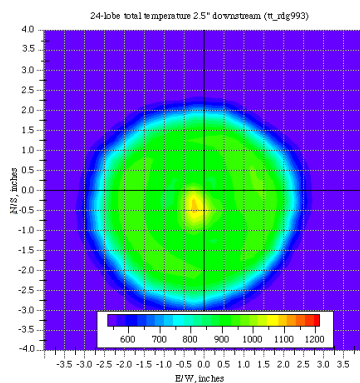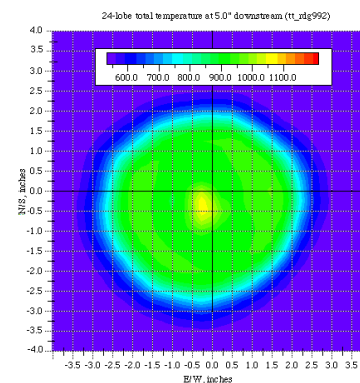
X =   1.0"   2.5"   5.0"   10.0"
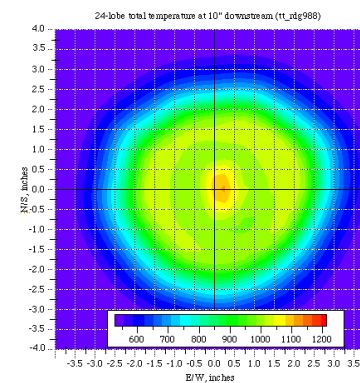
Figure 7.3.3: Total Temperature (degrees R) Traverses at X = 1.0, 2.5, 5.0, and 10.0 Inches Downstream of the Nozzle Exit Plane for the 24-Lobe Mixer
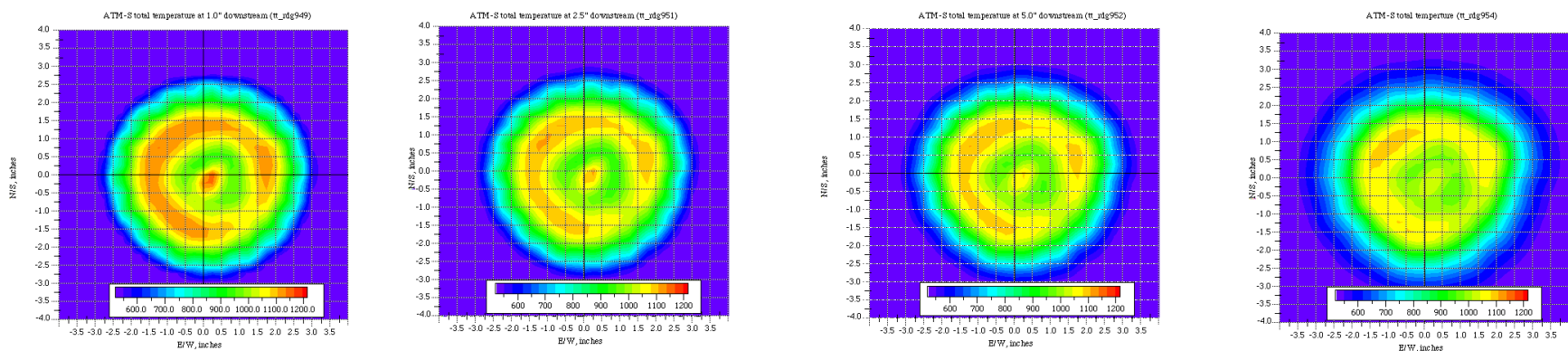
X =   1.0"   2.5"   5.0"   10.0"

Figure 7.3.4: Total Temperature (degrees R) Traverses at X = 1.0, 2.5, 5.0, and 10.0 Inches Downstream of the Nozzle Exit Plane for the ATM
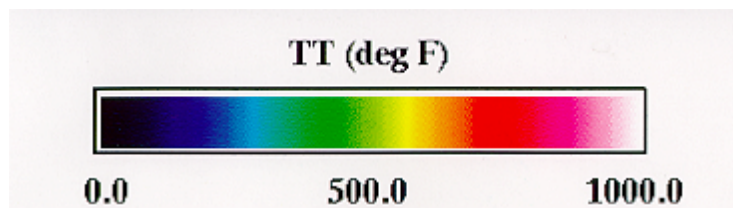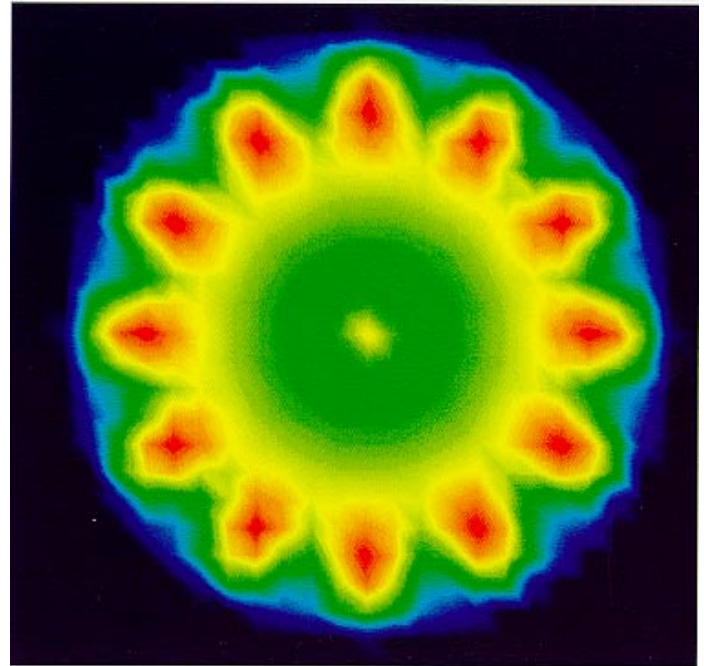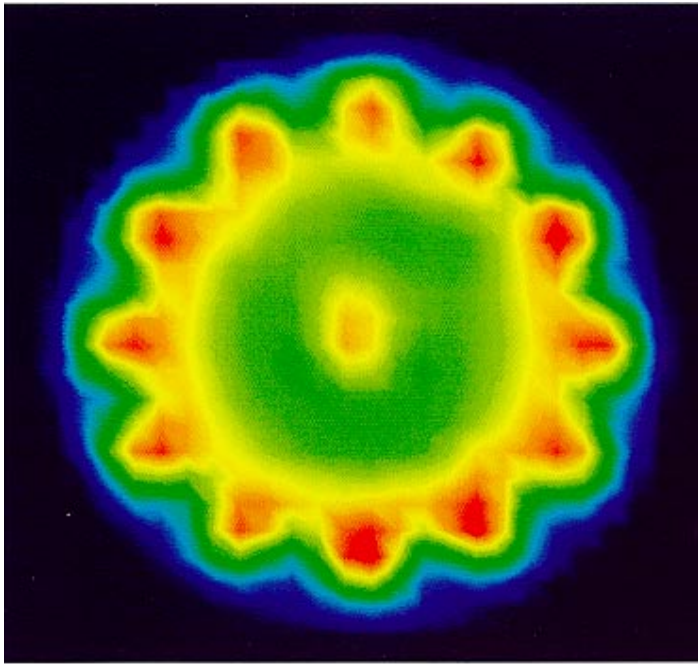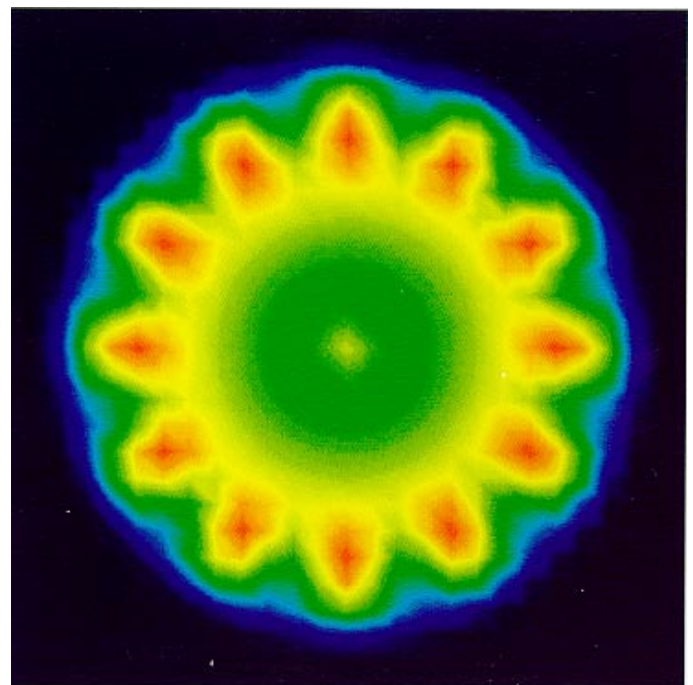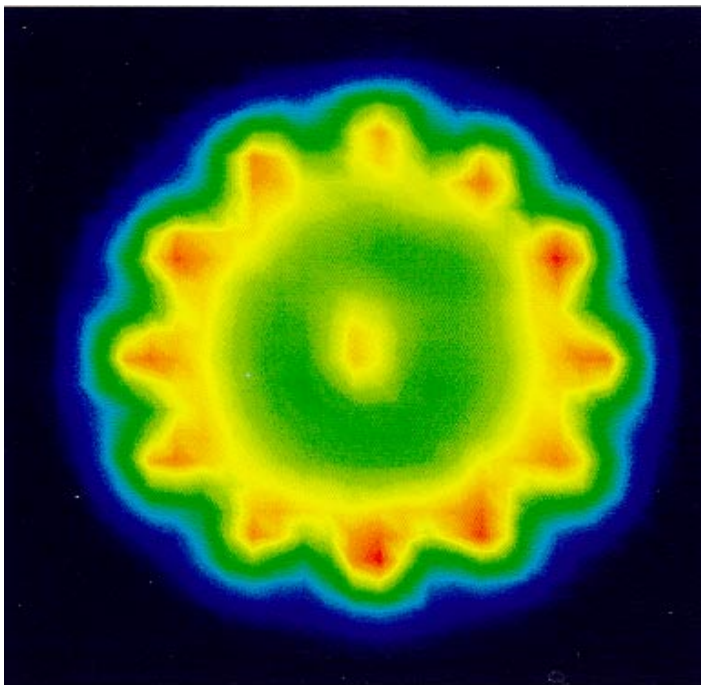
Figure 7.3.5: 12-Lobe Mixer Model Total Temperature Traverse Comparisons at X=1.0, and 2.5 Inches Downstream of the Nozzle Exit Plane
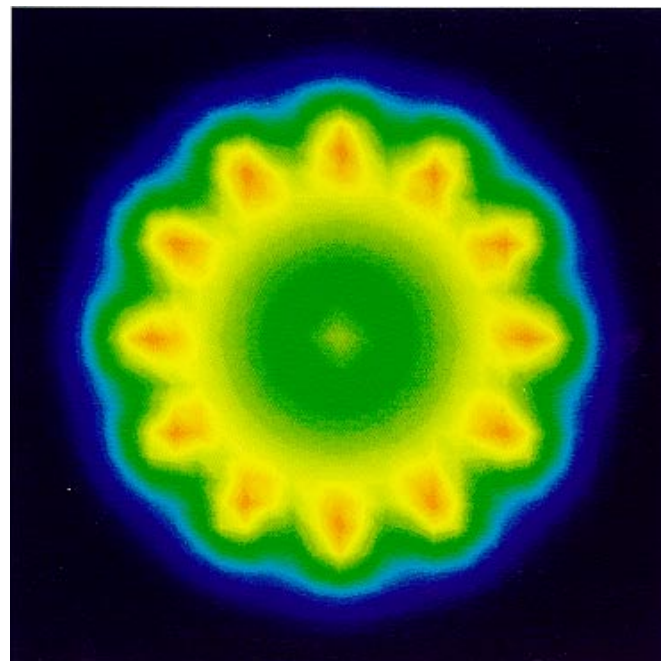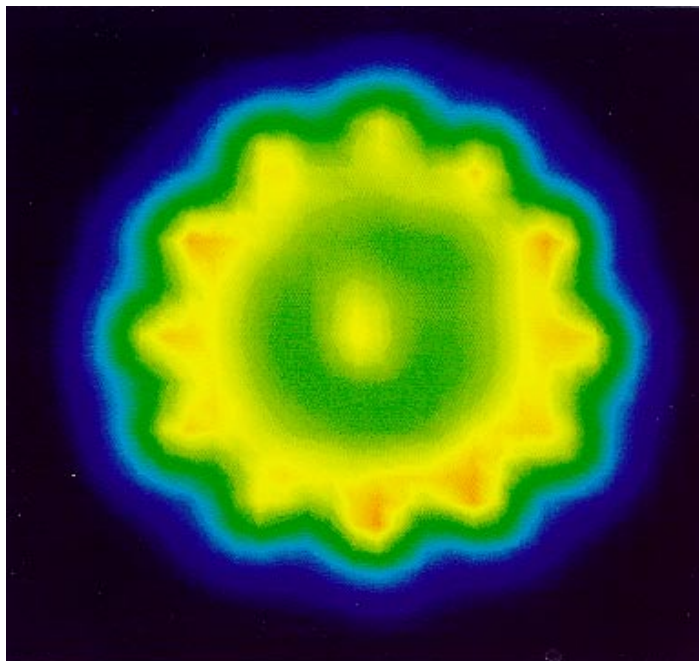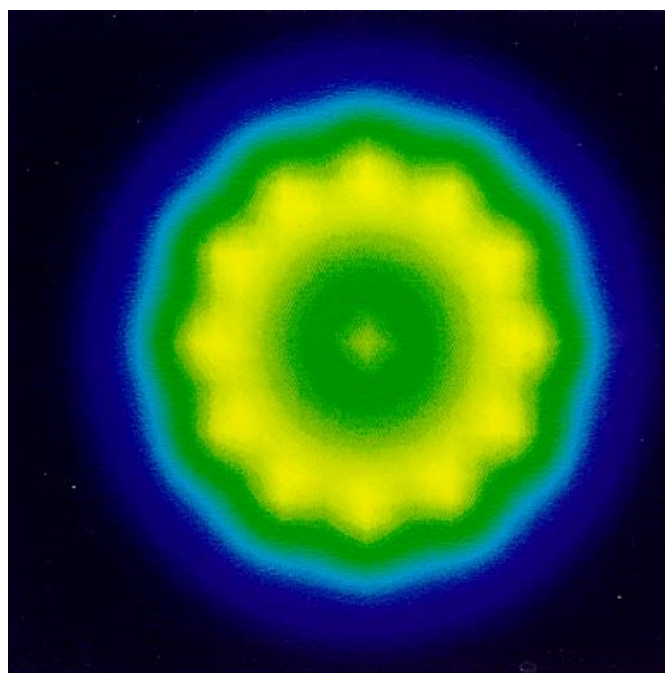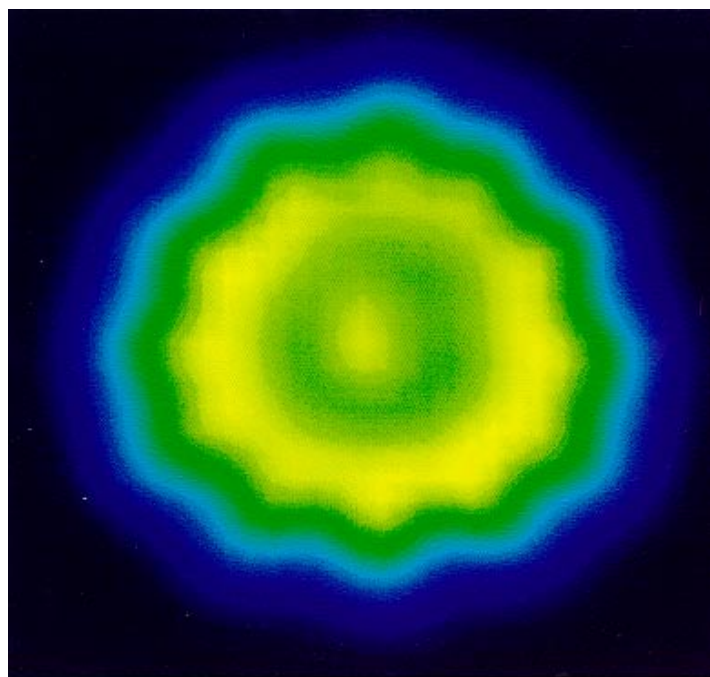
Figure 7.3.6: 12-Lobe Mixer Model Total Temperature Traverse Comparisons at X=5.0, and 10.0 Inches Downstream of the Nozzle Exit Plane

TT (deg F)

0.0   500.0   1000.0
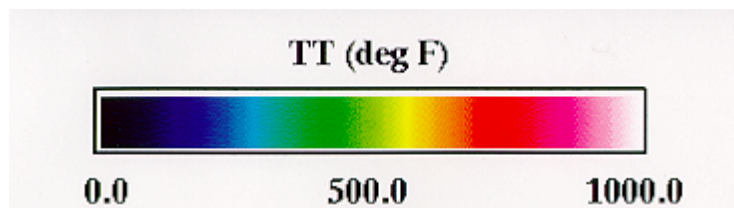
DATA   NASTAR
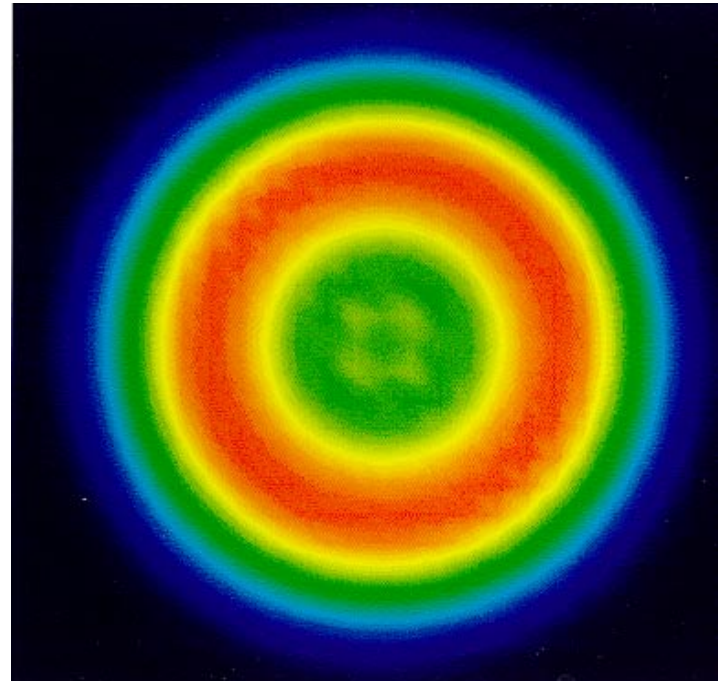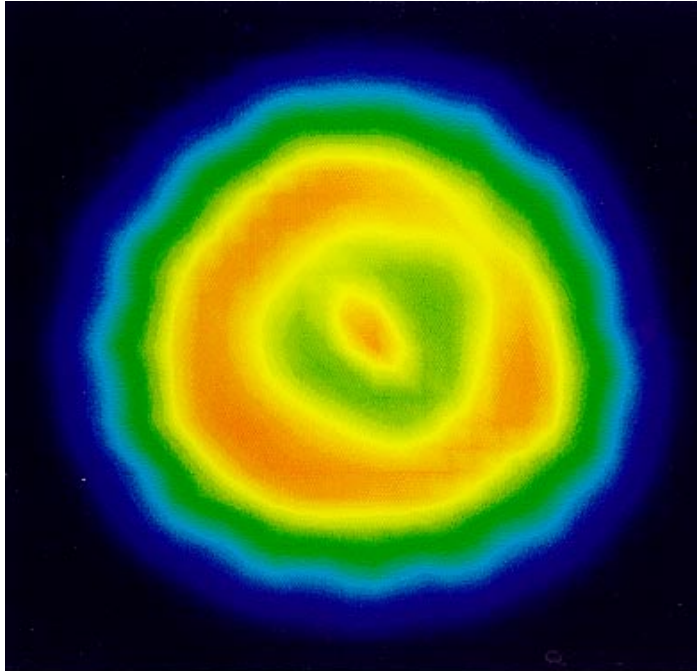
X = 5"
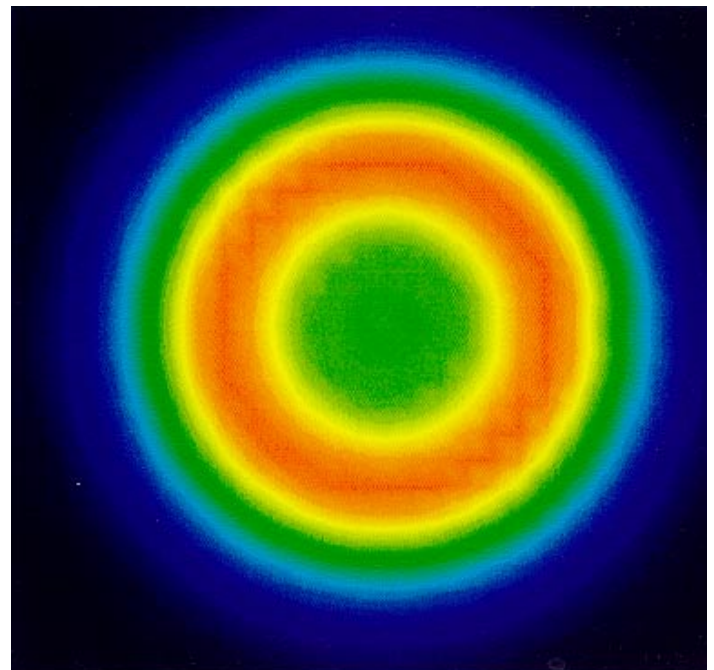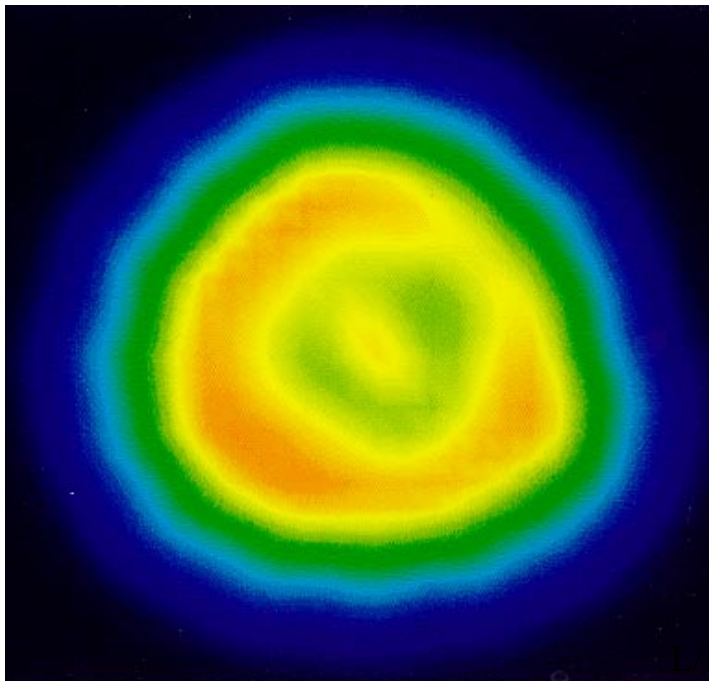
X = 10"

Figure 7.3.7: ATM Model Total Temperature Traverse Comparisons at X=5.0, and 10.0 Inches Downstream of the Nozzle Exit Plane
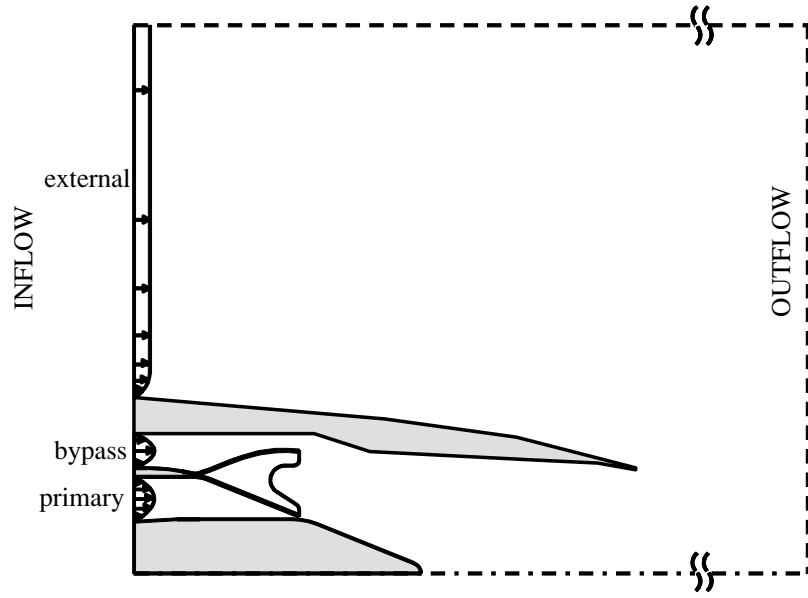
Figure 8.2.1: Computational Volume for Analysis
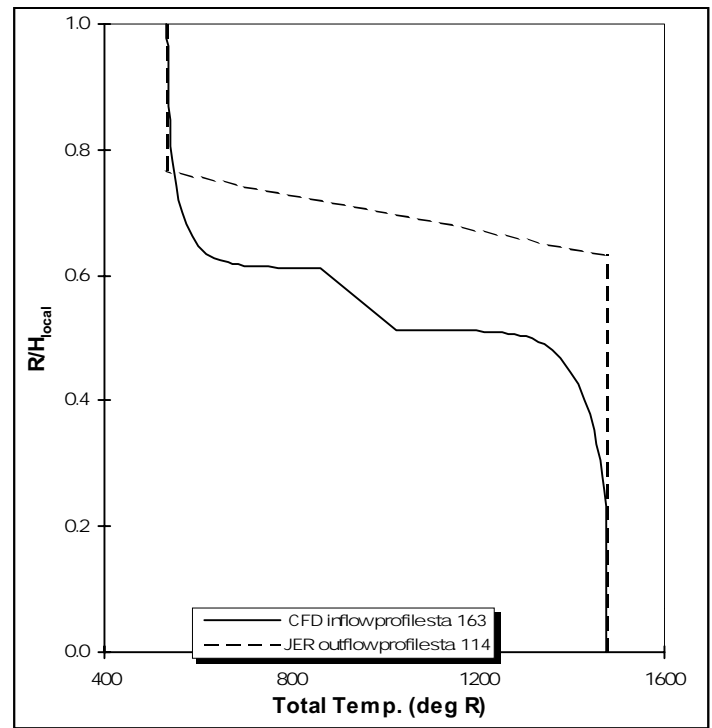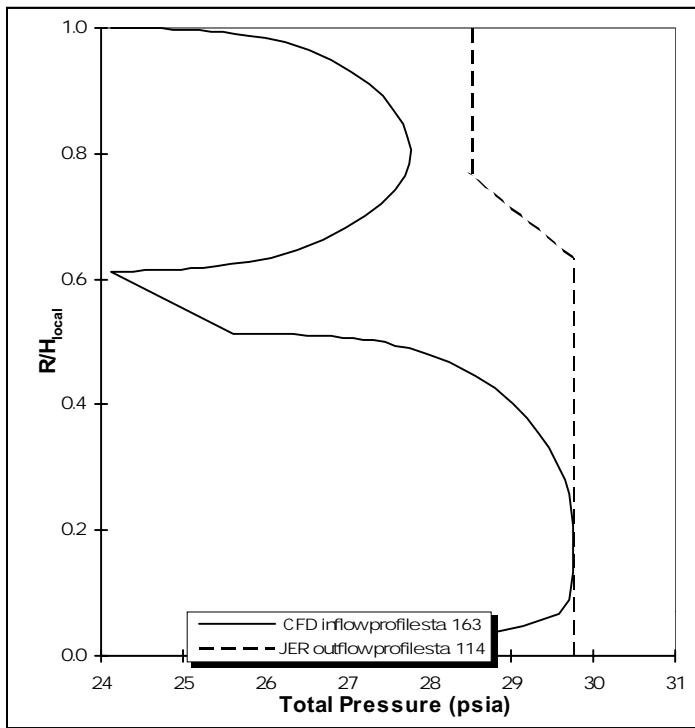
Figure 8.2.2: CFD Initialization Profiles
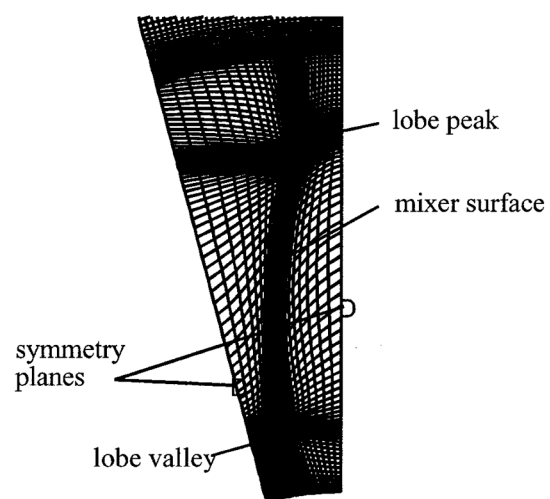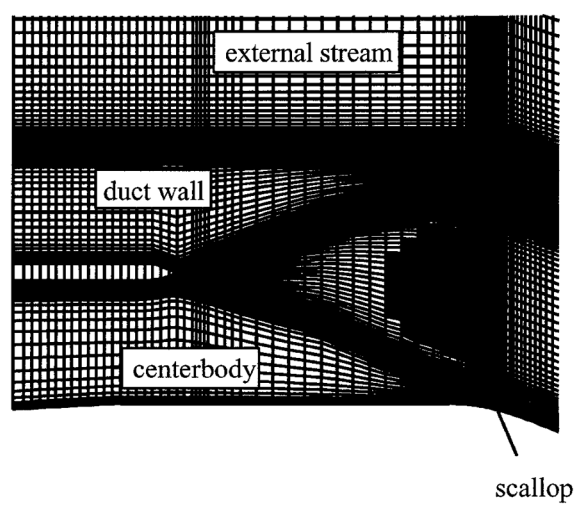
Figure 8.2.3: 3D Mixer Grid
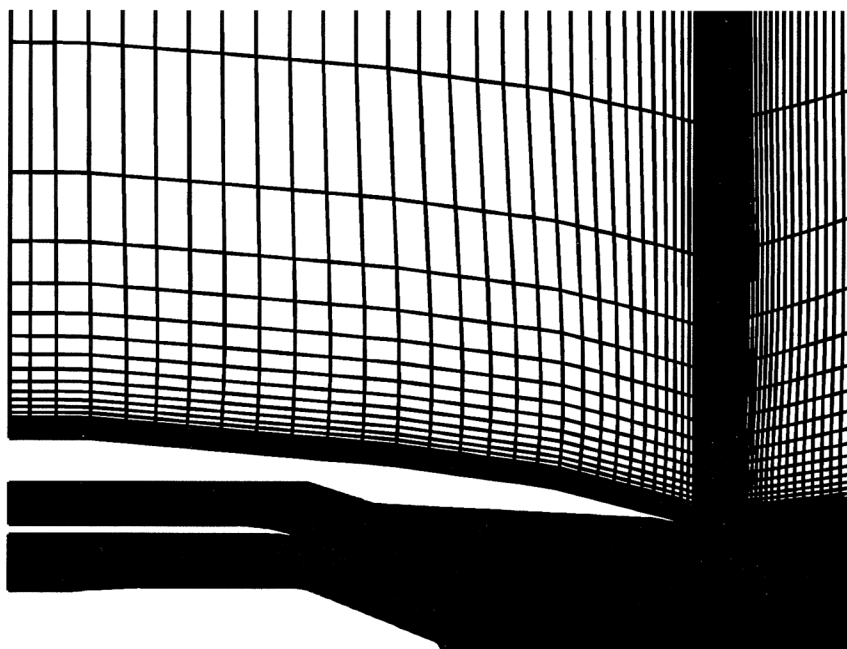
Figure 8.2.4: Axisymmetric Splitter CFD Grid
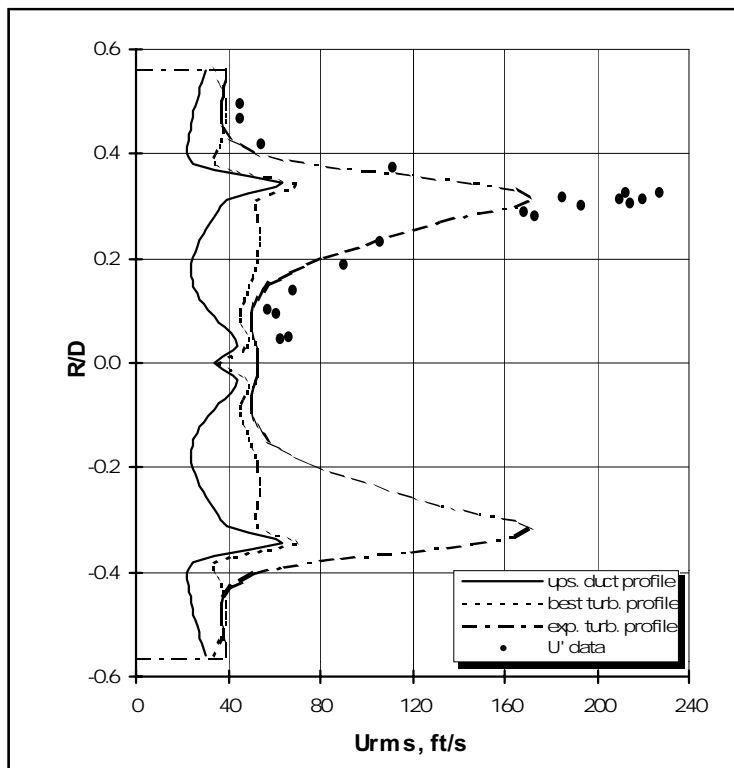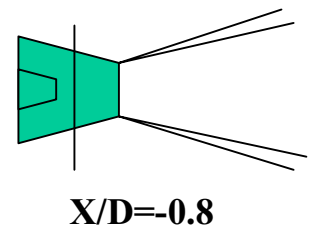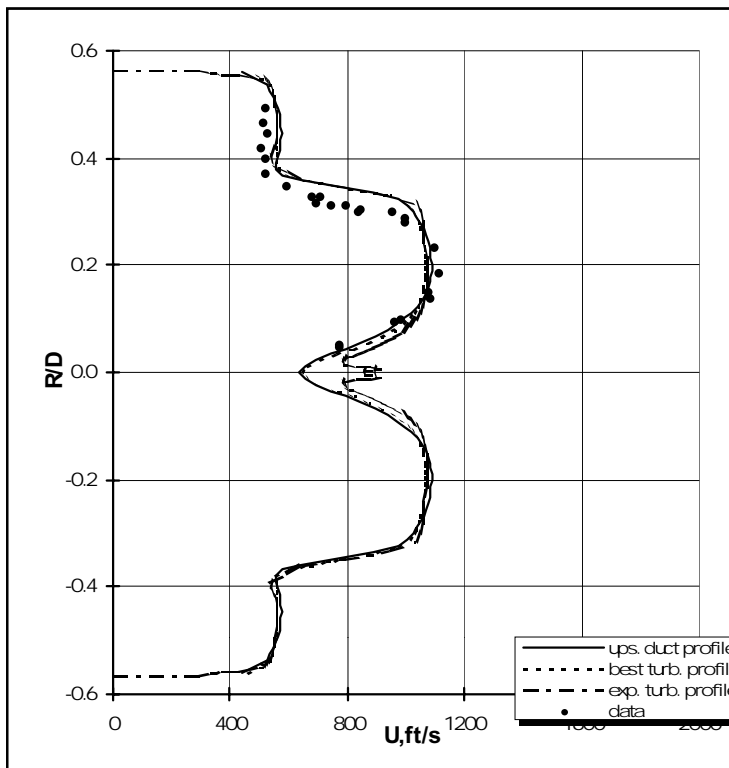
Figure 8.2.5a: Comparison of Splitter Analysis to Data
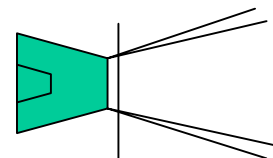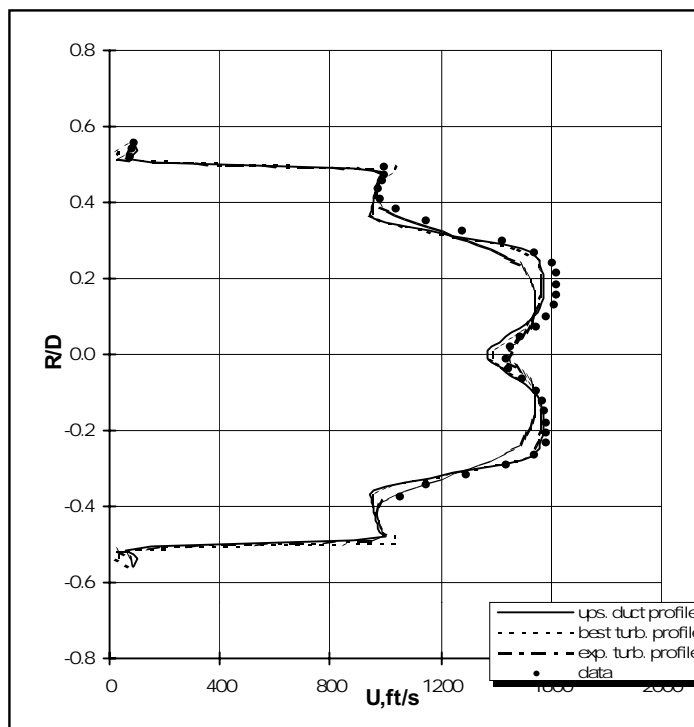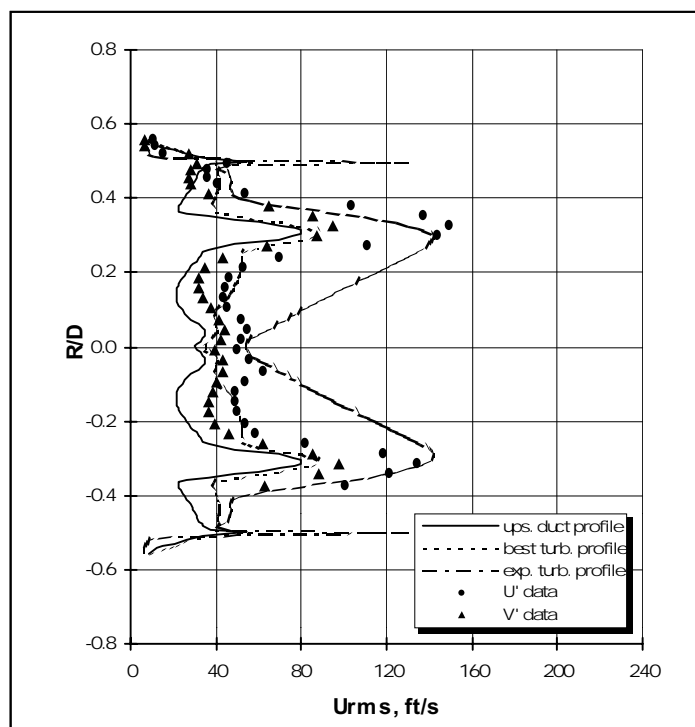
Figure 8.2.5b: Comparison of Splitter Analysis to Data
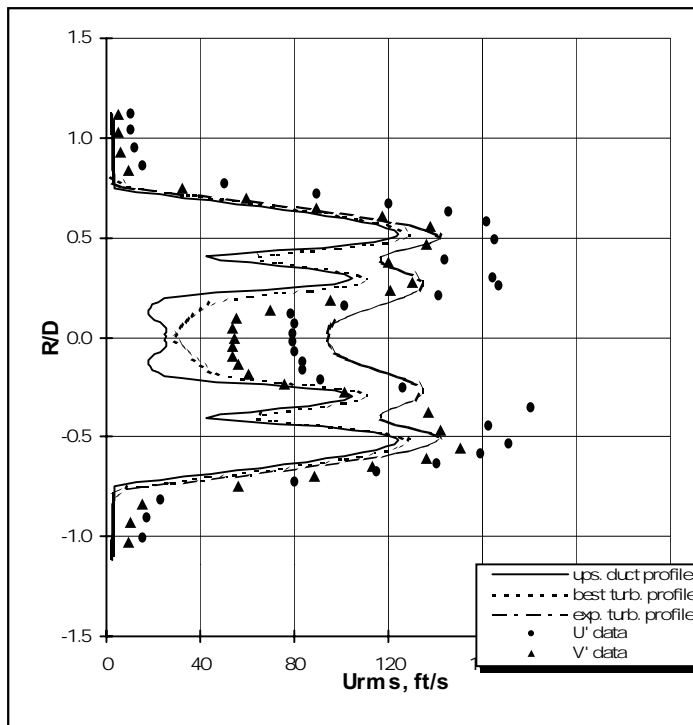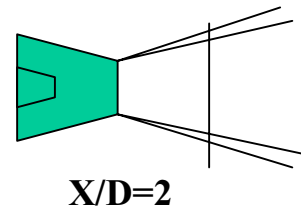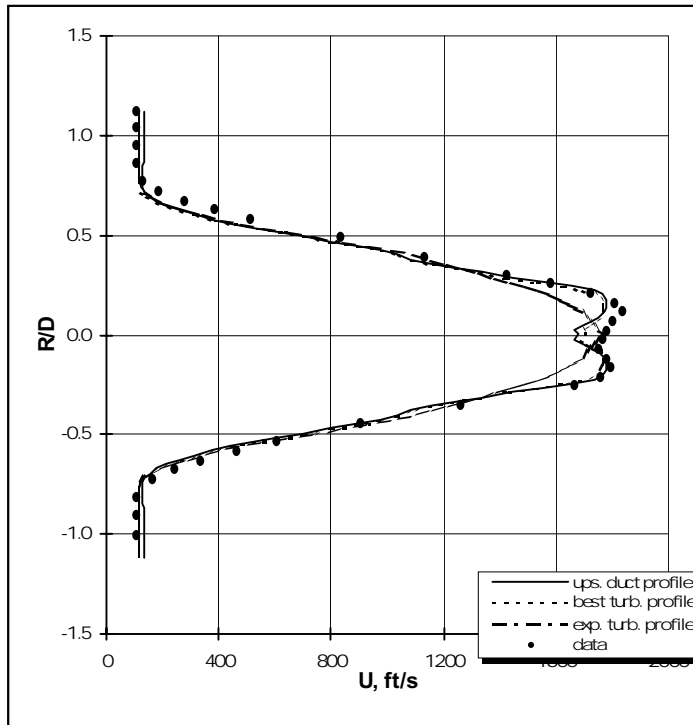
Figure 8.2.5c: Comparison of Splitter Analysis to Data
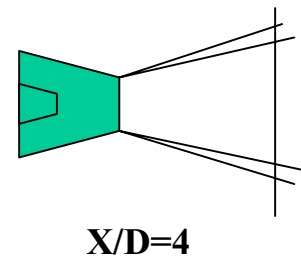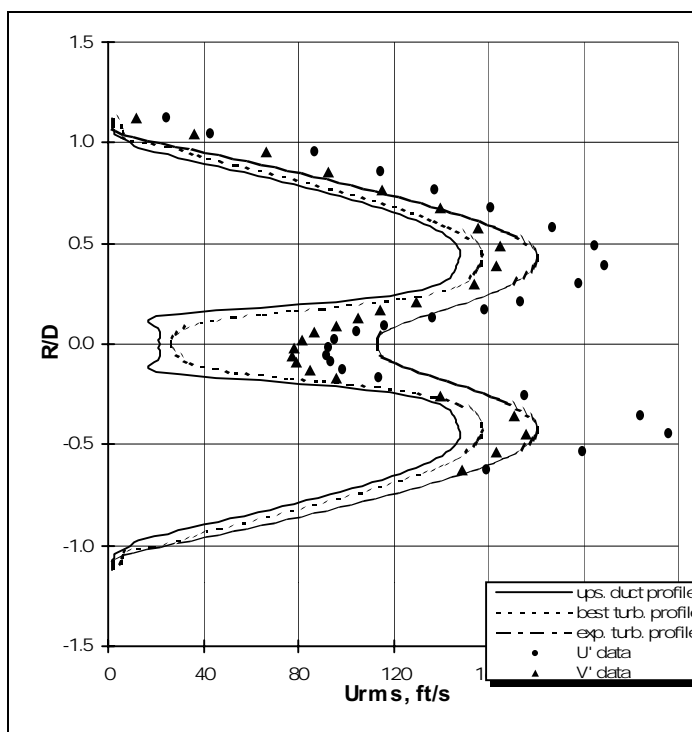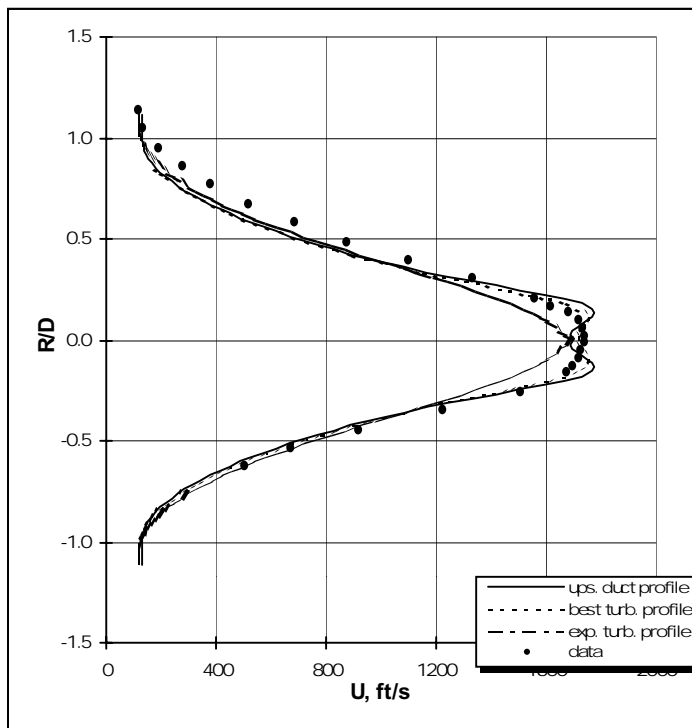
Figure 8.2.5d: Comparison of Splitter Analysis to Data
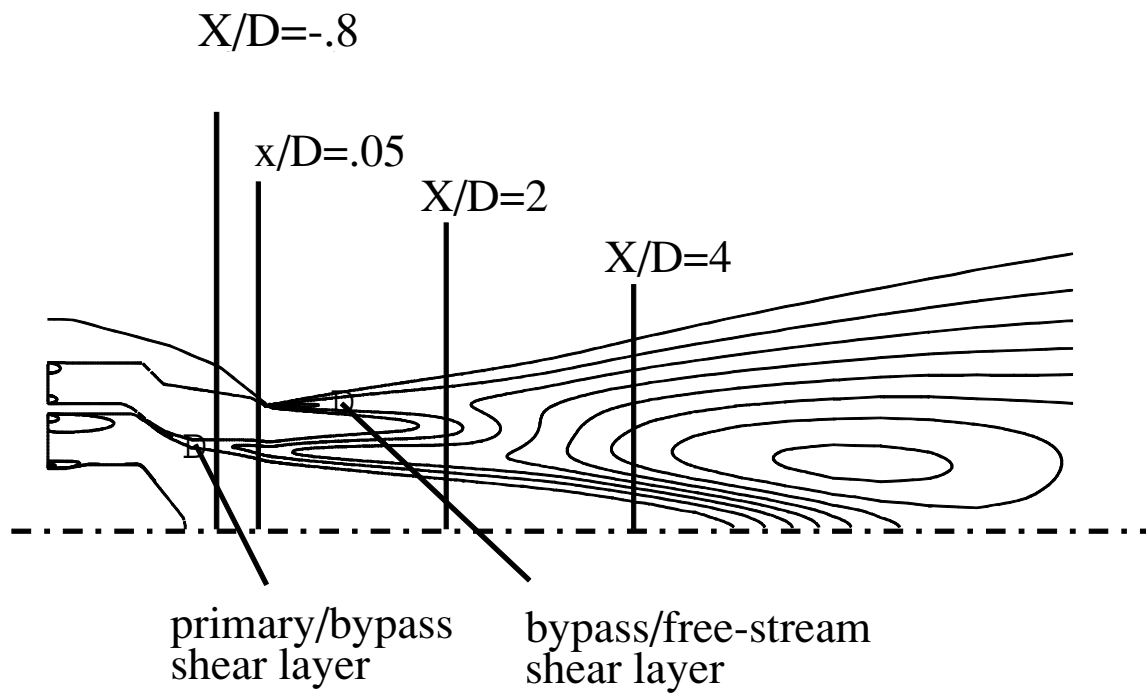
Figure 8.2.6: Turbulent Kinetic Energy Contours
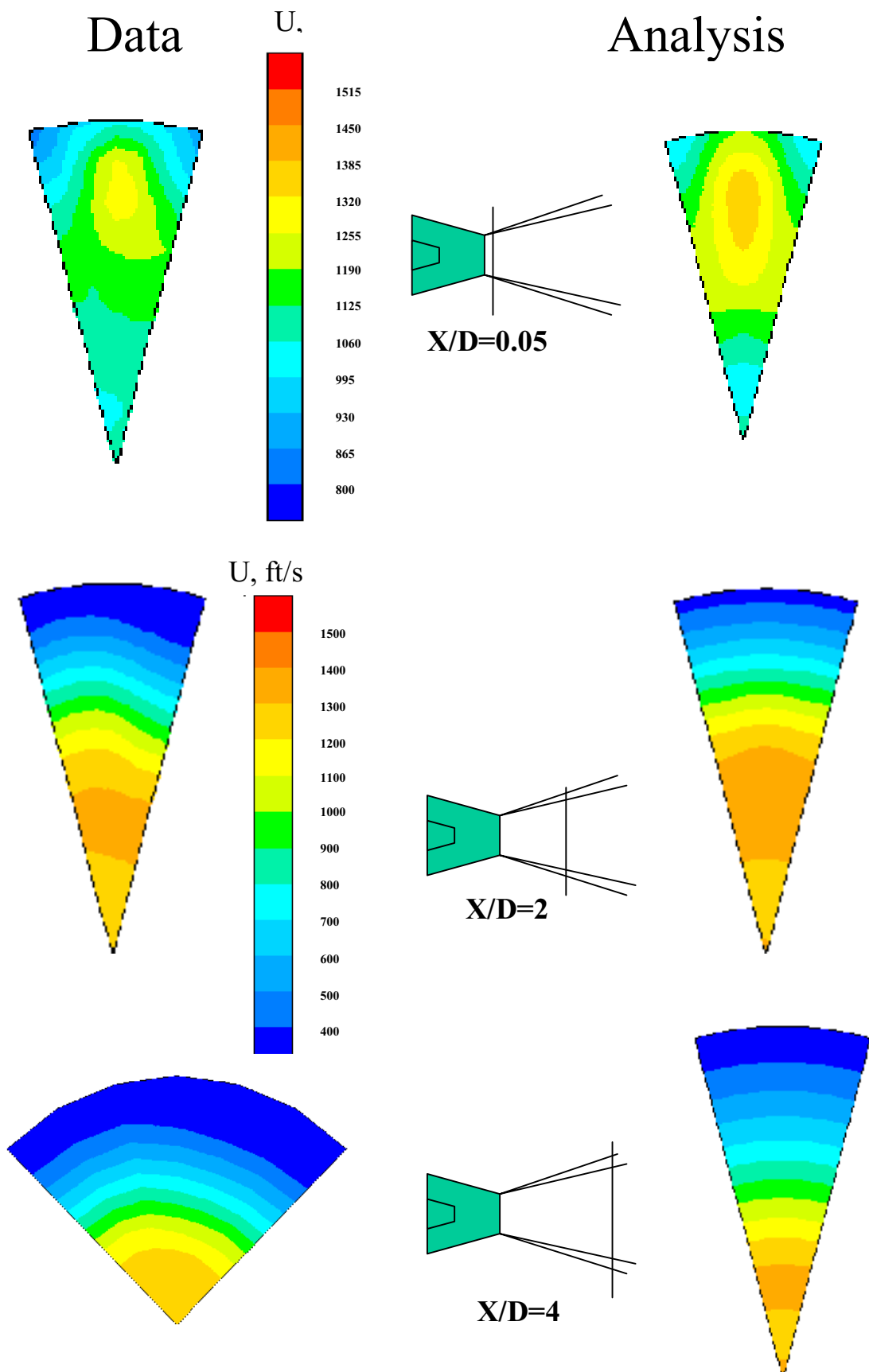
Figure 8.2.7: Comparison of 12-Lobe Mixer Analysis and Data
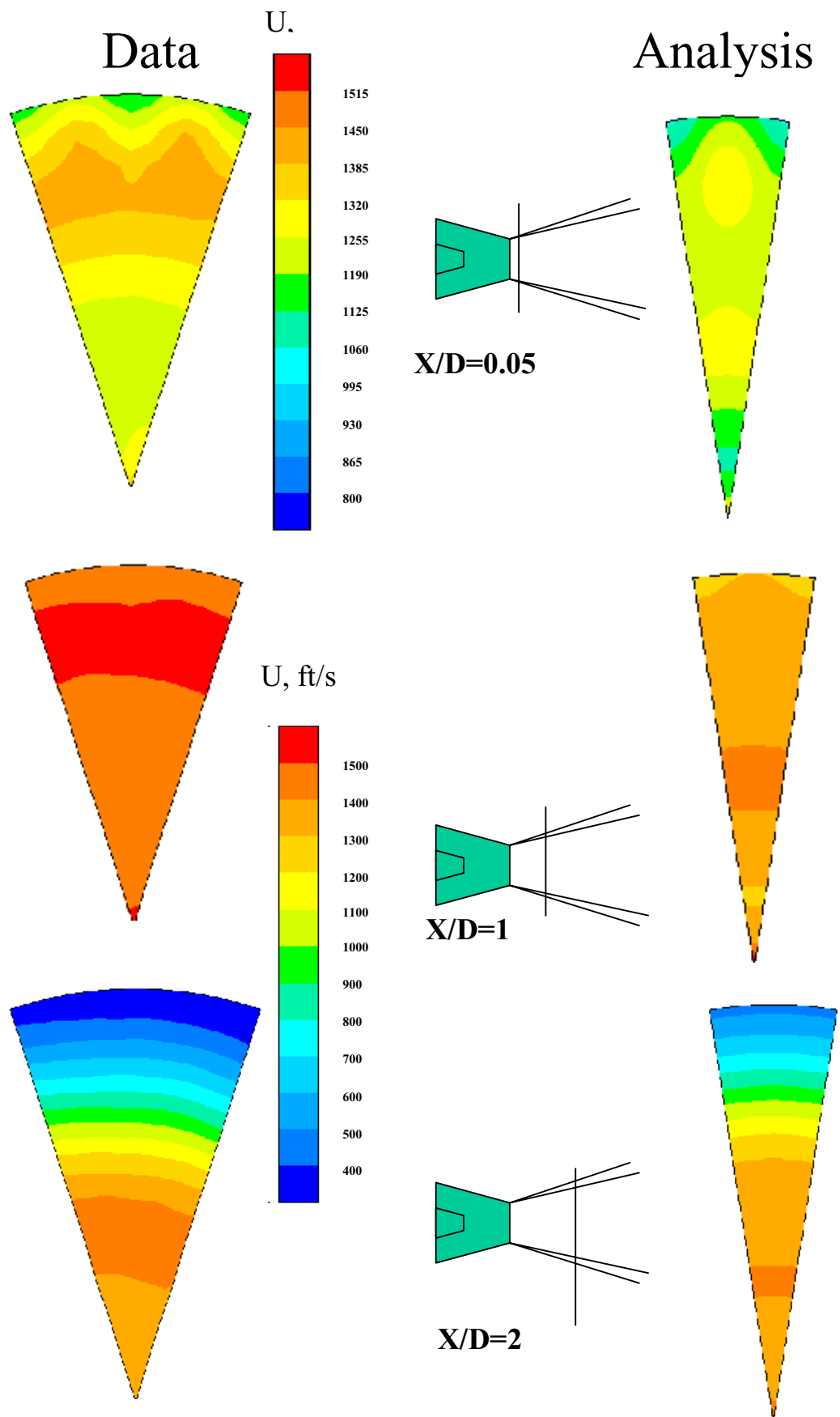
Figure 8.2.8: Comparison of 20-Lobe Mixer Analysis and Data
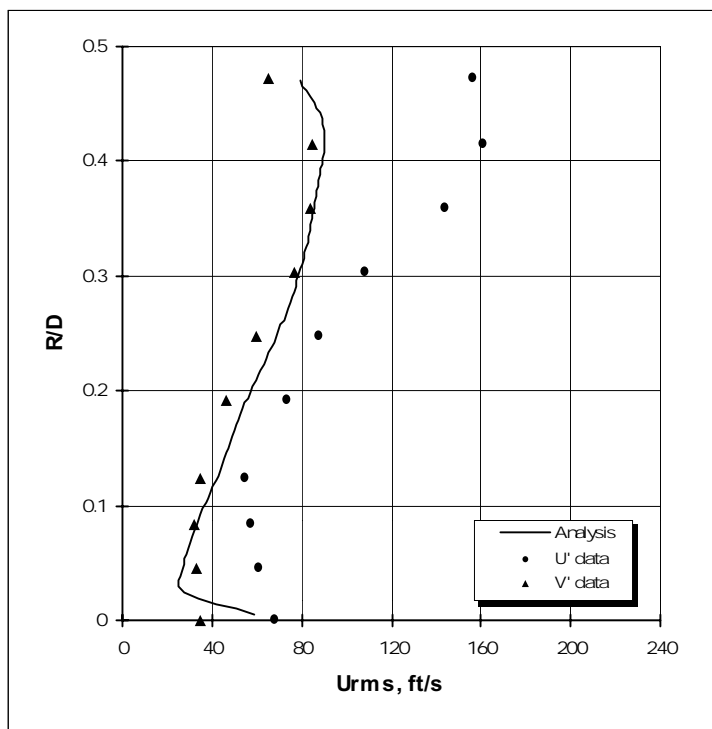
12-Lobe
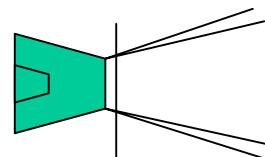
X/D=0.05
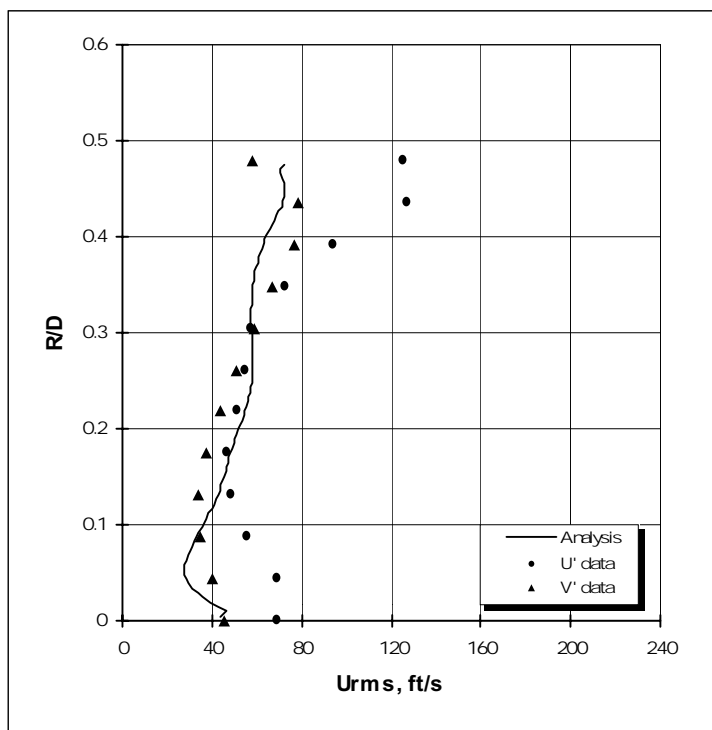
20-Lobe

Figure 8.2.9a: Comparison of 12 and 20-Lobe Mixer Analysis to Data
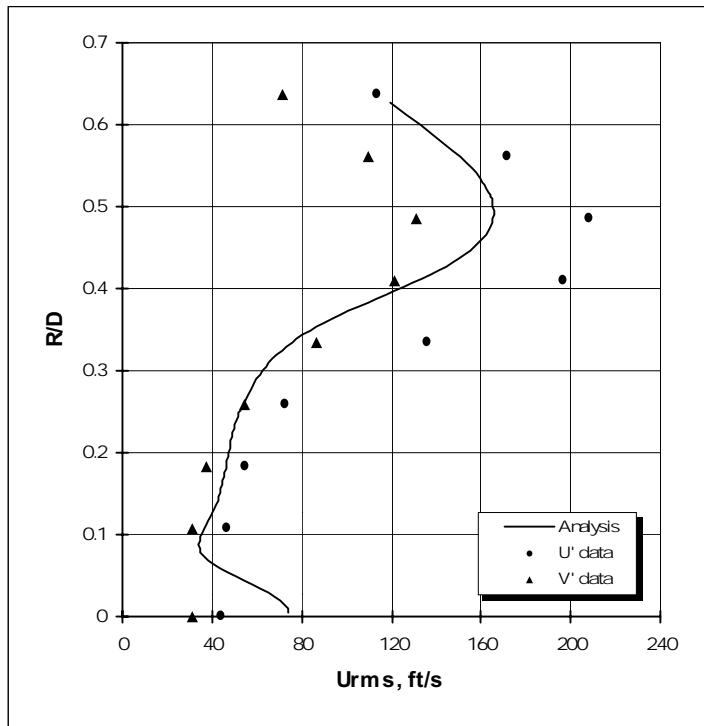
12-Lobe
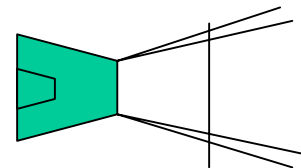
X/D=2
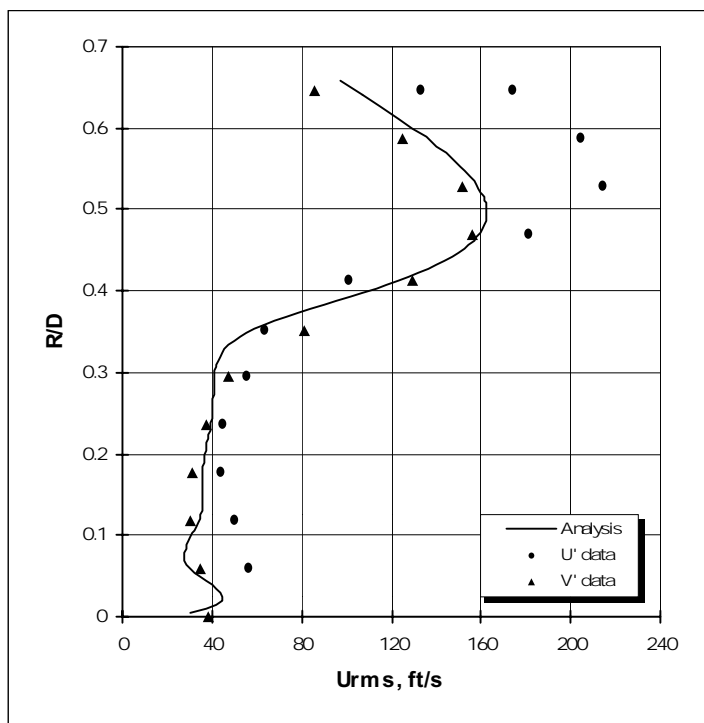
20-Lobe

Figure 8.2.9b: Comparison of 12 and 20-Lobe Mixer Analysis to Data
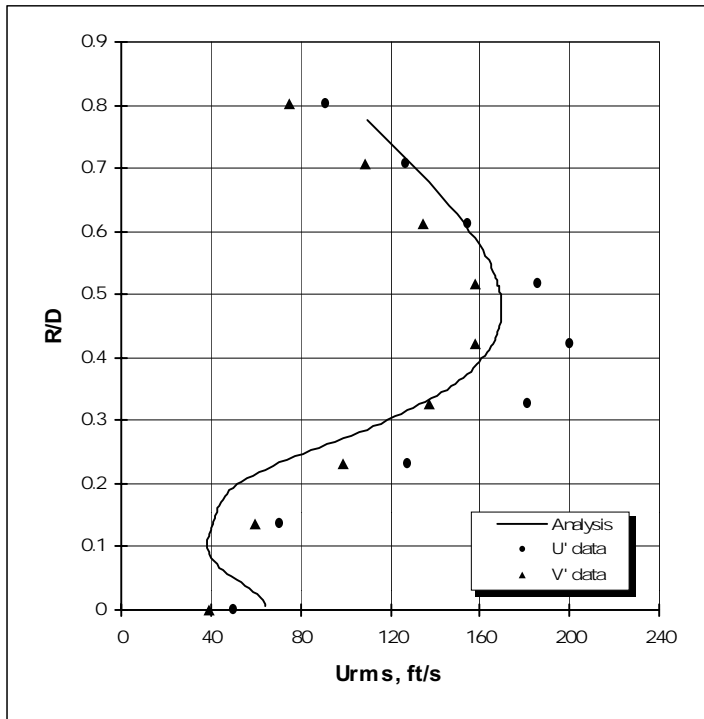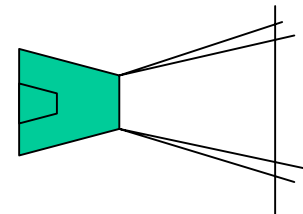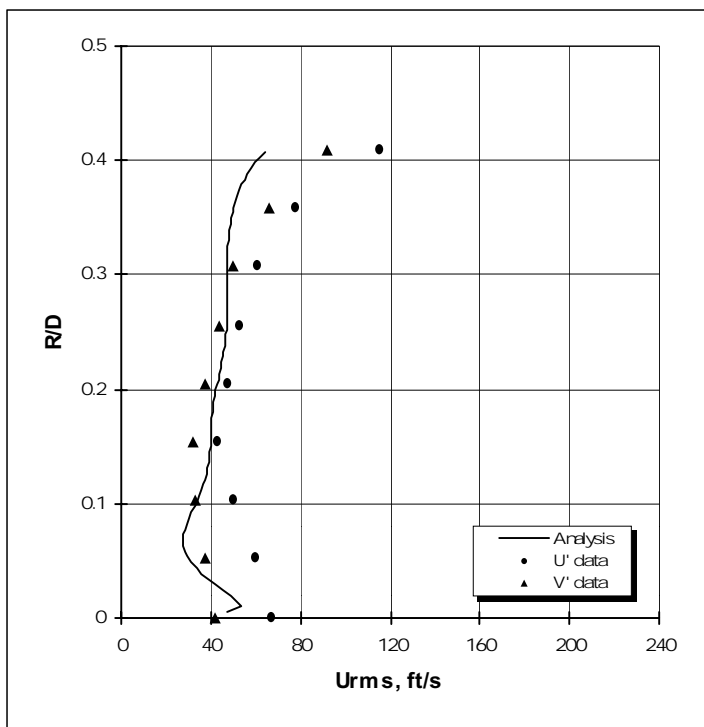
Figure 8.2.9c: Comparison of 12 and 20-Lobe Mixer Analysis to Data
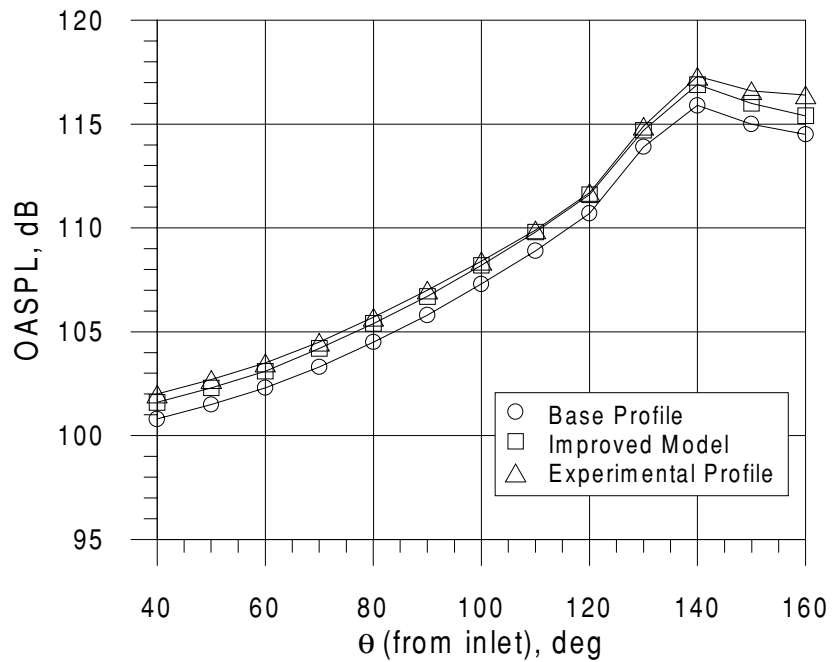
Figure 8.3.1: Effect of inlet turbulence profile on OASPL
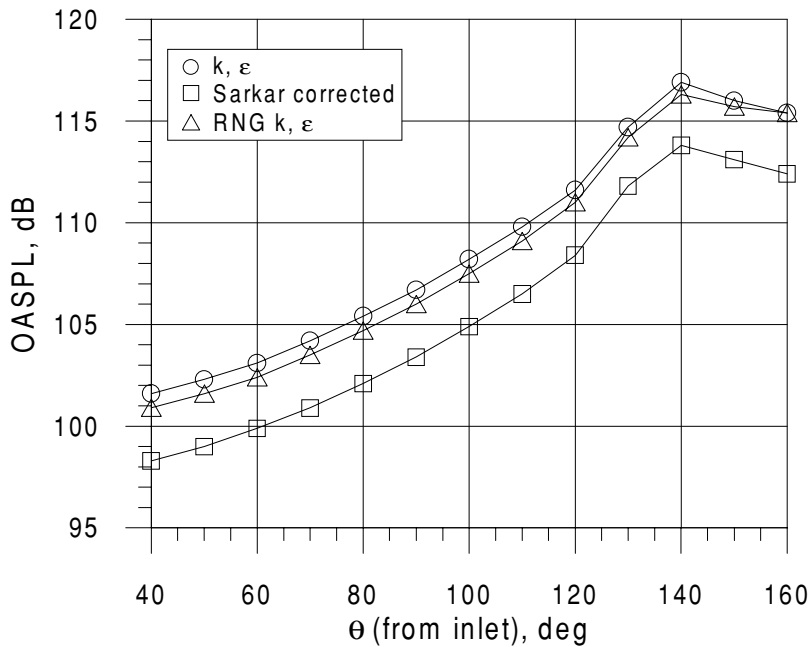
Figure 8.3.2: Effect of turbulence model on OASPL
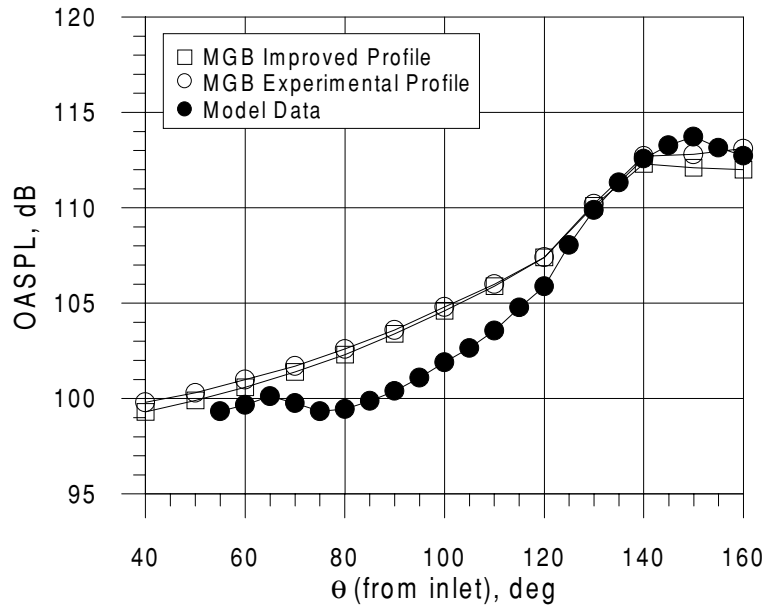
Figure 8.3.3: Model scale Splitter OASPL comparisons at 50 foot distance
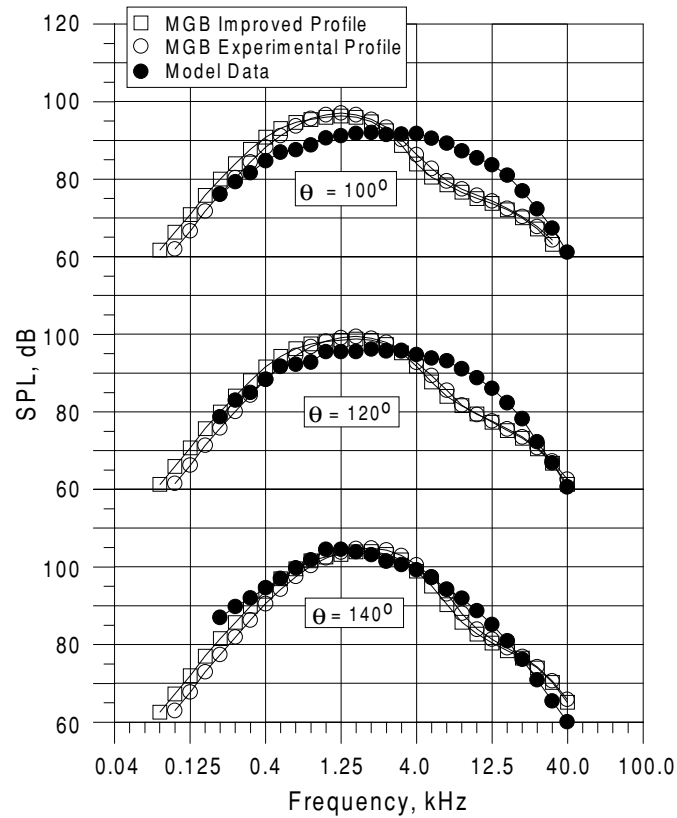
Figure 8.3.4: Model scale Splitter 1/3 octave spectra comparisons at 50 foot distance
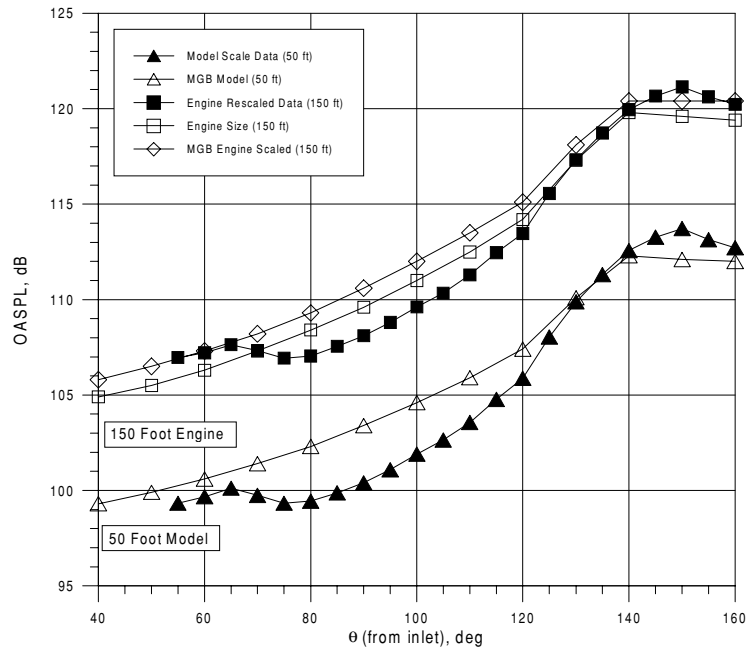
Figure 8.3.5: Engine scaled Splitter OASPL comparisons at 150 foot distance
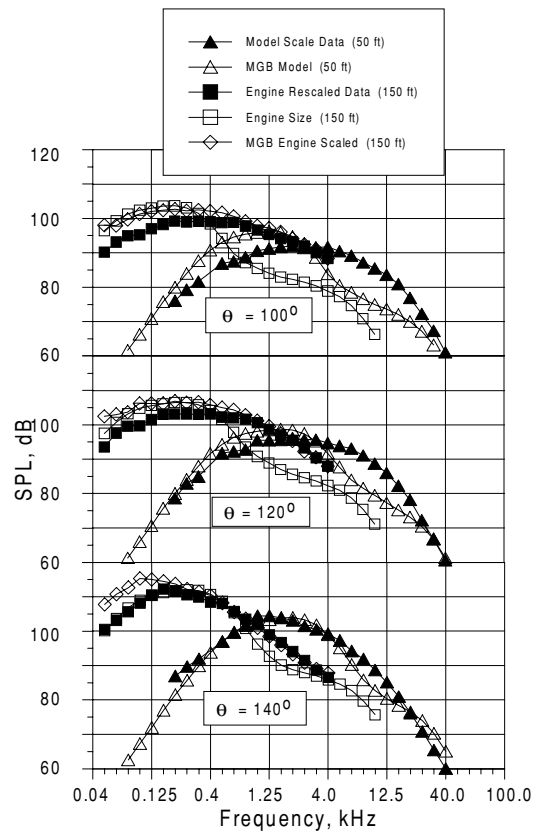
Figure 8.3.6: Engine scaled Splitter 1/3 octave spectra comparisons at 150 foot distance
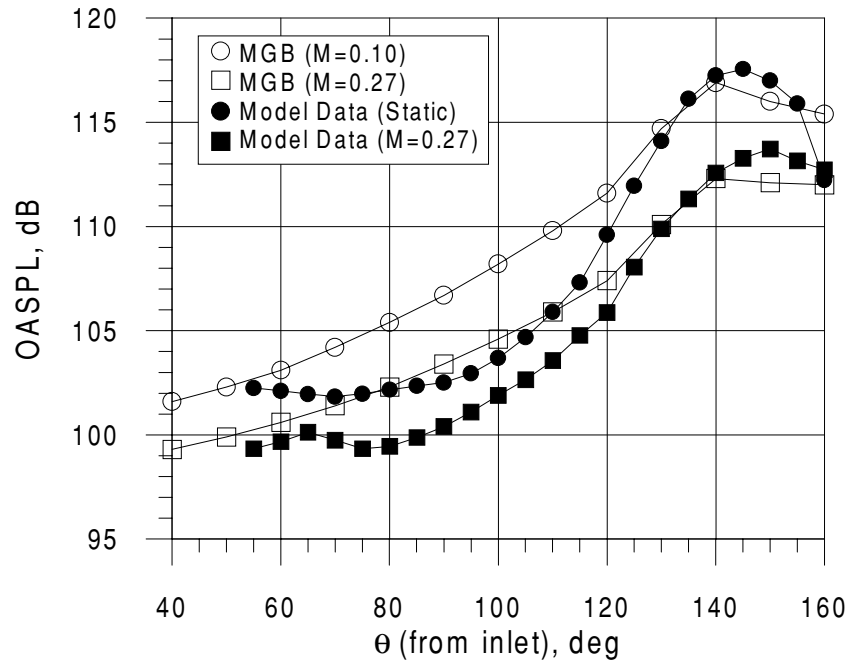
Figure 8.3.7: Forward flight effect on OASPL for model scale Splitter at 50 foot distance
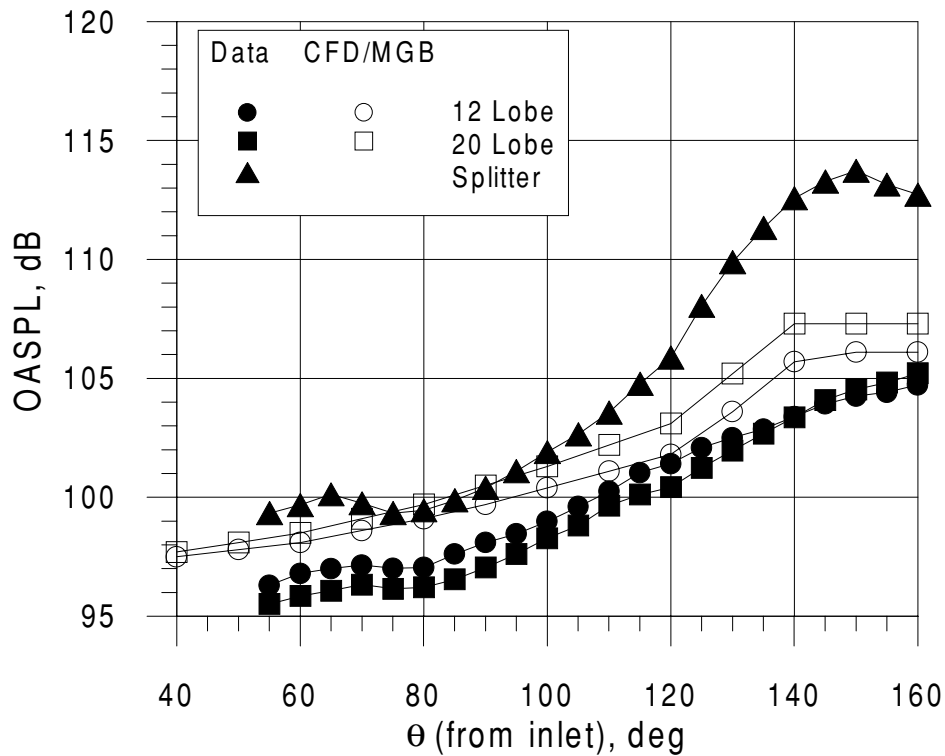
Figure 8.3.8: MGB/data comparisons of OASPL for 12/20-lobe mixer nozzles at 50 foot distance
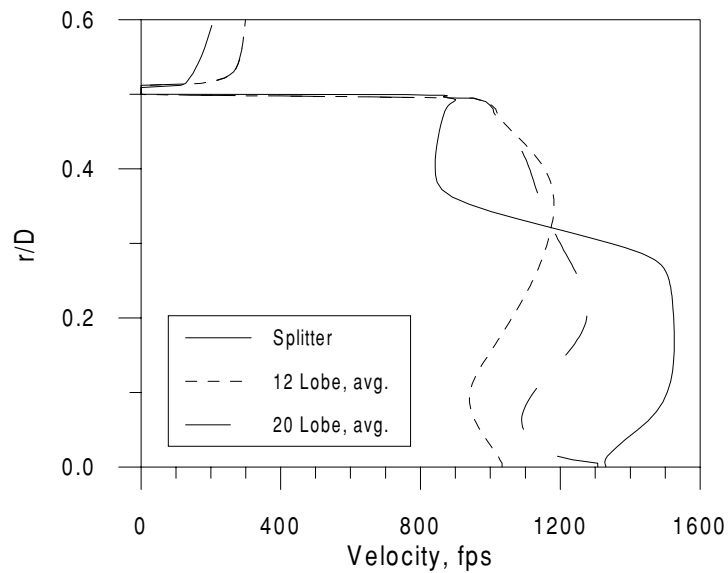
Figure 8.3.9: Circumferentially mass averaged exit plane axial velocity profiles for Splitter, 12-lobe and 20-lobe nozzles
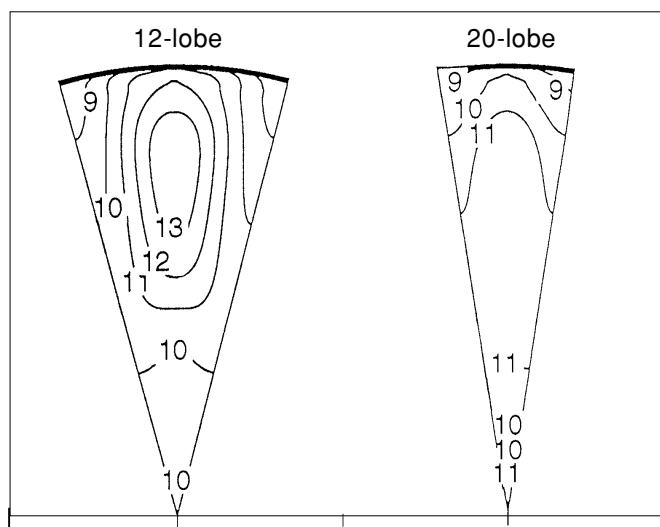
Figure 8.3.10: Exit plane velocity field for 12 and 20-lobe mixer nozzles (Ux10^{-2} fps)
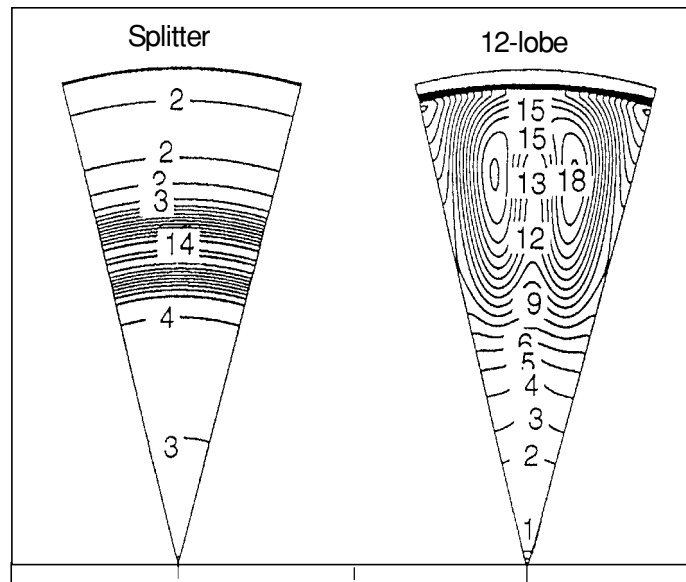
Figure 8.3.11: Exit plane turbulent kinetic energy contours for axisymmetric Splitter and 12-lobe mixer nozzles (kx10^{-3}, ft^2/s^2)
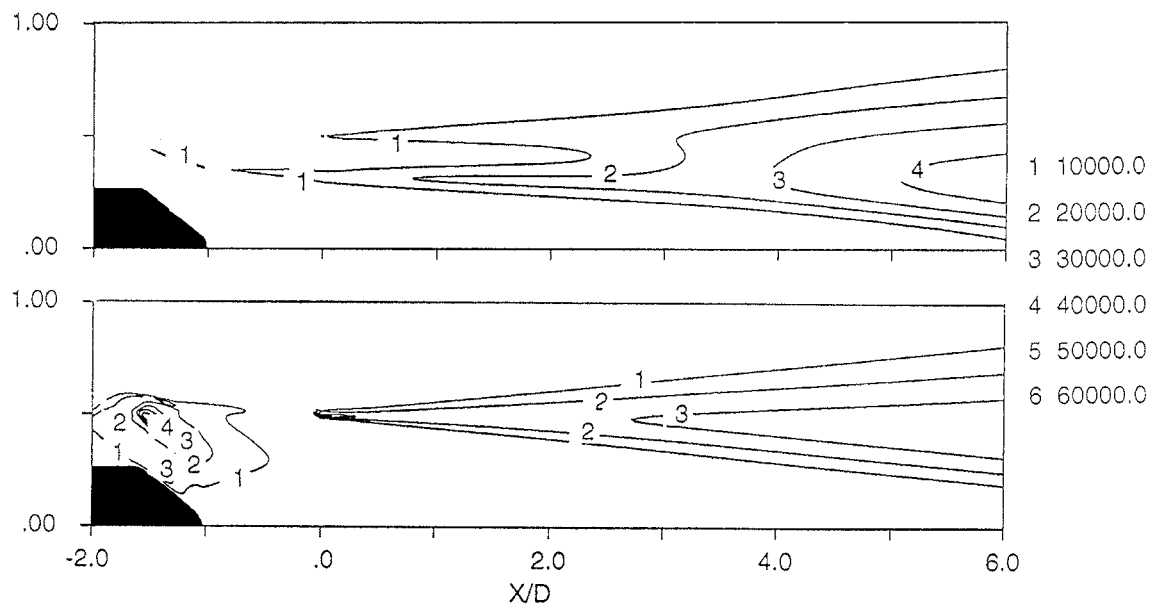
Figure 8.3.12: Axial view of turbulent kinetic energy contours in the exhaust of an axisymmetric Splitter and 20-lobe mixer nozzles (kx10^{-4}, ft^2/s^2)
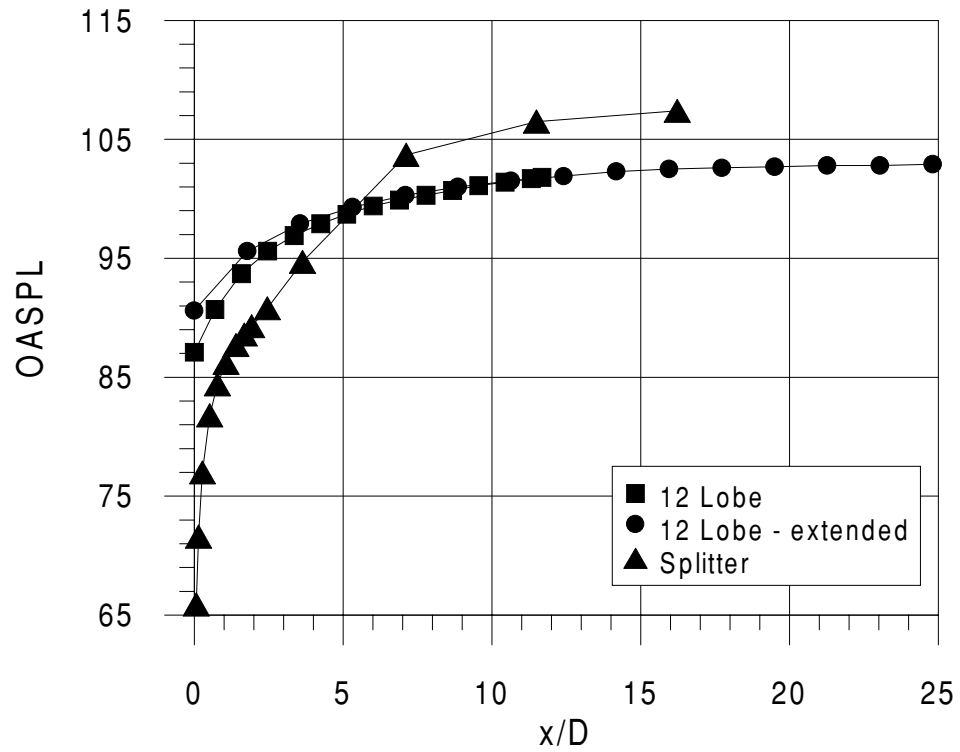
Figure 8.3.13: Calculated axial contribution of OASPL for axisymmetric Splitter and 12-lobe

mixer nozzles

Table A-1. EPNL and Performance Summary for Static (Mn = 0.0) Noise Data With Un-heated Fan Flow

Escort Number	Test Date	POWER CONDITION	Freejet Mach Number	Ambient Temp. (R)	Ambient Pressure (psia)	Core Ttpri (R)	Core Ptpri (psia)	Core Flow Rate (lbm/sec)	Fan Ttbyp (R)	Fan Ptbyp (psia)	Fan Flow Rate (lbm/sec)	Vjet (ft/sec)	Ttpri/T0	Ptpri/P0	Ttbyp/T0	Ptbyp/P0	Mixed Jet Mn (Vjet/C0)	1500' alt 1476' s/l EPNL
SPLITTER																		
492 *	Nov. 94	6	0	518.9	14.35	1363.20	25.87	3.55	520.70	26.6	6.54	1191	2.63	1.80	1.00	1.85	1.07	98.9
490 *	Nov. 94	9	0	518.9	14.35	1470.40	29.43	4.06	516.90	29.69	7.23	1335	2.83	2.05	1.00	2.07	1.20	103.4
20-LOBE MIXER																		
445	Nov. 94	2	0	527.6	14.25	1228.90	21.52	2.68	530.20	23.07	5.58	991	2.33	1.51	1.00	1.62	0.88	83.0
444	Nov. 94	6	0	527.2	14.25	1348.30	25.60	3.34	529.90	26.78	6.53	1195	2.56	1.80	1.01	1.88	1.06	90.6
443	Nov. 94	8	0	526.5	14.25	1431.30	28.45	3.74	530.90	28.81	6.93	1314	2.72	2.00	1.01	2.02	1.17	94.7
442	Nov. 94	9	0	526.5	14.25	1459.80	29.21	3.81	531.00	29.46	7.07	1345	2.77	2.05	1.01	2.07	1.20	95.7
ATM WITHOUT SCALLOPS																		
377	Nov. 94	6	0	520.1	14.28	1322.00	25.05	2.96	519.20	27.11	6.96	1148	2.54	1.75	1.00	1.90	1.03	89.9
382	Nov. 94	6	0	520.0	14.29	1319.30	26.24	3.36	523.30	26.76	6.57	1191	2.54	1.84	1.01	1.87	1.07	91.1
378	Nov. 94	8	0	520.1	14.28	1400.30	27.52	3.27	520.10	29.21	7.44	1251	2.69	1.93	1.00	2.05	1.12	93.5
379	Nov. 94	8	0	520.0	14.28	1433.90	28.56	3.41	520.70	30.06	7.6	1292	2.76	2.00	1.00	2.11	1.16	95.3
381	Nov. 94	9	0	519.8	14.28	1401.60	29.03	3.73	523.80	28.72	6.96	1304	2.70	2.03	1.01	2.01	1.17	95.1
380	Nov. 94	9	0	520.0	14.28	1430.50	30.01	3.84	523.10	29.57	7.16	1340	2.75	2.10	1.01	2.07	1.20	96.5
ATM WITH SCALLOPS																		
483	Nov. 94	3	0	520.3	14.35	1231.50	21.98	2.69	516.40	23.46	5.64	704	2.37	1.53	0.99	1.63	0.63	83.2
482	Nov. 94	6	0	520.3	14.35	1348.60	26.13	3.34	509.10	26.88	6.6	902	2.59	1.82	0.98	1.87	0.81	91.0
481	Nov. 94	8	0	520.0	14.35	1433.30	28.86	3.74	507.60	29.45	7	1013	2.76	2.01	0.98	2.05	0.91	95.0
480	Nov. 94	9	0	520.0	14.34	1460.70	30.06	3.85	507.20	30.78	7.51	1045	2.81	2.10	0.98	2.15	0.94	96.5

* Measured Noise Data Used For Comparison To MGB Analysis

Table A-2. EPNL and Performance Summary for Flight (Mn = 0.27) Noise Data With Un-heated Fan Flow

Escort Number	Test Date	POWER CONDITION	Freejet Mach Number	Ambient Temp. (R)	Ambient Pressure (psia)	Core Ttpri (R)	Core Ptpri (psia)	Core Flow Rate (lbm/sec)	Fan Ttbyp (R)	Fan Ptbyp (psia)	Fan Flow Rate (lbm/sec)	Vjet (ft/sec)	Ttpri/T0	Ptpri/P0	Ttbyp/T0	Ptbyp/P0	Mixed Jet Mn (Vjet/C0)	1500' alt 1476' s/l EPNL
								SPLITTER										
484	Nov. 94	5	0.27	519.3	14.35	1287.80	23.45	3.15	521.40	24.79	6.29	1068	2.48	1.63	1.00	1.73	0.96	84.1
485	Nov. 94	6	0.27	519.2	14.35	1357.60	25.90	3.54	507.30	25.82	6.95	1175	2.61	1.80	0.98	1.80	1.05	89.5
486 *	Nov. 94	8	0.27	519.0	14.35	1438.80	28.82	3.91	507.10	28.81	7.4	1291	2.77	2.01	0.98	2.01	1.16	95
488	Nov. 94	9	0.27	518.7	14.35	1474.60	29.51	4.06	516.40	29.56	7.25	1337	2.84	2.06	1.00	2.06	1.20	96.8
								12-LOBE MIXER										
459	Nov. 94	2	0.27	507.6	14.37	1245.80	21.70	2.76	505.50	22.15	5.48	978	2.45	1.51	1.00	1.54	0.89	76.3
451	Nov. 94	2	0.27	510.8	14.41	1248.60	21.74	2.75	518.00	22.71	5.42	983	2.44	1.51	1.01	1.58	0.89	76.8
452	Nov. 94	4	0.27	510.7	14.41	1268.50	22.58	2.93	517.80	23.4	5.6	1029	2.48	1.57	1.01	1.62	0.93	78.5
453	Nov. 94	5	0.27	510.5	14.41	1294.00	23.45	3.11	517.90	23.93	5.7	1075	2.53	1.63	1.01	1.66	0.97	80.2
454	Nov. 94	6	0.27	510.4	14.41	1364.10	26.04	3.52	517.70	26.14	6.27	1197	2.67	1.81	1.01	1.81	1.08	84.6
455	Nov. 94	6	0.27	510.2	14.4	1401.60	27.32	3.7	518.00	27.21	6.5	1255	2.75	1.90	1.02	1.89	1.13	86.4
456	Nov. 94	8	0.27	510.1	14.4	1443.20	28.82	3.89	518.40	28.24	6.69	1314	2.83	2.00	1.02	1.96	1.19	88.4
457 *	Nov. 94	9	0.27	510.0	14.4	1480.50	29.63	4	519.10	28.7	6.72	1352	2.90	2.06	1.02	1.99	1.22	89.4
								20-LOBE MIXER										
413	Nov. 94	2	0.27	525.0	14.25	1244.40	21.72	2.71	524.80	22.91	5.49	999	2.37	1.52	1.00	1.61	0.89	75.8
414	Nov. 94	4	0.27	525.0	14.25	1269.00	22.54	2.87	525.00	23.56	5.65	1043	2.42	1.58	1.00	1.65	0.93	77.4
415	Nov. 94	5	0.27	525.3	14.25	1290.10	23.49	3.06	525.40	24.22	5.80	1091	2.46	1.65	1.00	1.70	0.97	78.9
420	Nov. 94	5	0.27	525.3	14.24	1295.50	23.60	3.07	527.60	24.26	5.79	1099	2.47	1.66	1.00	1.70	0.98	79
416	Nov. 94	6	0.27	525.2	14.25	1359.80	25.99	3.46	526.10	26.29	6.29	1210	2.59	1.82	1.00	1.84	1.08	83
418	Nov. 94	8	0.27	525.3	14.25	1445.20	28.73	3.84	528.00	28.27	6.66	1327	2.75	2.02	1.01	1.98	1.18	86.7
422	Nov. 94	8	0.27	525.4	14.24	1447.40	28.68	3.83	529.30	28.11	6.60	1328	2.75	2.01	1.01	1.97	1.18	86.7
419 *	Nov. 94	9	0.27	525.3	14.25	1478.80	29.79	4.00	529.20	28.74	6.66	1371	2.82	2.09	1.01	2.02	1.22	88
								ATM WITHOUT SCALLOPS										
387	Nov. 94	4	0.27	519.8	14.28	1241.00	22.70	2.82	524.70	23.45	5.64	1032	2.39	1.59	1.01	1.64	0.92	76.2
388	Nov. 94	5	0.27	519.8	14.28	1259.60	23.61	2.98	524.70	24.19	5.84	1076	2.42	1.65	1.01	1.69	0.96	78
395	Nov. 94	9	0.27	520.0	14.28	1445.00	29.90	3.86	526.90	28.87	6.87	1344	2.78	2.09	1.01	2.02	1.20	87.4
								ATM WITH SCALLOPS										
468	Nov. 94	2	0.27	521.5	14.34	1242.10	21.78	2.66	523.30	23.04	5.53	972	2.38	1.52	1.00	1.61	0.87	74.4
469	Nov. 94	4	0.27	521.1	14.34	1269.70	22.78	2.84	522.80	23.79	5.7	1023	2.44	1.59	1.00	1.66	0.91	76.4
470	Nov. 94	5	0.27	520.8	14.34	1286.90	23.56	2.97	522.40	24.48	5.89	1061	2.47	1.64	1.00	1.71	0.95	77.9
471	Nov. 94	6	0.27	520.4	14.34	1359.30	26.22	3.39	522.20	26.6	6.4	1182	2.61	1.83	1.00	1.85	1.06	82.3
473	Nov. 94	7	0.27	520.3	14.34	1393.40	27.63	3.59	522.30	27.74	6.66	1240	2.68	1.93	1.00	1.93	1.11	84.3
479	Nov. 94	8	0.27	520.1	14.35	1437.00	29.02	3.77	507.50	29.06	7.04	1286	2.76	2.02	0.98	2.03	1.15	86.1
474	Nov. 94	8	0.27	520.0	14.34	1435.30	28.95	3.75	522.70	28.74	6.86	1293	2.76	2.02	1.01	2.00	1.16	86.1
476	Nov. 94	9	0.27	520.3	14.34	1470.10	29.92	3.86	523.20	29.42	6.99	1332	2.83	2.09	1.01	2.05	1.19	87.5

* Measured Noise Data Used For Comparison To MGB Analysis

Table A-3. EPNL and Performance Summary for Static (Mn = 0.0) Noise Data

Escort Number	Test Date	POWER CONDITION	Freejet Mach Number	Ambient Temp. (R)	Ambient Pressure (psia)	Core Ttpri (R)	Core Ptpri (psia)	Core Flow Rate (lbm/sec)	Fan Ttbyp (R)	Fan Ptbyp (psia)	Fan Flow Rate (lbm/sec)	Vjet (ft/sec)	Ttpri/T0	Ptpri/P0	Ttbyp/T0	Ptbyp/P0	Mixed Jet Mn (Vjet/C0)	1500' alt 1476' s/l EPNL
						SPLITTER WITH HEATED FAN FLOW												
815	3-29-96	5	0.02	507.8	14.40	1252.39	23.41	2.92	605.54	22.57	5.96	1091	2.47	1.63	1.19	1.57	0.99	92.5
816	3-29-96	7	0.02	506.3	14.40	1370.13	27.27	3.44	630.35	25.63	6.84	1277	2.71	1.89	1.24	1.78	1.16	99.0
817	3-29-96	8	0.02	505.8	14.40	1420.88	28.51	3.56	641.09	26.57	7.05	1335	2.81	1.98	1.27	1.85	1.21	100.9
						12-LOBE WITH HEATED FAN FLOW												
615	3-22-96	5	0.00	493.7	14.25	1208.65	23.32	2.95	584.74	22.50	5.77	1086	2.45	1.64	1.18	1.58	1.00	87.9
614	3-22-96	7	0.00	493.2	14.25	1334.02	26.84	3.37	613.78	25.22	6.41	1263	2.70	1.88	1.24	1.77	1.16	94.6
613	3-22-96	8	0.00	493.1	14.25	1382.10	28.18	3.50	622.43	26.30	6.72	1321	2.80	1.98	1.26	1.85	1.21	96.9
						12-LOBE WITH PROBES and HEATED FAN FLOW												
721	3-27-96	5	0.01	490.8	14.57	1210.32	23.84	2.94	588.61	22.92	6.03	1079	2.47	1.64	1.20	1.57	0.99	87.8
720	3-27-96	7	0.01	490.8	14.57	1321.78	27.52	3.42	617.21	25.97	6.72	1261	2.69	1.89	1.26	1.78	1.16	94.7
719	3-27-96	8	0.01	490.5	14.57	1378.17	28.86	3.55	626.30	26.92	6.95	1320	2.81	1.98	1.28	1.85	1.22	96.9
						20-LOBE WITH HEATED FAN FLOW												
649	3-25-96	5	0.00	496.8	14.34	1225.15	23.31	2.87	589.35	22.43	5.70	1081	2.47	1.63	1.19	1.56	0.99	87.5
647	3-25-96	7	0.00	495.1	14.34	1334.88	27.19	3.39	621.14	25.59	6.48	1273	2.70	1.90	1.25	1.78	1.17	94.7
648	3-25-96	8	0.00	496.1	14.34	1392.05	28.42	3.49	631.12	26.61	6.73	1331	2.81	1.98	1.27	1.86	1.22	97.2
						20-LOBE WITH ALTERNATING SCARF and HEATED FAN FLOW												
769	3-28-96	5	0.00	505.4	14.36	1248.16	23.41	2.84	603.02	22.49	5.81	1089	2.47	1.63	1.19	1.57	0.99	89.9
770	3-28-96	7	0.01	506.3	14.36	1366.80	27.17	3.33	634.17	25.55	6.49	1281	2.70	1.89	1.25	1.78	1.16	94.6
771	3-28-96	8	0.01	506.9	14.36	1426.65	28.48	3.45	642.47	26.60	6.74	1342	2.81	1.98	1.27	1.85	1.22	97.0
						24-LOBE WITH HEATED FAN FLOW												
683	3-26-96	5	0.01	493.8	14.55	1215.03	23.66	2.89	584.96	22.70	5.85	1072	2.46	1.63	1.18	1.56	0.98	87.3
682	3-26-96	7	0.00	494.0	14.55	1332.65	27.41	3.37	613.56	25.85	6.62	1260	2.70	1.88	1.24	1.78	1.16	94.7
681	3-26-96	8	0.00	492.6	14.55	1382.16	28.85	3.54	625.42	26.88	6.86	1322	2.81	1.98	1.27	1.85	1.22	97.0
						ATM WITH HEATED FAN FLOW												
528	3-16-96	5	0.00	498.8	14.24	1228.41	23.17	2.83	595.72	22.34	5.64	1086	2.46	1.63	1.19	1.57	0.99	87.1
527	3-16-96	7	0.00	498.9	14.24	1348.19	26.99	3.32	629.36	25.45	6.33	1281	2.70	1.90	1.26	1.79	1.17	94.9
525	3-16-96	8	0.01	498.6	14.24	1405.05	28.15	3.42	631.95	26.21	6.50	1331	2.82	1.98	1.27	1.84	1.22	96.5
526	3-16-96	8	0.00	498.6	14.24	1404.30	28.20	3.42	637.81	26.33	6.51	1337	2.82	1.98	1.28	1.85	1.22	97.1
1047	4-30-96	8	0.00	509.1	14.18	1429.29	28.11	3.45	649.40	26.28	6.58	1350	2.81	1.98	1.28	1.85	1.22	96.6
						ATM WITH PROBES and HEATED FAN FLOW												
755	3-28-96	5	0.02	504.3	14.36	1243.71	23.44	2.77	603.01	22.60	5.89	1088	2.47	1.63	1.20	1.57	0.99	87.4
756	3-28-96	7	0.02	504.3	14.36	1360.48	27.15	3.23	630.76	25.55	6.58	1271	2.70	1.89	1.25	1.78	1.15	94.4
757	3-28-96	8	0.02	504.4	14.36	1416.12	28.45	3.36	641.51	26.57	6.85	1330	2.81	1.98	1.27	1.85	1.21	96.6
1057	4-30-96	8	0.02	506.6	14.21	1421.74	28.12	3.44	642.86	26.24	6.58	1342	2.81	1.98	1.27	1.85	1.22	96.6
						ATM WITH PROBES and MUFFLER and HEATED FAN FLOW												
1111	5-2-96	8	0.02	527.4	14.33	1475.33	28.38	3.45	672.81	26.51	6.53	1373	2.80	1.98	1.28	1.85	1.22	96.8

Table A-4. EPNL and Performance Summary for Flight (Mn = 0.27) Noise Data for Splitter

Escort Number	Test Date	POWER CONDITION	Freejet Mach Number	Ambient Temp. (R)	Ambient Pressure (psia)	Core Ttpri (R)	Core Ptpri (psia)	Core Flow Rate (lbm/sec)	Fan Ttbyp (R)	Fan Ptbyp (psia)	Fan Flow Rate (lbm/sec)	Vjet (ft/sec)	Ttpri/T0	Ptpri/P0	Ttbyp/T0	Ptbyp/P0	Mixed Jet Mn (Vjet/C0)	1500' alt 1476' s/l EPNL
SPLITTER WITH HEATED FAN FLOW																		
808	3-29-96	1	0.27	506.0	14.38	1158.81	20.98	2.46	589.63	20.75	5.49	948	2.29	1.46	1.17	1.44	0.86	76.6
824	3-29-96	1	0.27	506.3	14.40	1152.82	21.07	2.49	589.45	20.74	5.47	948	2.28	1.46	1.16	1.44	0.86	77.1
807	3-29-96	3	0.27	506.4	14.38	1194.08	22.05	2.69	591.24	21.53	5.72	1010	2.36	1.53	1.17	1.50	0.92	79.8
806	3-29-96	5	0.27	506.5	14.38	1230.34	23.34	2.90	606.35	22.55	5.94	1086	2.43	1.62	1.20	1.57	0.98	83.6
822	3-29-96	5	0.27	506.2	14.40	1229.23	23.30	2.91	596.65	22.53	5.97	1079	2.43	1.62	1.18	1.56	0.98	83.4
805	3-29-96	6	0.27	505.9	14.38	1298.78	25.80	3.29	619.05	24.52	6.49	1209	2.57	1.79	1.22	1.71	1.10	89.1
821	3-29-96	6	0.27	505.7	14.40	1295.10	25.89	3.30	617.28	24.59	6.51	1209	2.56	1.80	1.22	1.71	1.10	89.2
804	3-29-96	7	0.27	505.6	14.38	1331.72	27.00	3.42	626.93	25.61	6.79	1264	2.63	1.88	1.24	1.78	1.15	91.4
820	3-29-96	7	0.27	505.8	14.40	1331.92	27.06	3.45	627.01	25.56	6.77	1264	2.63	1.88	1.24	1.78	1.15	91.8
803	3-29-96	8	0.27	505.3	14.38	1371.28	28.49	3.61	635.37	26.69	7.09	1324	2.71	1.98	1.26	1.86	1.20	94.0
826	3-29-96	8	0.27	507.2	14.40	1376.75	28.54	3.65	634.81	26.59	7.05	1325	2.71	1.98	1.25	1.85	1.20	94.5
802	3-29-96	9	0.27	504.3	14.38	1399.57	29.31	3.73	637.57	27.30	7.22	1359	2.78	2.04	1.26	1.90	1.23	95.2
825	3-29-96	9	0.27	506.1	14.40	1399.16	29.41	3.74	639.66	27.34	7.21	1361	2.76	2.04	1.26	1.90	1.23	95.6
SPLITTER WITH UN-HEATED FAN FLOW																		
833	3-29-96	1	0.27	505.0	14.41	1162.10	21.10	2.52	510.96	20.67	5.71	910	2.30	1.46	1.01	1.44	0.83	76.8
832	3-29-96	3	0.27	504.0	14.40	1191.27	22.24	2.75	511.39	21.56	6.06	972	2.36	1.54	1.01	1.50	0.88	80.2
831	3-29-96	5	0.27	505.1	14.40	1229.17	23.31	2.90	512.12	22.57	6.44	1031	2.43	1.62	1.01	1.57	0.94	83.3
830	3-29-96	6	0.27	504.0	14.40	1283.86	25.96	3.34	513.12	24.54	7.10	1144	2.55	1.80	1.02	1.70	1.04	89.4
829	3-29-96	7	0.27	505.5	14.40	1332.56	27.12	3.46	514.40	25.63	7.45	1196	2.64	1.88	1.02	1.78	1.09	91.8
827	3-29-96	8	0.27	507.0	14.40	1372.66	28.52	3.65	533.53	26.64	7.60	1261	2.71	1.98	1.05	1.85	1.14	94.3
828	3-29-96	9	0.27	505.4	14.40	1403.49	29.37	3.73	518.17	27.45	7.92	1285	2.78	2.04	1.03	1.91	1.17	95.9
SPLITTER WITH PROBES and HEATED FAN FLOW																		
1119	5-2-96	3	0.27	524.7	14.33	1236.13	22.08	3.60	614.72	21.47	4.21	1106	2.36	1.54	1.17	1.50	0.98	82.1
1118	5-2-96	5	0.27	524.6	14.33	1276.20	23.18	3.80	624.32	22.43	4.45	1177	2.43	1.62	1.19	1.57	1.05	85.2
1117	5-2-96	6	0.27	524.5	14.33	1346.46	25.85	4.33	641.85	24.50	4.82	1327	2.57	1.80	1.22	1.71	1.18	90.7
1116	5-2-96	7	0.27	525.0	14.33	1380.82	27.02	4.57	655.09	25.53	4.85	1397	2.63	1.89	1.25	1.78	1.24	92.9
1115	5-2-96	8	0.27	524.9	14.33	1424.27	28.32	4.81	660.83	26.41	4.99	1462	2.71	1.98	1.26	1.84	1.30	95.1
1120	5-2-96	8	0.27	524.3	14.33	1425.04	28.39	4.70	663.92	26.56	5.04	1461	2.72	1.98	1.27	1.85	1.30	94.8
1114	5-2-96	9	0.27	525.1	14.33	1452.73	29.27	4.93	672.70	27.23	5.15	1508	2.77	2.04	1.28	1.90	1.34	96.7

Table A-5 EPNL and Performance Summary for Flight (Mn = 0.27) Noise Data for 12-Lobe Mixer

Escort Number	Test Date	POWER CONDITION	Freejet Mach Number	Ambient Temp. (R)	Ambient Pressure (psia)	Core Ttpri (R)	Core Ptpri (psia)	Core Flow Rate (lbm/sec)	Fan Ttbyp (R)	Fan Ptbyp (psia)	Fan Flow Rate (lbm/sec)	Vjet (ft/sec)	Ttpri/T0	Ptpri/P0	Ttbyp/T0	Ptbyp/P0	Mixed Jet Mn (Vjet/C0)	1500' alt 1476' s/l EPNL
						12-LOBE MIXER WITH HEATED FAN FLOW												
601	3-22-96	1	0.27	492.0	14.24	1118.07	20.77	2.46	566.85	20.43	5.24	931	2.27	1.46	1.15	1.43	0.86	74.7
600	3-22-96	3	0.27	492.1	14.24	1171.37	21.91	2.68	572.02	21.28	5.47	1002	2.38	1.54	1.16	1.49	0.92	77.4
599	3-22-96	5	0.27	492.8	14.24	1195.54	23.00	2.85	589.57	22.46	5.80	1075	2.43	1.62	1.20	1.58	0.99	79.9
598	3-22-96	6	0.27	493.0	14.24	1264.98	25.70	3.27	598.56	24.41	6.24	1202	2.57	1.80	1.21	1.71	1.10	85.0
602	3-22-96	6	0.26	493.0	14.24	1260.01	25.64	3.28	605.45	24.42	6.22	1204	2.56	1.80	1.23	1.71	1.11	85.1
597	3-22-96	7	0.27	492.8	14.24	1294.34	26.82	3.43	611.03	25.37	6.49	1256	2.63	1.88	1.24	1.78	1.15	86.6
603	3-22-96	7	0.26	493.3	14.24	1298.15	26.78	3.45	613.75	25.39	6.44	1261	2.63	1.88	1.24	1.78	1.16	86.6
596	3-22-96	8	0.27	492.6	14.24	1326.99	28.12	3.62	621.33	26.32	6.60	1315	2.69	1.97	1.26	1.85	1.21	88.4
604	3-22-96	8	0.26	493.4	14.24	1333.11	28.13	3.60	621.43	26.37	6.65	1316	2.70	1.98	1.26	1.85	1.21	88.8
595	3-22-96	9	0.27	492.3	14.24	1363.57	29.08	3.71	629.46	27.10	6.78	1358	2.77	2.04	1.28	1.90	1.25	89.8
605	3-22-96	9	0.26	493.8	14.24	1365.05	29.08	3.69	635.99	27.05	6.78	1359	2.76	2.04	1.29	1.90	1.25	90.3
						12-LOBE MIXER WITH PROBES and HEATED FAN FLOW												
722	3-27-96	1	0.27	490.4	14.57	1122.41	21.23	2.43	571.14	20.91	5.49	928	2.29	1.46	1.16	1.44	0.85	75.9
712	3-27-96	1	0.27	490.7	14.57	1121.63	21.31	2.47	568.57	21.06	5.49	935	2.29	1.46	1.16	1.45	0.86	75.8
711	3-27-96	3	0.27	490.8	14.57	1166.50	22.50	2.71	570.35	21.86	5.76	1000	2.38	1.54	1.16	1.50	0.92	78.0
723	3-27-96	3	0.27	490.3	14.57	1155.98	22.49	2.67	578.94	21.89	5.83	1001	2.36	1.54	1.18	1.50	0.92	78.6
724	3-27-96	5	0.27	490.1	14.57	1193.35	23.64	2.88	582.22	22.80	6.15	1061	2.44	1.62	1.19	1.57	0.98	80.5
710	3-27-96	5	0.27	490.6	14.57	1183.54	23.61	2.90	583.70	22.86	6.04	1064	2.41	1.62	1.19	1.57	0.98	80.3
709	3-27-96	6	0.27	490.5	14.57	1258.25	26.21	3.29	599.23	24.87	6.49	1192	2.57	1.80	1.22	1.71	1.10	84.9
725	3-27-96	6	0.27	490.0	14.57	1254.07	26.18	3.27	601.91	25.03	6.55	1194	2.56	1.80	1.23	1.72	1.10	94.9
726	3-27-96	7	0.27	490.1	14.57	1292.26	27.32	3.44	608.14	25.82	6.76	1244	2.64	1.88	1.24	1.77	1.15	86.9
708	3-27-96	7	0.27	491.0	14.57	1291.88	27.36	3.43	610.93	26.01	6.76	1249	2.63	1.88	1.24	1.78	1.15	86.7
707	3-27-96	8	0.27	491.0	14.57	1331.96	28.88	3.61	617.75	26.94	7.03	1305	2.71	1.98	1.26	1.85	1.20	89.1
727	3-27-96	8	0.27	490.2	14.57	1331.05	28.81	3.62	620.79	27.03	7.00	1309	2.72	1.98	1.27	1.86	1.21	88.9
706	3-27-96	9	0.27	491.0	14.58	1357.15	29.74	3.75	619.74	27.63	7.07	1343	2.76	2.04	1.26	1.90	1.24	90.0
728	3-27-96	9	0.27	489.5	14.57	1355.92	29.71	3.73	621.87	27.65	7.16	1341	2.77	2.04	1.27	1.90	1.24	90.0

Table A-6. EPNL and Performance Summary for Flight (Mn = 0.27) Noise Data for 20-Lobe Mixer

Escort Number	Test Date	POWER CONDITION	Freejet Mach Number	Ambient Temp. (R)	Ambient Pressure (psia)	Core Ttpri (R)	Core Ptpri (psia)	Core Flow Rate (lbm/sec)	Fan Ttbyp (R)	Fan Ptbyp (psia)	Fan Flow Rate (lbm/sec)	Vjet (ft/sec)	Ttpri/T0	Ptpri/P0	Ttbyp/T0	Ptbyp/P0	Mixed Jet Mn (Vjet/C0)	1500' alt 1476' s/l EPNL
20-LOBE WITH HEATED FAN FLOW
636	3-25-96	1	0.27	495.3	14.32	1145.25	20.91	2.44	572.46	20.67	5.14	945	2.31	1.46	1.16	1.44	0.87	74.3
635	3-25-96	3	0.27	495.6	14.32	1162.13	22.08	2.70	577.11	21.45	5.43	1007	2.34	1.54	1.16	1.50	0.92	76.7
634	3-25-96	5	0.27	495.9	14.32	1205.72	23.19	2.85	588.13	22.38	5.71	1073	2.43	1.62	1.19	1.56	0.98	79.4
633	3-25-96	6	0.27	495.6	14.31	1271.62	25.74	3.25	604.39	24.46	6.21	1203	2.57	1.80	1.22	1.71	1.10	84.2
632	3-25-96	7	0.27	496.0	14.31	1301.13	26.87	3.40	612.24	25.38	6.43	1255	2.62	1.88	1.23	1.77	1.15	85.9
645	3-25-96	8	0.27	495.0	14.33	1341.54	28.43	3.58	628.02	26.45	6.67	1320	2.71	1.98	1.27	1.85	1.21	88.4
631	3-25-96	8	0.27	495.9	14.31	1346.92	28.45	3.60	629.34	26.46	6.63	1325	2.72	1.99	1.27	1.85	1.21	88.5
630	3-25-96	9	0.27	496.0	14.30	1372.10	29.22	3.66	631.53	27.15	6.85	1356	2.77	2.04	1.27	1.90	1.24	89.6
644	3-25-96	9	0.27	494.8	14.33	1375.16	29.28	3.66	634.43	27.27	6.87	1359	2.78	2.04	1.28	1.90	1.25	89.3
20-LOBE WITH UN-HEATED FAN FLOW
622	3-25-96	1	0.27	503.2	14.24	1152.36	20.75	2.45	504.45	20.43	5.24	909	2.29	1.46	1.00	1.43	0.83	73.1
628	3-25-96	3	0.27	495.6	14.30	1171.53	21.99	2.66	492.96	21.50	5.75	965	2.36	1.54	0.99	1.50	0.88	75.6
623	3-25-96	5	0.27	502.5	14.24	1219.90	23.16	2.85	500.23	22.32	6.02	1031	2.43	1.63	1.00	1.57	0.94	78.3
624	3-25-96	6	0.27	501.7	14.25	1281.26	25.70	3.20	499.43	24.32	6.71	1140	2.55	1.80	1.00	1.71	1.04	82.8
626	3-25-96	7	0.27	496.9	14.29	1308.63	26.86	3.30	496.35	25.39	7.14	1178	2.63	1.88	1.00	1.78	1.08	84.7
629	3-25-96	8	0.27	495.7	14.30	1346.83	28.34	3.53	494.98	26.48	7.32	1236	2.72	1.98	1.00	1.85	1.13	86.5
627	3-25-96	9	0.27	496.7	14.29	1374.65	29.22	3.62	496.76	27.20	7.49	1271	2.77	2.04	1.00	1.90	1.16	87.7
20-LOBE WITH VORTEX GENERATORS and HEATED FAN FLOW
659	3-26-98	1	0.27	494.1	14.51	1136.17	21.18	2.47	571.20	20.90	5.23	940	2.30	1.46	1.16	1.44	0.86	74.4
658	3-26-98	3	0.27	493.8	14.51	1173.88	22.27	2.69	575.62	21.66	5.52	1002	2.38	1.53	1.17	1.49	0.92	76.8
657	3-26-98	5	0.27	495.0	14.51	1205.25	23.53	2.87	589.37	22.75	5.84	1074	2.44	1.62	1.19	1.57	0.98	79.8
656	3-26-98	6	0.27	494.9	14.51	1263.64	26.07	3.28	600.53	24.73	6.34	1195	2.55	1.80	1.21	1.70	1.10	84.4
655	3-26-98	7	0.27	494.7	14.51	1298.11	27.17	3.39	608.11	25.77	6.62	1247	2.62	1.87	1.23	1.78	1.14	86.2
654	3-26-98	8	0.27	494.5	14.51	1339.68	28.74	3.61	623.24	26.79	6.79	1315	2.71	1.98	1.26	1.85	1.21	88.6
661	3-26-98	8	0.27	494.0	14.51	1338.93	28.78	3.62	623.79	26.86	6.81	1317	2.71	1.98	1.26	1.85	1.21	88.8
653	3-26-98	9	0.27	494.7	14.51	1370.18	29.67	3.69	633.05	27.67	7.01	1357	2.77	2.05	1.28	1.91	1.24	90.0

Table A-6. EPNL and Performance Summary for Flight (Mn = 0.27) Noise Data for 20-Lobe Mixer

Escort Number	Test Date	POWER CONDITION	Freejet Mach Number	Ambient Temp. (R)	Ambient Pressure (psia)	Core Ttpri (R)	Core Ptpri (psia)	Core Flow Rate (lbm/sec)	Fan Ttbyp (R)	Fan Ptbyp (psia)	Fan Flow Rate (lbm/sec)	Vjet (ft/sec)	Ttpri/T0	Ptpri/P0	Ttbyp/T0	Ptbyp/P0	Mixed Jet Mn (Vjet/C0)	1500' alt 1476' s/l EPNL
20-LOBE WITH ALTERNATING SCARF and HEATED FAN FLOW
789	3-28-96	1	0.27	503.9	14.36	1159.17	20.86	2.36	581.67	20.64	5.33	939	2.30	1.45	1.15	1.44	0.85	74.1
788	3-28-96	3	0.27	504.2	14.35	1194.02	22.06	2.62	586.64	21.47	5.58	1008	2.37	1.54	1.16	1.50	0.92	76.8
786	3-28-96	5	0.27	504.6	14.35	1224.70	23.28	2.80	597.33	22.56	5.86	1080	2.43	1.62	1.18	1.57	0.98	79.4
785	3-28-96	6	0.27	504.8	14.35	1303.81	25.82	3.18	617.07	24.57	6.34	1211	2.58	1.80	1.22	1.71	1.10	84.0
793	3-28-96	7	0.27	503.4	14.35	1326.15	27.01	3.34	624.37	25.56	6.59	1264	2.63	1.88	1.24	1.78	1.15	85.9
787	3-28-96	7	0.27	504.5	14.35	1331.87	27.01	3.33	627.52	25.62	6.60	1267	2.64	1.88	1.24	1.79	1.15	86.1
794	3-28-96	8	0.27	503.5	14.35	1362.65	28.42	3.52	637.69	26.62	6.79	1326	2.71	1.98	1.27	1.86	1.21	88.1
780	3-28-96	8	0.27	505.2	14.36	1370.39	28.49	3.52	637.65	26.64	6.79	1329	2.71	1.98	1.26	1.86	1.21	88.2
795	3-28-96	9	0.27	503.4	14.35	1393.24	29.30	3.63	639.24	27.26	6.93	1362	2.77	2.04	1.27	1.90	1.24	89.5
781	3-28-96	9	0.27	505.0	14.36	1402.48	29.32	3.61	643.00	27.25	6.91	1365	2.78	2.04	1.27	1.90	1.24	89.3
20-LOBE WITH ALTERNATING SCARF and UN-HEATED FAN FLOW
790	3-28-96	7	0.27	503.8	14.35	1324.53	26.93	3.29	507.67	25.53	7.15	1187	2.63	1.88	1.01	1.78	1.08	84.2
791	3-28-96	8	0.27	503.6	14.35	1365.97	28.45	3.53	507.64	26.53	7.32	1247	2.71	1.98	1.01	1.85	1.13	86.4
792	3-28-96	9	0.27	503.5	14.35	1395.86	29.31	3.60	507.35	27.28	7.55	1279	2.77	2.04	1.01	1.90	1.16	87.5

Table A-7. EPNL and Performance Summary for Flight (Mn = 0.27) Noise Data for 24-Lobe Mixer

Escort Number	Test Date	POWER CONDITION	Freejet Mach Number	Ambient Temp. (R)	Ambient Pressure (psia)	Core Ttpri (R)	Core Ptpri (psia)	Core Flow Rate (lbm/sec)	Fan Ttbyp (R)	Fan Ptbyp (psia)	Fan Flow Rate (lbm/sec)	Vjet (ft/sec)	Ttpri/T0	Ptpri/P0	Ttbyp/T0	Ptbyp/P0	Mixed Jet Mn (Vjet/C0)	1500' alt 1476' s/l EPNL
								24-LOBE WITH HEATED FAN FLOW										
667	3-26-96	1	0.27	494.5	14.53	1135.06	21.23	2.45	575.37	20.89	5.32	938	2.30	1.46	1.16	1.44	0.86	73.9
684	3-26-96	1	0.27	491.6	14.55	1120.73	21.30	2.46	575.60	20.97	5.33	939	2.28	1.46	1.17	1.44	0.86	74.1
668	3-26-96	3	0.27	494.3	14.53	1155.04	22.45	2.70	585.30	21.72	5.62	1005	2.34	1.55	1.18	1.50	0.92	76.7
685	3-26-96	3	0.27	489.9	14.55	1165.26	22.49	2.71	574.03	21.85	5.64	1005	2.38	1.55	1.17	1.50	0.93	76.8
686	3-26-96	5	0.27	489.5	14.56	1192.74	23.65	2.87	582.96	22.94	6.00	1069	2.44	1.62	1.19	1.58	0.99	79.2
669	3-26-96	5	0.27	494.3	14.53	1201.50	23.63	2.86	594.48	22.89	5.97	1077	2.43	1.63	1.20	1.58	0.99	79.5
687	3-26-96	6	0.27	489.1	14.55	1255.47	26.17	3.27	600.80	24.90	6.42	1194	2.57	1.80	1.23	1.71	1.10	83.9
670	3-26-96	6	0.27	494.1	14.53	1263.99	26.20	3.27	606.02	24.91	6.39	1201	2.56	1.80	1.23	1.71	1.10	84.3
688	3-26-96	7	0.27	488.5	14.56	1284.90	27.40	3.43	602.27	25.99	6.72	1245	2.63	1.88	1.23	1.78	1.15	85.9
671	3-26-96	7	0.27	494.0	14.53	1302.17	27.43	3.43	617.46	26.06	6.69	1262	2.64	1.89	1.25	1.79	1.16	86.2
672	3-26-96	8	0.27	493.7	14.53	1334.71	28.75	3.58	622.47	26.93	6.86	1312	2.70	1.98	1.26	1.85	1.20	88.2
689	3-26-96	8	0.27	488.5	14.56	1320.44	28.87	3.63	616.30	26.90	6.87	1306	2.70	1.98	1.26	1.85	1.21	88.2
673	3-26-96	9	0.27	493.5	14.53	1368.64	29.54	3.66	621.86	27.45	7.03	1341	2.77	2.03	1.26	1.89	1.23	89.2
690	3-26-96	9	0.27	488.1	14.57	1347.00	29.72	3.69	621.25	27.74	7.14	1340	2.76	2.04	1.27	1.90	1.24	89.4
								24-LOBE WITH UN-HEATED FAN FLOW										
696	3-26-96	3	0.27	486.6	14.57	1150.62	22.39	2.63	489.49	21.85	6.18	946	2.36	1.54	1.01	1.50	0.87	75.2
695	3-26-96	5	0.27	486.9	14.57	1183.04	23.68	2.85	489.73	22.91	6.53	1009	2.43	1.62	1.01	1.57	0.93	78.1
694	3-26-96	6	0.27	487.1	14.57	1244.85	26.22	3.20	490.56	24.88	7.17	1116	2.56	1.80	1.01	1.71	1.03	82.3
693	3-26-96	7	0.27	487.3	14.57	1280.82	27.40	3.33	491.43	25.99	7.52	1164	2.63	1.88	1.01	1.78	1.08	84.5
692	3-26-96	8	0.27	487.0	14.57	1316.89	28.75	3.50	492.21	26.97	7.78	1213	2.70	1.97	1.01	1.85	1.12	86.3
691	3-26-96	9	0.27	486.9	14.57	1349.53	29.79	3.63	492.80	27.68	7.94	1251	2.77	2.05	1.01	1.90	1.16	87.7

Table A-8. EPNL and Performance Summary for Flight (Mn = 0.27) Noise Data for ATM

Escort Number	Test Date	POWER CONDITION	Freejet Mach Number	Ambient Temp. (R)	Ambient Pressure (psia)	Core Ttpri (R)	Core Ptpri (psia)	Core Flow Rate (lbm/sec)	Fan Ttbyp (R)	Fan Ptbyp (psia)	Fan Flow Rate (lbm/sec)	Vjet (ft/sec)	Ttpri/T0	Ptpri/P0	Ttbyp/T0	Ptbyp/P0	Mixed Jet Mn (Vjet/C0)	1500' alt 1476' s/l EPNL
ATM WITH HEATED FAN FLOW
507	3-16-96	1	0.27	501.0	14.25	1144.85	20.80	2.39	579.36	20.46	5.08	942	2.29	1.46	1.16	1.44	0.86	73.0
484	3-15-96	1	0.27	497.0	14.26	1133.86	20.82	2.41	578.80	20.47	5.08	940	2.28	1.46	1.16	1.43	0.86	73.0
1042	4-30-96	3	0.27	508.3	14.18	1199.57	21.74	2.57	594.29	21.31	5.45	1016	2.36	1.53	1.17	1.50	0.92	75.7
506	3-16-96	3	0.27	501.1	14.25	1182.48	21.98	2.62	588.33	21.32	5.34	1014	2.36	1.54	1.17	1.50	0.92	91.7
483	3-15-96	3	0.27	496.9	14.26	1177.92	22.06	2.65	581.39	21.41	5.39	1013	2.37	1.55	1.17	1.50	0.93	76.0
1041	4-30-96	5	0.27	508.5	14.18	1237.24	22.89	2.80	605.11	22.13	5.58	1085	2.43	1.61	1.19	1.56	0.98	78.3
482	3-15-96	5	0.27	497.2	14.26	1203.95	23.15	2.84	590.60	22.45	5.67	1079	2.42	1.62	1.19	1.57	0.99	78.3
505	3-16-96	5	0.28	501.4	14.25	1216.14	23.13	2.82	598.65	22.38	5.63	1084	2.43	1.62	1.19	1.57	0.99	78.1
481	3-15-96	6	0.27	497.5	14.26	1269.68	25.62	3.20	606.18	24.37	6.11	1203	2.55	1.80	1.22	1.71	1.10	83.0
504	3-16-96	6	0.27	501.8	14.25	1286.90	25.70	3.21	617.41	24.36	6.05	1215	2.56	1.80	1.23	1.71	1.11	83.1
1040	4-30-96	6	0.27	508.5	14.18	1303.45	25.55	3.21	621.20	24.37	6.10	1224	2.56	1.80	1.22	1.72	1.11	83.3
503	3-16-96	7	0.28	502.4	14.25	1319.52	26.75	3.33	621.00	25.27	6.29	1264	2.63	1.88	1.24	1.77	1.15	85.0
1039	4-30-96	7	0.27	507.8	14.18	1338.63	26.56	3.34	629.78	25.22	6.29	1274	2.64	1.87	1.24	1.78	1.15	85.3
480	3-15-96	7	0.27	497.2	14.26	1306.39	26.87	3.37	618.56	25.56	6.35	1267	2.63	1.88	1.24	1.79	1.16	85.2
1038	4-30-96	8	0.27	508.0	14.18	1373.72	28.04	3.53	639.46	26.12	6.52	1332	2.70	1.98	1.26	1.84	1.21	87.4
1043	4-30-96	8	0.27	508.4	14.18	1376.66	28.13	3.53	641.59	26.30	6.58	1338	2.71	1.98	1.26	1.85	1.21	87.9
485	3-15-96	8	0.27	496.8	14.27	1344.52	28.28	3.57	625.26	26.40	6.54	1323	2.71	1.98	1.26	1.85	1.21	87.5
502	3-16-96	8	0.27	502.4	14.25	1362.13	28.21	3.53	638.45	26.42	6.49	1334	2.71	1.98	1.27	1.85	1.21	87.3
501	3-16-96	9	0.27	502.7	14.25	1394.68	29.09	3.62	638.40	27.11	6.64	1369	2.77	2.04	1.27	1.90	1.25	88.5
1037	4-30-96	9	0.27	507.4	14.18	1410.69	28.94	3.65	647.61	26.83	6.58	1378	2.78	2.04	1.28	1.89	1.25	88.8
ATM WITH UN-HEATED FAN FLOW
493	3-16-96	1	0.27	505.4	14.25	1154.80	20.69	2.34	502.15	20.53	5.41	902	2.28	1.45	0.99	1.44	0.82	71.4
494	3-16-96	3	0.27	505.5	14.25	1194.86	21.98	2.63	501.97	21.31	5.65	971	2.36	1.54	0.99	1.50	0.88	74.4
495	3-16-96	5	0.28	504.7	14.25	1224.77	23.12	2.79	502.00	22.30	6.02	1028	2.43	1.62	0.99	1.56	0.93	77.0
498	3-16-96	6	0.27	503.7	14.25	1291.02	25.68	3.16	503.21	24.37	6.62	1146	2.56	1.80	1.00	1.71	1.04	80.6
497	3-16-96	7	0.27	503.7	14.25	1326.13	26.79	3.29	503.91	25.32	6.91	1192	2.63	1.88	1.00	1.78	1.08	83.1
499	3-16-96	8	0.28	503.0	14.25	1362.01	28.23	3.48	505.80	26.32	7.10	1247	2.71	1.98	1.01	1.85	1.13	85.6
500	3-16-96	9	0.27	502.8	14.25	1392.35	29.07	3.55	505.97	27.09	7.31	1280	2.77	2.04	1.01	1.90	1.16	86.7
ATM WITH PROBES and HEATED FAN FLOW
748	3-28-96	1	0.27	504.9	14.36	1155.63	20.99	2.31	581.10	20.69	5.41	939	2.29	1.46	1.15	1.44	0.85	75.2
747	3-28-96	3	0.27	505.3	14.36	1195.28	22.13	2.53	594.10	21.56	5.64	1010	2.37	1.54	1.18	1.50	0.92	77.7
1055	4-30-96	3	0.27	506.6	14.21	1195.15	21.83	2.57	594.24	21.30	5.49	1013	2.36	1.54	1.17	1.50	0.92	77.2
746	3-28-96	5	0.27	505.3	14.36	1221.53	23.25	2.73	605.03	22.56	5.92	1077	2.42	1.62	1.20	1.57	0.98	79.6
1054	4-30-96	5	0.27	506.6	14.21	1235.72	23.08	2.79	603.14	22.30	5.73	1086	2.44	1.62	1.19	1.57	0.98	79.5
745	3-28-96	6	0.27	505.6	14.37	1297.16	25.84	3.08	618.71	24.64	6.46	1204	2.57	1.80	1.22	1.71	1.09	84.2
1053	4-30-96	6	0.27	507.2	14.21	1292.62	25.67	3.22	619.29	24.25	6.15	1215	2.55	1.81	1.22	1.71	1.10	83.5
744	3-28-96	7	0.27	505.8	14.37	1332.82	26.96	3.22	627.13	25.50	6.62	1257	2.63	1.88	1.24	1.77	1.14	86.0
767	3-28-96	7	0.27	502.0	14.35	1319.08	27.01	3.26	625.71	25.50	6.60	1257	2.63	1.88	1.25	1.78	1.14	85.7
1052	4-30-96	7	0.27	506.9	14.21	1325.44	26.78	3.35	629.30	25.28	6.40	1271	2.61	1.88	1.24	1.78	1.15	85.5
766	3-28-96	8	0.27	501.5	14.36	1361.32	28.36	3.41	630.45	26.53	6.82	1313	2.71	1.98	1.26	1.85	1.20	87.9
743	3-28-96	8	0.27	505.6	14.37	1370.02	28.43	3.40	637.59	26.61	6.87	1319	2.71	1.98	1.26	1.85	1.20	88.0
1051	4-30-96	8	0.27	507.2	14.21	1369.55	28.12	3.54	642.38	26.28	6.55	1333	2.70	1.98	1.26	1.85	1.21	87.5
1056	4-30-96	8	0.27	506.2	14.21	1370.62	28.17	3.54	642.38	26.25	6.55	1335	2.71	1.98	1.27	1.85	1.21	87.5
742	3-28-96	9	0.27	505.2	14.37	1397.62	29.23	3.47	641.83	27.28	7.05	1352	2.77	2.03	1.27	1.90	1.23	89.3
765	3-28-96	9	0.27	501.4	14.36	1392.89	29.26	3.49	641.83	27.33	7.01	1355	2.78	2.04	1.28	1.90	1.23	89.3
1050	4-30-96	9	0.27	506.8	14.21	1398.70	28.97	3.61	646.35	26.90	6.71	1369	2.76	2.04	1.28	1.89	1.24	88.8

Table A-8. EPNL and Performance Summary for Flight (Mn = 0.27) Noise Data for ATM

Escort Number	Test Date	POWER CONDITION	Freejet Mach Number	Ambient Temp. (R)	Ambient Pressure (psia)	Core Ttpri (R)	Core Ptpri (psia)	Core Flow Rate (lbm/sec)	Fan Ttbyp (R)	Fan Ptbyp (psia)	Fan Flow Rate (lbm/sec)	Vjet (ft/sec)	Ttpri/T0	Ptpri/P0	Ttbyp/T0	Ptbyp/P0	Mixed Jet Mn (Vjet/C0)	1500' alt 1476' s/l EPNL
full: **ATM WITH PROBES and UN-HEATED FAN FLOW**
764	3-28-96	1	0.27	501.3	14.35	1144.38	20.97	2.37	506.67	20.63	5.44	904	2.28	1.46	1.01	1.44	0.82	73.3
763	3-28-96	3	0.27	501.3	14.35	1180.62	22.13	2.58	506.64	21.50	5.85	964	2.36	1.54	1.01	1.50	0.88	75.5
762	3-28-96	5	0.27	501.2	14.35	1215.58	23.29	2.73	506.69	22.50	6.27	1022	2.43	1.62	1.01	1.57	0.93	77.9
761	3-28-96	6	0.27	501.4	14.35	1283.80	25.78	3.08	508.03	24.48	6.89	1132	2.56	1.80	1.01	1.71	1.03	82.0
760	3-28-96	7	0.27	501.5	14.35	1318.82	26.97	3.23	508.53	25.45	7.14	1182	2.63	1.88	1.01	1.77	1.08	84.0
759	3-28-96	8	0.27	501.7	14.35	1360.62	28.45	3.42	509.83	26.47	7.39	1237	2.71	1.98	1.02	1.84	1.13	85.9
758	3-28-96	9	0.27	502.1	14.36	1391.62	29.35	3.51	510.45	27.22	7.58	1272	2.77	2.04	1.02	1.90	1.16	87.5
full: **ATM WITH PROBES and MUFFLER and HEATED FAN FLOW**
1108	5-2-96	3	0.27	526.1	14.33	1239.23	21.95	2.68	617.68	21.47	5.39	1036	2.36	1.53	1.17	1.50	0.92	77.6
1110	5-2-96	3	0.27	526.3	14.33	1248.53	21.95	2.83	618.32	21.49	5.46	1044	2.37	1.53	1.17	1.50	0.93	77.8
1106	5-2-96	5	0.27	526.2	14.33	1285.64	23.29	2.93	624.73	22.58	5.66	1117	2.44	1.62	1.19	1.58	0.99	80.1
1105	5-2-96	6	0.27	525.7	14.33	1346.74	25.78	3.27	645.99	24.52	6.13	1243	2.56	1.80	1.23	1.71	1.11	84.3
1104	5-2-96	7	0.27	525.7	14.33	1381.83	26.86	3.35	650.98	25.56	6.41	1294	2.63	1.87	1.24	1.78	1.15	85.8
1101	5-2-96	8	0.27	525.0	14.33	1428.52	28.31	3.42	664.81	26.55	6.65	1352	2.72	1.98	1.27	1.85	1.20	88.1
1109	5-2-96	8	0.27	526.2	14.33	1423.59	28.39	3.59	664.90	26.51	6.60	1361	2.71	1.98	1.26	1.85	1.21	88.1
1100	5-2-96	9	0.27	524.3	14.33	1445.37	29.29	3.56	668.73	27.22	6.78	1390	2.76	2.04	1.28	1.90	1.24	89.5

REPORT DOCUMENTATION PAGE

Public reporting burden for this collection of information is estimated to average 1 hour per response, including the time for reviewing instructions, searching existing data sources, gathering and maintaining the data needed, and completing and reviewing the collection of information. Send comments regarding this burden estimate or any other aspect of this collection of information, including suggestions for reducing this burden, to Washington Headquarters Services, Directorate for Information Operations and Reports, 1215 Jefferson Davis Highway, Suite 1204, Arlington, VA 22202-4302, and to the Office of Management and Budget, Paperwork Reduction Project (0704-0188), Washington, DC 20503.

1. AGENCY USE ONLY (Leave blank)	2. REPORT DATE	3. REPORT TYPE AND DATES COVERED
	March 2001	Final Contractor Report

4. TITLE AND SUBTITLE

Large Engine Technology (LET) Task XXXVII Low-Bypass Ratio Mixed Turbofan Engine Subsonic Jet Noise Reduction Program Test Report

5. FUNDING NUMBERS

WU–522–81–11–00
NAS3–26618
Task Order 37

6. AUTHOR(S)

Joseph R. Hauser, Steven H. Zysman, and Thomas J. Barber

7. PERFORMING ORGANIZATION NAME(S) AND ADDRESS(ES)

United Technologies Corporation
Pratt & Whitney
East Hartford, Connecticut 06108

8. PERFORMING ORGANIZATION REPORT NUMBER

E–12537

9. SPONSORING/MONITORING AGENCY NAME(S) AND ADDRESS(ES)

National Aeronautics and Space Administration
Washington, DC 20546–0001

10. SPONSORING/MONITORING AGENCY REPORT NUMBER

NASA CR—2001-210571

11. SUPPLEMENTARY NOTES

Joseph R. Hauser and Steven H. Zysman, United Technologies Corporation, Pratt & Whitney Division, East Hartford, Connecticut 06108; and Thomas J. Barber, United Technologies Corporation, Research Center, East Hartford, Connecticut 06108. Project Manager, Naseem Saiyed, Structures and Acoustics Division, NASA Glenn Research Center, organization code 5940, 216–433–6736.

12a. DISTRIBUTION/AVAILABILITY STATEMENT

Unclassified - Unlimited
Subject Category: 71   Distribution: Nonstandard

Available electronically at http://gltrs.grc.nasa.gov/GLTRS

This publication is available from the NASA Center for AeroSpace Information, 301–621–0390.

12b. DISTRIBUTION CODE

13. ABSTRACT (Maximum 200 words)

NASA Glenn Research Center supported a three year effort to develop the technology for reducing jet noise from low-bypass ratio engines. This effort concentrated on both analytical and experimental approaches using various mixer designs. CFD and MGB predictions are compared with LDV and noise data, respectively. While former predictions matched well with data, experiment shows a need for improving the latter predictions. Data also show that mixing noise can be sensitive to engine hardware upstream of the mixing exit plane.

14. SUBJECT TERMS

Acoustic nozzles; Aeroacoustics; Aircraft noise; Engine noise; Exhaust nozzles; Jet aircraft noise; Jet engines; Mixers; Noise reduction; Noise suppressors; Sonic nozzles

15. NUMBER OF PAGES

166

16. PRICE CODE

A08

17. SECURITY CLASSIFICATION OF REPORT	18. SECURITY CLASSIFICATION OF THIS PAGE	19. SECURITY CLASSIFICATION OF ABSTRACT	20. LIMITATION OF ABSTRACT
Unclassified	Unclassified	Unclassified	